

PhD Thesis

# **Development and validation of methods used to compute time values of indoor daylight illuminances**

Presented in front of:

University of Ljubljana  
Faculty of Electrical Engineering

L'Institut National des Sciences Appliquées de LYON  
Formation doctorale: Génie Civil  
Ecole doctorale: M.E.G.A.

By:

Matej Bernard KOBAV

Presented on January 30, 2009

---

Reviewer	prof. dr. Peter Žunko
Reviewer	prof. dr. Pierre Ineichen
Thesis supervisor	prof. dr. Grega Bizjak
Thesis supervisor	prof. dr. Dominique Dumortier
Member	prof. dr. Marc Fontoynt
Member	prof. dr. Stanislav Kovačič

---

*Research laboratories:*

Laboratoire des Sciences de l'Habitat, DGCB, Ecole Nationale des Travaux Publics de l'Etat, rue Maurice Audin, 69120 Vaulx-en-velin, France.

Laboratory of the Lighting and Photometry, Faculty of Electrical Engineering, University of Ljubljana, Tržaška 25, SI-1000 Ljubljana, Slovenia



*Dedicated to Manja, Ema and Matija*



## **Acknowledgments**

This PhD thesis is a result of my post-graduate study at Faculty of Electrical Engineering and very good collaboration with Laboratoire des Sciences de l'Habitat, Ecole Nationale des Travaux Publics de l'Etat, Vaulx-en-Velin.

I wish to thank my two mentors for their support, patience and spent time. Their gentle but firm direction has been most appreciated. Dr. Grega Bizjak was particularly helping in guiding me toward the finish. Dr. Dominique Dumortier had always the right answers to all my questions and doubts. He was more than just a mentor when I was staying in Lyon and he lent me a working table in his office when I was at ENTPE.

Since working conditions are always an important issue, I would like to thank also my mates in the office. Boštjan, Tomaž, Ambrož and Uroš, thank you.

I would also like to thank Manja for being with me, giving me all the needed support and love and giving birth to two beautiful children, who fill me up with energy and love.

Finally I would like to thank my parents and brother and sister for giving me support to continue with my postgraduate study.



# Table of contents

<b>ACKNOWLEDGMENTS .....</b>	<b>I</b>
<b>TABLE OF CONTENTS .....</b>	<b>III</b>
<b>LIST OF ABBREVIATIONS AND SYMBOLS .....</b>	<b>1</b>
<b>ABSTRACT OF THE THESIS.....</b>	<b>5</b>
<b>RESUME .....</b>	<b>9</b>
<b>POVZETEK .....</b>	<b>13</b>
<b>INTRODUCTION.....</b>	<b>17</b>
<b>1 DESCRIPTION OF THE SKY SCANNER.....</b>	<b>21</b>
<b>1.1 Sky scanner and measurements .....</b>	<b>21</b>
<b>1.2 Calibration of the sky scanner .....</b>	<b>23</b>
1.2.1 Calibration of the sky scanner under artificial sky .....	23
1.2.1.1 Zenith luminance .....	24
1.2.1.2 Horizontal and vertical illuminances .....	26
1.2.1.3 Checking the Li-cor sensors .....	28
1.2.2 Calibration of the sky scanner under real sky .....	30
1.2.2.1 Calculated vertical illuminances and measured data from IDMP station... ..	30
<b>1.3 Setting up the sky scanner .....</b>	<b>33</b>
1.3.1 Description of the IDMP station. ....	33
1.3.2 Correction of orientation of vertical illuminance sensors .....	34
1.3.3 Correction of orientation of the sky scanner.....	39
<b>2 ANALYSIS OF THE SKY SCANNER DATA .....</b>	<b>41</b>
<b>2.1 Description of the visualization .....</b>	<b>41</b>
<b>2.2 Defining CIE sky type based on CIE standard.....</b>	<b>43</b>
2.2.1 Determination of the gradation group .....	45
2.2.2 Determination of the indicatrix group .....	53
2.2.3 Calculation of the CIE sky type with gradation and indicatrix.....	60
<b>2.3 Calculation of the CIE sky type based on Lz/Dv ratio.....</b>	<b>61</b>

2.3.1	Calculation of the diffuse horizontal illuminance (Dv).....	65
2.3.2	Calculation of the vertical illuminances .....	68
<b>2.4</b>	<b>Calculation of the CIE sky type with Tregenza statistical method.....</b>	<b>69</b>
<b>2.5</b>	<b>Results of measurements .....</b>	<b>70</b>
<b>3</b>	<b>USING DIGITAL CAMERA AS A SKY SCANNER.....</b>	<b>75</b>
<b>3.1</b>	<b>Introduction.....</b>	<b>75</b>
<b>3.2</b>	<b>Transforming sky images to .05D files.....</b>	<b>75</b>
<b>3.3</b>	<b>Linking sky scans and images from digital camera.....</b>	<b>77</b>
3.3.1	Flipping and rotating an image .....	77
3.3.2	Flipping and rotating a sky scanner grid .....	80
<b>3.4</b>	<b>Comparing results derived with sky scanner and digital images.....</b>	<b>81</b>
<b>3.5</b>	<b>Database of sky luminance measurements .....</b>	<b>84</b>
<b>3.6</b>	<b>Conclusion on the use of digital images .....</b>	<b>87</b>
<b>4</b>	<b>SKY LUMINANCE MODELS .....</b>	<b>89</b>
<b>4.1</b>	<b>All weather model for sky luminance distribution - Perez .....</b>	<b>89</b>
<b>4.2</b>	<b>ASRC - CIE .....</b>	<b>92</b>
<b>4.3</b>	<b>Igawa All sky model.....</b>	<b>92</b>
<b>4.4</b>	<b>Comparison of sky luminance models.....</b>	<b>96</b>
4.4.1	Results of comparison - all cases .....	101
4.4.2	Results of comparison dependent on CIE sky type.....	105
4.4.3	Results of comparison.....	109
4.4.4	Results of comparison dependent on sky types and sun altitudes .....	111
4.4.4.1	Sun altitudes 5 - 20 <sup>0</sup> .....	112
4.4.4.2	Sun altitudes 20 - 35 <sup>0</sup> .....	114
4.4.4.3	Sun altitudes 35 - 50 <sup>0</sup> .....	115
4.4.4.4	Sun altitudes over 50 <sup>0</sup> .....	117
4.4.4.5	Problems of Igawa model for intermediate skies.....	120
<b>4.5</b>	<b>Conclusion on sky luminance models .....</b>	<b>126</b>
<b>5</b>	<b>MEASUREMENTS IN SCALE MODEL .....</b>	<b>129</b>
<b>5.1</b>	<b>Introduction.....</b>	<b>129</b>
<b>5.2</b>	<b>Description of the model and method.....</b>	<b>129</b>
5.2.1	Illuminance and luminance measurements in scale model.....	132

5.2.1.1	Illuminance .....	132
5.2.1.2	Indoor luminances .....	132
5.2.1.3	Outdoor luminances .....	132
5.2.2	View from a scale model .....	134
<b>5.3</b>	<b>Calculation of directional daylight factors .....</b>	<b>136</b>
<b>5.4</b>	<b>Calculation of illuminance values in scale model .....</b>	<b>144</b>
5.4.1	Calculation of luminance values of sky elements .....	144
5.4.2	Calculation of illuminance values in scale model with daylight factors.....	146
5.4.2.1	Daylight factors with DIALux.....	146
5.4.2.2	Daylight factors with illuminance .....	147
5.4.3	Calculation of illuminance values in scale model from luminance values from sky scanner.....	148
<b>5.5</b>	<b>Mean bias error between measured and calculated illuminance values in scale model .....</b>	<b>148</b>
<b>5.6</b>	<b>Database of scale model measurements .....</b>	<b>149</b>
<b>5.7</b>	<b>Results of the scale model measurements .....</b>	<b>152</b>
<b>5.8</b>	<b>Conclusions for scale model measurements .....</b>	<b>156</b>
<b>6</b>	<b>CONCLUSION.....</b>	<b>157</b>
	<b>CONTRIBUTIONS OF THE THESIS TO THE SCIENCE .....</b>	<b>159</b>
	<b>STATEMENT OF THE AUTHORSHIP .....</b>	<b>161</b>
	<b>REFERENCES.....</b>	<b>163</b>



## List of abbreviations and symbols

### List of abbreviations

IDMP	International Daylight Measurement Programme
CCD	Charge-coupled device
CIE	Commission Internationale de l'Eclairage (International Commission on Illumination)
DDF	Directional daylight factor
DF	Daylight factor
ENTPE	Ecole Nationale des Travaux Publics de l'Etat
FE	Faculty of Electrical engineering of University of Ljubljana
LASH	Laboratoire des Sciences de l'Habitat
MA	Mean absolute
MBD	Mean bias difference
MBE	Mean bias error
RMS	Root mean square
RMSD	Root mean square difference
SLR (camera)	Single-lens reflex (camera)

### List of symbols used in chapter 1

$f_c$	Calibration factor of sky scanner (110.6),
$k_{SS}$	Factor we defined based on measurements under artificial sky (1.65)
$L_F$	Luminance of a sky element in .05D file

### List of symbols additionally used in chapter 2

$a, b, c, d, e$	Parameters defining gradation and indicatrix groups in Standard CIE S 011/E:2003 /ISO 15469.2004
$A_z$	Angular difference between azimuth of the sun and azimuth of the sky element,
$A^{90}$	Difference in azimuth of ideal $L_{90}$ sky element and solar meridian
$B, C, D, E$	Standard parameters defining $L_z/D_v$ curves

$D_V$	Diffuse horizontal illuminance
$E_h$	Horizontal illuminance from sky scanner measurement
$E_{hCIEx}$	Horizontal illuminance for CIE sky type x
$\delta E$	contribution to horizontal illuminance from a single sky patch
$\delta E_v$	contribution to vertical illuminance from a single sky patch
$f(\chi)$	Indicatrix function
$L_\alpha$	Luminance of a sky element
$L_\alpha'$	Measured luminance of a sky element
$L_{a-rel}$	Relative sky element luminance
$L_p$	Luminance of a sky patch
$L_p'$	Normalized luminance of a sky patch
$L_{pCIEx}$	Luminance of a sky patch for CIE sky type x
$L_{pCIEx}'$	Normalized luminance of a sky patch for CIE sky type x
$L_Z$	Zenith luminance
$L_Z'$	Measured zenith luminance
$L(90^0)$	Normalizing luminance, luminance of sky element with angular distance $90^0$ towards sun
$L(90^0)'$	Measured normalizing luminance $L(90)$
$L(\chi)$	Luminance of sky element with angular distance $\chi$ towards sun
$L(\chi)'$	Measured luminance of sky element with angular distance $\chi$ towards sun
$n_{X>15}$	Number of patches with scattering angle larger than 15 degrees
$rms_{CIEx}$	RMS error between measured values and CIE sky type x
$Z$	Zenith angle of a sky element
$Z_S$	Solar zenith angle
$\alpha_S$	Solar azimuth
$\alpha$	Azimuth of a sky element
$\gamma$	Elevation angle of a sky element
$\gamma_S$	Solar altitude
$\Delta\alpha$	Angular difference in azimuth between sky patch and normal of the plane

$\varepsilon_{\xi}$	Altitude of the almucantar (imaginary circle on the celestial sphere, parallel to the horizon. The circle connects sky elements with same altitudes)
$\varphi(Z)$	Gradation function
$\chi$	Scattering angle
$d\omega$	Solid angle of a sky patch

**List of symbols additionally used in chapter 4**

$a_p, b_p, c_p, d_p, e_p$	Coefficients in Perez All weather model
$a', b', c', d', e'$	Coefficients in Igawa model
$C_e$	Cloud ratio
$C_{le}$	Cloudless index
$C_{es}$	Standard cloud ratio
$E_{ed}$	Horizontal diffuse irradiance
$E_{eg}$	Global irradiance
$E_{es}$	Normal incident direct irradiance
$E_{es0}$	Extraterrestrial direct normal irradiance
$K_C$	Clear sky index
$L_{pIgawa}$	Luminance of a patch in Igawa model,
$L_{pSS}$	Luminance of a patch measured with sky scanner.
$mbd_{Igawa}$	Mean bias difference between Igawa model and sky scanner measurement,
$S_{egg}$	Standard global irradiance
$m$	Optical air mass
$mbd_{Igawa}'$	Mean bias difference between Igawa model and sky scanner measurement without elements on first almucantar and without element with $\chi < 15^\circ$
$rd_{IgawaCIEx}$	Relative difference for Igawa luminance model for CIE sky type X
$rmsd_{Igawa}$	RMSD between Igawa model and sky scanner measurement
$rmsd_{IgawaCIEx}$	RMSD for Igawa luminance model for CIE sky type X
$rmsd_{BestCIEx}$	RMSD for best luminance model for CIE sky type X

$rmsd_{I_{gawa}}$	RMSD between Igawa model and sky scanner measurement and without elements on first almucantar and without element with $\chi < 15^{\circ}$
$Si$	Sky index
$\varepsilon$	Sky brightness
$\Delta$	Sky clearness

**List of symbols additionally used in chapter 5**

$DDF_{Ap}$	Directional daylight factor related to a sky element for a point A in the model
$DDQ_{Ap}$	Directional daylight quotient related to a sky element p for a point A in the model
$DF_A$	Daylight factor for a given point
$E_A$	Total illuminance at a given point
$E_{Ap}$	Illuminance at a given point contributed by a sky element
$E_{AIntp}$	Indoor illuminance at a given point A, produced by sky element p
$E_{AExt p}$	Outdoor (unobstructed) illuminance at a given point A, produced by sky element p
$E_{diff}$	Diffuse illuminance on unobstructed horizontal plane
$E_{Licor-A1}$	Measured illuminance with Licor sensor in point A1
$E_{sky13-A1}$	Calculated illuminance from 13 sky zone luminances in point A1
$MBE_{sky13}$	Mean bias error for sky modelled with 13 zones
$RMSE_{sky13}$	Root mean square error for sky modelled with 13 sky zones
$Z_p'$	Incidence angle between surface in point and sky element
$Z_p$	Zenith angle of a sky element
$\Delta S_p$	Solid angle of a sky element
$\Delta S_p'$	Solid angle of a sky element seen from indoor

## **Abstract of the thesis**

The presented doctoral thesis concentrates on daylight availability calculations with an emphasis on models of the sky luminance distribution. The main goal of the thesis is to recommend the most appropriate sky luminance model used to calculate time values of indoor daylight illuminances and to define the needed accuracy of the sky luminance model, by the number of zones used in the model. Both conclusions are based on measurements.

The first chapter introduces the equipment needed to perform sky luminance distribution measurements. The most important device is a sky scanner. The sky scanner that was used with our research was produced by company EKO and is capable to measure sky luminance distribution with accuracy of 145 sky zones in approximate 3 minutes. Before realization of the measurements the calibration of the sky scanner was carried out. Calibration of the sky scanner was carried out with different methods, firstly under artificial sky. Under artificial sky, zenith luminance and horizontal and vertical illuminances were checked. Second calibration was performed under real sky. In this case we compared calculated horizontal illuminance with illuminances measured on IDMP station. After the sky scanner was calibrated and set up on IDMP station it was possible to correct the orientation of the IDMP vertical sensors for illuminance, since they were not perfectly in line with correct azimuths.

In the second chapter, we describe how to analyse luminance data gained with sky scanner. In this part also the CIE S 011/2003 standard is explained with an emphasis on gradation and indicatrix function. Determination of the gradation group is based on calculation of luminance ratio between two elements on every almucantar (imaginary circle on the celestial sphere, parallel to the horizon. The circle connects sky elements with same altitudes) with scattering angle as close as possible to solar zenith angle and zenith luminance. Determination of the indicatrix group is also based on luminance ratio. In this case in the numerator is luminance of an element on certain almucantar and in denominator we can find the normalizing luminance. Normalizing luminance is a luminance of a part of the sky with angular distance 90 degrees towards sun. There are 36 combinations of gradation and indicatrix groups and only 15 of them are listed in the CIE standard. Since some of combinations are really rare, we provide the table how to include 36 combinations in 15 standard CIE sky types.

CIE sky type can be also defined with ratio between zenith luminance and diffuse horizontal illuminance. Later on in chapter two, we explain how to calculate diffuse illuminance from sky scan and how to derive CIE sky type from before mentioned ratio.

Another method, which is also explained in this chapter, provides CIE sky type based on statistical method. The mentioned method is based on statistical approach. Luminances gained with sky scanner and the ones in the luminance model, described with a standard, are normalised with diffuse horizontal illuminance and compared with each other. If comparison is made between measurements and all 15 CIE sky types, the one with smallest discrepancy can be found.

At the end of chapter two results are gathered and frequencies of CIE sky types derived with different methods are shown.

Chapter three introduces a digital camera with fish-eye lens as a sky scanner. Our goal was to compare sky luminance values captured with sky scanner and the ones with digital camera and fish-eye. Since luminance values gained with sky scanner are gathered in a text file with sophisticated structure, also the luminances gained with digital camera were with help of Photolux software written in such a file. Both files (for the same time period) were processed in the same manner for 160 cases. As the luminance data were processed it was possible to compare significant sky type characteristics. When gained data were compared, we checked horizontal diffuse illuminance, zenith illuminance, Lz/Dv ratio, gradation group, indicatrix group, sky type based on Lz/Dv ratio, sky type based on statistical method and also all 145 luminance values were compared with each other. In this chapter a reader can find described also the whole procedure how to transform fish-eye image into luminance map and how to extract 145 luminances of the CIE sky partitioning, which is also used by the sky scanner. At the end of the chapter we conclude that a digital camera can be easily (with some limitations) used as a sky scanner.

In chapter four, a description of different sky luminance models is given. The emphasis is on the following models: Perez all weather model, ASRC-CIE model and Igawa model. For the times, when we had sky scanner measurements (13.006 cases), sky luminance distributions were modelled with all three models. The modelled luminances are calculated with model's equations and irradiance data measured by IDMP station. In this chapter a problem of high luminance values of the solar corona is exposed. Neither sky luminance models nor sky scanner are capable to model or measure (truthfully) high luminance values of sky elements with low scattering angle towards sun. For this reason in our comparison, all sky elements with scattering angle smaller than  $15^{\circ}$  were eliminated. This decision is based on calculated mean bias error for all sky elements and only for those with scattering angle higher than  $15^{\circ}$ . Later on, a comparison between three models and sky scanner measurements is introduced. Comparison was carried out with calculation of MB error and RMS error between each modelled and measured sky element. In similar way also CIE sky types were compared. A comparison was carried out for two methods used to derive sky scanner sky type; the one based on gradation and indicatrix group and the statistical one and for two sets of luminance values; for all sky elements without the ones with scattering angle less than  $15^{\circ}$  and the ones on first almucantar. In continuation of chapter four, we present quality of luminance models depending on the sky type and on sun altitude. Conclusion on all comparisons in this chapter is that Igawa model is best for extremely cloudy sky types, Perez All weather model gives best results with intermediate sky types and ASRC-CIE model is in most cases in between upper two models, but always close to the best model.

In the fifth chapter, we are talking about scale model measurements. Scale model is fully described and also all measuring problems are listed. In this chapter we introduce sky partitioning into different number of zones (212, 145, 97, 26 and 13) and we also introduce directional daylight factors (DDF) and traditionally used daylight factor.

Illuminances in the model were measured with illuminance sensors and later compared with calculated values. The calculated values of illuminances were calculated with directional daylight factors and averaged luminance of the sky zone and with daylight factors and diffuse illuminance measured by IDMP station. In continuation, we describe also the database of scale model measurements (available as an attachment on a CD-rom) and the results. Results show us that the number of sky zones has practically no influence to MBE and after that we can conclude that 13 zones are enough to model sky luminance if we are considering only sky vault without direct sun.



## Résumé

Cette thèse de doctorat traite des calculs de disponibilité de la lumière du jour à l'intérieur des bâtiments en s'intéressant particulièrement aux modèles permettant de décrire la distribution des luminances du ciel. Son objectif principal est de recommander les modèles les plus appropriés au calcul des valeurs instantanées des éclairements lumineux intérieurs et de définir la finesse du maillage utilisé pour représenter les variations de luminance sur la voûte céleste.

Le premier chapitre présente le dispositif expérimental utilisé pour mesurer la distribution des luminances du ciel sur le site de l'ENTPE. L'appareil le plus important est le scanner de ciel. Celui que nous avons utilisé est de la marque EKO. Il est capable de mesurer les luminances de 145 points de la voûte céleste en 3 minutes. Nous avons d'abord étalonné le scanner. Dans un premier temps, nous avons placé le scanner sous le ciel artificiel de l'ENTPE. Cette source de lumière parfaitement contrôlée nous a permis de nous assurer de la cohérence des mesures effectuées par le scanner et des valeurs calculées à partir des mesures : luminances, luminance du zénith, éclairement horizontal, éclairements verticaux... Dans un deuxième temps, le scanner de ciel a été installé sur le lieu de la station de mesure de la lumière de l'ENTPE. Nous avons vérifié que les cellules de mesure des éclairements verticaux de la station étaient correctement orientées. Nous avons ensuite orienté le scanner puis nous l'avons étalonné de manière à ce que toutes les informations calculables à partir de ses mesures de luminance soient cohérentes avec les mesures de la station. Le scanner de ciel a été programmé pour effectuer des mesures automatiques des luminances du ciel toutes les 10 minutes pendant un peu moins d'une année.

Dans le deuxième chapitre, nous décrivons comment les mesures de luminances provenant du scanner de ciel ont été analysées. Nous présentons la classification des ciels standardisée par la Commission Internationale de l'Eclairage (CIE) en 2003. Nous expliquons le principe des fonctions de gradation et de diffusion utilisées par la classification et nous montrons comment obtenir ces fonctions à partir des mesures. La détermination du groupe de gradation est basée sur la variation en fonction de l'angle au zénith, du rapport entre les luminances de deux points de mesure ayant le même angle au zénith et un angle avec le soleil, le plus proche possible de l'angle au zénith du soleil. La détermination du groupe de diffusion est basée sur la variation en fonction de l'angle de diffusion (angle entre le soleil et un point du ciel) du rapport entre la luminance d'un point du ciel et la luminance moyenne des points du ciel situés à 90 degrés du soleil. La combinaison des 6 groupes de gradation et des 6 groupes de diffusion conduit à un total de 36 types de ciels dont 15 seulement font partie du standard CIE. Nous proposons donc une table d'équivalence. Certains auteurs ont proposé d'autres méthodes ne nécessitant pas les luminances de la voûte céleste pour déterminer les types de ciel CIE. Nous les avons aussi testées. L'une est basée sur le rapport entre la luminance du zénith et l'éclairement horizontal diffus. L'autre est basée sur une approche statistique comparant la distribution des luminances mesurée avec la distribution des luminances calculée à partir de modèles n'utilisant que des

éclairagements horizontaux. La fin de ce chapitre permet de comparer toutes ces méthodes sur la base des fréquences de ciels CIE obtenus pendant la période de mesures.

Le chapitre 3 nous permet de présenter et de valider une nouvelle méthode de mesure des luminances du ciel basée sur l'utilisation d'un appareil photo numérique étalonné en luminances. Le système appelé PHOTOLUX et développé à l'ENTPE, avait jusqu'ici été utilisé pour l'évaluation du confort visuel dans les ambiances intérieures. Notre objectif était de l'utiliser à l'extérieur en parallèle avec le scanner de ciel et de vérifier la qualité des informations qu'il était capable de produire. Nous présentons d'abord le système et sa mise en place sur la station. L'appareil est équipé d'un objectif fish-eye à 180° qui lui permet de voir l'intégralité de la voûte céleste. Comme pour le scanner de ciel, sa mise en place s'est accompagnée d'une mise en cohérence avec les mesures de la station. Nous avons ensuite utilisé le système pendant des journées bien précises. Au total, nous avons effectué 160 mesures. La carte des luminances générée par PHOTOLUX (plus de 400000 pixels) a été utilisée pour calculer les éclairagements lumineux horizontaux et verticaux mesurés sur la station. Pour pouvoir comparer ce système avec le scanner de ciel, nous avons calculé les luminances moyennes des 145 zones vues par le scanner. Nous avons aussi utilisé le système pour produire des informations liées à la classification des ciels de la CIE. Chacune des 160 mesures est présentée dans une fiche constituant une base de données utile pour comprendre la classification des ciels. La fin du chapitre nous permet de conclure que le système fournit des informations beaucoup plus riches qu'un scanner de ciel (photo et distribution très fine des luminances) malgré quelques limitations liées à l'impact du soleil direct.

Dans le chapitre 4, nous décrivons différents modèles de luminances de ciel. Nous nous intéressons aux modèles les plus récents ou les plus utilisés : « tout temps Perez », « ASRC-CIE Perez » et « Igawa ». Nous comparons leurs performances sur la base des 13000 mesures effectuées avec le scanner de ciel. Pour tenir compte du fait que ni les modèles, ni le scanner de ciel ne peuvent déterminer avec précision les luminances très élevées de la zone circumsolaire, nous n'avons pas pris en compte les luminances correspondant aux zones dont l'angle par rapport au soleil était inférieur à 15°. Nous nous sommes intéressés à l'écart moyen et l'écart quadratique moyen entre les luminances des modèles et les luminances mesurées. Nous nous sommes aussi intéressés à la capacité de chacun des modèles à restituer les ciels types de la CIE. Nous présentons la performance de chacun des modèles en fonction du type de ciel et de la hauteur du soleil. Même si le modèle « Igawa » est le plus performant pour la modélisation des ciels couverts. Même si le « tout temps Perez » est le plus performant pour la modélisation des ciels intermédiaires. Le modèle « ASRC-CIE Perez » est souvent proche des deux autres dans les catégories citées précédemment et globalement le meilleur.

Le cinquième chapitre s'intéresse au calcul des éclairagements intérieurs et notamment à l'influence de la finesse du maillage utilisé pour représenter les variations de luminance sur la voûte céleste. Pour tester les calculs, nous avons mis en place un dispositif expérimental original s'appuyant sur une maquette placée à l'extérieur. La maquette représente un bureau avec une ouverture en façade. Les parois de la maquette ont été

peintes en noir pour supprimer au maximum les réflexions multiples. Nous nous sommes donc intéressés au calcul de la composante directe de la lumière du jour résultant d'un ciel de distribution de luminance quelconque. Nous avons mesuré les éclairagements lumineux sur les parois de la maquette (sol et murs). Nous avons utilisé deux systèmes PHOTOLUX (donc deux appareils photos) : l'un pour produire la carte des luminances du ciel vus par l'ouverture, l'autre la carte des luminances des parois de la maquette. Nous avons calculé les éclairagements lumineux directs correspondant aux points de mesure dans la maquette en utilisant la notion de facteur de lumière du jour directionnel (DDF). Ce facteur permet de décrire la contribution d'une zone du ciel à l'éclairage d'un point de la pièce. Nous l'avons calculé analytiquement pour chacun des points de mesure dans la maquette et pour chacune de zones du ciel d'un maillage variant de 13 à 212 zones. Nous les avons ensuite combinés avec les luminances moyennes de chaque zone du ciel pour déterminer l'éclairage à l'intérieur de la maquette aux différents points de mesure. Les mesures et les résultats des calculs sont documentées dans des fiches qui facilitent leur interprétation. La comparaison entre les mesures et les calculs montre que la méthode des facteurs de lumière du jour directionnels fournit des meilleurs résultats que la méthode classique du facteur de lumière du jour. Pour la configuration correspondant à notre maquette, un nombre minimum de 13 zones semble suffisant pour prendre en compte la diversité des distributions de luminances des ciels rencontrés dans la réalité



## Povzetek

Pričujoča doktorska disertacija se osredotoča na izračun razpoložljive dnevne svetlobe s poudarkom na modelih svetlosti neba. Prvi cilj naloge je predlagati najbolj primeren model svetlosti neba za izračun trenutnih vrednosti osvetljenosti z dnevno svetlobo v notranjih prostorih. Drugi cilj naloge pa je določitev potrebne natančnosti modela svetlosti neba. Natančnost modela svetlosti neba je določena s številom uporabljenih elementov v modelu. Oba zaključka sta osnovana na meritvah, ki so bile opravljene v Lyonu.

V prvem poglavju je opisana oprema, ki je potrebna za opravljanje meritev porazdelitve svetlosti neba. Najbolj pomembna naprava je vsekakor merilnik porazdelitev svetlosti neba (sky scanner). Merilnik, ki smo ga uporabili pri meritvah, je znamke EKO in je sposoben meritve porazdelitve svetlosti neba v 145 točkah v času približno treh minut. Pred opravljanjem meritev je bilo potrebno merilnik tudi kalibrirati. Kalibracija je izvedena z uporabo različnih metod. Prva kalibracija je bila izvedena v simulatorju dnevne svetlobe. Pri tej kalibraciji smo preverjali meritve svetlosti zenita in izračunane vrednosti vertikalnih in horizontalne osvetljenosti. Druga kalibracija je bila izvedena pod resničnim nebom. V tem primeru smo primerjali izračunane vrednosti vertikalnih in horizontalne osvetljenosti z vrednostmi, ki so bile izmerjene z merilniki postaje IDMP (International Daylight Measuring Program), ki so nameščeni že od leta 1992. Ko je bil merilnik porazdelitve svetlosti neba umerjen in nameščen na IDMP postaji, smo lahko popravili usmerjenosti merilnikov vertikalnih osvetljenosti IDMP postaje. Ti merilniki namreč niso imeli popolnoma ustrezne usmerjenosti.

V drugem poglavju je opisan postopek analize meritev porazdelitve svetlosti neba. V tem delu je opisan način določitve CIE tipa neba in tudi CIE standard S 011/2003 s poudarkom na funkcijah postopnosti (gradation) in razpršenosti (indicatrix). Določitev skupine postopnosti temelji na razmerju svetlosti dveh elementov na vsakem almukantarju (Krog na nebesni polobli, ki je vzporeden s horizontom. Krog povezuje točke z enako kotno višino.) in svetlosti zenita. Elementa na vsakem almukantarju morate imeti kotno razdaljo do sonca čim bližje zenitnemu kotu sonca. Tako dobimo na vsaki strani sončnega poldnevnika en element, ki ustreza zahtevi. Prav tako tudi določitev skupine razpršenosti temelji na razmerju dveh svetlosti. V tem primeru je v števcu svetlost posameznega elementa na almukantarju, v imenovalcu pa se nahaja normalna svetlost almukantarja. Normalna svetlost almukantarja je svetlost elementa neba na almukantarju, ki ima kotno razdaljo  $90^{\circ}$  do sonca. Ker imamo šest skupin postopnosti in šest skupin razpršenosti, imamo skupno 36 kombinacij. Nekatere od kombinacij so izjemno redke in s pomočjo tabele, ki je v nalogi podana, lahko vseh 36 kombinacij uvrstimo med 15 osnovnih tipov, kolikor jih je tudi v CIE standardu.

CIE tip neba se lahko določi iz razmerja svetlosti zenita ( $L_z$ ) in difuzne horizontalne osvetljenosti ( $D_v$ ). V nadaljevanju drugega poglavja je opisan postopek izračuna horizontalne osvetljenosti iz meritev porazdelitve svetlosti neba in postopek določitve CIE tipa neba iz omenjenega razmerja.

V tem poglavju je opisan tudi postopek določitve CIE tipa neba s pomočjo statistične metode. Izmerjene vrednosti svetlosti elementov neba se normirajo z difuzno horizontalno osvetljenostjo. Na enak način se normirajo tudi vrednosti vseh 15 tipov neba, ki so opisani s standardom. Nato primerjamo izmerjene normirane vrednosti z normiranimi izračunanimi vrednostmi za vseh 15 tipov. Tip neba, pri katerem je odstopanje najmanjše, je rezultat metode.

Na koncu poglavja so podane tabele frekvenc pojavljanj posameznih tipov neba izračunanih z različnimi metodami.

V tretjem poglavju predstavimo digitalni fotoaparatus s širokokotnim objektivom kot merilnik porazdelitve svetlosti. Cilj, ki smo ga imeli, je primerjava porazdelitve svetlosti neba, ki jo dobimo s pomočjo digitalnega fotoaparata s širokokotnim objektivom in porazdelitve, ki jo izmeri merilnik porazdelitve svetlosti neba. Meritve, izmerjene z merilnikom so zapisane v tekstovni datoteki s specifično obliko zapisa, zato smo morali podatke dobljene z digitalnim fotoaparatom in obdelane s pomočjo programske opreme Photolux, zapisati v datoteko z enako obliko zapisa. Obe datoteki (za isto časovno obdobje) smo analizirali na enak način za vseh 160 primerov, kolikor smo imeli digitalnih fotografij. Z analizo vrednosti svetlosti elementov neba smo lahko primerjali tudi značilne lastnosti neba. Ko so bili vsi podatki zbrani, smo med seboj primerjali horizontalno difuzno osvetljenost, svetlost zenita, razmerje  $Lz/Dv$ , skupino postopnosti in razpršenosti, tip neba določen z razmerjem  $Lz/Dv$  in tip neba določen s statistično metodo. Na koncu smo med seboj primerjali tudi pare vseh 145 svetlosti elementov. Na koncu poglavja zaključujemo, da lahko digitalni fotoaparatus s širokokotnim objektivom uporabimo kot merilnik svetlosti, pri tem pa moramo upoštevati nekatere omejitve.

V četrtem poglavju so opisani modeli porazdelitve svetlosti neba. Poudarek je na modelih, ki se največ uporabljajo: Perez-ov model za vse tipe neba, ASRC-CIE model in Igawa model. Za vse čase (13.006 meritev), ko je deloval merilnik svetlosti neba (april 2005 – december 2005) smo izdelali porazdelitve svetlosti neba za vse tri modele. Vrednosti svetlosti so bile izračunane na podlagi modelov in meritev obsevanosti na IDMP postaji. V tem poglavju je opisan tudi problem visokih vrednosti svetlosti sonca in sončeve korone. Niti modeli porazdelitve svetlosti neba niti merilnik porazdelitve svetlosti neba ne morejo modelirati oz. izmeriti visokih nivojev svetlosti elementov neba, ki imajo majhno kotno razdaljo do sonca. Prav zaradi tega razloga smo pri analizi podatkov izločili vse elemente neba, ki imajo kotno razdaljo do sonca manjšo od  $15^{\circ}$ . Ta odločitev temelji na izračunu povprečne razlike svetlosti elementov neba z upoštevanjem vseh elementov neba in le tistih s kotno razdaljo do sonca večjo od  $15^{\circ}$ . V nadaljevanju je predstavljena primerjava izračunanih vrednosti svetlosti elementov neba z modeli in vrednosti izmerjenih z merilnikom porazdelitve. Primerjava je bila izvedena z izračunom povprečne vrednosti razlike in efektivne vrednosti razlike med posameznim modelom in izmerjeno vrednostjo. Na podoben način smo primerjali tudi CIE tip neba. Primerjava je bila izvedena za dve metodi določitve CIE tipa neba, za določitev na podlagi postopnosti in razpršenosti in za določitev na podlagi statistične metode. Primerjava smo izvedeli na dveh skupnih podatkih o vrednostih svetlosti; za vse vrednosti in le za tiste, katerih elementi imajo kotno razdaljo do sonca večjo od  $15^{\circ}$  in višino večjo od  $6^{\circ}$ . Prvi elementi so bili izvzeti zaradi sončeve korone, drugi pa zaradi

ovir-stavb, ki so v okolici IDMP postaje. V nadaljevanju četrtega poglavja je predstavljena kakovost modelov svetlosti neba v odvisnosti od tipa neba in višine sonca. Na koncu poglavja so podani zaključki, da je Igawa model najboljši zelo oblačne tipe neba, Perezov model je najboljši za srednje tipe neba, ASRC-CIE model neba pa je v povprečju najboljši model. ta model je namreč v večini primerov po kakovosti med prej omenjenima, vedno pa blizu najboljšega modela.

Peto poglavje opisuje meritve na modelu prostora in analizo le-teh. Model prostora je natančno opisan, prav tako pa so omenjeni tudi problemi, ki so nastali ob meritvah. Na tem mestu predstavimo tudi delitev neba na različno število elementov (212, 145, 97, 26 in 13), faktor dnevne svetlobe in direktni faktor dnevne svetlobe. Osvetljenosti v modelu so bile merjene z merilniki osvetljenosti, nato pa so bile te vrednosti primerjane z modeliranimi. Modelirane vrednosti so bile izračunane na podlagi direktnega faktorja dnevne svetlobe in srednje vrednosti svetlosti elementa neba na podlagi faktorja dnevne svetlobe in izmerjenih vrednosti osvetljenosti na IDMP postaji. V nadaljevanju je opisana tudi baza podatkov, ki so bili izmerjeni z meritvami na modelu prostora. Rezultati meritev in primerjave kažejo, da natančnost modela (število elementov neba) praktično ne vpliva na velikost napake pri izračunu osvetljenosti. Tako zaključujemo, da je pri izračunih, kjer ne upoštevamo direktne sončne svetlobe, dovolj delitev neba na 13 elementov.



## **Introduction**

Our life is closely connected to daylight. It has a bearing on our schedule, way of life and biological processes in the body. In fact, we cannot even imagine our life without daylight.

Daylight constitutes a renewable source of energy. Consequently, we would like to exploit it to the greatest extent possible. If we strive for its rational exploitation, we need to provide for at least an approximate forecast. Thus, all over the world different methods for calculating the daylight contribution to the indoor illuminances are being developed.

The sky is the main contributor to the indoor illuminances, whereas the smaller portion is contributed directly by the sun. The prerequisite for the calculation of indoor daylight illuminances is the knowledge of the distribution of sky luminances, which in turn enables the calculation of the indoor illuminances.

First mathematical descriptions of the distribution of sky luminances can be traced as far back as beginning of 20<sup>th</sup> century, yet their focus was only on a cloudy sky [11, 12]. Complexity of the problem was the reason why the majority of researchers limited their work at the beginning to two basic sky types, i.e. clear and cloudy. It was only later that intermediate types were described as well. Researchers formulated mathematical equations for the description of sky luminances on the basis of local measurements. Most equations are consequently adapted to local conditions or sky types. 2003 saw the adoption of the standard by CIE - Commission Internationale de l'Eclairage (International Commission on Illumination). The standard [16] gives mathematical description of the distribution of luminances for 15 different sky types, five for a cloudy sky, five for a partly cloudy and five for a clear sky. These 15 sky types now constitute an instrument allowing for the worldwide description of the most frequent sky types.

Various methods can be employed for the calculation of the daylight contribution to indoor illuminances on the basis of the recorded distribution of sky luminances. The most frequent method of calculation is the daylight factor. The calculation by way of computer simulations of the room conditions has been gaining ground recently. In 2003, our Laboratory of Lighting and Photometry developed a simulation procedure [17] whereby the calculation of indoor daylight illuminances employs photometry of the window through which the daylight comes into a room.

### **Description of the problem**

The basis for the method developed at the Faculty of Electrical Engineering in Ljubljana is the sky division into 77 zones. The luminances of certain zones provide the basis for subsequent calculation of photometric data giving luminances for certain directions of the window through which the light comes into the premises. Similar methods have also been developed in other labs. ENTPE-LASH developed a method founded on sky division into 13 zones. It is presented in [1] and is also available at the website [www.satel-light.com](http://www.satel-light.com). The method is based on the calculation of the contribution which the individual sky zone makes to the illuminances of a certain point in a room. The method is also called Directional Daylight Factor – DDF. The methods used for the

calculation of the daylight contribution have unfortunately not yet been adequately verified, the primary reason being the lack of comparable measurements.

The use of different software (e.g. Photolux enabling the measurement of distribution of sky luminances and the drawing of the luminance maps on the basis of the photographs taken by the digital camera and wide-angle lens) and measurements on a model hold promises for certain progress in the field.

### **Rationale of the contribution to the science**

In 2003, CIE issued a standard which describes the distribution of sky luminances in different weather conditions. The standard provides for universal equations enabling the calculation of luminances of the sky element in an arbitrary direction and gives the coefficient table used for the determination of 15 different sky types, ranging from cloudy to clear skies. Not long ago after the standard had been issued, it became evident that the frequency of emergence of certain sky types at a certain location also needed to be determined so that the described model would be used correctly. Hence, the purpose of this doctoral thesis is to develop an adequate method which shall make this possible.

Tables denoting the frequency of emergence of certain sky types at certain locations would be compiled in the easiest way by employing measurements of the distribution of sky luminances. Such measurements, however, are extremely rare since only 17 measurement stations in the world make use of the "sky scanner" for the measurements of sky luminances. There is not enough data on luminance distribution or, what is more, there is none for most of the locations. Therefore, the method in question shall be based on more comprehensive and accessible measurements. Satellite images obtained from geostationary satellites shall be used. The satellites provide permanent coverage of the surface of the Earth, with their resolution reaching the accuracy of up to 5 km. Each image of the Earth surface is made every 30 minutes, which allows for a great amount of data for the purpose of the analysis. Most of this data for Europe and Africa is to be accessed via the Internet. The accessibility of the data has led to the decision to develop a new method. This method shall allow us to determine the frequency of emergence of CIE sky types at a specific location on the basis of global and diffuse horizontal irradiances.

We shall be able to carry out calculations to determine time values of indoor daylight illuminances by way of devised tables and known algorithms.

### **Method description**

We shall carry out the method by comparing the measurements of sky luminance distribution, the measurements of spatial illuminance by way of the model, and the illuminance calculation by way of various simulation programmes. The measurements shall be carried out at ENTPE (Ecole Nationale des Travaux Publics de l'Etat) Vaulx-en-Velin, France, which is home to one of IDMP (International Daylight Measurement Programme) locations. Our efforts shall (simultaneously) focus on the following:

- measurement of sky luminance distribution by way of the sky scanner (a special measuring device);
- measurement of zenith luminance ( $1^{\circ}$  – spatial angle) by way of a luminance measuring device on a stand;
- measurement of sky luminance distribution by way of a digital camera, wide-angle lens and Photolux program package, and the drawing of sky luminance maps;
- measurement of luminance distribution within the scale model by way of a digital camera, wide-angle lens and Photolux program package, as well as the drawing of maps for wall luminance within the model;
- measurements of illuminance in the model by way of Li-cor sensors.

When processing the data, all additional data collected through calculations within the IDMP locations shall be taken into consideration.

The corresponding sky type shall be determined for each scan of sky luminance distribution (obtained through sky scanner) according to CIE standards. As for classifying individual sky luminance scans, Kittler's method shall be used.

Furthermore, we shall also determine the corresponding sky type for both the sky scan and the measurements carried out at the IDMP location, which shall be measured at the same time as the scan of sky luminance distribution. In this case, the Perez method shall be used for determining the sky type. The method is instrumental in determining sky clearness and sky brightness and also the corresponding sky type on the basis of the measurements obtained from IDMP.

The results of the measurements and both methods shall be duly compared. On the basis of the results, a new method for determining CIE sky types from satellites scans shall be devised.

In the second part, we shall carry out computer simulation of illuminances in the model by way of various methods. As far as the calculation is concerned, the illuminances in the scale model shall be calculated with different sky luminance models and with daylight quotients. Input data for sky luminance models shall consist of the maps developed by a digital camera and PhotoLux programme.

Computer simulations results shall be compared to the measurements on a model. Focus shall be placed on comparing the values of illuminances. This will allow for evaluating the applicability of the method as regards determining CIE sky type when calculating indoor daylight illuminances.



# 1 Description of the sky scanner

The sky scanner measures the spatial distribution of the luminance or radiance of the entire sky automatically.

## 1.1 Sky scanner and measurements

For measuring purposes a sky scanner (Fig. 1.1) was kindly borrowed from Kyushu University (Japan) for one year (January 2005 - January 2006). Sky scanner was made by Japanese company EKO Instruments CO., LTD and it was already used for measurements in Japan. Its measurement head is mounted on a two axis turning table, the luminance sensor is a Si-photodiode with a  $V(\lambda)$  filter. An amplifier and automatic temperature compensation is assembled in the sensor head. Sky scanner came together with acquisition system (I/O controller and portable computer) and power supply since the input voltage sky scanner acquisition system and computer is 110 V.

Sky scanner measures luminance and radiance of 145 patches in sky hemisphere (Fig. 1.2), following the CIE recommendations [44]. The solid angle of each measured sky patch is  $11^\circ$ . Measured value represents the average value of luminance and radiance in the solid angle of  $11^\circ$ . Measurement takes place on eight almucantars (imaginary circle on the celestial sphere, parallel to the horizon. The circle connects sky elements with same altitudes) - altitudes ( $6^\circ$ ,  $18^\circ$ ,  $30^\circ$ ,  $42^\circ$ ,  $54^\circ$ ,  $66^\circ$ ,  $78^\circ$ ,  $90^\circ$ ). Number of measurements at different altitudes is changing and depends on the size of virtual bend at that altitude (Table 1.1).

*Table 1.1. Number of measurements according to the altitude of the point*

Altitude ( $^\circ$ ) - Almucantar	No. of measurements
6	30
18	30
30	24
42	24
54	18
66	12
78	6
90	1
<i>SUM</i>	<i>145</i>



*Fig. 1.1. Sky scanner*



Fig. 1.2. 145 sky patches

Measurement takes place every 10 minutes from sunrise to sunset. Time needed to perform one measurement of the sky luminance distribution is a little bit more than 3 minutes, which can cause problems under dynamic weather conditions, since a single moving cloud can cover different patches of sky in a single measurement. The sky scanner has two measuring heads, one for luminance and the other for radiance.

After one measurement is finished, the computer creates two files with data, the first one is for luminance and the second one is for radiance. In our thesis, we used only data for luminance, but we stored also the one for the radiance. All files are in ASCII format and they include data from the scanner, date and time of the beginning and the end of the measurement, inserted constants and location of the measurement. (Fig. 1.3).

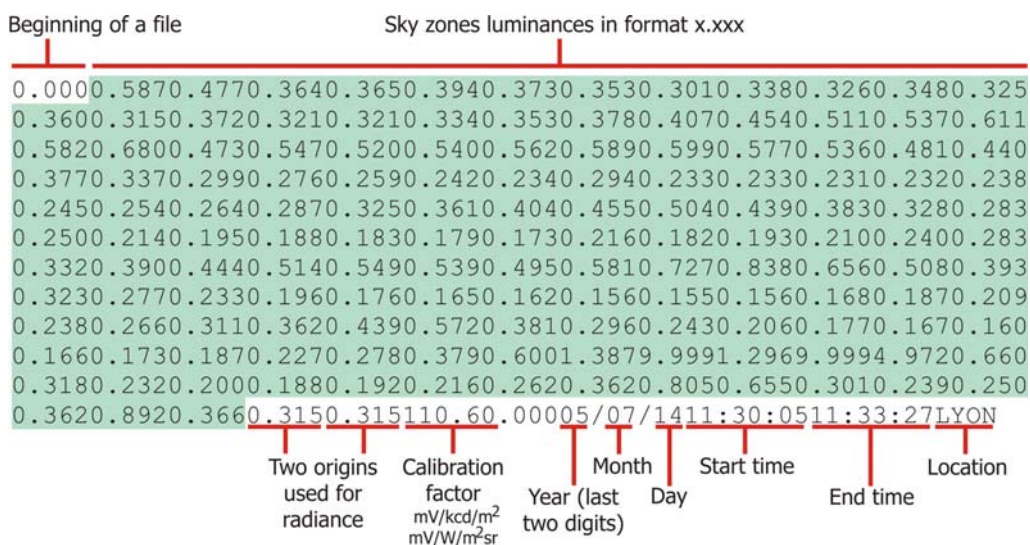


Fig. 1.3. Example of the data file.

Luminance data are written in a file .05D (in year 2005), where luminances of all 145 sky patches are listed one after another without any punctuation mark (Fig. 1.3 and Fig. 1.4). Luminances in a file have number format of X.XXX and they are not given in absolute values, but they are divided by constant  $k$  (Fig. 1.4). Factor  $k$  can be calculated with next equation:

$$L = k \cdot L_F$$

$$L = 10^6 / f_C \cdot k_{SS} \cdot L_F \Rightarrow k = 10^6 / f_C \cdot k_{SS} \quad (1.1)$$

Where:

- $L$  luminance of a sky patch,
- $f_C$  calibration factor of sky scanner (110.6),
- $k_{SS}$  factor we defined based on calibration under artificial sky (1.65) – (see Chapter 1.2)
- $L_F$  luminance in .05D file.

Calculated value of the factor  $k$  is 14.918,63.

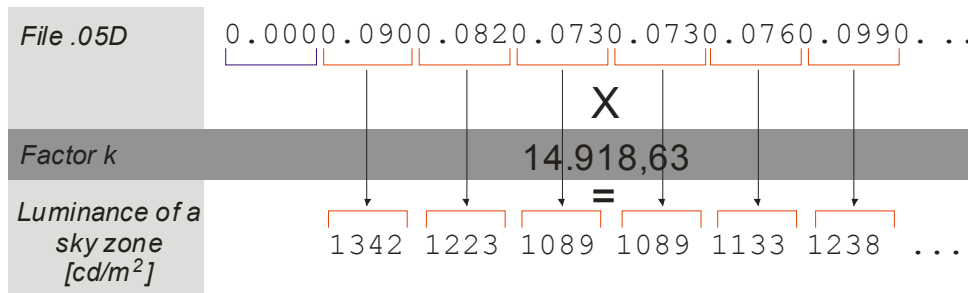


Fig. 1.4. Calculation of luminances of sky patches from a .05D file

## 1.2 Calibration of the sky scanner

The sky scanner was last used in Japan in 2000/2001 and it has not been calibrated since then. And so we had to calibrate it before performing any measurements. First calibration was done under artificial sky and second under real sky conditions.

### 1.2.1 Calibration of the sky scanner under artificial sky

For calibration of sky scanner under artificial sky we used the artificial sky of ENTPE (Vaulx-en-Velin). This is a uniform sky with adjustable luminance.

### **1.2.1.1 Zenith luminance**

As a first calibration, we decided to compare the "zenith luminance" of the sky scanner with luminance of the artificial sky. Zenith luminance is the 145<sup>th</sup> patch, which is measured by the sky scanner. Luminance value of this patch was compared with value measured with Minolta handheld luminance meter LS-100 with 1<sup>o</sup> aperture and with the value derived with digital camera and software Photolux.

The sky scanner was placed in the middle of a room with artificial sky and it was lifted to a height where luminance and radiance heads were facing mirror on side walls (Fig. 1.5, Fig. 1.6). The scanner was placed also in horizontal position with water level. When the scanner was placed in right position, the door was closed and the automatic measurement was started.

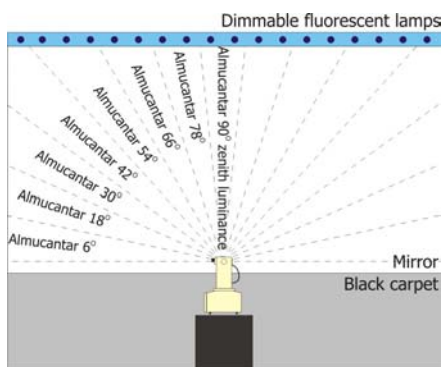


*Fig. 1.5. Diagram of the sky scanner under artificial sky*



*Fig. 1.6. Picture of the sky scanner under artificial sky*

With the same luminance level, a picture with calibrated digital camera (Nikon Coolpix 5000) with fish eye lens was taken. Digital camera was placed on tripod in the middle of a room with artificial sky and it was lifted to a level, where top of the fish-eye lens was in the same height as luminance and radiance heads of the sky scanner. When the digital camera was placed in right position, the door was closed and the picture was taken.

With the same luminance level also luminance of the "zenith" was measured with handheld luminance meter. The "zenith" zone was marked on ceiling with transparent adhesive tape, using plumb line and calculating the area which is covered at height 1.7 m with solid angle of 11<sup>o</sup> (Fig. 1.7)

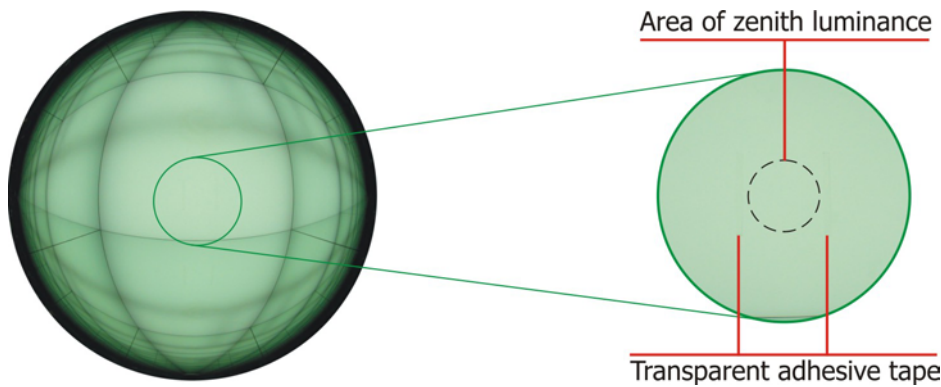


Fig. 1.7. Digital image of artificial sky with zoomed area of zenith luminance

The same procedure was used for eight times with different luminance levels. Measured results are gathered in Table 1.2.

The luminances of sky patch number 145, measured with the sky scanner were derived using calibration factor and data from files produced by the scanner. The luminances measured with digital camera and fish-eye lens were obtained with Photolux. Photolux is a software in a system including a digital camera calibrated in terms of luminance and a software which translated the image(s) produced by the camera into a luminance map.

The measurements were performed on April 14<sup>th</sup>, 2005.

Table 1.2. Results of "zenith" luminance measurements.

Measurement No. (time)	Zenith Luminance (EKO) [cd/m <sup>2</sup> ]	Zenith Luminance Minolta (cd/m <sup>2</sup> )	Zenith Luminance Photolux (cd/m <sup>2</sup> )	Coefficient Minolta/EKO	Coefficient Photolux /EKO
M1 (10:20)	651	1070	1080	1.644	1.659
M2 (10:30)	940	1540	1550	1.638	1.649
M3 (10:40)	1573	2580	2612	1.640	1.660
M4 (10:50)	2495	4140	4158	1.659	1.667
M5 (11:00)	2975	4920	4504	1.654	1.514
M6 (11:10)	3400	5620	5062	1.653	1.489
M7 (11:20)	3770	6400	5833	1.698	1.547
M8 (11:30)	3128	5150	4713	1.646	1.507
<b>Average coefficient</b>				<b>1.654</b>	<b>1.576</b>

From the measurements we calculated the coefficients between Minolta luminance meter and sky scanner and Photolux and sky scanner values. The average coefficient between Minolta luminance meter and the scanner is 1.654 and the average coefficient between Photolux and sky scanner is 1.576.

As it is seen from the most right column in Table 1.2 deviation of values of coefficient between luminances calculated with Photolux and luminances from sky scanner are more fluctuating than values of coefficient between Minolta luminance meter and sky scanner. Due to this fact we decided to take coefficient 1.65 for further calculations.

In this sense, we plotted diagram (Fig. 1.8), where almost perfect match between corrected values of sky scanner luminances and luminances measured with Minolta is seen.

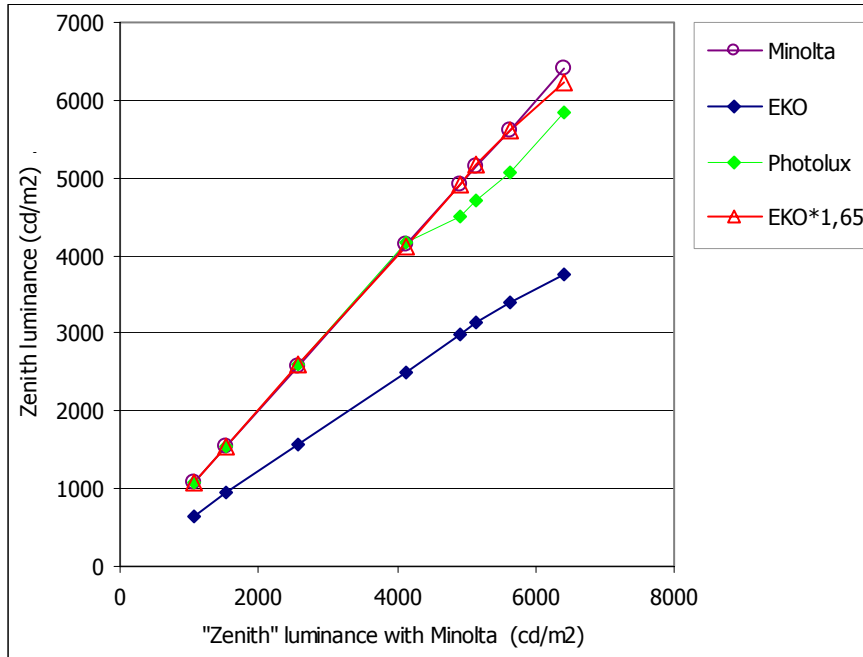


Fig. 1.8. Measured luminances under artificial sky

### 1.2.1.2 Horizontal and vertical illuminances

The second calibration was done also under the artificial sky. At this time, we compared illuminances derived from the sky scanner and from the illuminance meter. We compared horizontal and 4 vertical illuminances. Illuminances from sky scanner are calculated by integrating of all luminances for horizontal illuminance (see chapter 2.3.1) and by integrating of only certain luminances for vertical illuminances. Measured illuminances were measured with Li-cor sensors and stored on logger.

Li-cor sensors and a logger (Fig. 1.9) is a system capable of reading and storing different values depending on type of measurement we perform. In our case we were measuring illuminances, so illuminance sensors were attached to the logger. We used five illuminance sensors, one for horizontal illuminance and four for vertical illuminances. Sensors were fixed on a specially designed wooden cube (Fig. 1.10), which was painted black and fixed together with black wooden plate to a tripod (Fig. 1.11).



*Fig. 1.9. Li-cor illuminance sensors and data logger*



*Fig. 1.10. Illuminance sensors fixed on a black wooden cube*



*Fig. 1.11. Illuminance sensors with wooden cube fixed on a plate and on a tripod*

But before doing the comparison, Li-cor sensors had to be checked (see chapter 1.2.1.3). After the validation of Li-cor sensors we installed the sky scanner under the artificial sky in the same way as we did it when checking zenith luminance. When the scanner was in place we started measurement and when the measurement was finished, the sky scanner was removed from the artificial sky room and on the same position as there was the measuring head of the sky scanner we put the tripod with 5 sensors.

One sensor was set up in horizontal position and the other four in four vertical positions (N, E, S, W). Then again the room with artificial sky was closed and from the data logger, which was placed outside, reading of all five illuminances from sensors was done.

The same procedure was used for six different settings of illuminance levels under artificial sky.

Illuminance values from sky scanner were obtained with integration of all or only certain luminances (for vertical illuminances) and then compared with measurement readings from Li-cor logger. The procedure of computation of horizontal and vertical illuminances from the sky scanner is explained in section 2.3.1 and 2.3.2.

For all six different illuminance setups we calculated coefficients between illuminances from Li-cor sensors and illuminances calculated from sky scans. Coefficients were calculated for horizontal and for four vertical illuminances. For each measurement those five coefficients were averaged and values are collected in Table 1.3.

*Table 1.3. Average Li-cor/sky scanner coefficient for all measurements*

<b>Measurement</b>	<b>Average coefficient Li-cor/Sky scanner</b>
M1	1.626458
M2	1.653968
M3	1.697119
M4	1.62945
M5	1.679245
M6	1.627261
<b>Average</b>	<b>1.65225</b>

With averaging the average coefficient at all six measurements we got practically the same coefficient as we got it with luminance validation. So we can conclude that taking the coefficient 1.65 is the right decision

### **1.2.1.3 Checking the Li-cor sensors**

Li-cor sensors were last calibrated in July 2002 and they should be calibrated every two year. Instead of an absolute calibration we did a relative calibration and we compared sensors between each other. Comparison was done under artificial sky. All sensors were lied down on a horizontal plane and the artificial sky was switched on. At eight

different luminance levels illuminance measurements were done and results are in table Table 1.4. After measurements the average illuminance and deviation of all measurements from average illuminance was calculated for all luminance levels. After that illuminance profiles on Fig. 1.12 were plotted. In the diagram, we can see the measured illuminances from all 5 sensors compared to average illuminance.

Table 1.4. Calibration of illuminance sensors

Probe	E1 lx	E2 lx	E3 lx	E4 lx	E5 lx	E6 lx	E7 lx	E8 lx	Mean deviation %
A-I1	1522	1977	2860	4059	5975	7120	8560	10150	-0.563
A-I2	1552	2006	2907	4170	6083	7280	8720	10360	1.401
A-I3	1508	1940	2815	4057	5895	7075	8430	9956	-1.786
A-I4	1556	1980	2853	4145	6050	7228	8630	10160	0.421
A-I5	1549	1988	2864	4146	6055	7305	8650	10070	0.528
<b>Average</b>	<b>1537.4</b>	<b>1978.2</b>	<b>2859.8</b>	<b>4115.4</b>	<b>6011.6</b>	<b>7201.6</b>	<b>8598.0</b>	<b>10139.2</b>	

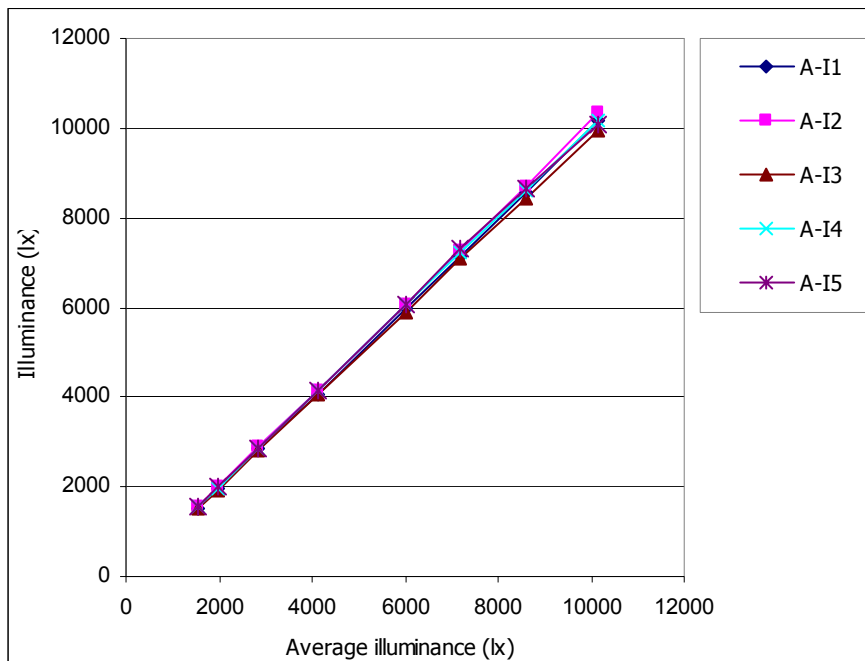


Fig. 1.12. Measured illuminance under artificial sky.

Deviation of illuminances when compared to average illuminance is less than 2 % and from that result, we can conclude, that sensors are coherent and they don't need calibration.

## 1.2.2 Calibration of the sky scanner under real sky

### 1.2.2.1 Calculated vertical illuminances and measured data from IDMP station

The same validation of illuminances as it was done under the artificial sky was also done under real sky conditions. After the installation of the sky scanner we compared four vertical illuminances calculated from sky luminance distribution and illuminances from IDMP station.

With comparison it was possible to calculate the coefficient between IDMP measurements and sky scanner calculated values. The coefficient was calculated for each illuminance, but only for times when, there was no direct sun component since the sky scanner can't measure direct sun luminance. This fact is best viewed on next diagrams (Fig. 1.13 - Fig. 1.16), where sky scanner curve can not follow high values obtained from IDMP station for times with direct component of sun. Calculated coefficient was 1.62. Since almost the same coefficient was already calculated with measurements under artificial sky and it is 1.65, we decided to use 1.65 and plot diagrams of all four vertical illuminances for time from July 19 5:10:00 to July 22 14:50:00.

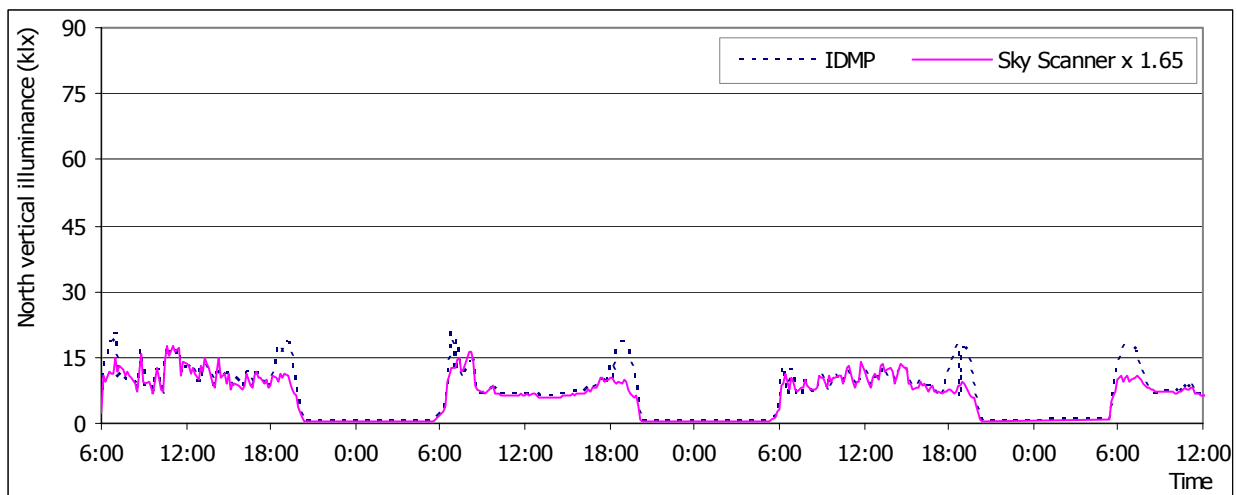


Fig. 1.13. Diagram of North vertical illuminance measured on IDMP station and calculated from sky scanner data

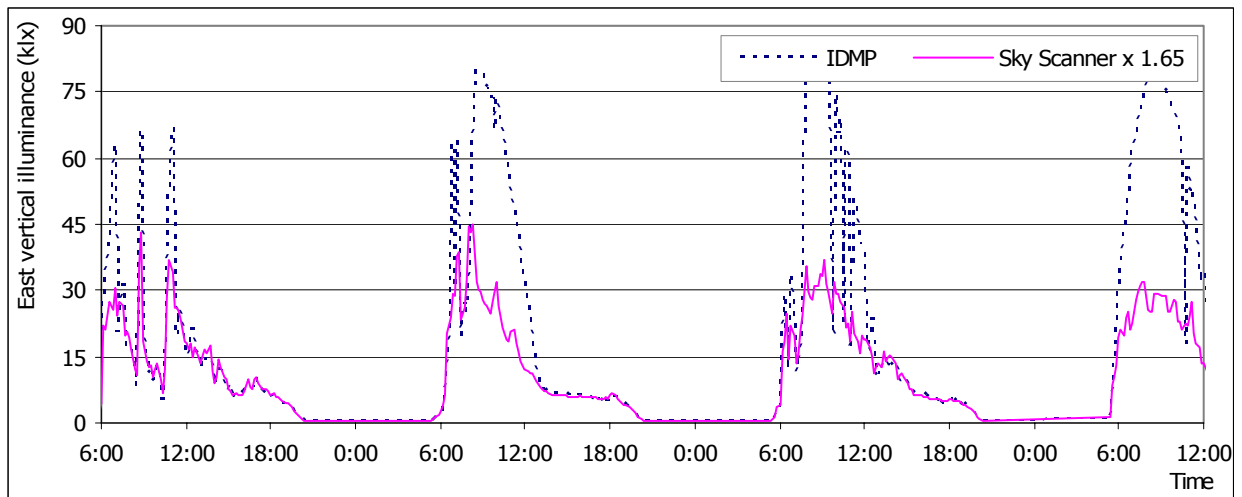


Fig. 1.14. Diagram of East vertical illuminance measured on IDMP station and calculated from sky scanner data

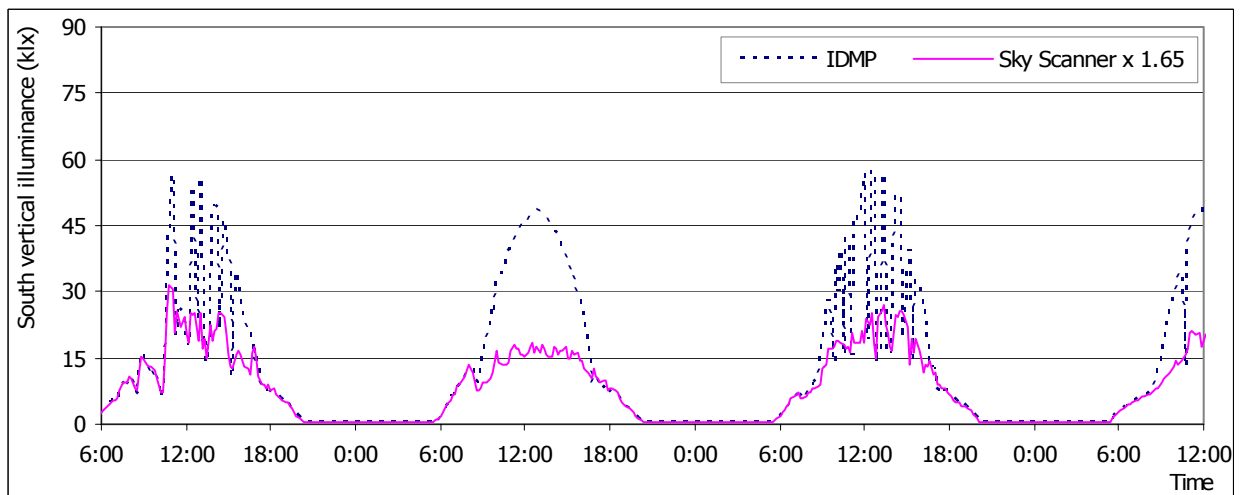


Fig. 1.15. Diagram of South vertical illuminance measured on IDMP station and calculated from sky scanner data

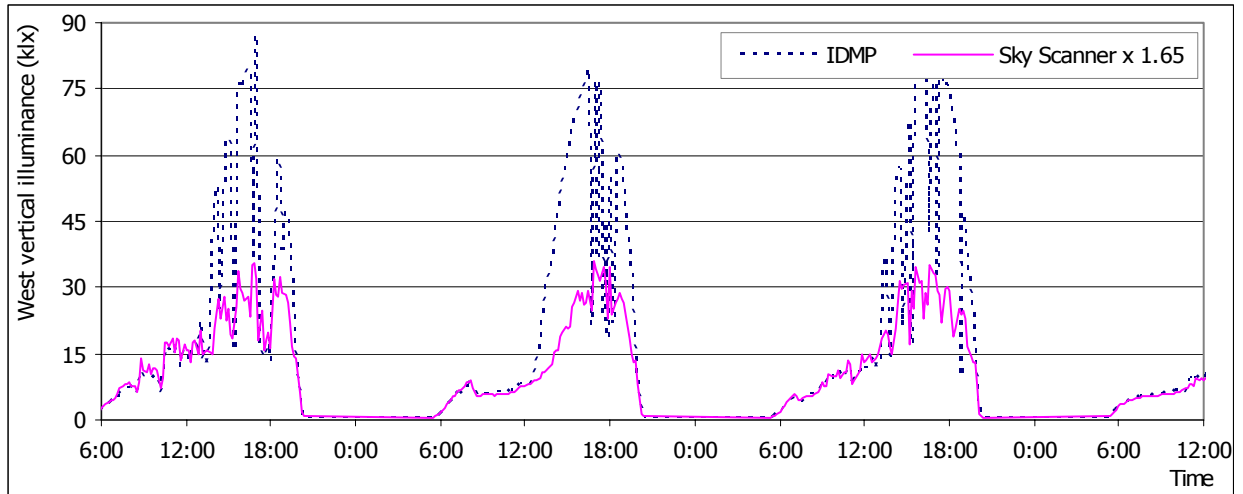


Fig. 1.16. Diagram of West vertical illuminance measured on IDMP station and calculated from sky scanner data

## 1.3 Setting up the sky scanner

### 1.3.1 Description of the IDMP station

The IDMP (International Daylight Measuring Program) Vaulx-en-Velin station (Fig. 1.17) was set up with the IDMP project in 1992. On the station there are the following measurements (Fig. 1.18):

#### **Illuminances:**

- Global horizontal
- Diffuse horizontal
- North vertical
- East vertical
- South vertical
- West vertical

#### **Irradiances:**

- Global horizontal
- Diffuse horizontal

#### **Others:**

- Zenith luminance
- Dry Bulb Temperature
- Wind direction
- Wind speed
- Normal incidence direct solar radiation
- UV-A, UV-B



Fig. 1.17. Outlook of the IDMP station Vaulx-en-Velin

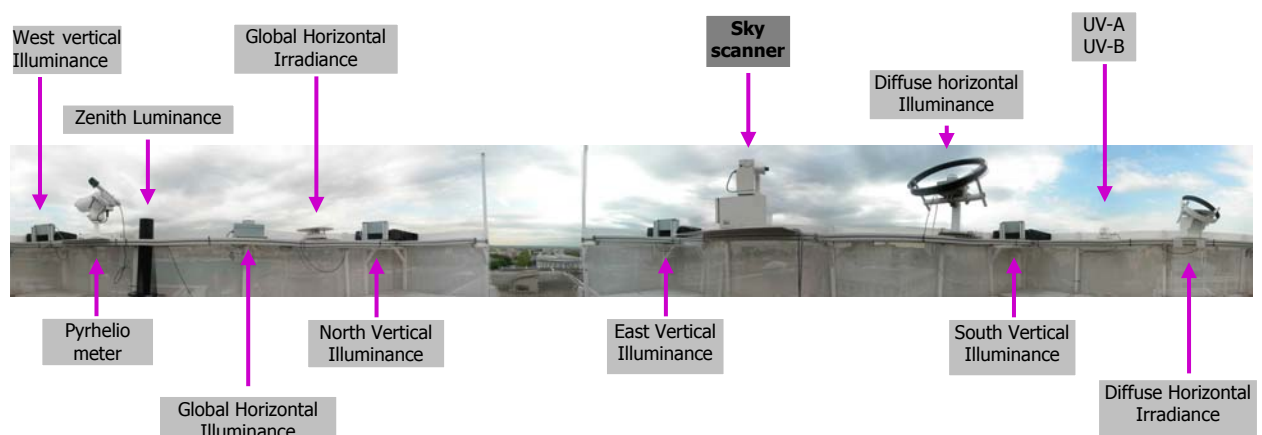


Fig. 1.18. IDMP station measurements (360° view)

Beside these measurements, in April 2005, an EKO sky scanner was added. It was placed on the south east part of the station.

### **1.3.2 Correction of orientation of vertical illuminance sensors**

Although the station has been working more than ten years, the actual orientation of vertical illuminance meters was not checked in last two years. The orientation was checked before we did the comparison between vertical illuminances derived from the sky scanner and from the IDMP station. Precise positioning of measuring devices with normal magnetic compass is on the IDMP station almost impossible since the whole station is made of iron tubes.

To define correct orientation of vertical illuminance meters, we compared data from IDMP station and data derived from a program with *Perez – All weather* sky luminance model [14]. The input data for the Perez model were global and diffuse illuminances and position of the Sun (date, time). In the sky luminance model, the whole hemisphere was divided into patches with a grid of  $1^\circ$ . For all patches, luminance was calculated and from luminance values four vertical illuminances were calculated.

To find the best matching orientation we calculated profiles for rotations from  $10^\circ$  counter-clockwise to  $10^\circ$  clockwise and in some cases up to  $12^\circ$  clockwise for every degree. Suggested corrections were calculated with root mean square (RMS) differences between measurements and values from Perez All weather sky luminance model.

Comparison was done under clear sky conditions. For all four vertical illuminances RMS difference was calculated for different orientation setups for 4 cloudless or semi cloudless days (May 26, 27, 31 and July 3, 2005). In next tables (Table 1.5 - Table 1.8) we present diagrams with original setup, diagrams with calculated values if sensors would be rotated for 5 degrees in clockwise and 5 degrees in counter-clockwise and the last diagram is plotted with suggested correction of the direction of vertical sensors. All diagrams in tables (Table 1.5 - Table 1.8) present illuminance values for July 3, 2005.

From the results for all four days we concluded that vertical illuminance meters should be rotated for:

- North vertical illuminance:  $4^\circ$  counter-clockwise
- East vertical illuminance:  $5^\circ$  counter-clockwise
- South vertical illuminance:  $2.5^\circ$  counter-clockwise
- West vertical illuminance:  $12^\circ$  clockwise

Table 1.5. North Global Vertical Illuminance

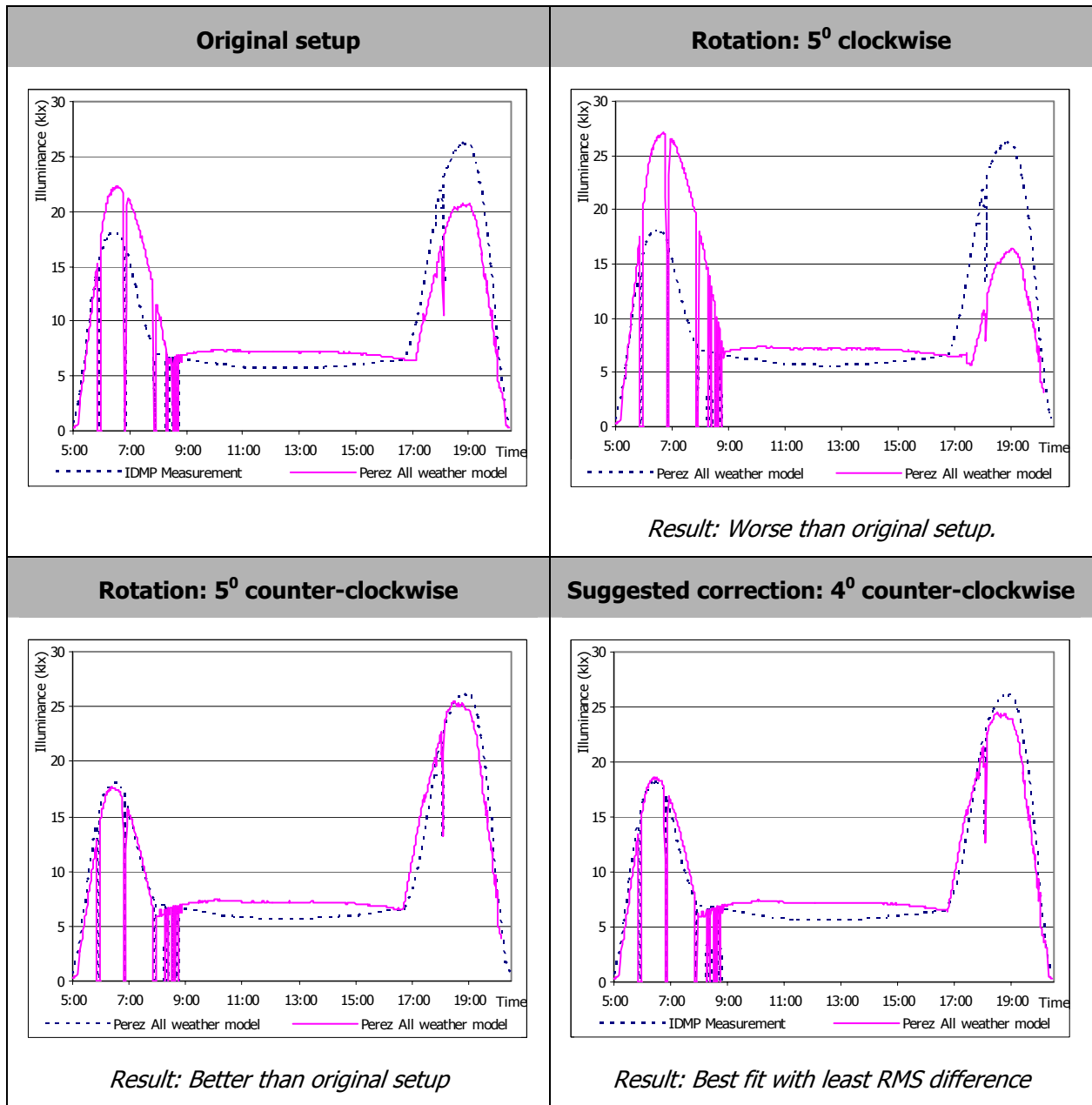


Table 1.6. East Global Vertical Illuminance

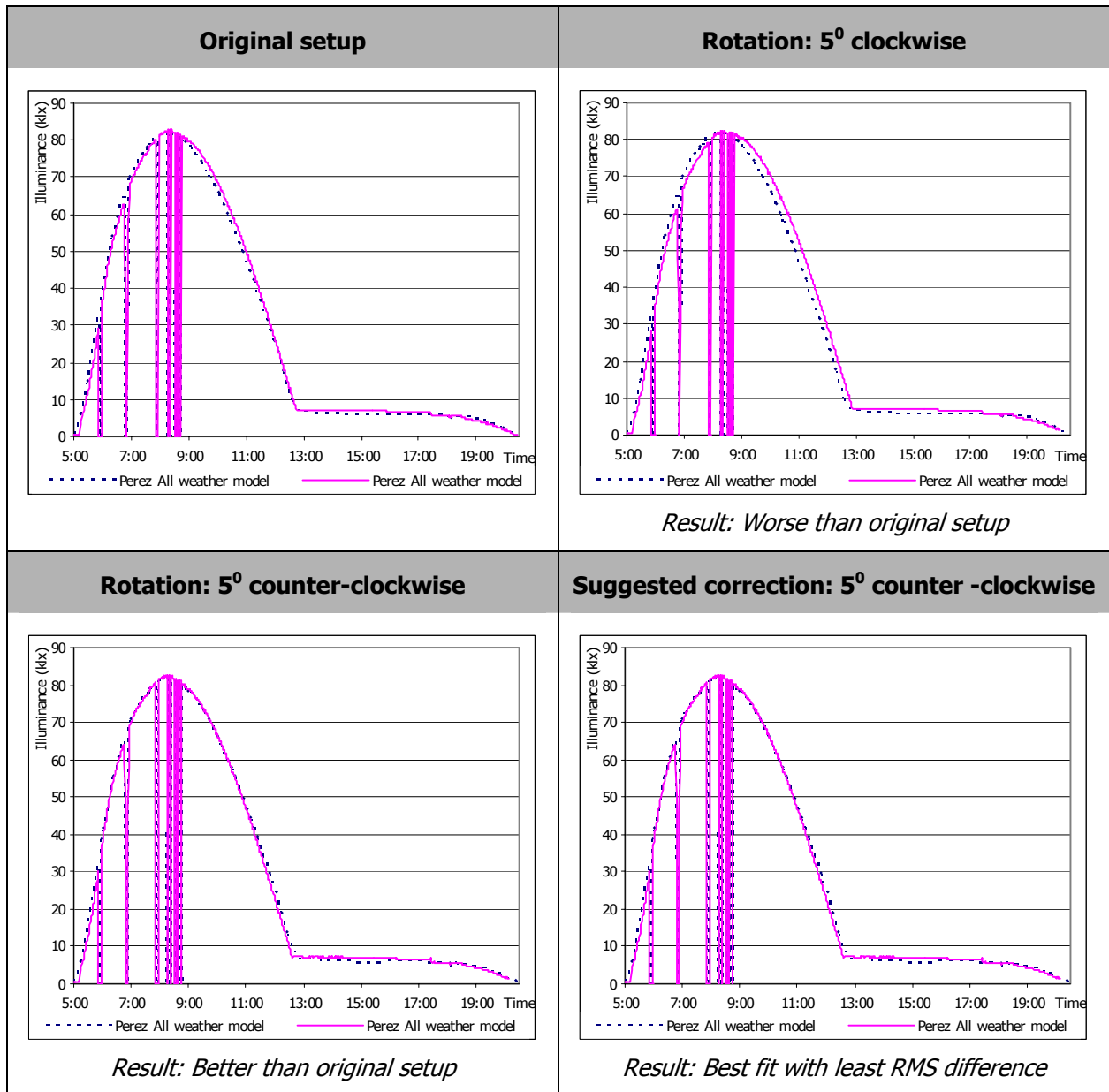


Table 1.7. South Global Vertical Illuminance

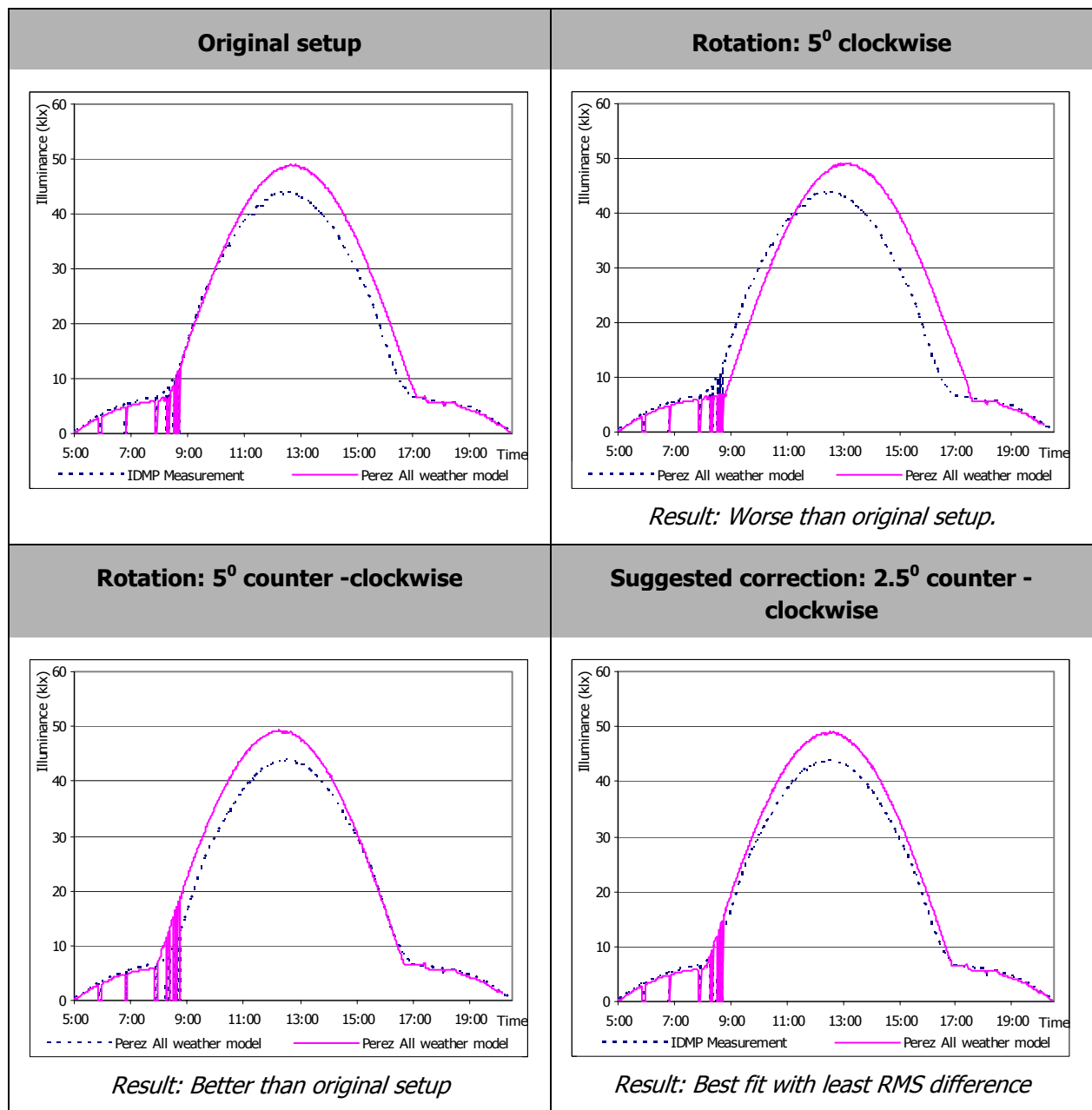
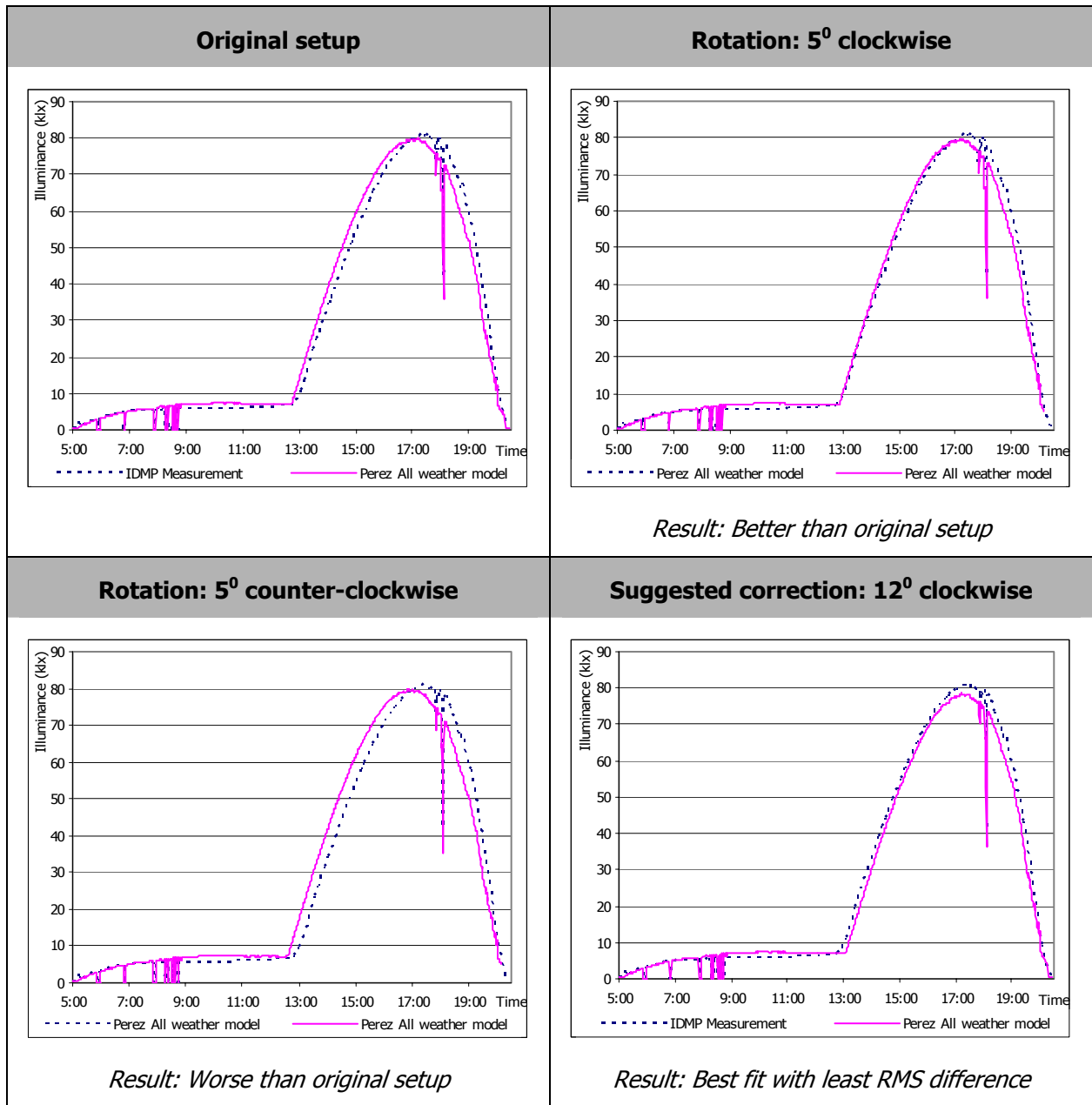


Table 1.8. West Global Vertical Illuminance



### 1.3.3 Correction of orientation of the sky scanner

The sky scanner was positioned on a new aluminium plate, which was fixed on the metallic frame of the IDMP station. The scanner was placed in horizontal position with spirit level. Orientation of the scanner was approximately defined and checked with compass. Setting the sky scanner in the right orientation with only compass is impossible since the sky scanner and also the frame of the IDMP station is made of metal. The influence of surrounding objects to the compass was noticeable up to a distance of 1 meter above metal frame of the station. Approximate orientation was set up with a handheld compass from a distance 1 meter from sky scanner. After the approximate set up, first measurement were performed under real sky.

From measurements on a cloudless sky it was possible to check the orientation of the sky scanner. First orientation was not correct (Fig. 1.19). Calculated position of sun (yellow dot) which was calculated from date and time and location, was not on the brightest part of sky, which was measured with sky scanner. If the orientation of the sky scanner would be correct, the calculated position of the sun would be on the brightest part of the sky. After first positioning, sky scanner was rotated for 10 degrees counter-clockwise. From image with new setup (Fig. 1.20), we can conclude that repositioning of the sky scanner was successful.

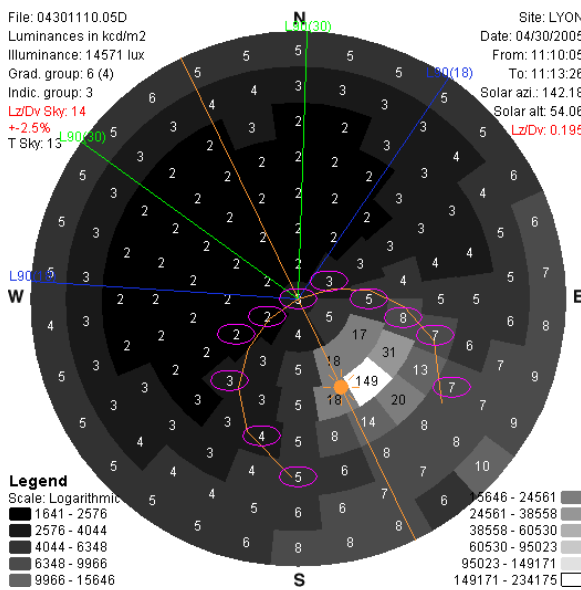


Fig. 1.19. Measurements done with original setup

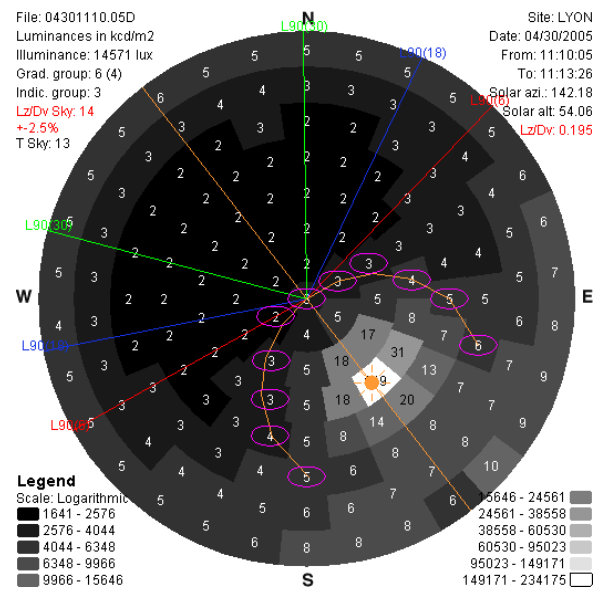


Fig. 1.20. Measurements done with original setup with rotation 10 degrees counter-clockwise



## 2 Analysis of the sky scanner data

### 2.1 Description of the visualization

Data got from sky scanner are in raw format. With a Java program, we did visualisation of the data as shown on Fig. 2.1. First and most important matter was to present the sky luminance distribution in a graphical way. The whole hemisphere was flattened onto 2D circle. Every measured part of the sky is presented as trapezoid with curved top and bottom borders, except the last one, the zenith luminance is presented as a circle. All elements are coloured in shades of grey, where the brightest sky element is coloured in white and the darkest in black. On all elements there are values of luminance of that sky element. If the brightest sky element has a value less than  $1100 \text{ cd/m}^2$ , the values are in  $\text{cd/m}^2$  otherwise values are in  $\text{kcd/m}^2$ . On the luminance distribution map there is also a position of sun drawn. The position of the sun is calculated from date and time and the location of measurement.

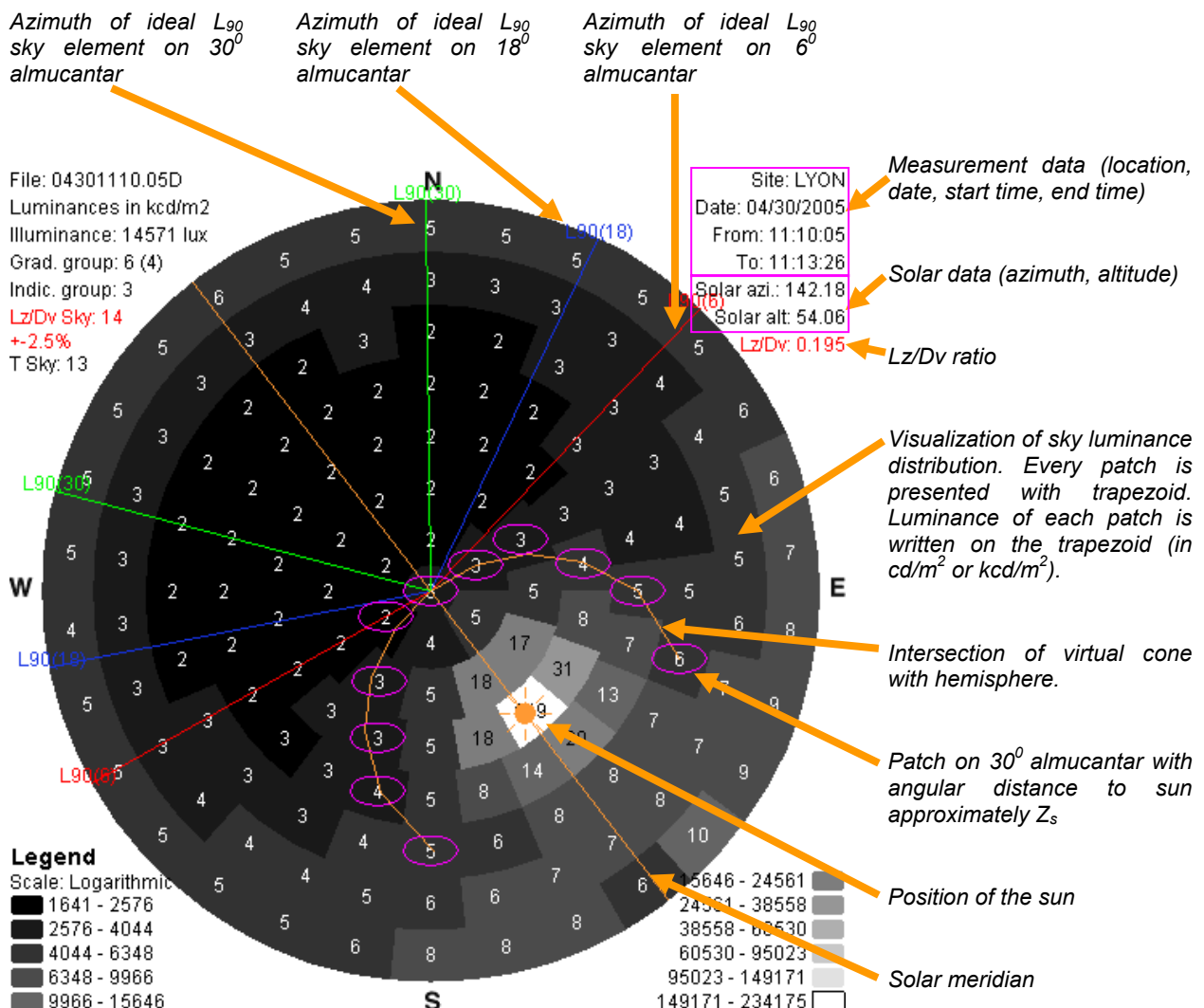


Fig. 2.1. Visualization of the sky scanner data

## 2.2 Defining CIE sky type based on CIE standard

Calculation of gradation and indicatrix for all sky scans was performed on the basis of the CIE and ISO standard CIE S 011/E:2003 /ISO 15469.2004 "Spatial distribution of daylight – CIE standard general sky" [16]. The standard defines 15 standard skies; 5 overcast, 5 intermediate and 5 clear skies. Skies are defined with next equations and parameters a, b, c, d and e that can be found in Table 2.7.

$$L_{a-rel} = \frac{L_{\alpha}}{L_z} = \frac{f(\chi) \cdot \varphi(Z)}{f(Z_s) \cdot \varphi(0)} \quad (2.1)$$

$$f(\chi) = 1 + c \cdot \left[ \exp(d\chi) - \exp\left(d \frac{\pi}{2}\right) \right] + e \cdot \cos^2 \chi \quad (2.2)$$

$$\varphi(Z) = 1 + a \cdot \exp\left(\frac{b}{\cos Z}\right) \quad (2.3)$$

Where:

- $L_{a-rel}$  relative sky element luminance,
- $L_{\alpha}$  luminance of a sky element,
- $L_z$  zenith luminance,
- $f(\chi)$  indicatrix function,
- $\varphi(Z)$  gradation function,
- $\chi$  scattering angle,
- $Z$  zenith angle of a sky element,
- $Z_s$  solar zenith angle.

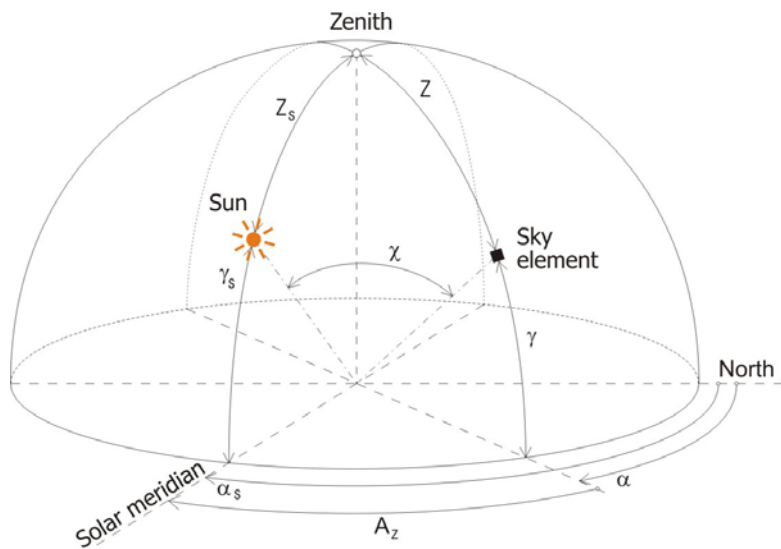


Fig. 2.2. Angles defining the position of the sun and a sky element

Scattering angle  $\chi$  is angular distance (Fig. 2.2) between sun and sky element and it is defined with next equation:

$$\chi = \arccos(\cos Z_s \cdot \cos Z + \sin Z_s \cdot \sin Z \cdot \cos Az) \quad (2.4)$$

$$A_z = |\alpha - \alpha_s| \quad (2.5)$$

Where:

- $A_z$  angular difference between azimuth of the sun and azimuth of the sky element,
- $\alpha_s$  solar azimuth,
- $\alpha$  azimuth of a sky element.

### 2.2.1 Determination of the gradation group

The gradation function connects the luminance of a sky element with its zenith angle. For overcast skies there is typical vertical drop in luminance from zenith to horizon (Fig. 2.3a). Uniform skies, as it is seen from their name, have constant luminance over the whole hemisphere (Fig. 2.3b). And on the other side, there are clear skies where luminance is increasing from zenith to horizon (Fig. 2.3c).

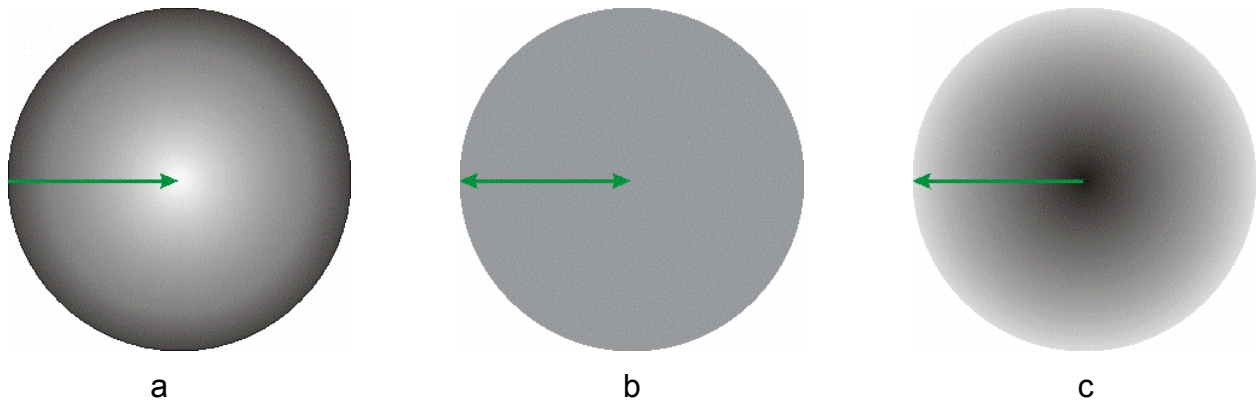


Fig. 2.3. Gradation for overcast (a), uniform (b) and clear skies (c)

In the standard CIE S 011/E:2003 /ISO 15469:2004 "Spatial distribution of daylight – CIE standard general sky" [16] table (Table 2.7) with six gradation groups is given. Gradation groups are defined with parameters  $a$  and  $b$  and next equation:

$$\varphi(Z) = 1 + a \cdot \exp\left(\frac{b}{\cos Z}\right), \quad \text{where } 0 \leq Z \leq \frac{\pi}{2} \quad (2.6)$$

Where:

$\varphi(Z)$  gradation of sky element,

$Z$  zenith angle of sky element.

Gradation function in horizon:  $\varphi(\pi / 2) = 1$  (2.7)

And in zenith:  $\varphi(0) = 1 + a \cdot \exp(b)$  (2.8)

Waveforms belonging to six standard gradation functions are drawn on next figure.

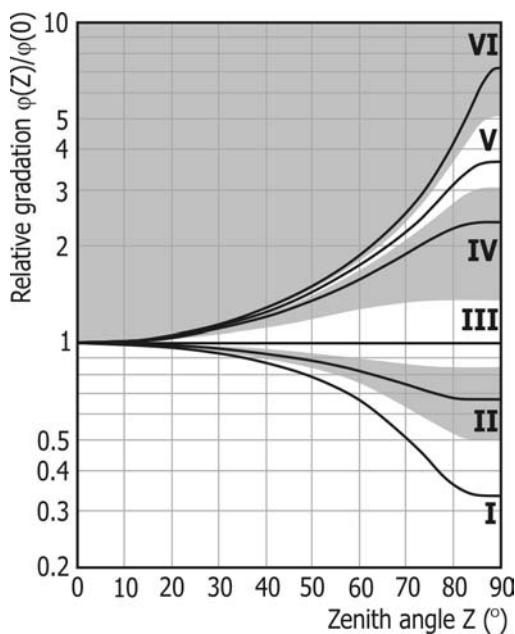


*Fig. 2.4. Standard gradation function groups*

From the sky scan, we had to find out the appropriate sky elements to calculate gradation function. Since both gradation and indicatrix functions have influence on all sky elements, it is necessary for gradation calculation to exclude influence of indicatrix function. Influence of indicatrix function is excluded if all sky elements we use for gradation calculation have the same angular distance from sun. And if we want to include also zenith luminance in calculations, the angular distance of sky elements must be the same as angular distance between zenith and sun. On every almucantar we have to find elements, which have angular distance to sun equal to  $Z_s$  (zenith angle of sun). As there are only limited numbers of sky elements on every almucantar and it is impossible to find a sky patch with exact angular distance  $Z_s$  to sun, it's necessary to take an element with angular distance as close as possible to  $Z_s$ .

On every almucantar there are two points with angular distance  $Z_s$  to sun. Points are connected on visualization (Fig. 2.1) with orange curve. Orange curve represents intersection of virtual cone with hemisphere. Cone has angular distance  $2 \cdot Z_s$  and its top in the centre of the hemisphere (Fig. 2.5).

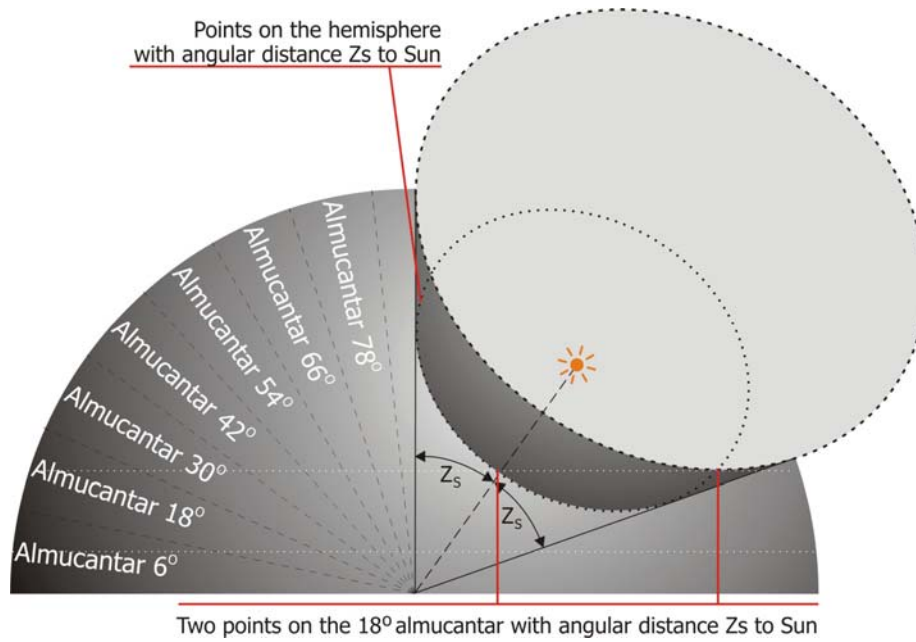


Fig. 2.5. Intersection of cone and hemisphere

Luminance of a sky element is with standard [16] defined in a relative way. From the basic equation in standard and knowing that the angular distance towards sun of all chosen sky elements is  $Z_s$  or close to  $Z_s$  it's possible to transform the basic equation 2.9 to equation 2.10.

$$L_{a-rel} = \frac{L_\alpha}{L_Z} = \frac{f(\chi) \cdot \varphi(Z)}{f(Z_s) \cdot \varphi(0)} \quad (2.9)$$

With  $\chi = Z_s$

$$\frac{L_\alpha}{L_Z} = \frac{\varphi(Z)}{\varphi(0)} \quad (2.10)$$

Equation 2.10 describes relative gradation, which is the fact of decision when searching gradation group. This equation can be applied on measured values on all almucantars and gradation can be calculated by equation 2.11.

$$\frac{\varphi(Z)}{\varphi(0)} = \frac{L_\alpha'}{L_Z'} \quad (2.11)$$

Where:

$L_\alpha'$  measured luminance of a sky element,

$L_Z'$  measured zenith luminance.

As sky elements with angular distance  $Z_s$  towards the sun are known on all almucantars, relative gradation values can be calculated and plotted on the relative

gradation diagram. And finally gradation group can be defined. Sky elements with angular distance approximately  $Z_s$  towards sun or better their luminance values are on graphical presentation (Fig. 2.1) encircled with purple ellipses.

Intersection of virtual cone with hemisphere defines two elements with angular distance  $Z_s$  towards sun on every almucantar. One is clockwise and other is counter-clockwise from sun meridian. The average of both sky elements on each almucantar is taken for calculation of relative gradation. At higher sun altitudes there are no points on lower almucantars, where angular distance to sun would be  $Z_s$ . In next table (Table 2.1) for every almucantar, the highest sun altitudes are given for which it is possible to find sky elements with angular distance  $Z_s$ . The table was filled based on next equation:

$$Z_s + Z_s + \gamma = 90^0 \quad (2.12)$$

Where:

- $Z_s$             solar zenith angle,
- $\gamma$             elevation angle of a sky element (almucantar).

*Table 2.1. Highest sun altitudes with existing sky elements with angular distance  $Z_s$  towards sun*

<b>Elevation angle of almucantar</b> [ <sup>0</sup> ]	<b>Highest sun altitude</b> [ <sup>0</sup> ]
6	48
18	54
30	60
42	66
54	72
66	78
78	84
90	90

With respect to the fact about highest sun altitudes for gradation calculations only existing sky elements are taken.

Gradation group is defined by calculation of RMS error between averaged measured sky elements (two on every almucantar) luminance and standard gradation functions. When calculating gradation function, we do not take into account sky elements on almucantar 6 degrees due to fact that the station is being obstructed by surrounding building. An obvious drop in sky luminance was noticed especially on clear days at zenith angles of  $84^0$ . Unfortunately IDMP station and also sky scanner is not the highest point around and there are surrounding obstacles up to  $6^0$  on all sides of station (Fig.

2.6). In case of zenith angle of  $84^{\circ}$ , sky scanner is measuring luminance of buildings façades and not sky luminance.

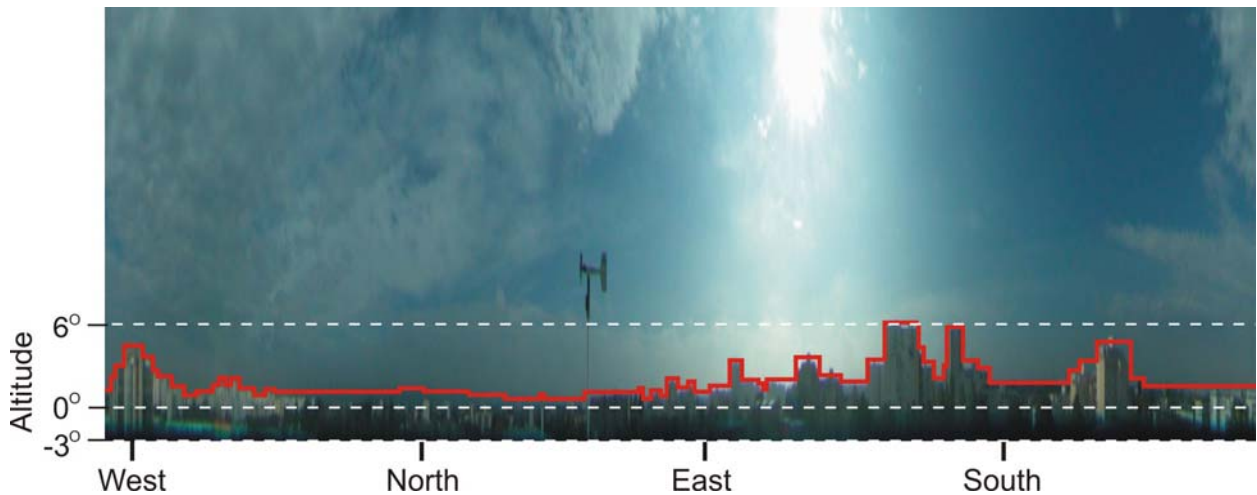


Fig. 2.6. Surrounding obstructions around the IDMP station

**Example:**

With this example, we are showing calculation of gradation group for measurement performed on July 14, 2005 at 17:30. Sky luminance distribution with luminance values are shown on Fig. 2.8. Altitude of the sun is  $28.41^{\circ}$  and calculated solar zenith angle is  $61.59^{\circ}$ .

Table 2.2. Table of values for example

Almucantar [ $^{\circ}$ ]	Zenith Angle [ $^{\circ}$ ]	Azimuth of sky element with smallest difference (clockwise) [ $^{\circ}$ ]	Azimuth of sky element with smallest difference (counter clockwise) [ $^{\circ}$ ]	Luminance of 1 <sup>st</sup> element [ $\text{cd}/\text{m}^2$ ]	Luminance of 2 <sup>nd</sup> element [ $\text{cd}/\text{m}^2$ ]	Average luminance [ $\text{cd}/\text{m}^2$ ]	Average luminance /Zenith Luminance (relative gradation)
6	84	336	216	6877.48	8205.24	7541.36	3.859
18	72	336	204	5683.99	6071.88	5877.93	3.008
30	60	345	195	3744.57	3714.73	3729.65	1.908
42	48	345	195	2700.27	3073.23	2886.75	1.477
54	36	0	200	2163.20	2879.29	2521.24	1.290
66	24	0	180	2014.01	2118.44	2066.22	1.057
78	12	0	180	1954.33	1984.17	1969.25	1.008
90	0	0	0	1954.33	-----	1954.33	1.000

With known solar zenith angle and equation 2.4 we are able to find two sky elements on every almucantar with scattering angle as close as possible to solar zenith angle. For 6 degree almucantar we find elements with azimuths  $336^{\circ}$  and  $216^{\circ}$  to have the smallest difference between scattering angle and solar zenith angle. When those two sky elements are defined we can calculate the average luminance and divide it with zenith luminance. The result is relative gradation for certain almucantar. Using the same method we can compute relative gradation values for all almucantars and fill in the Table 2.2.

With the zenith angle and calculated relative gradation (from Table 2.2) it's possible to draw the relative gradation function (Fig. 2.7).

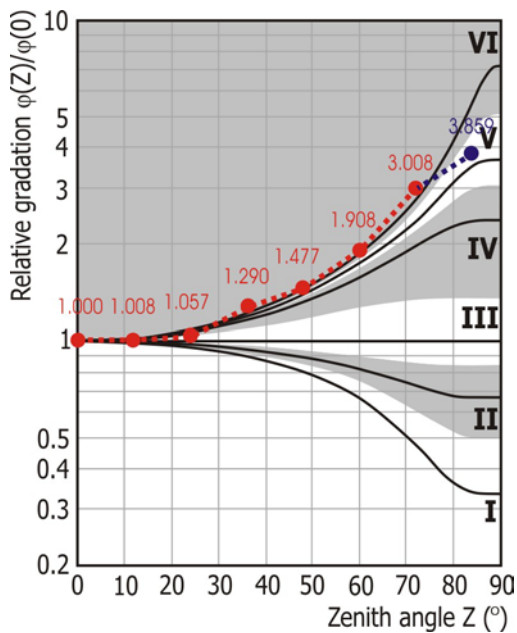


Fig. 2.7. Standard gradation groups and calculated values of relative gradation

When relative gradation values from the measured values of the luminances for all almucantars are calculated we have to find the difference between measured (calculated) values of the relative gradation and values defined with the CIE standard, which are defined with equation 2.6. Values of relative gradation for the CIE standard gradation groups are listed in Table 2.3. When differences (Table 2.4) are calculated it's possible to calculate RMS difference for all CIE gradation groups and we can find the gradation group with the smallest RMS difference. Since we already know that there are obstructions around the IDMP station, we do not take into account sky elements on first (6 degree) almucantar. If we would take into account all sky elements we would end up with gradation group V but if we exclude the almucantar with obstructions, we end up with gradation group VI. With the same reason all measured (calculated) relative gradations in Fig. 2.7 are coloured in red, except the one for the first almucantar, which is coloured in blue, since we do not take it into account when defining gradation group.

Table 2.3. Values of relative gradation for six gradation groups defined with equations 2.6 – 2.8.

Almucantar [°]	Zenith Angle [°]	Relative gradation					
		Gradation group					
		I	II	III	IV	V	VI
6	84	0.337	0.670	1.000	2.352	3.481	5.470
18	72	0.474	0.725	1.000	1.965	2.355	2.761
30	60	0.665	0.818	1.000	1.577	1.726	1.861
42	48	0.805	0.892	1.000	1.325	1.388	1.442
54	36	0.899	0.943	1.000	1.166	1.193	1.215
66	24	0.957	0.976	1.000	1.069	1.079	1.087
78	12	0.990	0.994	1.000	1.017	1.019	1.021
90	0	1.000	1.000	1.000	1.000	1.000	1.000

Table 2.4. Absolute and RMS differences between measured and standard relative gradation

Almucantar [°]	Zenith Angle [°]	Relative gradation (measured)	Difference between measured and standard relative gradation					
			Gradation group					
			I	II	III	IV	V	VI
6	84	3.859	3.522	3.189	2.859	1.507	0.378	1.611
18	72	3.008	2.534	2.283	2.008	1.043	0.653	0.247
30	60	1.908	1.243	1.090	0.908	0.331	0.182	0.047
42	48	1.477	0.672	0.585	0.477	0.152	0.089	0.035
54	36	1.290	0.391	0.347	0.290	0.124	0.097	0.075
66	24	1.057	0.100	0.081	0.057	0.012	0.022	0.030
78	12	1.008	0.018	0.014	0.008	0.009	0.011	0.013
90	0	1.000	0.000	0.000	0.000	0.000	0.000	0.000
RMS difference with all almucantars			4.581	4.129	3.653	1.873	<b>0.788</b>	1.633
RMS difference without 6 deg. almucantar			2.929	2.621	2.274	1.112	0.691	<b>0.267</b>

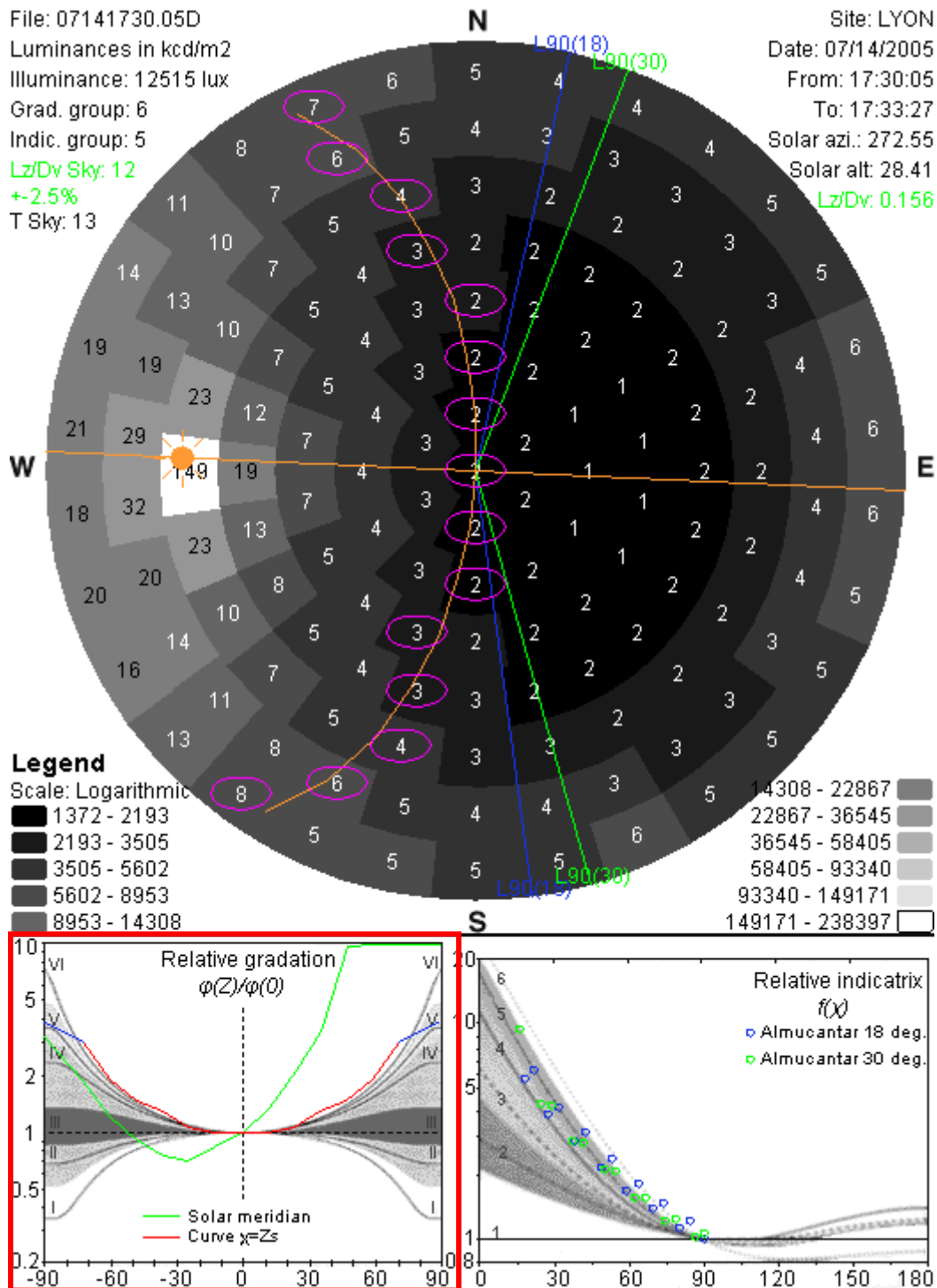


Fig. 2.8. Determination of the gradation curve for 14<sup>th</sup> July, 2005

On Fig. 2.8 a sample of relative gradation diagram with standard gradation functions and measured data is shown.

On the diagram two profiles are drawn. First one is in green and represents relative luminance profile on solar meridian. Solar meridian profile represents relative luminance values of sky elements with the same azimuth as the sun is and with the azimuth of the sun  $\pm 180^\circ$ . Although we don't need this profile for further calculations, it is a useful way to represent luminance distribution and it was also used in [15].

The second profile is in red and represents relative gradation on circular profile with elements with angular distance  $Z_s$  to sun. Last part of profile (high zenith angle) is colored in blue, since it's not taken into account for determination of the gradation group because of surrounding obstructions. From the sample case, it's also seen that relative gradation is steeply increasing from zenith towards horizon but only up to zenith angle  $72^\circ$ .

From  $72^\circ$  further towards horizon increasing of the relative gradation is not so obvious due to surrounding obstacles with lower luminances.

From the relative gradation function profile, it is possible to read the gradation group. In the sample, gradation group is 6, and it means that luminance is gradually increasing from zenith towards horizon. Sky luminance at horizon can be up to 10 times higher than the zenith luminance. In a presented case, the sky was without a cloud.

### **2.2.2 Determination of the indicatrix group**

The indicatrix function connects the relative luminance of the sky element and the angular distance between the sky element and the sun. It also takes into account turbidity of the atmosphere and describes the scattering of sun beams. Under densely overcast skies, the diffusion of sun beams is very high and relative scattering indicatrix function is the same in all directions and it has a unity value. Under overcast conditions direct sunlight is absent as well as any azimuth irregularities in luminance distribution.

In the CIE standard [16] and in Table 2.7 six indicatrix groups are given. Indicatrix groups are defined with parameters  $c$ ,  $d$  and  $e$  and next equations:

$$f(\chi) = 1 + c \cdot \left[ \exp(d\chi) - \exp\left(d \frac{\pi}{2}\right) \right] + e \cdot \cos^2 \chi \quad (2.13)$$

Its value in zenith is:

$$f(Z_s) = 1 + c \cdot \left[ \exp(dZ_s) - \exp\left(d \frac{\pi}{2}\right) \right] + e \cdot \cos^2 Z_s \quad (2.14)$$

Waveforms belonging to six standard indicatrix functions are drawn on next figure.

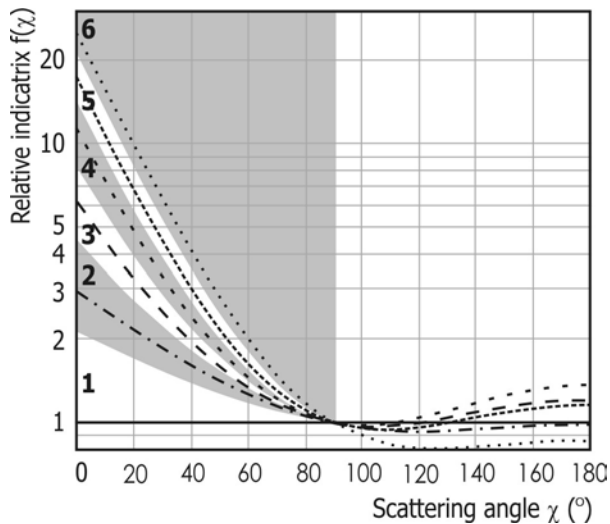


Fig. 2.9. Standard indicatrix function groups

From basic equation (2.9), where a relative luminance of sky element is given, the influence of gradation function has to be excluded. If gradation is excluded that means that for indicatrix calculations we have to find sky elements on the same almucantar, i.e. at the same altitude [45, 46].

Relative indicatrix on certain almucantar can be calculated with next equation:

$$f(\chi) = \frac{L(\chi)}{L(90^\circ)} \quad (2.15)$$

Where:

$L(\chi)$  Luminance of sky element with angular distance  $\chi$  towards sun,

$L(90^\circ)$  Normalizing luminance, luminance of sky element with angular distance  $90^\circ$  towards sun,

On next figure (Fig. 2.10) angles and elements defining indicatrix group are shown.

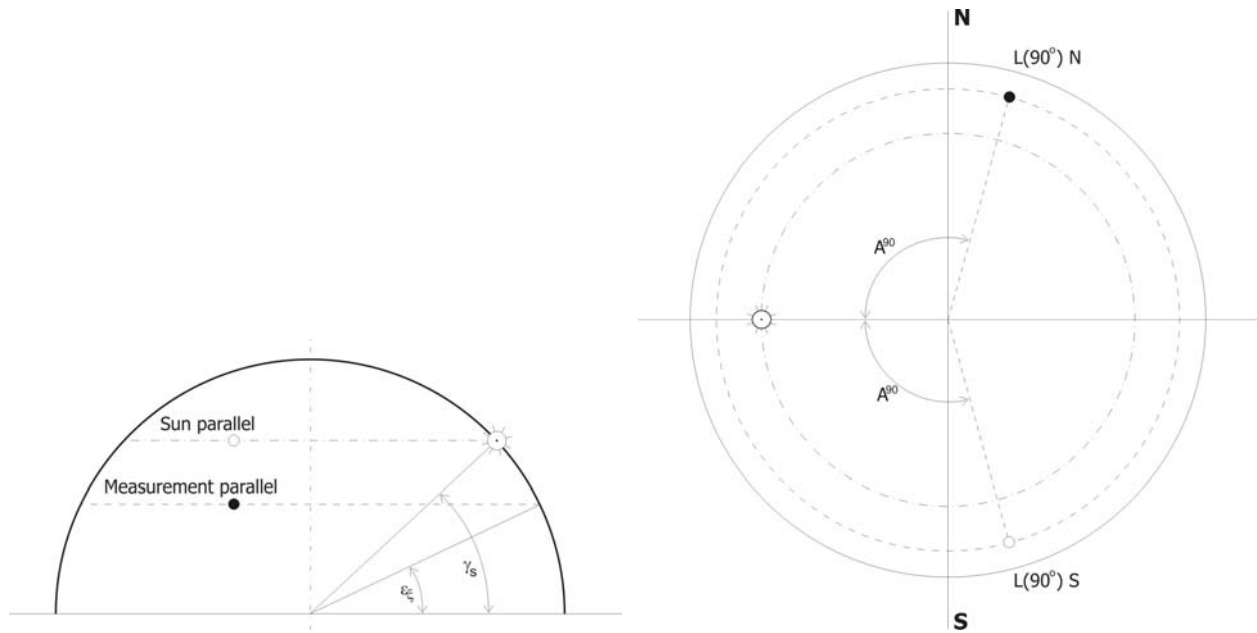


Fig. 2.10. Geometry of sky hemisphere, solar and sky element almucantar and normalizing luminance.

After relative indicatrix function is calculated for all sky elements, it is possible to plot the points on relative indicatrix diagram and to define the indicatrix group.

When processing real sky scans, first we have to find normalizing luminance  $L_{90}$ . Normalizing luminance is a luminance value of a sky element with angular distance  $90^\circ$  towards sun. As there is only a limited number of sky elements on every almucantar, we have to find the one with the smallest difference between its azimuth and the azimuth of ideal  $L_{90}$ . Difference in azimuth of ideal  $L_{90}$  and solar meridian is calculated with next equation:

$$A^{90} = \arccos(-\tan \gamma_s \cdot \tan \varepsilon_\xi) \quad (2.16)$$

Where:

- $A^{90}$  Difference in azimuth of ideal  $L_{90}$  sky element and solar meridian
- $\gamma_s$  Sun altitude.
- $\varepsilon_\xi$  Altitude of the almucantar.

Calculated values of  $L_{90}$  for  $18^\circ$  and  $30^\circ$  almucantars are plotted in graphical presentation (Fig. 2.1) with colored lines; blue for 18 degree almucantar and green for 30 degree almucantar.

Measurements on  $6^\circ$  almucantar were excluded from the analysis because of the same reason as in gradation group calculation (because of the surrounding obstacles).

Indicatrix group decision is based on measurements on lower almucantars ( $18^{\circ}$  and  $30^{\circ}$ ). But also at low almucantars a new problem arises.  $A^{90}$  can exceed value  $180^{\circ}$  and this is not possible. On next diagram (Fig. 2.11)  $A^{90}$  is plotted as a function of sun altitude. From the graph it can be seen that the highest sun altitude to calculate relative indicatrix from measurements on  $18^{\circ}$  almucantar is  $72^{\circ}$  and  $60^{\circ}$  for measurements on  $30^{\circ}$  almucantar.

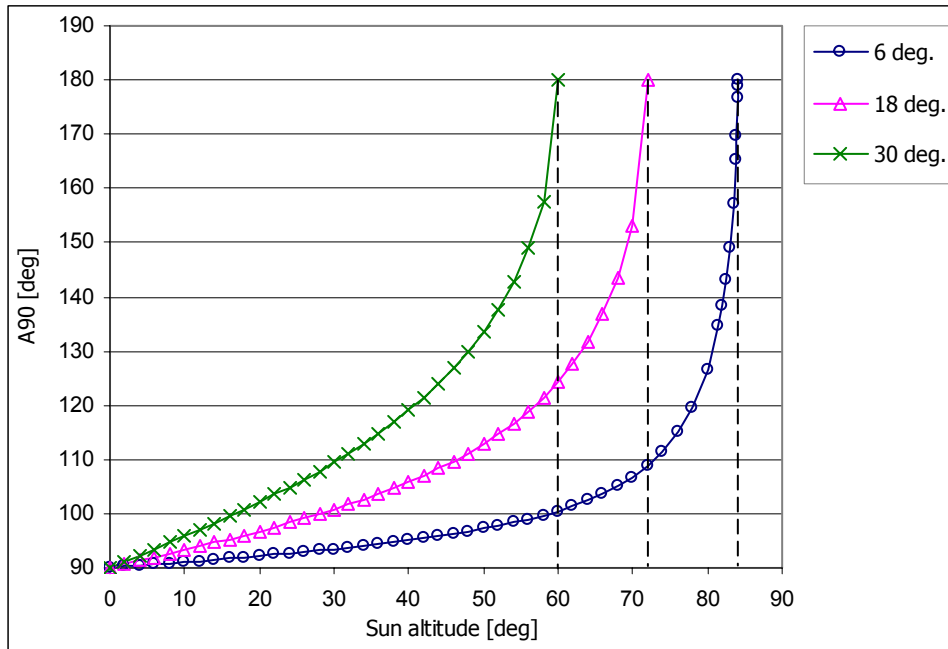


Fig. 2.11. Angle between sun meridian and normalizing sky element as a function of sun altitude

Similar to gradation calculation, also in this case we have to find two normalizing luminances, one in clockwise and the other in counter-clockwise position of the sun. Both luminances are averaged and the result is taken as  $L(90^{\circ})$ .

The relative indicatrix for each sky element on  $18^{\circ}$  and  $30^{\circ}$  almucantar is calculated by next equation.

$$f(\chi) = \frac{L(\chi)'}{L(90^{\circ})'} \quad (2.17)$$

Where:

$f(\chi)$  Relative indicatrix,

$L(\chi)'$  Measured luminance of sky element with angular distance  $\chi$  towards sun,

$L(90^{\circ})'$  Measured normalizing luminance  $L(90)$ .

Indicatrix group is defined by calculation of RMS error between calculated relative indicatrix for every sky elements on almucantars ( $18^{\circ}$  and  $30^{\circ}$ , if sun altitude is not too high) and standard gradation functions.

**Example:**

With this example, we are showing calculation of indicatrix group for measurement performed on July 14, 2005 at 17:30. Sky luminance distribution with luminance values are shown on Fig. 2.8. Azimuth of the sun is  $272.55^{\circ}$ .

First we have to find normalising sky elements on  $18^{\circ}$  and  $30^{\circ}$  almucantar and their luminances. Angle between solar meridian and normalising sky element is defined by equation. 2.16. Angular distance between solar meridian and normalising element for  $18^{\circ}$  almucantar is  $100.12^{\circ}$  and for  $30^{\circ}$  almucantar  $108.20^{\circ}$ . On every almucantar we have two normalising sky elements; the first one is in clockwise direction and the other is in counter-clockwise direction from solar meridian. Calculated azimuths of normalising elements for  $18^{\circ}$  almucantar are  $12.76^{\circ}$  and  $172.42^{\circ}$  and on  $30^{\circ}$  almucantar  $20.74^{\circ}$  and  $164.35^{\circ}$ . Since we have only a limited number of sky elements on every almucantar, we have to find the luminance of normalising sky elements with linear interpolation between two neighbouring sky elements. The azimuth of the first element ( $12.76^{\circ}$ ) on  $18^{\circ}$  almucantar is between elements with azimuths  $12^{\circ}$  and  $24^{\circ}$ . Luminance of the sky element with azimuth  $12^{\circ}$  is  $3416.36 \text{ cd/m}^2$  and luminance of the element with azimuth  $24^{\circ}$  is  $3282.09 \text{ cd/m}^2$ . With linear interpolation calculated value of the first normalising element on  $18^{\circ}$  almucantar is  $3408.83 \text{ cd/m}^2$ . The same procedure is used to calculate luminance of the second normalising element on the  $18^{\circ}$  almucantar and also for both normalising elements on the  $30^{\circ}$  almucantar (Table 2.5).

*Table 2.5. Table of azimuths and luminance values for example*

Almucantar [ $^{\circ}$ ]	Azimuth of normalising element [ $^{\circ}$ ]	First bordering azimuth [ $^{\circ}$ ]	Second bordering azimuth [ $^{\circ}$ ]	Luminance of the first bordering azimuth [ $\text{cd/m}^2$ ]	Luminance of the second bordering azimuth [ $\text{cd/m}^2$ ]	Calculated luminance of normalising elements [ $\text{cd/m}^2$ ]	Luminance of normalising element for almucantar [ $\text{cd/m}^2$ ]
18	12.76	12	24	3416.36	3282.09	3408.83	3581.56
	172.42	168	180	3550.63	4102.62	3754.29	
30	20.74	15	30	2491.41	2327.30	2428.52	2492.43
	164.35	150	165	2342.22	2566.00	2556.33	

With calculated normalising luminances it's now possible to calculate relative indicatrix with equation (3.17) for elements on  $18^{\circ}$  and  $30^{\circ}$  almucantar. Since difference between indicatrix groups is noticeable only for scattering angles less than  $90^{\circ}$ , it makes sense to calculate relative indicatrix only for elements with scattering angles lower than  $90^{\circ}$ . Another problem arises with sky elements with low scattering angle. If scattering angle is less than  $15^{\circ}$ , high luminance of a sky element can be measured because of a bright solar corona. When we are looking for the indicatrix group regarding relative indicatrix,

all elements with scattering angle less than  $15^\circ$  and more than  $90^\circ$  are excluded. With all suitable elements, practically with their scattering angles and relative indicatrixes it's possible to draw relative indicatrix function on standard indicatrix function graph (Fig. 2.12).

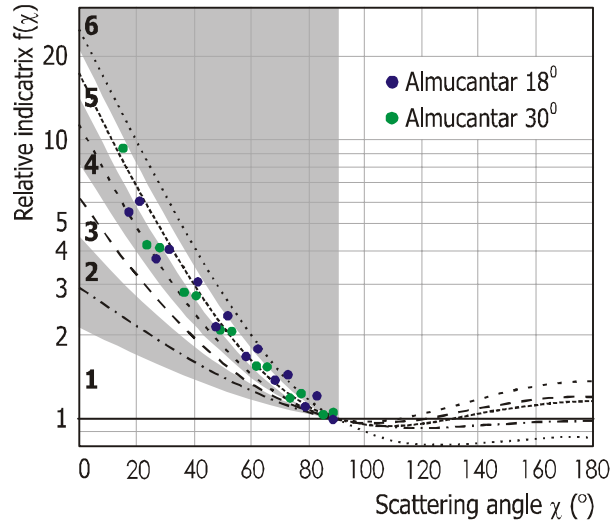


Fig. 2.12. Relative indicatrixes and standard indicatrix function groups

Relative indicatrixes can now be compared to standard indicatrix groups. RMS difference between appropriate sky elements and standard indicatrix function is calculated and based on this result indicatrix group is defined.

In our example indicatrix group with least RMS difference is number 5 (Table 2.6).

Table 2.6. RMS differences for all indicatrix groups

Standard gradation group	1	2	3	4	5	6
RMS difference	1.786	1.286	0.910	0.447	<b>0.441</b>	1.535

On Fig. 2.13 a sample of relative indicatrix diagram with standard indicatrix functions and measured data are shown.

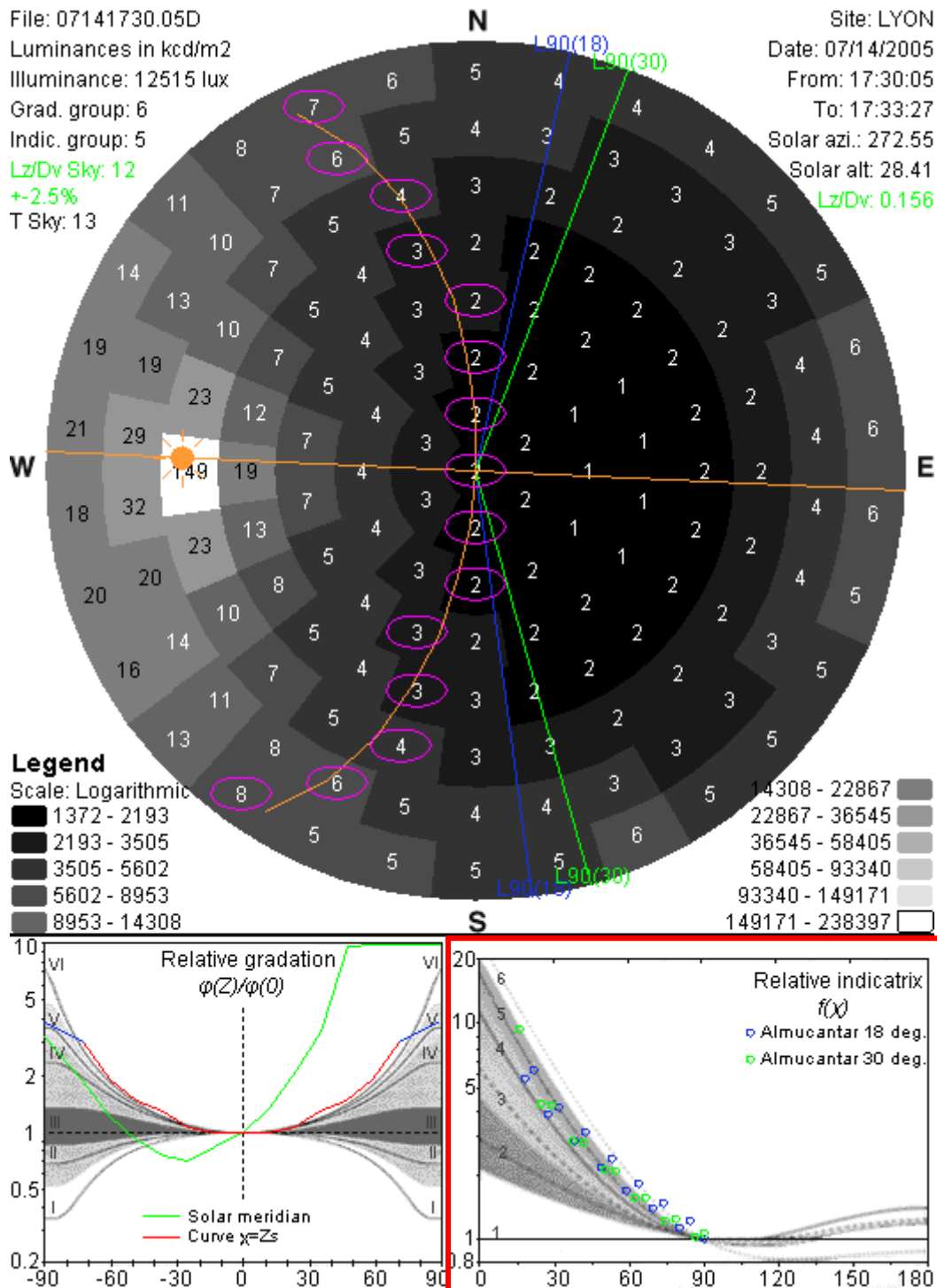


Fig. 2.13. Determination of relative indicatrix group for 14<sup>th</sup> July, 2005

On the diagram of relative indicatrix, calculated values are plotted with colored small circles. The circles in blue color represent sky elements on 18<sup>o</sup> almucantar with its relative indicatrix and with their angular distance towards sun and the ones in green color they represent relative indicatrix and their angular distances towards for elements on 30<sup>o</sup> almucantar (same example is also shown on Fig. 2.12).

From the points on relative indicatrix diagram it is possible to read out the indicatrix group. In the shown sample indicatrix group is 5, and it means that luminance is gradually increasing towards the sun position.

### 2.2.3 Calculation of the CIE sky type with gradation and indicatrix

CIE Standard [16] defines 15 sky types (Table 2.7). Although with six gradation and six indicatrix groups we would get 36 sky types. Some combinations of gradation and indicatrix are extremely rare and those combinations are not included in 15 CIE sky types.

Table 2.7. 15 standard skies with gradation and indicatrix groups and parameters which define those groups

CIE sky type	Gradation	Indicatrix	<i>a</i>	<i>b</i>	<i>c</i>	<i>d</i>	<i>e</i>	Description of luminance distribution
1	I	1	4	-0,7	0	-1	0	<b>CIE Standard Overcast Sky, alternative form Steep luminance gradation towards zenith, azimuthal uniformity</b>
2	I	2	4	-0,7	2	-1,5	0,15	Overcast, with steep luminance gradation and slight brightening towards the sun
3	II	1	1,1	-0,8	0	-1	0	Overcast, moderately graded with azimuthal uniformity
4	II	2	1,1	-0,8	2	-1,5	0,15	Overcast, moderately graded and slight brightening towards the sun
5	III	1	0	-1	0	-1	0	<b>Sky of uniform luminance</b>
6	III	2	0	-1	2	-1,5	0,15	Partly cloudy sky, no gradation towards zenith, slight brightening towards the sun
7	III	3	0	-1	5	-2,5	0,3	Partly cloudy sky, no gradation towards zenith, brighter circum solar region
8	III	4	0	-1	10	-3	0,45	Partly cloudy sky, no gradation towards zenith, distinct solar corona
9	IV	2	-1	-0,55	2	-1,5	0,15	Partly cloudy, with the obscured sun
10	IV	3	-1	-0,55	5	-2,5	0,3	Partly cloudy, with brighter circumsolar region
11	IV	4	-1	-0,55	10	-3	0,45	White-blue sky with distinct solar corona
12	V	4	-1	-0,32	10	-3	0,45	<b>CIE Standard Clear Sky, low illuminance turbidity</b>
13	V	5	-1	-0,32	16	-3	0,3	<b>CIE Standard Clear Sky, polluted atmosphere</b>
14	VI	5	-1	-0,15	16	-3	0,3	Cloudless turbid sky with broad solar corona
15	VI	6	-1	-0,15	24	-2,8	0,15	White-blue turbid sky with broad solar corona

Table 2.8. Matrix with gradation and indicatrix combinations for 15 CIE sky types.

		<b>Gradation</b>					
		<b>I</b>	<b>II</b>	<b>III</b>	<b>IV</b>	<b>V</b>	<b>VI</b>
<b>Indicatrix</b>	<b>1</b>	1	3	5	9	9	9
	<b>2</b>	2	4	6	9	9	9
	<b>3</b>	2	7	7	10	10	12
	<b>4</b>	8	8	8	11	12	14
	<b>5</b>	8	8	8	11	13	14
	<b>6</b>	8	8	8	13	13	15

Reduction from 36 sky types to 15 CIE sky types was done with Tregenza statistical [37] method for different sun altitudes which is shortly described in chapter 2.4.

### 2.3 Calculation of the CIE sky type based on Lz/Dv ratio

In several papers, Kittler [15, 22, 36, 38, 42, 43] proposed that CIE sky types from measurements should be considered based on Lz/Dv values. Lz/Dv curves are defined by next equation:

$$L_z / D_v = \frac{B \cdot (\sin \gamma_s)^c / (\cos \gamma_s)^d + E \cdot \sin \gamma_s}{133.8 \cdot \sin \gamma_s} \quad (2.18)$$

Where:

- $L_z$  Zenith luminance,
- $D_v$  Diffuse horizontal illuminance,
- $\gamma_s$  Solar altitude,
- $B, C, D, E$  Standard parameters defined with Table 2.9

Table 2.9. Parameters B, C, D, E for Lz/Dv curves

CIE Sky Type	Gradation group	Indicatrix group	Description of luminance distribution	Parameters			
				B	C	D	E
1	I	1	<b>CIE Standard Overcast Sky</b> , Steep luminance gradation towards zenith, azimuthal uniformity	54.63	1.00	0	0
2	I	2	Overcast, with steep luminance gradation and slight brightening towards the sun	12.35	3.68	0.59	50.47
3	II	1	Overcast, moderately graded with azimuthal uniformity	48.3	1.00	0	0
4	II	2	Overcast, moderately graded and slight brightening towards the sun	12.23	3.57	0.57	44.27
5	III	1	<b>Sky of uniform luminance</b>	42.59	1.00	0	0
6	III	2	Partly cloudy sky, no gradation towards zenith, slight brightening towards the sun	11.84	3.53	0.55	38.78
7	III	3	Partly cloudy sky, no gradation towards zenith, brighter circum solar region	21.72	4.52	0.64	34.56
8	III	4	Partly cloudy sky, no gradation towards zenith, distinct solar corona	29.35	4.94	0.70	30.41
9	IV	2	Partly cloudy, with the obscured sun	10.34	3.45	0.50	27.47
10	IV	3	Partly cloudy, with brighter circumsolar region	18.41	4.27	0.63	24.04
11	IV	4	White-blue sky with distinct solar corona	24.41	4.60	0.72	20.76
12	V	4	<b>CIE Standard Clear Sky, low illuminance turbidity</b>	23.00	4.43	0.74	18.52
13	V	5	<b>CIE Standard Clear Sky, polluted atmosphere</b>	27.45	4.61	0.76	16.59
14	VI	5	Cloudless turbid sky with broad solar corona	25.54	4.40	0.79	14.56
15	VI	6	White-blue turbid sky with broad solar corona	28.08	4.13	0.79	13.00

For all 15 sky types Lz/Dv curves are plotted and grouped for overcast (Fig. 2.14), intermediate (Fig. 2.15) and cloudless (Fig. 2.16) skies.

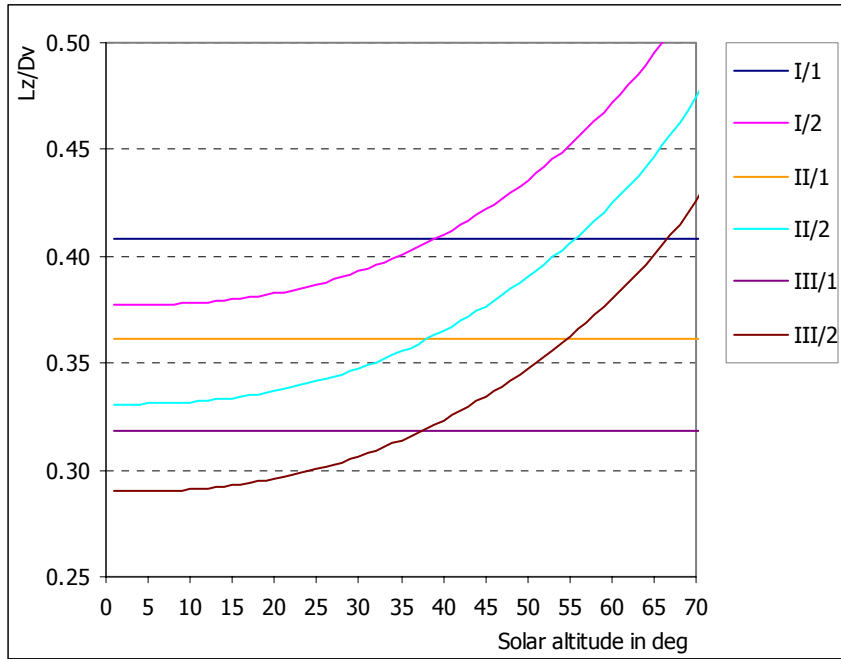


Fig. 2.14.  $Lz/Dv$  curves for overcast skies

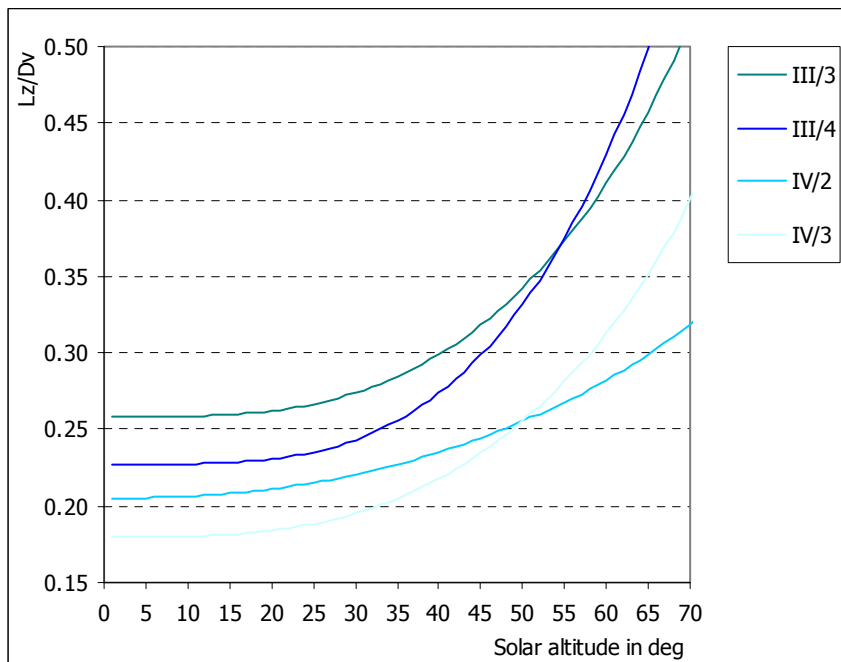


Fig. 2.15.  $Lz/Dv$  curves for intermediate skies

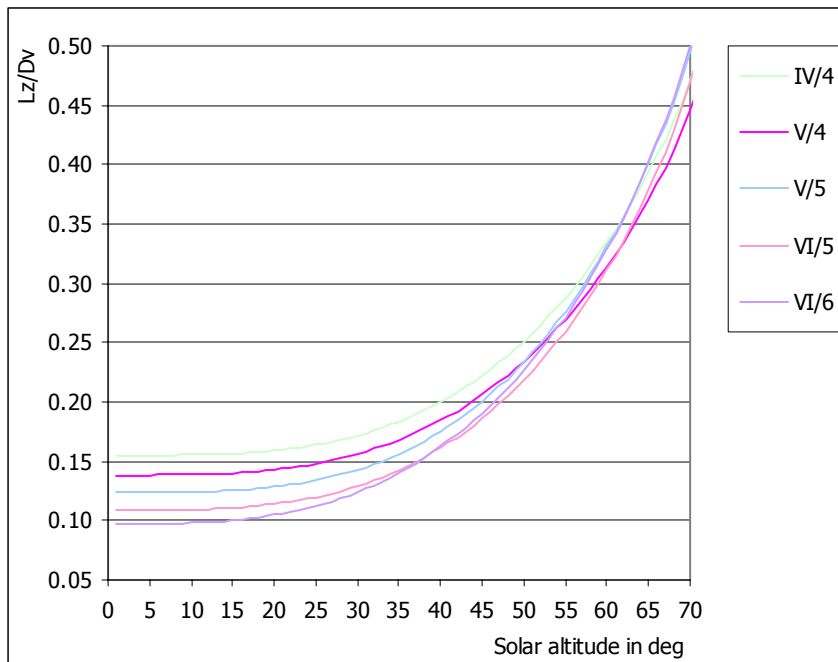


Fig. 2.16.  $Lz/Dv$  curves for cloudless skies

Around every  $Lz/Dv$  curve a surrounding strip  $\pm 2.5\%$  should be drawn (Fig. 2.17). This is the proposed band of trust. If measurement is inside the band, then the measurement can be trusted (Point 3 on Fig. 2.17). The problem arises, when a measurement is inside two or more bands of trust (Point 2 on Fig. 2.17). In this case we can find the nearest  $Lz/Dv$  curve, but we can not trust the measurement. It is the same if a measurement is not in any of those  $\pm 2.5\%$  strips (Point 1 on Fig. 2.17). Also in this case  $Lz/Dv$  can be calculated and regarding this value and solar altitude, nearest  $Lz/Dv$  curve can be defined with relative RMS difference.

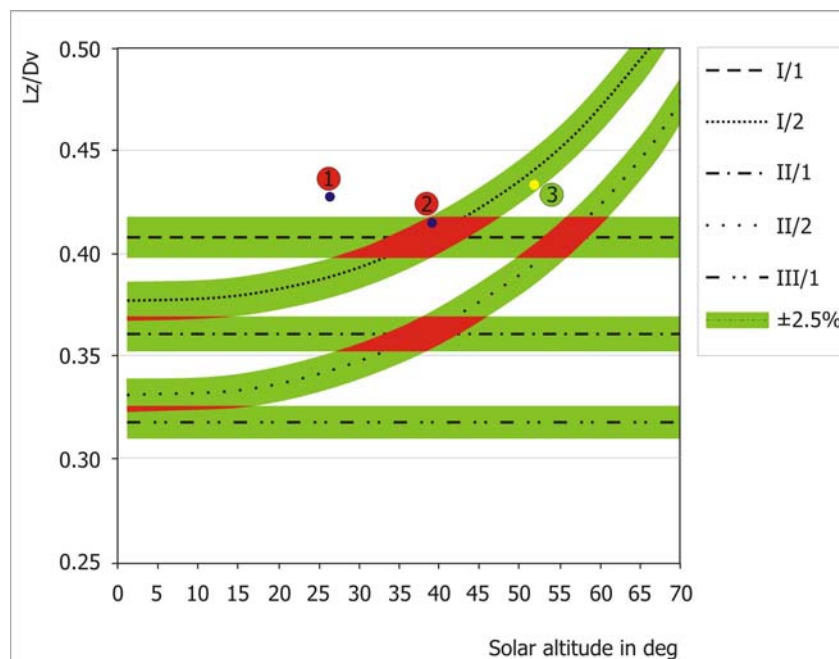


Fig. 2.17.  $Lz/Dv$  curves for overcast skies with  $\pm 2.5\%$  surrounding strips

### 2.3.1 Calculation of the diffuse horizontal illuminance ( $D_v$ )

Diffuse horizontal illuminance is calculated from sky scans with integration of illuminance contributions from every patch. For calculations of diffuse illuminance the following equation is used:

$$\delta E = L_p \cdot \cos(Z) \cdot d\omega \quad (2.19)$$

Where:

$\delta E$  contribution to horizontal illuminance from a single sky patch.

$L_p$  luminance of a sky patch.

$Z$  zenith angle of sky patch.

$d\omega$  solid angle of a sky patch.

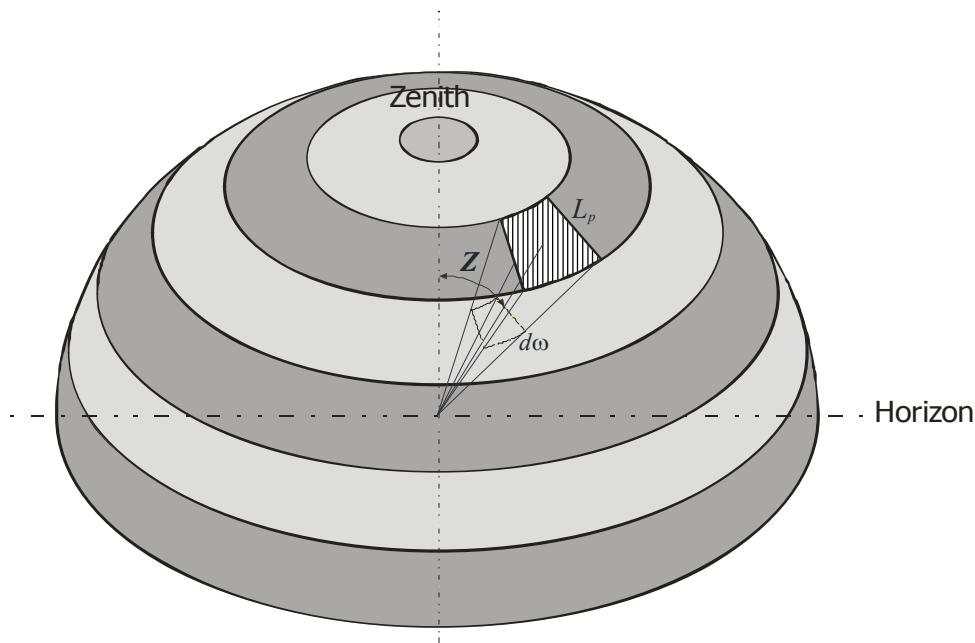


Fig. 2.18. Contribution of a single sky patch to diffuse horizontal illuminance.

Since we have to calculate diffuse horizontal illuminance, direct part of sunlight has to be removed. Direct component of sunlight can be removed with eliminating contribution of sky element with sun to illuminance. The corresponding sky element is defined with calculated sun position.

Calculated illuminance values were compared with measured illuminance from IDMP station. The first calculations we performed overestimated diffuse horizontal illuminance, although sky element with sun was removed.

Calibration of the sky scanner was performed under cloudy sky, where global and diffuse illuminances have practically the same value. In cases of cloudy conditions, horizontal illuminance was calculated correctly. Zenith luminance from sky scans was

calculated correctly in all types of sky conditions also in cases of intermediate and clear skies (Fig. 2.19), but on the other hand, diffuse illuminance on horizontal plane was overestimated. (Fig. 2.20)

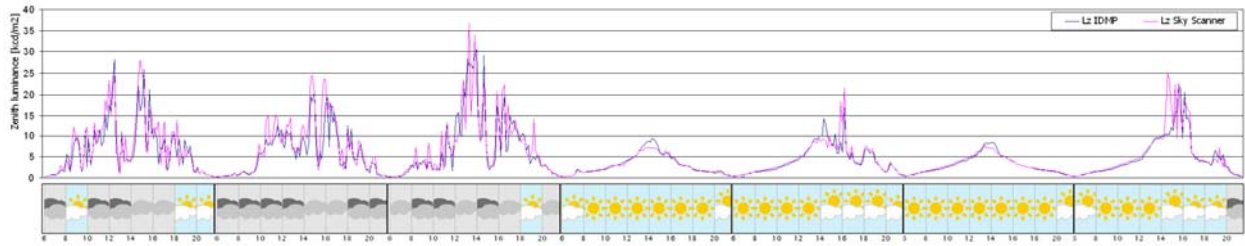


Fig. 2.19. Zenith luminance for a week in July 2005

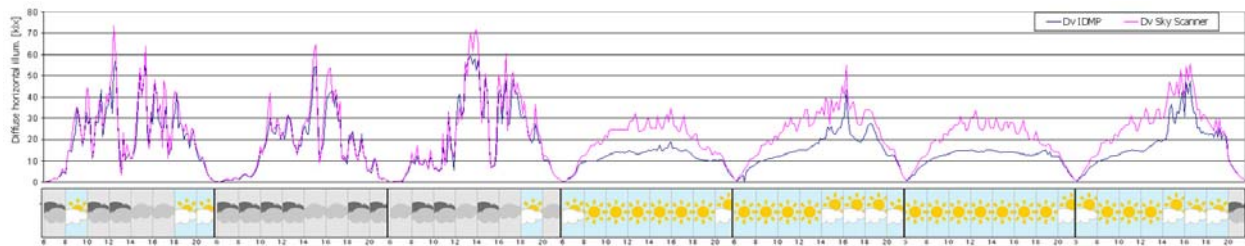


Fig. 2.20. Diffuse horizontal illuminance for a week in July 2005

As it is seen from Fig. 2.20 the calculated diffuse horizontal illuminance is far too estimated when compared with measured values from IDMP station. The only reason for that could be solar corona, which is also scanned with sky scanner. From some sample sky scans it can be seen that two or even more sky elements near sun can have almost the same (very high) luminance. (Fig. 2.21).

Removing only one sky element might not be enough. In next step we tried to near curves for diffuse horizontal illuminance from IDMP measurements and from sky scans. In calculations with sky scans sky patches near sun were excluded. Patches were selected on the basis of the scattering angle ( $\chi$ ), which is defined with equation 2.4.

For a cloudless day (June 1<sup>st</sup> 2005) we did comparison between measured diffuse horizontal illuminance and calculated one. When calculating diffuse horizontal illuminance from sky scans different number of sky elements near the sun was excluded. Number of excluded elements depends on angle  $\chi$ , which was changed from 8 degree to 15 degree. Results of different calculations can be seen on diagram on next page (Fig. 2.22).

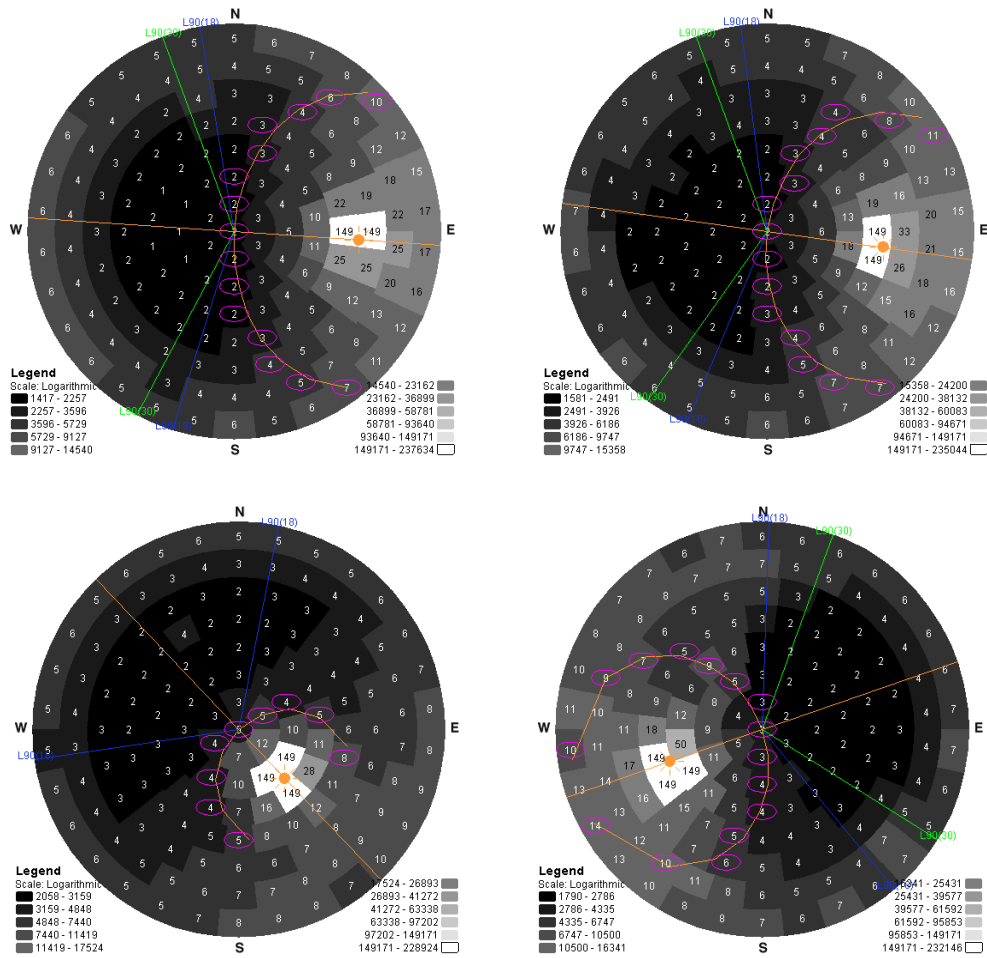


Fig. 2.21. Number of sky elements with very high luminance around sun, can be more than one or two.

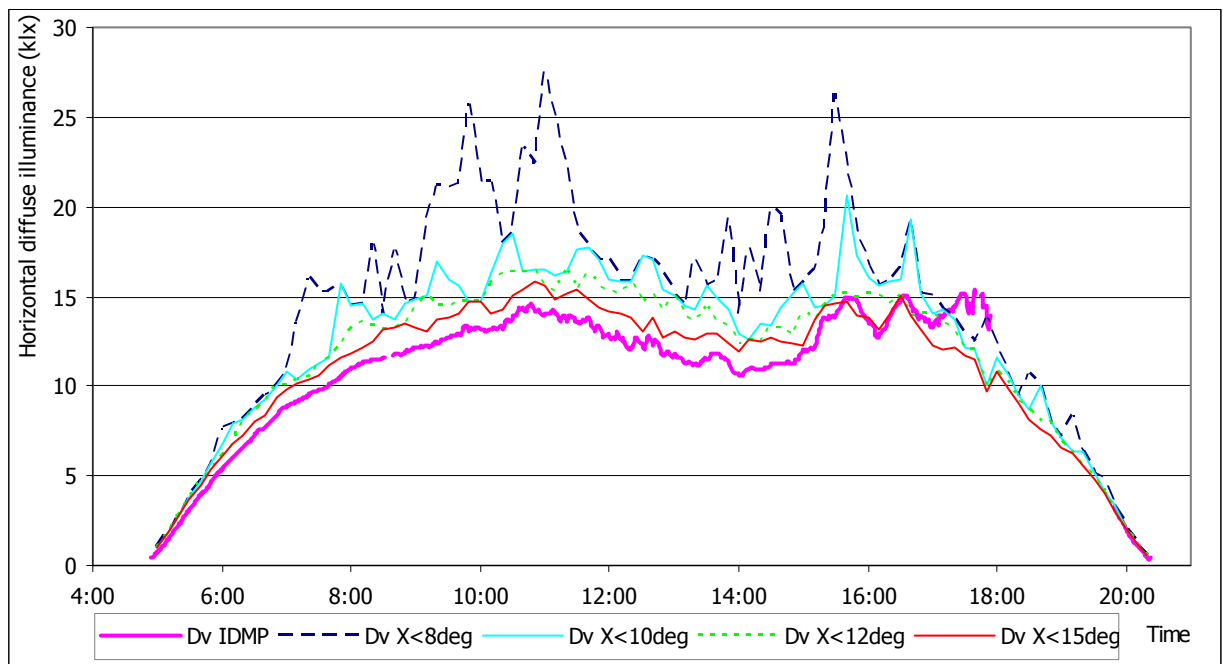


Fig. 2.22. Diffuse horizontal illuminance with different number of excluded sky elements near sun

For further calculations all sky elements with scattering angle below 15 degrees from sun were excluded in diffuse horizontal illuminance calculation. When we applied this method to data for week in July 2005 we got new diffuse horizontal illuminance diagram (Fig. 2.23).

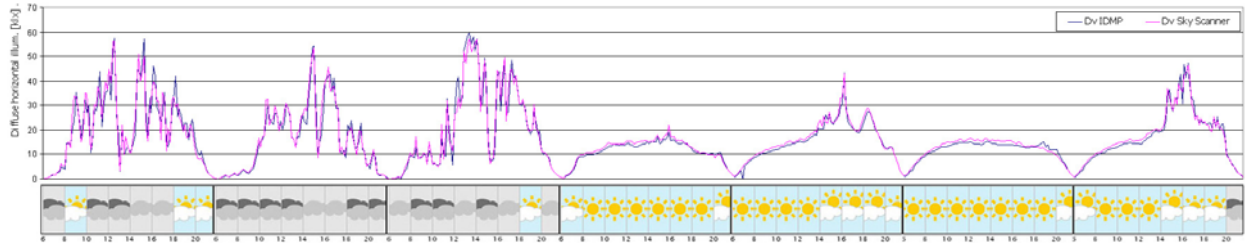


Fig. 2.23. Diffuse horizontal illuminance for a week in July with new calculation method

When new method was applied to the data set from a week in July the illuminance values from IDMP station and calculated values from the sky scans are practically the same (Fig. 2.23).

### 2.3.2 Calculation of the vertical illuminances

Vertical illuminances were calculated from sky scans with integration of illuminance contributions of all sky patches that are seen from the vertical plane. Visibility depends on the azimuth of the sky patch. North vertical illuminance is illuminance on a plane that is facing north. From this plane sky elements with azimuths higher than  $270^{\circ}$  or smaller than  $90^{\circ}$  are visible. For visibility we have next conditions:

$$\begin{array}{l}
 \text{North} \\
 \text{East} \\
 \text{South} \\
 \text{West}
 \end{array}
 \begin{array}{l}
 \left\{ \begin{array}{l} \alpha > 270^{\circ} \\ \alpha < 90^{\circ} \end{array} \right. \\
 \left\{ 0 < \alpha < 180^{\circ} \right. \\
 \left\{ 90 < \alpha < 270^{\circ} \right. \\
 \left\{ 180 < \alpha < 360^{\circ} \right.
 \end{array}
 \quad (2.20)$$

For calculations of diffuse illuminance the following equation is used:

$$\delta E_v = L_p \cdot \sin(Z) \cdot d\omega \cdot \cos(\Delta\alpha) \quad (2.21)$$

Where:

- $\delta E_v$  contribution to vertical illuminance from a single sky patch
- $L_p$  luminance of a sky patch
- $Z$  zenith angle of sky patch
- $d\omega$  solid angle of a sky patch
- $\Delta\alpha$  angular difference in azimuth between sky patch and normal of the plane

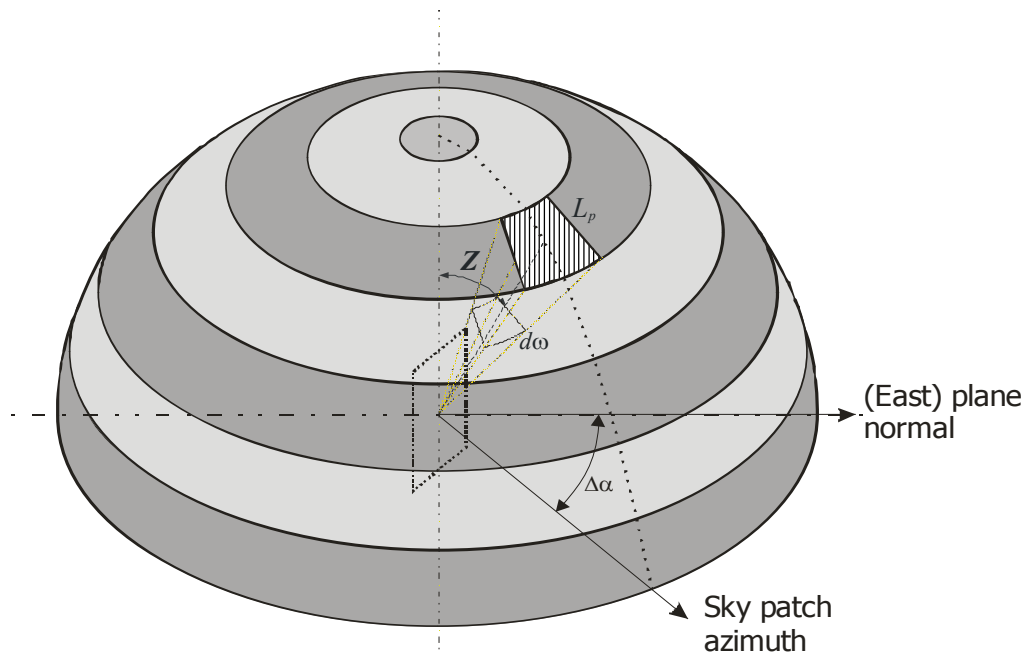


Fig. 2.24. Contribution of a single sky patch to diffuse vertical illuminance.

## 2.4 Calculation of the CIE sky type with Tregenza statistical method

Determination of the CIE sky type based on Tregenza [37] method is practically a statistical method due to comparison based on RMS error between measured luminance and theoretical luminance defined by CIE standard [16].

From every sky scan measurement horizontal illuminance has to be calculated. Also in this method, we use only patches with scattering angle larger than 15 degrees. After that normalized luminance distribution can be calculated by the following equation:

$$L_p' = \frac{L_p}{E_h} \quad (2.22)$$

Where:

- $L_p'$  normalized luminance of a sky patch,
- $L_p$  luminance of a sky patch,
- $E_h$  horizontal illuminance from sky scan measurement.

Next step is to calculate luminance distribution of each CIE sky type with solar elevation and azimuth at the time of the measurement. Calculation is performed for the centre of every of 145 sky patches. After the luminance distribution for all CIE sky types is

calculated, we have to calculate horizontal illuminance for all CIE skies and then normalized luminance distribution for CIE sky types by next equation

$$L_{pCIEx}' = \frac{L_{pCIEx}}{E_{hCIEx}} \quad (2.23)$$

Where:

- $L_{pCIEx}'$  normalized luminance of a sky patch for CIE sky type x,  
 $L_{pCIEx}$  luminance of a sky patch for CIE sky type x,  
 $E_{hCIEx}$  horizontal illuminance for CIE sky type x.

The last step is to calculate RMS error between each type of CIE sky and measured values by next equation:

$$rms_{CIEx} = \sqrt{\frac{1}{n_{X>15}} \sum_{p=1}^{n_{X>15}} (L_p' - L_{pCIEx}')^2} \quad (2.24)$$

Where:

- $rms_{CIEx}$  RMS error between measured values and CIE sky type x,  
 $n_{X>15}$  number of patches with scattering angle larger than 15 degrees.

Tregenza sky is defined by the smallest RMS error between measured values and CIE sky type.

## **2.5 Results of measurements**

When measurements with sky scanner in December 2005 were finished, calculations of CIE sky type were carried out for all measured cases. CIE sky type was defined with three previously mentioned methods. Together with these calculations CIE sky type was also calculated for data measured at IDMP station. From the IDMP data it was only possible to define CIE sky type based on  $L_z/D_v$  ratio. Although zenith luminance and diffuse illuminance are measured every minute, CIE sky type was calculated only for every tenth measurement. We decided to calculate CIE sky type only for times when sky scanner started to measure. The zenith luminances and diffuse illuminances we used for further calculation were carried out every full ten minutes (00, 10, 20, 30, 40, 50).

When all calculations were carried out we had to synchronize measurements database. In some cases sky scanner data were missing. This was due to problems with sky scanner. Sky scanner was checked every day in the morning and sometimes it was not working due to unknown reason. The sky scanner stopped also at all voltage drops and dips. Voltage drops were mostly problematic during weekends when it was not possible

to get to the IDMP station because of the security alarm which was switched on at corridors leading to the station.

On the other hand in some cases zenith luminance and diffuse illuminance measurements were missing. Practically they were not missing, but they did not pass the quality control. For example if diffuse illuminance is higher than global illuminance, the measured data does not meet the quality control conditions.

All cases when one of the measurements was missing were excluded. After the synchronization of the sky scanner and zenith luminance/diffuse illuminance database, the final database was created. In this database we have all together 14172 measurements. If we apply sun altitude limitations and limitation for Lz/Dv ratio to the dataset, we get fewer cases that meet the limitations (Table 2.10). The best quality data are the ones that meet both limitations (Table 2.11).

*Table 2.10. Number of cases with different limitations*

		Sky scanner data		IDMP data	
		Lz/Dv in $\pm 2.5\%$ band		Lz/Dv in $\pm 2.5\%$ band	
	Sun altitude	YES	5905	NO	8313
< 5°	1317	all cases	14172	all cases	14172
≥ 5°	12855				
all cases	14172				

*Table 2.11. Number of cases in cross-section of sun altitude and Lz/Dv limitations*

Sun altitude	Lz/Dv in $\pm 2.5\%$ band	Sky scanner data	IDMP data
≥ 5°	YES	5338	5452
	NO	7516	7402
	all cases	12854	12854

On next charts (Fig. 2.25 - Fig. 2.28) frequencies of CIE sky types are presented for data with sun altitude above 5° and Lz/Dv (calculated from sky scanner data) in  $\pm 2.5\%$  band.

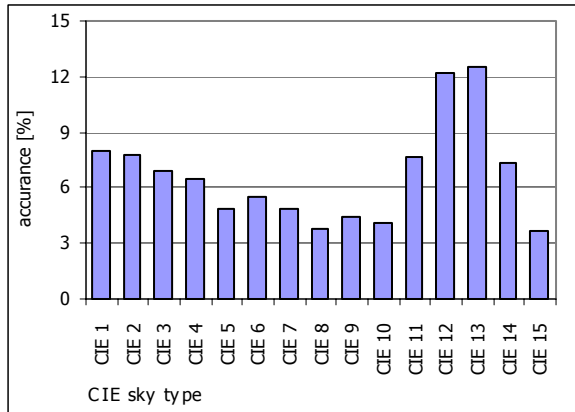


Fig. 2.25. Frequencies of CIE sky types for sky scanner data (sun altitude  $\geq 5^\circ$ , Lz/Dv in  $\pm 2.5\%$  band.) – based on Lz/Dv ratio.

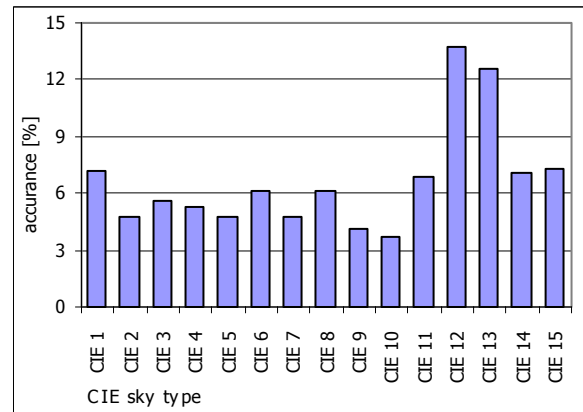


Fig. 2.26. Frequencies of CIE sky types for IDMP data (sun altitude  $\geq 5^\circ$ , Lz/Dv in  $\pm 2.5\%$  band.) – based on Lz/Dv ratio.

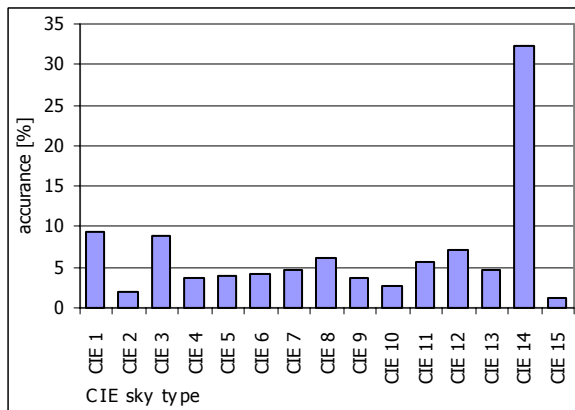


Fig. 2.27. Frequencies of CIE sky types for sky scanner data (sun altitude  $\geq 5^\circ$ , Lz/Dv in  $\pm 2.5\%$  band.) – based on gradation and indicatrix groups

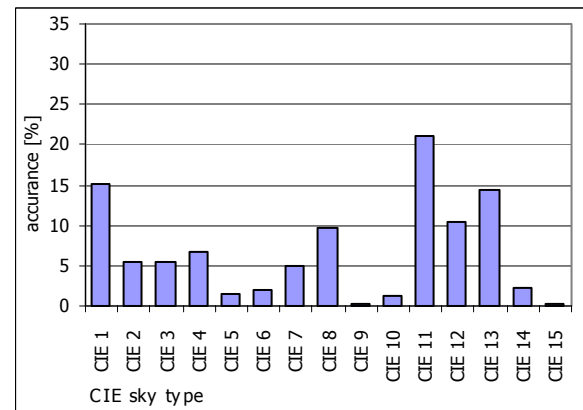


Fig. 2.28. Frequencies of CIE sky types for scanner data (sun altitude  $\geq 5^\circ$ , Lz/Dv in  $\pm 2.5\%$  band.) – based on Tregenza method.

On next charts (Fig. 2.29 - Fig. 2.32) frequencies of CIE sky types are presented for all data with sun altitude above  $5^{\circ}$  regardless of Lz/Dv ratio.

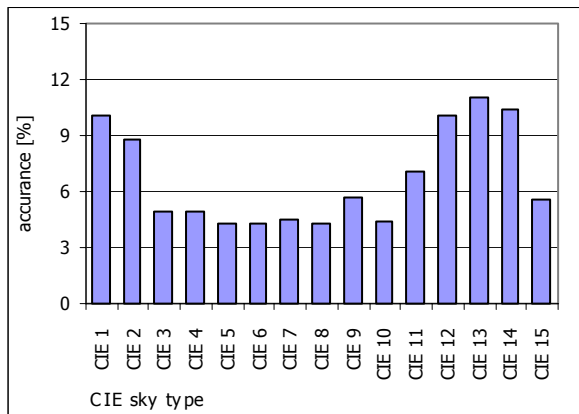


Fig. 2.29. Frequencies of CIE sky types for sky scanner data (sun altitude  $\geq 5^{\circ}$ ) – based on Lz/Dv ratio.

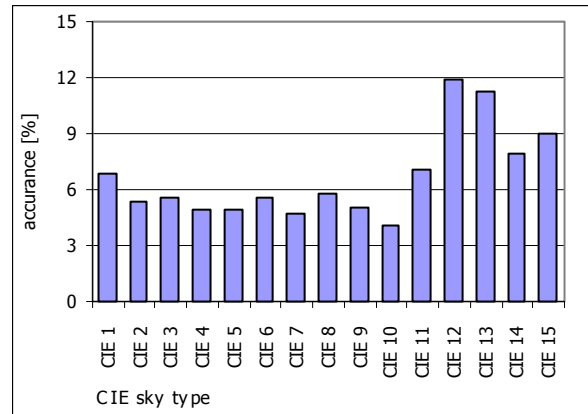


Fig. 2.30. Frequencies of CIE sky types for IDMP data (sun altitude  $\geq 5^{\circ}$ ) – based on Lz/Dv ratio.

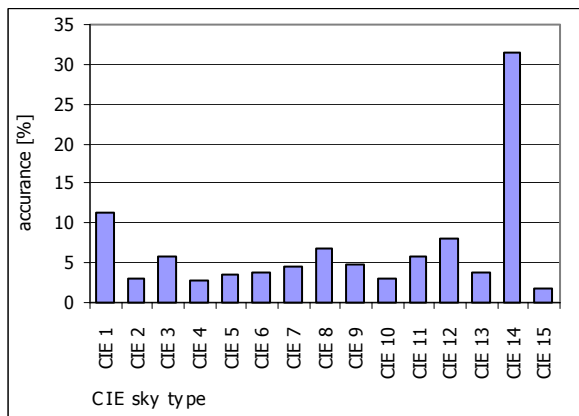


Fig. 2.31. Frequencies of CIE sky types for sky scanner data (sun altitude  $\geq 5^{\circ}$ ) – based on gradation and indicatrix groups

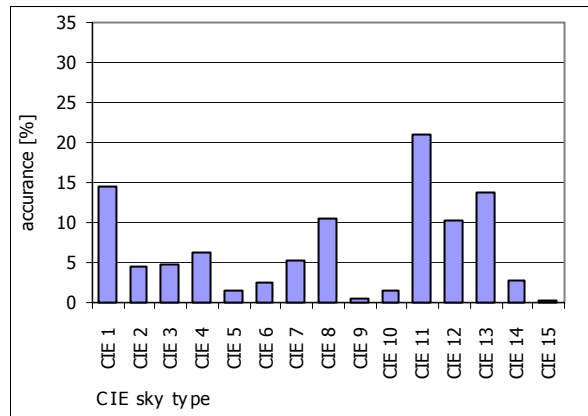


Fig. 2.32. Frequencies of CIE sky types for scanner data (sun altitude  $\geq 5^{\circ}$ ) – based on Tregenza method.

On next charts (Fig. 2.33 - Fig. 2.34), the frequencies of CIE sky types are presented for data with sun altitude above  $5^{\circ}$  regarding and regardless of Lz/Dv ratio. On these charts, the difference between both selections can be seen.

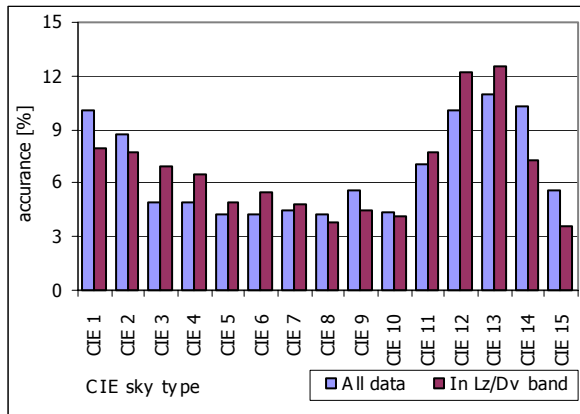


Fig. 2.33. Frequencies of CIE sky types for sky scanner data (sun altitude  $\geq 5^{\circ}$ ) – based on Lz/Dv ratio for all data and data with Lz/Dv in  $\pm 2.5$  % band.

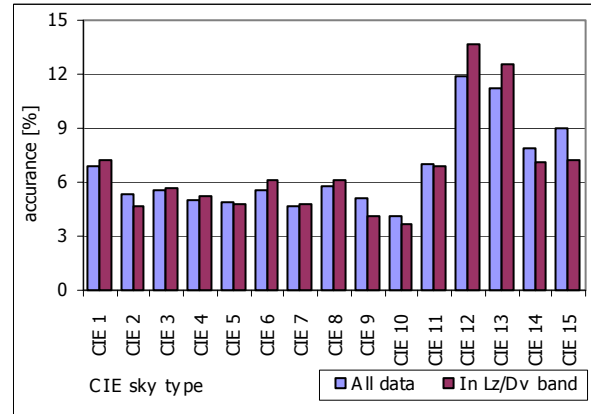


Fig. 2.34. Frequencies of CIE sky types for IDMP data (sun altitude  $\geq 5^{\circ}$ ) – based on Lz/Dv ratio for all data and data with Lz/Dv in  $\pm 2.5$  % band.

Based on graphs on Fig. 2.33 and Fig. 2.34 we can conclude that the method based on Lz/Dv gives similar frequencies of CIE sky types for data from IDMP station and from sky scanner. The gradation and indicatrix method and the Tregenza method, which could be only applied to sky scanner data, do not provide similar CIE sky frequencies as the Lz/Dv method.

### 3 Using digital camera as a sky scanner

#### 3.1 Introduction

Sky scanner that was installed at ENTPE IDMP station was borrowed from Kyushu University for a period of one year. Since one year is not especially long period for sky observations, we wanted to continue with measurements also without sky scanner. Instead of using sky scanner we would use digital camera with fish-eye lens and software to derive sky luminance distribution from digital images.

On certain days when sky scanner was still installed, we were also taking pictures of sky vault with digital camera and fish-eye lens (Fig. 3.1). The main purpose of taking pictures at the same time as the sky scanner is working, was to evaluate sky images taken with digital camera.

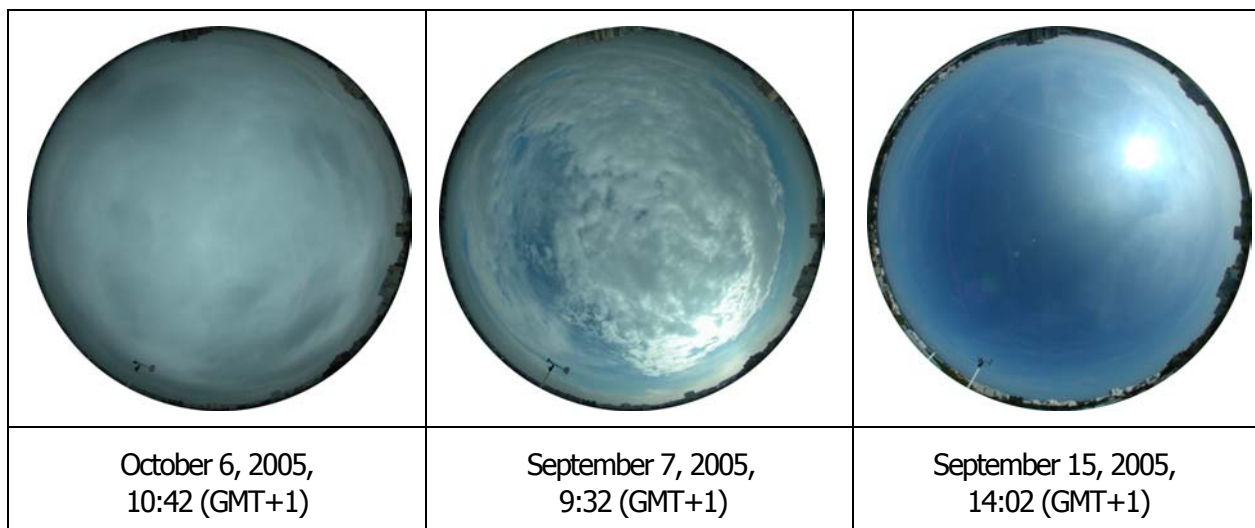


Fig. 3.1. Sample images for different sky types

#### 3.2 Transforming sky images to .05D files

To do the comparison between sky scans taken with sky scanner and fish-eye pictures it is necessary to transform sky images to the same data format as the sky scan data are. 145 averaged luminances extracted from the digital image were saved in the same format as the one used by the sky scanner.

Sky images were taken with two different digital cameras. The first one was Nikon Coolpix 5000 owned by ENTPE and the second one was also Nikon Coolpix 5000 but owned by FE (Faculty of Electrical engineering of University of Ljubljana).

After the fish-eye sky images were taken (Fig. 3.2a), the first step was to import them to Photolux and to calculate luminances (Fig. 3.2b). After the luminances were calculated we had to save them in an organized text format so we would be able to use them for next calculations.

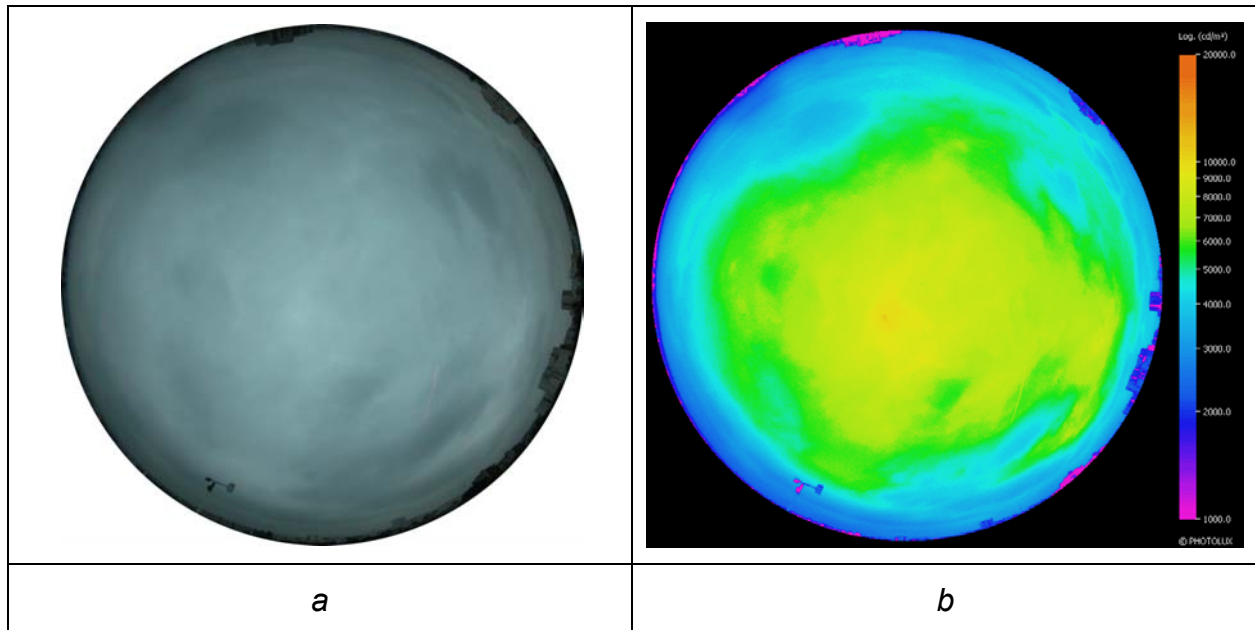


Fig. 3.2. Original image (a) and belonging to luminance map (b) for October 6<sup>th</sup>, 2005, 10:42 (GMT+1)

In Photolux calculated luminance values can be saved in different format. The most useful format is Genelux format. The whole sky luminance map is covered with a grid. The grid divides the luminance map into zones with practically the same solid angle. Density of a grid can be set between 1 degree and 30 degrees in zenith angle. Together with the density of the grid also the number of zones and size of a zone is changed (Table 3.1).

Table 3.1. Number of zones and solid angles with different Genelux grid.

Genelux grid [°]	1	2	3	5	6	10	15	30
<b>Number of zones</b>	20673	5181	2310	835	583	212	97	26
<b>Solid angle [sr]</b>	0.000304	0.001213	0.002720	0.007525	0.010777	0.029638	0.064775	0.241661

In the Genelux format the luminance values are listed in lines, with one luminance per line. In the same line there are also bordering azimuths and zenith angles (Fig. 3.3).

Cell#	Zenl Dg	ZenS Dg	Azil DgN->E	AziS DgN->E	SAngle Sr	Luminance Cd/m2
1	0.00	1.00	0.00	90.00	0.0002392	3813
2	0.00	1.00	90.00	180.00	0.0002392	3936
3	0.00	1.00	180.00	270.00	0.0002392	3926
4	0.00	1.00	270.00	360.00	0.0002392	3766
5	1.00	2.00	0.00	36.00	0.0002871	3863
6	1.00	2.00	36.00	72.00	0.0002871	3850
7	1.00	2.00	72.00	108.00	0.0002871	3892
8	1.00	2.00	108.00	144.00	0.0002871	3883
9	1.00	2.00	144.00	180.00	0.0002871	3857
10	1.00	2.00	180.00	216.00	0.0002871	3908
11	1.00	2.00	216.00	252.00	0.0002871	3900
12	1.00	2.00	252.00	288.00	0.0002871	3927
13	1.00	2.00	288.00	324.00	0.0002871	3751
14	1.00	2.00	324.00	360.00	0.0002871	3888

Fig. 3.3. Sample data from Genelux format file (with 1 degree grid)

Although we had the opportunity to save Photolux luminances also with CIE grid (145 sky zones), we did not use it because the camera was not perfectly in line with points of sky when taking pictures of sky. Since we were trying to get data as accurate as it was possible we decided to use the Genelux format with most dense grid: 1 degree. With this setting we exported Photolux luminances in Genelux files with 20673 luminance values, which were listed in lines together with bordering azimuths and zenith values (Fig. 3.3).

### 3.3 Linking sky scans and images from digital camera

When the image is taken with a digital camera and a fish-eye lens, the picture is turned upside down. The picture is the same as we would lie on the floor and we would be facing towards zenith. If our body is in line with north-south line and our head is facing north, then west is on our right side and east is on our left side. With the sky scanner is the opposite. Image taken with sky scanner has the correct orientation and points of a compass are in line with our understanding (North-top, South-bottom, East-right and West-left).

#### 3.3.1 Flipping and rotating an image

As it is seen from the paragraph above, all images taken with digital camera and fish-eye lens have to be horizontally flipped.

When the pictures were taken, the top of the camera was facing west, because this was the best way to get the camera in line with points of a compass, although it was not possible to get 100% in line. As we mentioned before, the top of the camera (and the picture) should be facing north.

Besides flipping the image, the image should also be rotated. To define the right angle of rotation, images of a certain day were compared with the position of sun on sunny days and with surroundings obstacles. Before the first images were taken, azimuths of some higher and observable obstacles were measured (Fig. 3.4).

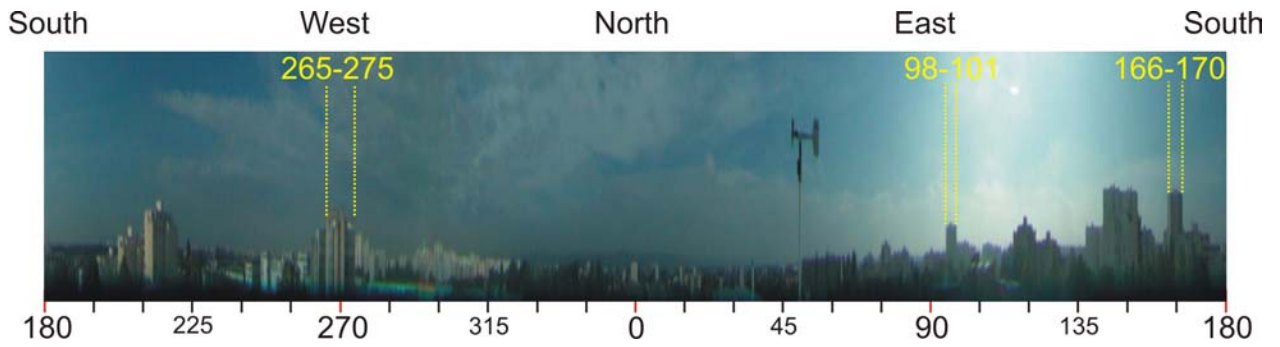


Fig. 3.4. Azimuths of some higher and observable obstacles

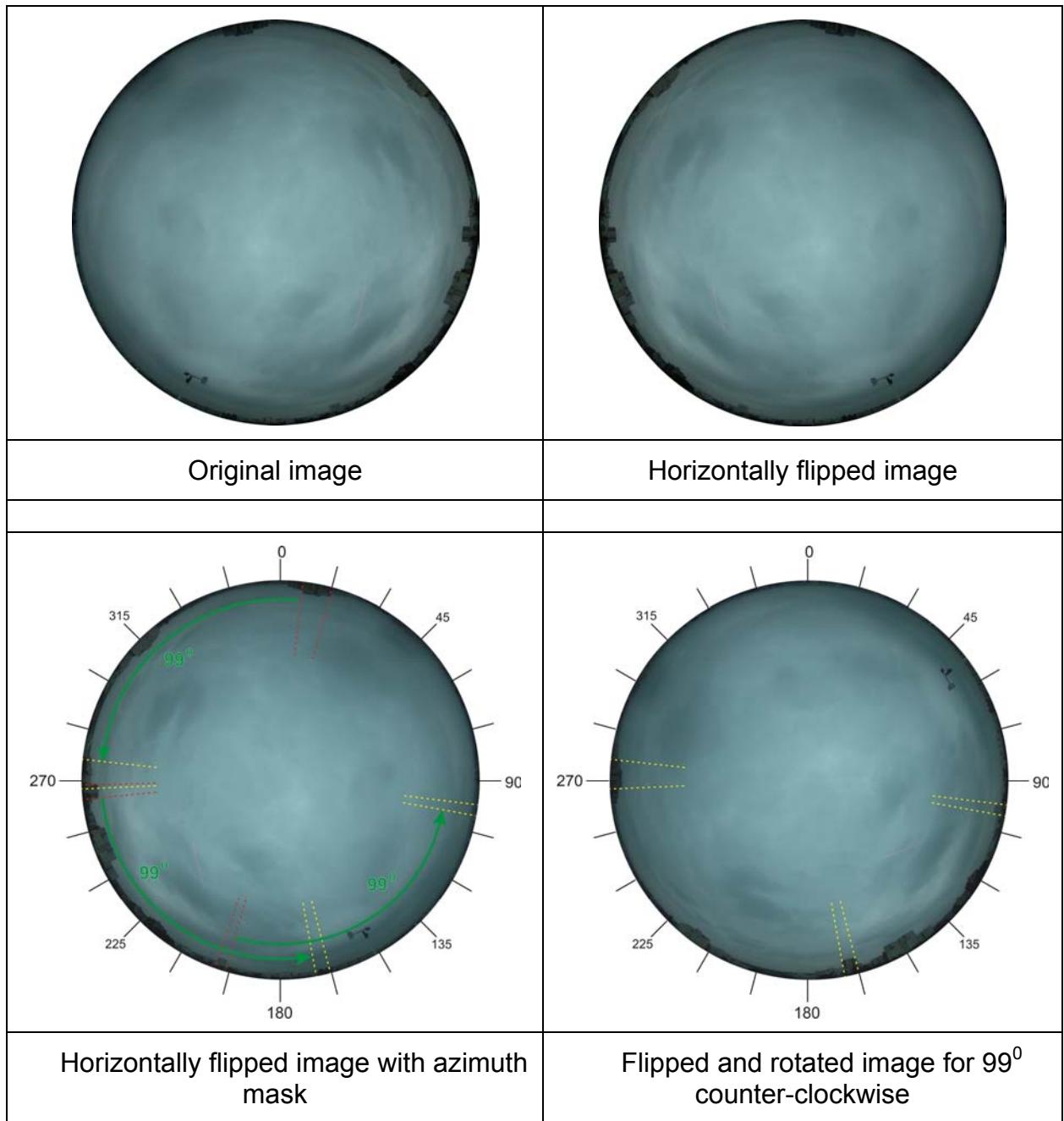


Fig. 3.5. Image transformation

Once the image is flipped and oriented a mask of 145 CIE patches has to be applied (Fig. 3.6). After the mask is applied, fields (calculation area) in Genelux grid have to be defined for all 145 sky scanner zones (Fig. 3.7).

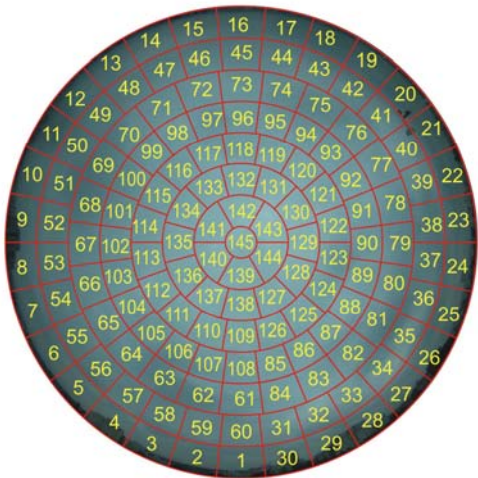


Fig. 3.6. Flipped and rotated digital image with applied sky scanner mask.

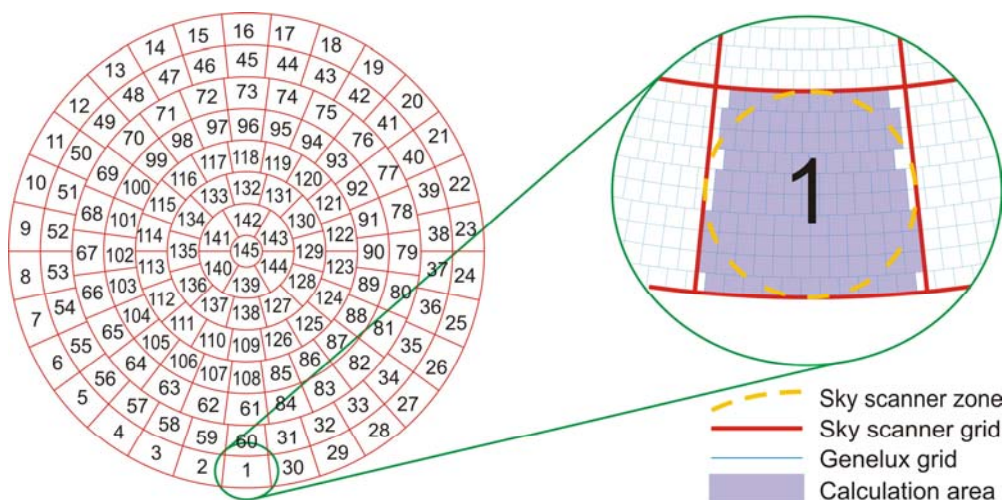


Fig. 3.7. Finding fields in Genelux grid for sky scanner zone number 1

When all zones from Genelux file that belong to one element in sky scanner grid are defined, an average luminance of all this Genelux zones is calculated. The calculated value represents luminance of a CIE sky patch derived with digital camera. The same procedure is used to define all 145 luminances of CIE grid.

When luminance values are calculated they are divided by factor  $k$  and calibration factor for camera and written in a .05D file, together with official beginning "0.000" and ending of the file "0.0070.010110.60.00005/10/0610:00:0510: 00:28LYON". In last part of the file there are also a date and time when picture was taken. Those data are saved in Genelux file and could be read out and saved in .05D file.

### 3.3.2 Flipping and rotating a sky scanner grid

Flipping an image and/or rotating an image in programs like Photoshop has irreparable consequences. When flipped and rotated file is saved, all information about the camera and exposure value are lost, what makes it impossible for use in Photolux. This is the reason why images are first handled in Photolux and then flipped and rotated. For further calculation also luminances in Genelux file should be "flipped and rotated". As it is almost impossible to flip and exactly rotate more than 20.000 luminances in Genelux file, it is easier to flip and rotate sky scanner grid. Flipped and rotated (Fig. 3.8) sky scanner grid can be applied when defining fields - calculation area for every sky scan zone.

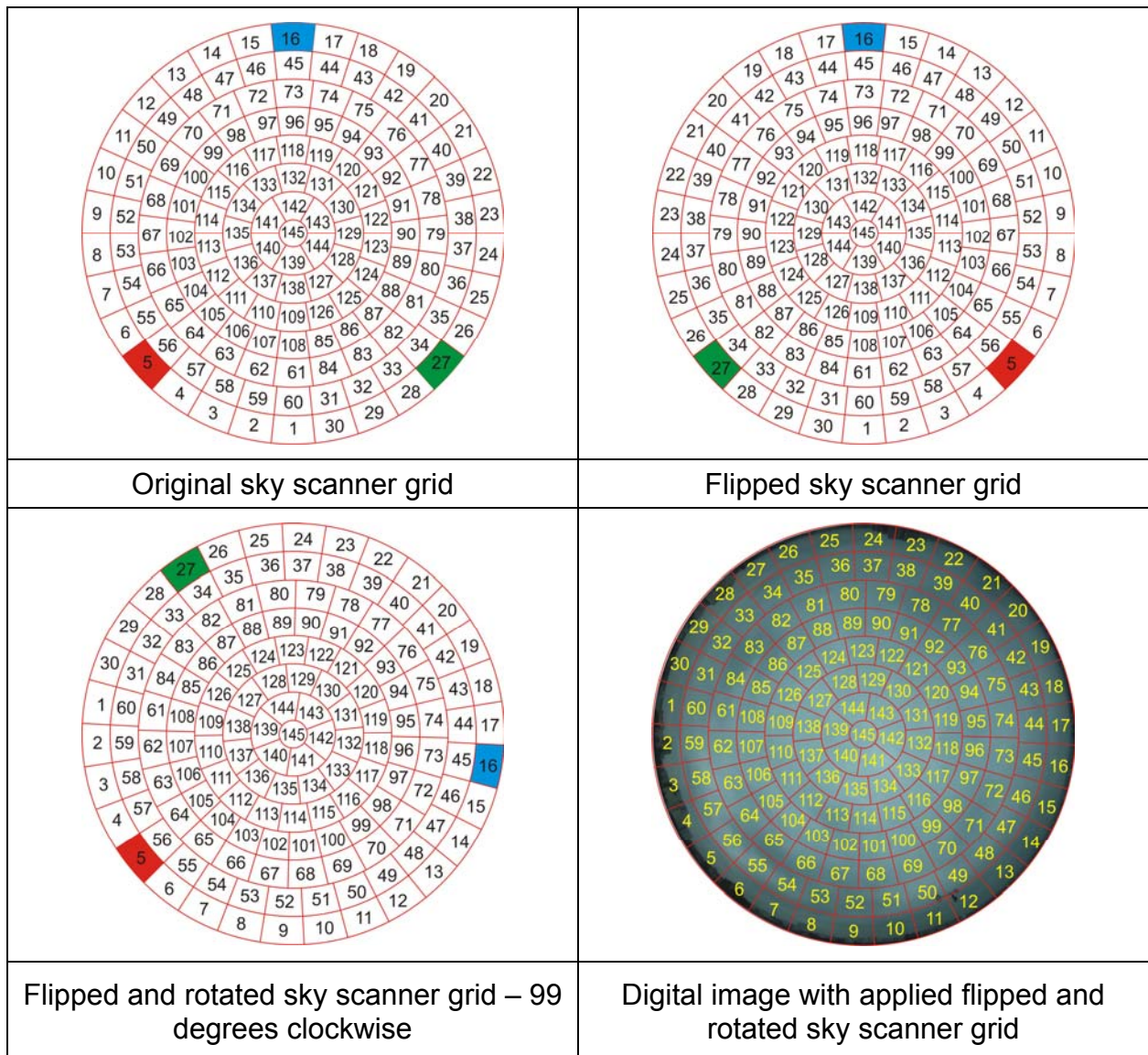


Fig. 3.8. Transformation of sky scanner grid

This procedure was used to get luminance of all 145 sky patches. The image was imported in Photolux, and luminance values were saved in Genelux format. At the end flipped and rotated sky scanner grid was applied and average luminances were calculated. Calculated luminance values were divided and written in .05D file as mentioned in previous chapter.

### 3.4 Comparing results derived with sky scanner and digital images

For evaluation purposes, we analyzed two sets of pictures. The first set consists of 112 digital images taken with ENTPE Nikon CoolPix 5000 camera on September 7<sup>th</sup>, 8<sup>th</sup>, 13<sup>th</sup>, 15<sup>th</sup>, 16<sup>th</sup> and October 6<sup>th</sup>, 2005. The second one consists of 48 digital images taken with FE Nikon CoolPix 5000 camera on November 30, December 1, 2 and 7.

With the software we developed and described in chapter 2, we did analysis of all 160 .05D files derived from digital images and later on compared results with sky scanner results (Fig. 3.9).

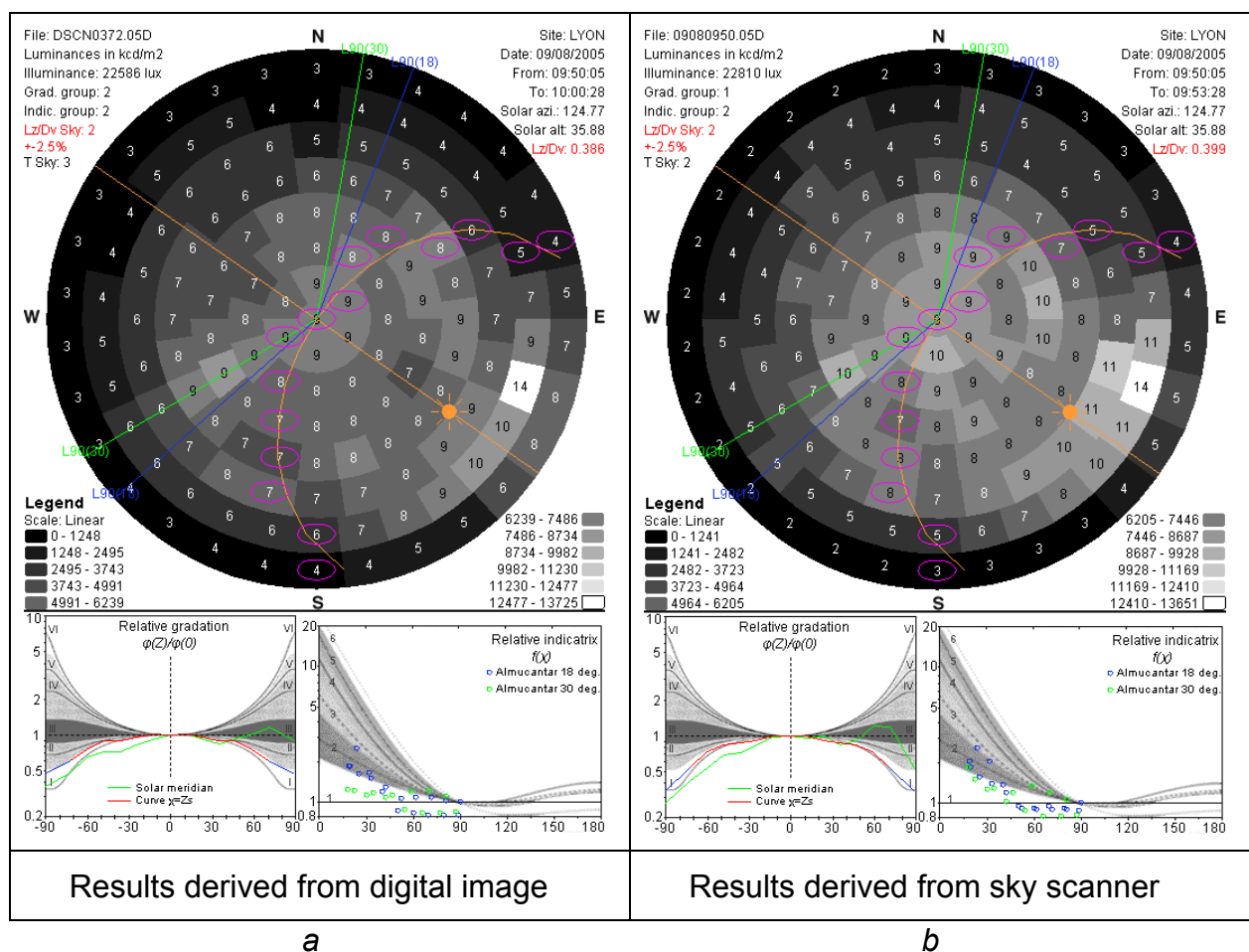


Fig. 3.9. Visualization of luminance distribution from digital image (a) and from sky scan (b)

For visualization we also processed digital image in a similar way that was presented in previous paragraph, only in false colors (Fig. 3.10).

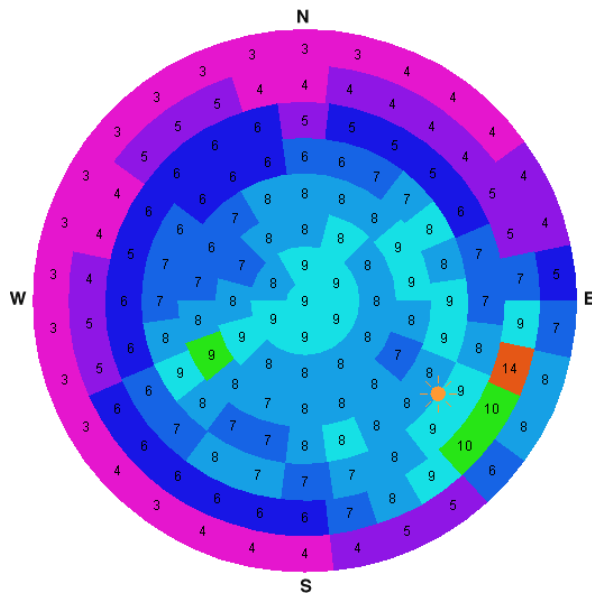


Fig. 3.10. Visualization of luminance distribution from digital image in false colors

For all 160 images we did comparison on all data derived from analysis (horizontal illuminance, four vertical illuminances, zenith luminance,  $L_z/D_v$  and 145 luminances of sky zones). Major differences in luminance values between digital images and sky scans were found on first almucantar (0-12 degrees). Differences on this almucantar are almost 3 times higher than on other almucantars (Fig. 3.11). The most probable reason for higher differences is the impact of the surroundings.

For further analysis luminances of sky zones with zenith angles higher than 78 degrees were eliminated. Most of those sky zones are at least partly covered with surrounding obstacles and we also eliminate them when we do analysis sky scanner data.

When creating .05D files we applied new factor  $k$  for each camera. The new value that was applied for ENTPE Nikon CoolPix 5000 camera was 15945.9 and it's 6,9% higher than the original value. The calculated average horizontal diffuse illuminance from digital image with the original value of factor  $k$  was 6.9 % higher than calculated horizontal diffuse illuminance from sky scans. Due to this we decided to change factor  $k$ . Due to the same reason new factor was applied also for FE Nikon CoolPix 5000 ( $k_{FE}=18018.9$ ).

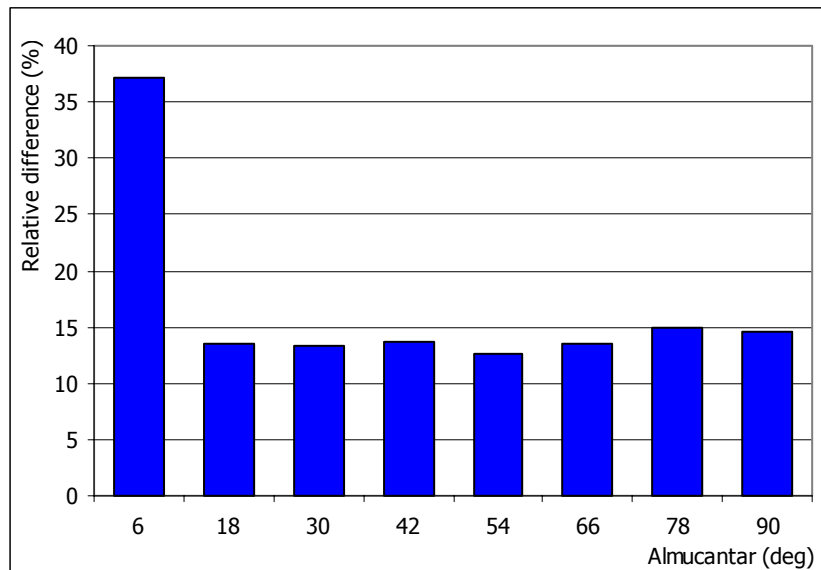


Fig. 3.11. Relative difference in luminances of sky zones on different almucantars.

Table 3.2. A sample comparison table for measurement on September 8<sup>th</sup>, 2005, 9:50 (GMT+1)

	Digital image	Sky scanner	Difference
Horizontal illuminance $lx$	22586	22810	- 0.98%
Zenith Luminance $cd/m^2$	8712	9100	+ 4.45%
Lz/Dv $cd/m^2 lx$	0.386	0.399	- 3.28%
Gradation	2	1	+1
Indicatrix	2	2	0
Lz/DV sky	2	2	0
Tregenza Sky	4	2	+2
115 sky zones luminance	Average difference		0.77 %
	RMS bias difference		8.63 %

For both sets of data we created tables with most important data (Table 3.2), and then summarized results from all tables like that in next tables (Table 3.3 and Table 3.4):

Table 3.3. Average and RMS bias differences for first set of measurements

	Average difference	RMS bias difference
Horizontal illuminance $lx$	+ 0.48 %	5.06 %
Zenith Luminance $cd/m^2$	+ 0.80 %	14.66 %
Lz/Dv $cd/m^2 lx$	+ 0.537 %	13.47 %
115 sky zones luminance	+ 3.25 %	13.42 %

Table 3.4. Average and RMS bias differences for second set of measurements

	Average difference	RMS bias difference
Horizontal illuminance $lx$	- 1.34 %	5.50 %
Zenith Luminance $cd/m^2$	- 4.60 %	9.51 %
Lz/Dv $cd/m^2 lx$	- 3.31 %	7.14 %
115 sky zones luminance	+ 2.66 %	8.82 %

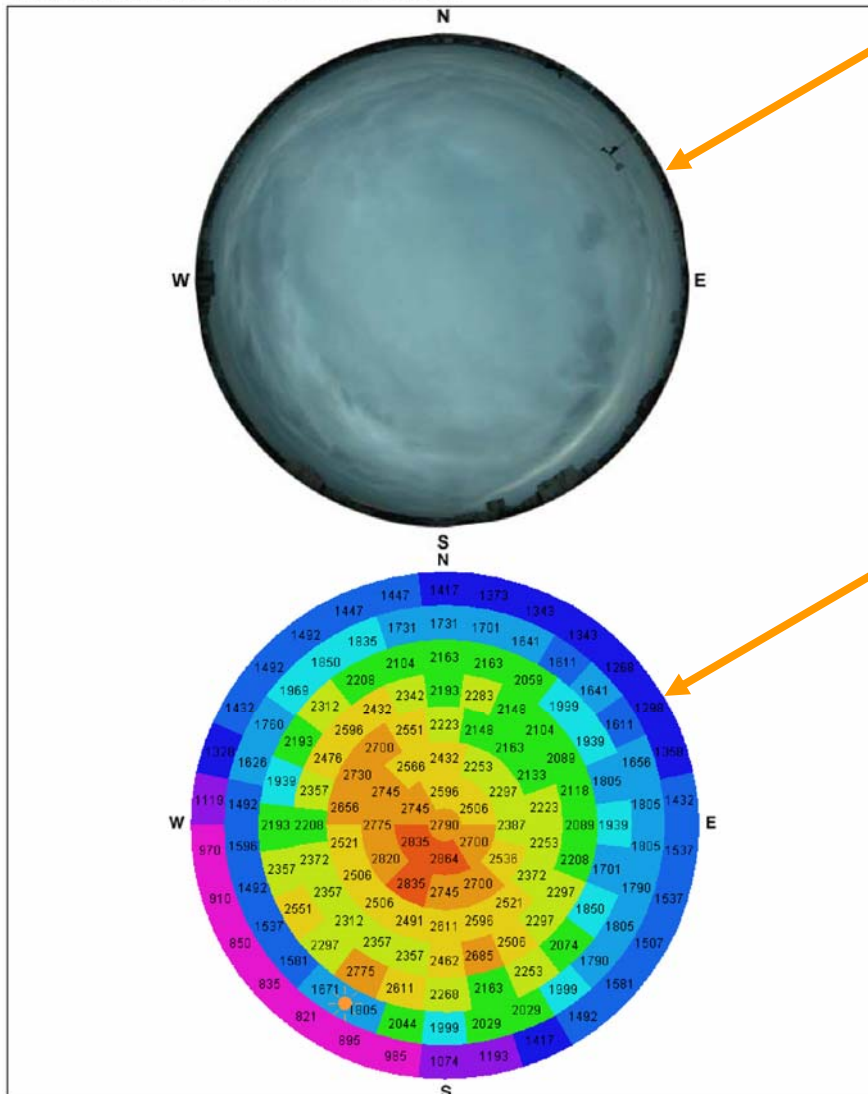
### 3.5 Database of sky luminance measurements

In the database we include all relevant data of the whole sky measurements and analysis of the measured values. The database consists of two pages for each measurement. On the first page, one can find a fish-eye image of the sky vault and false colour luminance map for 145 sky patches created with Photolux and procedure described in previous chapter. On the second page complete analysis of the sky scan, illuminance and luminance measurements and CIE sky type classification are presented

The measurements were carried out on September 7<sup>th</sup>, 8<sup>th</sup>, 13<sup>th</sup>, 15<sup>th</sup>, 16<sup>th</sup>, October 6<sup>th</sup>, November 30<sup>th</sup>, December 1<sup>st</sup>, 2<sup>nd</sup> and 7<sup>th</sup>. All together we performed 160 measurements. All measurements are collected in the database.

**November 30, 2005, 14:31 (GMT+1)**

**Fish-eye picture and luminance map**

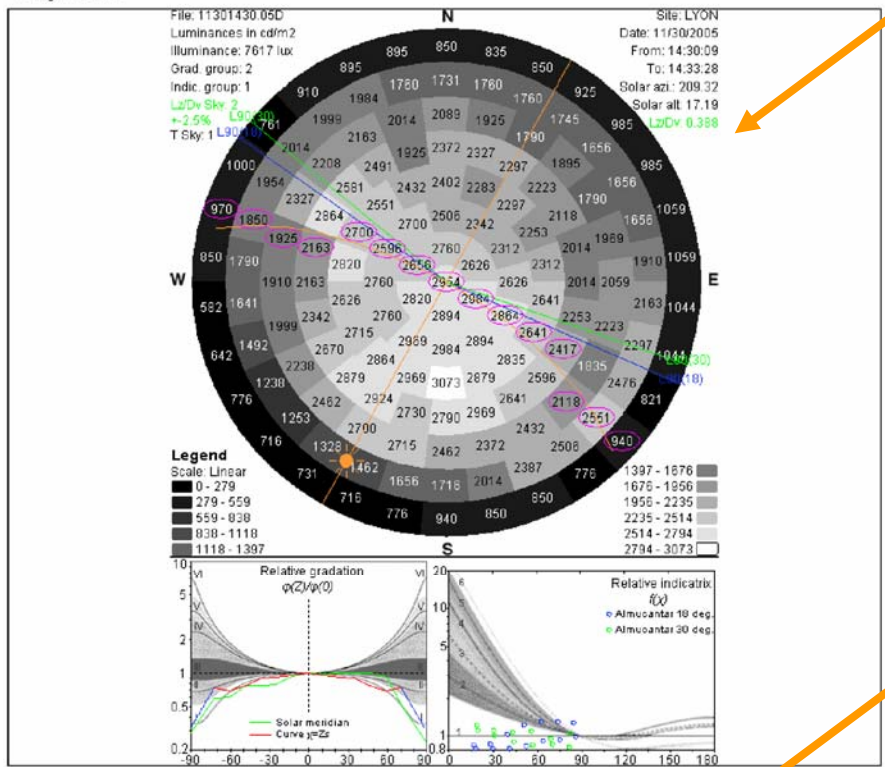


Fish-eye picture of a sky vault. Picture is taken at the start of sky scanner measurement.

False colour luminance map created from fish-eye image with a procedure described in previous chapter

**November 30, 2005, 14:30 (GMT+1)**

**Sky scan**



Complete analysis of the sky scanner measurement.

Global horizontal illuminance, diffuse horizontal illuminance, vertical illuminances (North, east, South, West), zenith luminance measured by the IDMP station.

**Whole sky measurements**

Time GMT+1	Gv lux	Dv lux	Gvn lux	Gve lux	Gvs lux	Gvw lux	Lz cd/m²	Tvl
14:30	7120	6966	2951	3011	3158	2891	2438	16.8
14:31	7040	6897	2901	2990	3158	2891	2282	16.9
14:32	6968	6829	2857	2970	3174	2862	2282	16.9
14:33	6877	6733	2808	2950	3158	2813	2360	16.7
14:34	6816	6665	2768	2939	3158	2774	2438	16.4

**CIE sky type classification (1 to 15)**

From sky scan			From whole sky measurements				
Indicatrices	Tregenza	Lz/Dv	Time	Lz/Dv	SI_Igawa	Igawa	Perez
3	1	2	14:30	3?	3	1	4
			14:31	4	1	1	4
			14:32	4	1	1	4
			14:33	3?	3	1	4
			14:34	3	3	1	4

CIE sky type classification based on three different methods (gradation/indicatrix method, Tregenza statistical method, LZ/Dv method) from sky scanner measurements (pink) and from Fish-eye image (blue).

Calculated CIE sky type with different sky models. Luminance values in models are based on global and diffuse horizontal irradiances from whole sky measurements (IDMP).

### **3.6 Conclusion on the use of digital images**

From those 160 comparisons, we can conclude that calibrated digital camera can be used as a sky scanner.

Use of digital cameras as sky scanners has some limitations. The most important limitation is weather. Digital camera can not be used in rain or snow since cameras are not water resistant. This problem could be solved with a special spherical glass cover which should cover the whole camera and fish-eye lens, but it should not have any impact of image received to the camera CCD.

The other and even more destructible problem is also connected with weather. The camera CCD sensor can be easily damaged if its sensor is exposed to direct sun light for a long time. The camera should be kept under protection screen in time between two pictures are taken or another type of camera should be used. Single-lens reflex (SLR) cameras have a different construction; their CCD is exposed to sunlight only when capturing the image. The SLR camera uses an automatic moving mirror system which permits the photographer to see exactly what will be captured by the film or digital imaging system, as opposed to non-SLR cameras where the view through the viewfinder could be significantly different from what was captured on film.



## 4 Sky luminance models

Sky models generate continuous sky luminance patterns. Researchers all over the world have tried to describe and to model sky luminance distribution for more than 100 years. The first measurements were performed by Schramm [48] in 1901, by Khaeler [11] in 1908 and by Kimball and Hand [12] in 1921. The measurements were performed under overcast skies and the gradual decrease of luminance from zenith to horizon in ratio between 1:0.5 to 1:0.3 was noted. Moon and Spencer [41] surveyed and arranged the previous research work and in year 1942 proposed luminance distribution of the overcast sky as a standard. The CIE has adopted a simplified version of the proposed standard as a CIE overcast sky only in year 1955.

Parallel to the measurements on overcast skies, in year 1929 Pokrowsky [48] found gradual increase in luminance from zenith to horizon in case of clear skies in ratio of 1:3.65 and more. On bases of work performed by Boldyrev [49] in year 1935 and Krat [50] in year 1943, Kittler [51] recommended standard clear sky in year 1967. Kittler's proposal was adopted in year 1973 as a CIE standard clear sky [52].

Since then several different approaches and concepts were used to describe sky luminance distribution under various intermediate skies.

In year 2003 CIE adopted a standard "Spatial distribution of daylight" [16], which is describing 15 different sky types (five overcast, five intermediate and five clear). In this chapter we describe three sky models that are mostly used to model sky luminance distribution from simple parameters such as irradiances. Irradiances (global and diffuse) are measured within IDMP stations or could be derived from the images of geostationary satellites [29] These satellites provide a continuous coverage of the earth, at least every half hour, at a spatial resolution of 5 km or less. For western and central Europe, this data is available on a Web server ([www.satel-light.com](http://www.satel-light.com)).

### 4.1 All weather model for sky luminance distribution - Perez

Model [14] is based on 5 different parameters, which are related to darkening or brightening of the horizon ( $a_p$ ), luminance gradient near the horizon ( $b_p$ ), relative intensity of the circumsolar region or solar aureole ( $c_p$ ), width of the circumsolar region ( $d_p$ ) and relative backscattered light ( $e_p$ ). This model is based on more than 16.000 all-sky scans recorded in Berkeley, California in years 1985 and 1986 which are covering a wide range of insolation conditions from overcast to clear through intermediate skies.

The model is given by next equation:

$$\frac{L}{L_z} = \frac{g(\gamma, \chi)}{g\left(\frac{\pi}{2}, \frac{\pi}{2} - \gamma_s\right)} \quad (4.1)$$

$$g(\gamma, \chi) = \left(1 + a_p \cdot \exp\left(\frac{b_p}{\sin \gamma}\right)\right) \cdot \left(1 + c_p \cdot \exp(d_p \cdot \chi) + e_p \cdot \cos^2 \chi\right) \quad (4.2)$$

Where  $a_p$ ,  $b_p$ ,  $c_p$ ,  $d_p$  and  $e_p$  are the distribution parameters and they describe atmospheric conditions. Parameters depend on sky brightness and sky clearness. Sky brightness and sky clearness are calculated from horizontal diffuse irradiance and normal incident direct irradiance with next equations:

$$\varepsilon = \frac{\frac{E_{es}}{E_{ed}} + 1 + 1.041Z_S^3}{1 + 1.041Z_S^3} \quad (4.3)$$

$$\Delta = \frac{m \cdot E_{ed}}{E_{es0}} \approx \frac{E_{ed}}{E_{es0} \cdot \cos(Z_S)} \quad (4.4)$$

where:

- $\varepsilon$  sky brightness
- $\Delta$  sky clearness
- $E_{ed}$  horizontal diffuse irradiance
- $E_{es}$  normal incident direct irradiance
- $Z_S$  solar zenith angle

Sky clearness and sky brightness describes two distinct characteristics of the atmosphere. The first one describes turbidity of a sky and the second one describes thickness of clouds.

Regarding sky clearness, eight categories of skies are described (Table 4.1).

*Table 4.1. Discrete sky clearness categories*

$\varepsilon$	category	Lower bound	Upper bound
1	Overcast	1.000	1.065
2		1.065	1.230
3		1.230	1.500
4		1.500	1.950
5		1.950	2.800
6		2.800	4.500
7		4.500	6.200
8	Clear	6.200	--

Distribution parameters are all calculated with equation of a same form. Next equation is an analytical form, using coefficient  $a_p$  as an example:

$$a_p = a_1(\varepsilon) + a_2(\varepsilon) \cdot Z_s + \Delta[a_3(\varepsilon) + a_4(\varepsilon) \cdot Z_s] \quad (4.5)$$

The terms  $a_i(\varepsilon)$  are discrete function of the parameter  $\varepsilon$  represented by eight-term vectors corresponding to each  $\varepsilon$  interval. Parameters  $a_i(\varepsilon)$  are given with a Table 4.2

Among all cases, there are only two exceptions. Those two exceptions are in the first  $\varepsilon$  interval for coefficients  $c_p$  and  $d_p$ . The functions for those two coefficients are:

$$c_p = \exp[(\Delta(c_1 + c_2 \cdot Z_s))^{c_3}] - c_4 \quad (4.6)$$

$$d_p = \exp[\Delta(d_1 + d_2 \cdot Z_s)] + d_3 - \Delta d_4 \quad (4.7)$$

Table 4.2. Model coefficients for Perez All weather model.

		<b>Sky clearness interval</b>							
$\varepsilon$	from	1.000	1.065	1.230	1.500	1.950	2.800	4.500	6.200
	to	1.065	1.230	1.500	1.950	2.800	4.500	6.200	-----
<b>Coefficients</b>									
$a_1$		1.3525	-1.2219	-1.1000	-0.5484	-0.6000	-1.0156	-1.0000	-1.0500
$a_2$		-0.2576	-0.7730	-0.2515	-0.6654	-0.3566	-0.3670	0.0211	0.0289
$a_3$		-0.2690	1.4148	0.8952	-0.2672	-2.5000	1.0078	0.5025	0.4260
$a_4$		-1.4366	1.1016	0.0156	0.7117	2.3250	1.4051	-0.5119	0.3590
$b_1$		-0.7670	-0.2054	0.2782	0.7234	0.2937	0.2875	-0.3000	-0.3250
$b_2$		0.0007	0.0367	-0.1812	-0.6219	0.0496	-0.5328	0.1922	0.1156
$b_3$		1.2734	-3.9128	-4.5000	-5.6812	-5.6812	-3.8500	0.7023	0.7781
$b_4$		-0.1233	0.9156	1.1766	2.6297	1.8415	3.3750	-1.6317	0.0025
$c_1$		2.8000	6.9750	24.7219	33.3389	21.0000	14.0000	19.0000	31.0625
$c_2$		0.6004	0.1774	-13.0812	-18.3000	-4.7656	-0.9999	-5.0000	-14.5000
$c_3$		1.2375	6.4477	-37.7000	-62.2500	-21.5906	-7.1406	1.2438	-46.1148
$c_4$		1.0000	-0.1239	34.8438	52.0781	7.2492	7.5469	-1.9094	55.3750
$d_1$		1.8734	-1.5798	-5.0000	-3.5000	-3.5000	-3.4000	-4.0000	-7.2312
$d_2$		0.6297	-0.5081	1.5218	0.0016	-0.1554	-0.1078	0.0250	0.4050
$d_3$		0.9738	-1.7812	3.9229	1.1477	1.4062	-1.0750	0.3844	13.3500
$d_4$		0.2809	0.1080	-2.6204	0.1062	0.3988	1.5702	0.2656	0.6234
$e_1$		0.0356	0.2624	-0.0156	0.4659	0.0032	-0.0672	1.0468	1.5000
$e_2$		-0.1246	0.0672	0.1597	-0.3296	0.0766	0.4016	-0.3788	-0.6426
$e_3$		-0.5718	-0.2190	0.4199	-0.0876	-0.0656	0.3017	-2.4517	1.8564
$e_4$		0.9938	-0.4285	-0.5562	-0.0329	-0.1294	-0.4844	1.4656	0.5636

## 4.2 ASRC - CIE

Perez et al [40] modified Matsuzawa's model to take into account the high turbid intermediate skies. This model is a linear combination of four skies - the CIE or Kittler clear sky, the Gusev turbid clear sky, the intermediate sky and the CIE overcast sky [23]. The coefficients of linear combination are computed using the sky clearness and the sky brightness factors [40, 29].

**for  $\varepsilon \leq 1.2$ :**

$$\frac{L}{L_z} = (1-a) \left( \frac{L}{L_z} \right)_{CIE-Overcast} + a \left( \frac{L}{L_z} \right)_{Intermediate} \quad (4.8)$$

$$\text{where: } a = \min \left\{ 1, \max \left[ 0, \frac{\varepsilon - 1}{0.2}, \frac{\Delta - 0.05}{0.4} \right] \right\} \quad (4.9)$$

**for  $1.2 < \varepsilon \leq 3.0$ :**

$$\frac{L}{L_z} = (1-b) \left( \frac{L}{L_z} \right)_{Intermediate} + b \left( \frac{L}{L_z} \right)_{Clear-Gusev} \quad (4.10)$$

$$\text{where: } b = \frac{\varepsilon - 1.2}{1.8} \quad (4.11)$$

**for  $3.0 < \varepsilon$ :**

$$\frac{L}{L_z} = (1-c) \left( \frac{L}{L_z} \right)_{Clear-Gusev} + c \left( \frac{L}{L_z} \right)_{Clear-Kittler} \quad (4.12)$$

$$\text{where: } c = \min \left\{ 1, \frac{\varepsilon - 3}{3} \right\} \quad (4.13)$$

## 4.3 Igawa All sky model

This model is the most recent one and it was introduced in 2004 on basis of previous models for sky luminance and radiance from Matsuzawa, Igawa and Nakamura. Model was tested on IDMP data for Tokyo and Fukuoka [39].

Also in this model, the input data are irradiances from IDMP or any other weather station and zenith angle of the sun. Similar to other models, also in this case model we

have two parameters which describe atmosphere conditions. First parameter is **clear sky index**, which is defined with next equation:

$$K_c = \frac{E_{eg}}{S_{eeg}} \quad (4.14)$$

Where:

- $K_c$  clear sky index,  
 $E_{eg}$  global irradiance,  
 $S_{eeg}$  standard global irradiance.

Standard global irradiance is a global irradiance of clear sky with TL (turbidity) of 2.5, and therefore defined with next equation:

$$S_{eeg} = \frac{0.84 \cdot E_{e0}}{m} \cdot \exp(-0.0675 \cdot m) \quad (4.15)$$

Where:

- $E_{e0}$  extraterrestrial direct normal irradiance,  
 $m$  relative optical mass.

The relative optical mass can be calculated with next equation:

$$m = \frac{1}{\cos(Z_s) + 0.50572 \cdot (96.07995 - Z_s)^{-1.6364}} \approx \frac{1}{\cos(Z_s)} \quad (4.16)$$

Second parameter is **cloudless index**. Since the lower bound values of the cloud ratio (4.17) appear in the clear sky and depend on the solar altitude, an index without solar altitude dependency is needed.

$$C_e = \frac{E_{ed}}{E_{eg}} \quad (4.17)$$

Where:

- $C_e$  cloud ratio,  
 $E_{ed}$  horizontal diffuse irradiance.

The cloudless indices of all the solar altitude are almost in the range from 1 to 0 though they vary a little when the solar altitude is low. The cloudless index proposed here can be used as the index without solar altitude dependency to classify sky conditions from clear sky to overcast sky, and can be calculated with next equation:

$$C_{le} = \frac{1 - C_e}{1 - C_{es}} \quad (4.18)$$

Where:

$C_{le}$  cloudless index,  
 $C_{es}$  standard cloud ratio.

Standard cloud ratio is a cloud ratio with TL of 2.5 and can be obtained with next equation:

$$C_{es} = 0.01299 + 0.07698 \cdot m - 0.003857 \cdot m^2 + 0.0001054 \cdot m^3 - 0.000001031 \cdot m^4 \quad (4.19)$$

With this two parameters sky conditions are given and sky luminance distribution can be calculated with equation that is the same as for CIE sky, only gradation and indicatrix functions are different and they are depended on the sky index.

$$L_{a-rel} = \frac{L_\alpha}{L_Z} = \frac{f(\chi) \cdot \varphi(Z)}{f(Z_s) \cdot \varphi(0)} \quad (4.20)$$

$$\varphi(Z) = 1 + a' \cdot \exp\left(\frac{b'}{\cos Z}\right) \quad (4.21)$$

$$f(\chi) = 1 + c' \cdot \left[ \exp(d' \chi) - \exp\left(d' \frac{\pi}{2}\right) \right] + e' \cdot \cos^2 \chi \quad (4.22)$$

In gradation and indicatrix functions parameters a, b, c, d and e are chosen from the table with 15 sky types, on the other hand in Igawa model, the parameters a', b', c', d' and e' are obtained as a function of the sky index and calculated with next equations:

$$\begin{aligned} a' &= \frac{4.5}{1 + 0.15 \cdot \exp(3.4 \cdot Si)} - 1.04 \\ b' &= \frac{-1}{1 + 0.17 \cdot \exp(1.3 \cdot Si)} - 0.05 \\ c' &= 1.77 \cdot (1.22 \cdot Si)^{3.56} \cdot \exp(0.2 \cdot Si) \cdot (2.1 - Si)^{0.8} \\ d' &= \frac{-3.05}{1 + 10.6 \cdot \exp(-3.4 \cdot Si)} \end{aligned} \quad (4.23)$$

$$e' = \frac{0.48}{1 + 245 \cdot \exp(-4.13 \cdot Si)}$$

where:

$Si$             sky index

The sky index is defined as a sum of the clear sky index and the root of the cloudless index:

$$Si = K_C + C_{le}^{0.5} \tag{4.24}$$

#### **4.4 Comparison of sky luminance models**

For all the times when we have measurements from sky scanner, we modelled sky luminance distribution of 145 sky patches with Perez All weather model, ASRC CIE model and Igawa model. Modelled luminances were compared to luminances measured with sky scanner and differences have been calculated. Sky luminance distributions in all models were calculated based on models equations and irradiance measurements from IDMP station.

To define the quality of a model, mean bias differences (MBD) and root mean square differences (RMSD), both in absolute values and in relative values have been calculated.

In the first step, calculations were performed on all 145 sky patches. In the second step we eliminated from calculation, patches with scattering angle less than  $15^{\circ}$ . And in the third step we eliminated from calculation patches on first almucantar because surrounding obstacles and patches with scattering angle less than  $15^{\circ}$ .

Sky luminance models are not capable to predict very high luminances in direction of sun and around it, practically the models are not taking into account sun luminance. Although the sky scanner measuring head is not capable to measure very high luminances in direction of sun and around it, differences between measured luminances and luminances predicted with models were very high. This was the reason why patches with scattering angles less than  $15^{\circ}$  were eliminated from calculation. With elimination of sky patches around sun, RMSD was extremely lowered. A sample case is shown for September 15, 2005 at 14:10, when sky was without a cloud (Fig. 4.1)

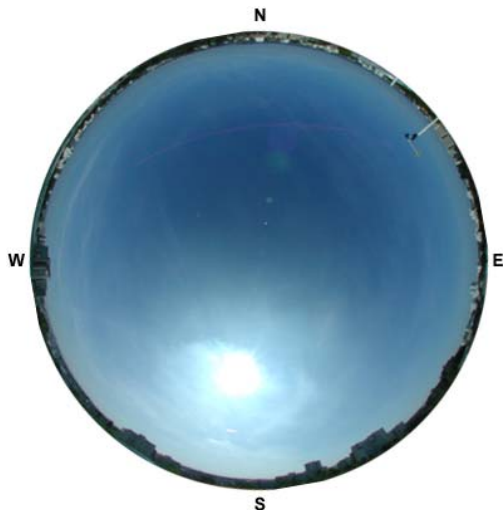


*Fig. 4.1. Fish-eye image of sky hemisphere on September 15, 2005 at 14:10*

For this case RMSD was first calculated taking into account all sky patches and latter with eliminated one and two and so on up to 8 eliminated patches around sun. Calculated RMSD are collected in Table 4.3 and presented in Fig. 4.2. Sky patches luminance profile for all sky patches (also the ones in solar corona) is plotted on Fig. 4.3

and for all sky patches except the ones with  $\chi < 15^\circ$  on Fig. 4.4. In the same way we calculated MBD for both cases, results are presented on Fig. 4.5 and Fig. 4.6.

From luminance profiles, it is seen that values measured with sky scanner in direction of sun ( $149 \text{ kcd/m}^2$ ) are up to 800 % higher than predicted luminance values with model (Perez-All weather:  $26.5 \text{ kcd/m}^2$ , Igawa:  $24.3 \text{ kcd/m}^2$ , ASRC-CIE:  $22.9 \text{ kcd/m}^2$ ).

From this case it is seen that it is essential to eliminate patches around sun from calculation of MBD and RMSD.

As it can be read from Fig. 4.6 all three sky luminance models overestimate luminance on first almucantar (Zenith angle of centre of patches on this almucantar is  $84^\circ$ ). Especially with clear skies, which in case of September 15, 2005 at 14:10 is, the horizon is brighter than zenith. Unfortunately around sky scanner there are surrounding obstacles in this almucantar and luminances of the obstacles are lower that the luminance of the horizon.

Table 4.3. RMSD depending on number of eliminated patches around sun (for September 15, 2005 at 14:10)

Sky luminance Model	Root mean square difference $\text{cd/m}^2$								
	Number of eliminated patches ( $\chi$ )								
	0 ( $0^\circ$ )	1 ( $3^\circ$ )	2 ( $10^\circ$ )	3 ( $12.6^\circ$ )	4 ( $13^\circ$ )	5 ( $14^\circ$ )	6 ( $15^\circ$ )	7 ( $16^\circ$ )	8 ( $19^\circ$ )
Perez-All Weather	10797.8	3578.8	3511.7	3136.8	3137.7	2794.8	2338.3	2337.9	2256.0
Igawa	10909.1	3391.0	3277.4	2836.2	2836.6	2460.0	1913.5	1916.4	1854.5
ASRC-CIE	11058.6	3535.0	3396.9	2963.9	2944.8	2550.8	2023.3	2009.0	1914.1

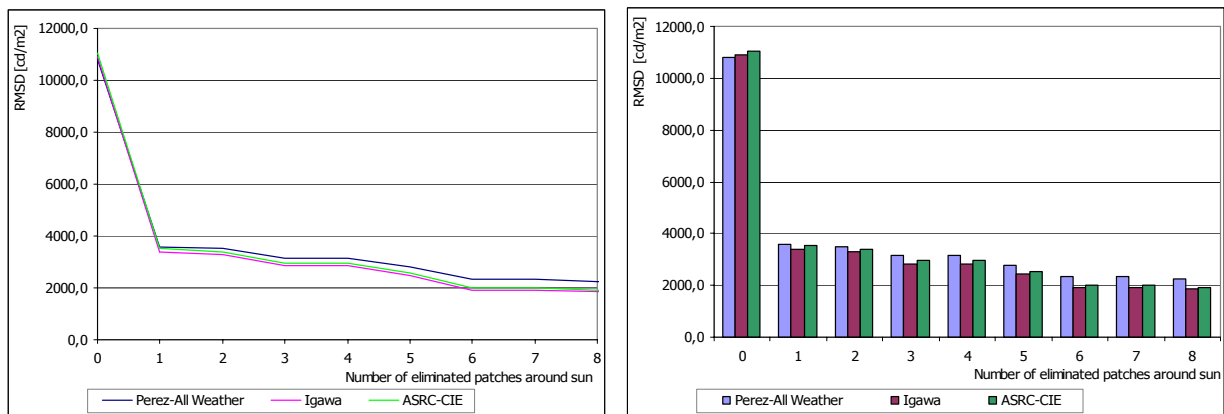


Fig. 4.2. RMSD depending on number of eliminated patches around sun (for September 15, 2005 at 14:10)

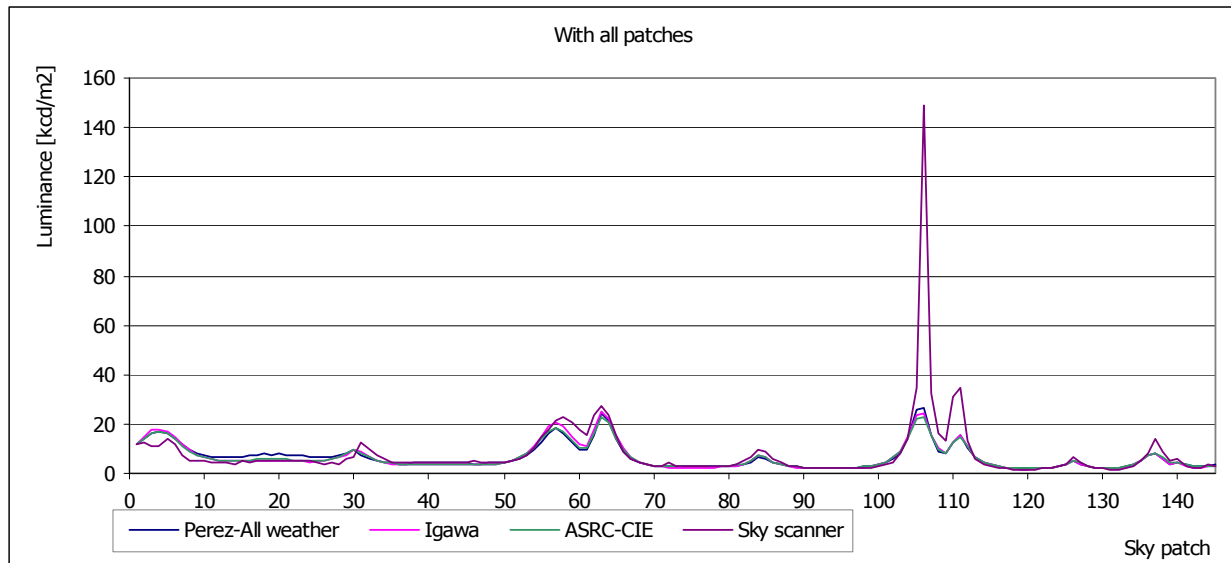


Fig. 4.3. Sky patches luminance profile for all sky patches (for September 15, 2005 at 14:10)

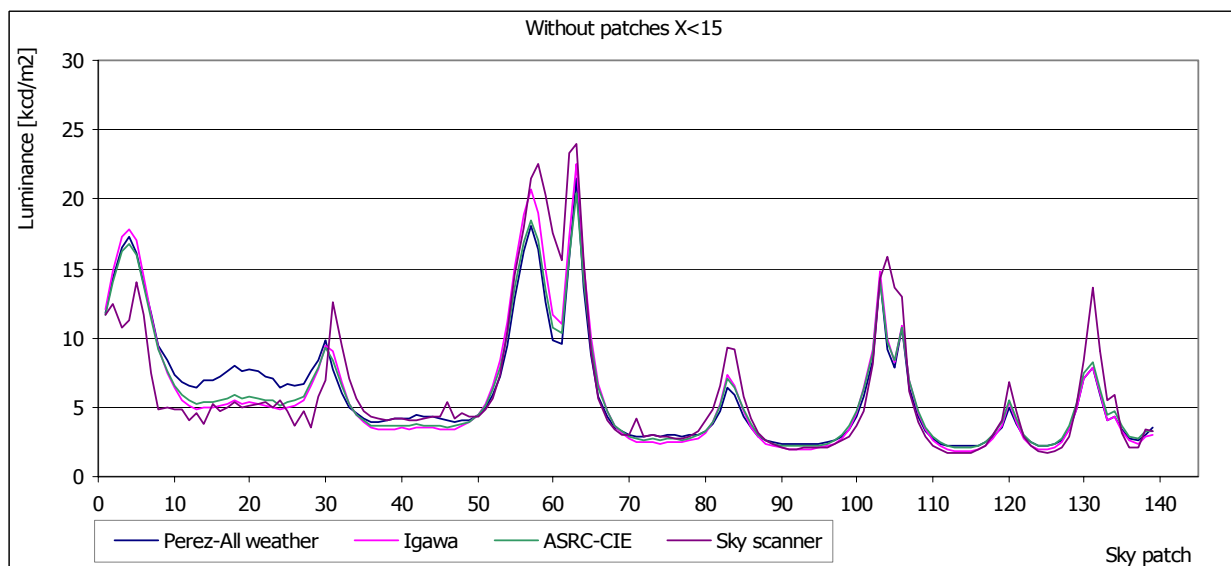


Fig. 4.4. Sky patches luminance profile for all sky patches except the ones with  $\chi < 15^0$  (for September 15, 2005 at 14:10)

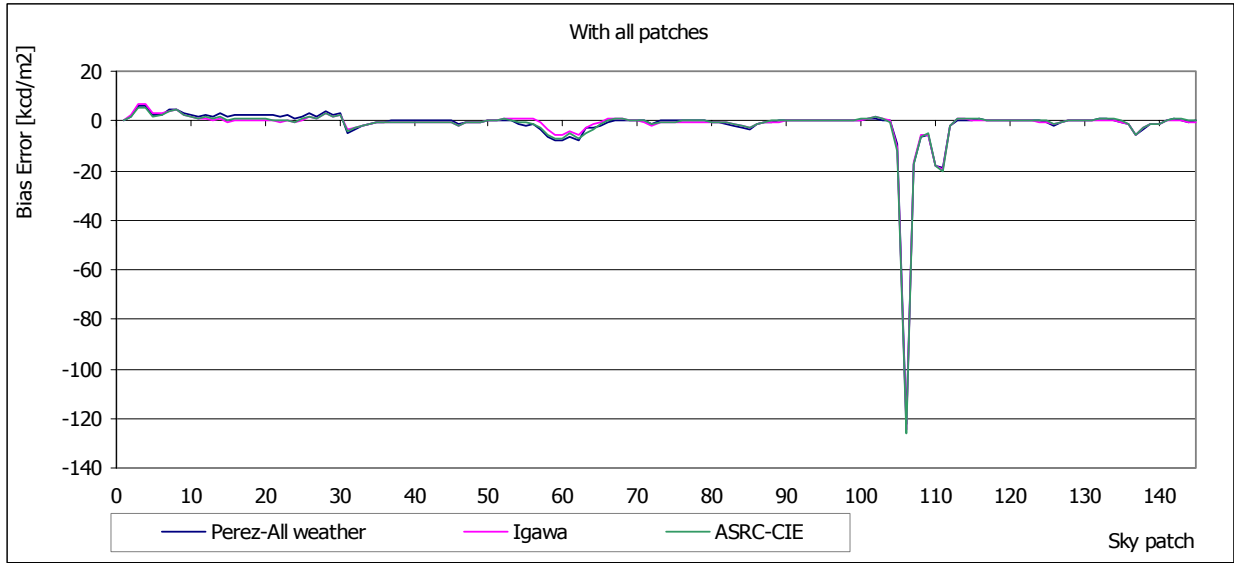


Fig. 4.5. Bias Error for all sky patches (for September 15, 2005 at 14:10)

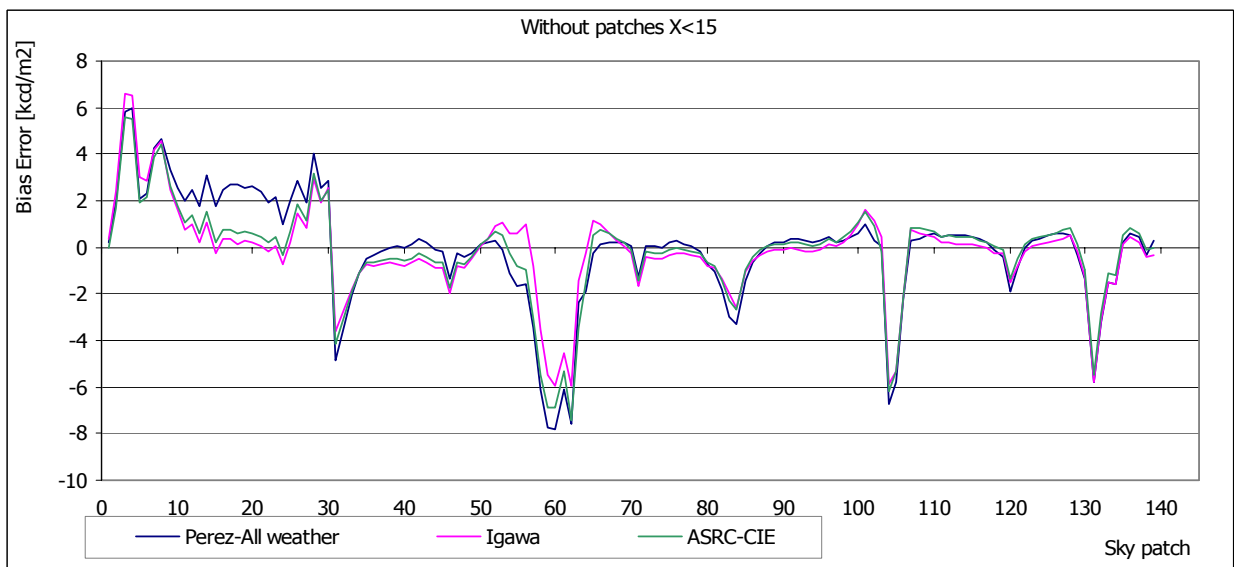


Fig. 4.6. Bias Error for all sky patches except the ones with  $\chi < 15^\circ$  (for September 15, 2005 at 14:10)

In the first step for mean bias differences next equation was used (a sample for Igawa model):

$$mbd_{Igawa} = \frac{1}{145} \sum_{p=1}^{145} (L_{pIgawa} - L_{pSS}) \quad (4.25)$$

Where:

$mbd_{Igawa}$  mean bias difference between Igawa model and sky scanner measurement,

$L_{pIgawa}$  luminance of a patch in Igawa model,

$L_{pSS}$  luminance of a patch measured with sky scanner.

In the second (and third) step for mean bias differences next equation was used (a sample for Igawa model):

$$mbd_{Igawa}' = \frac{1}{n_{X<15}} \sum_{p=1}^{n_{X<15}} (L_{pIgawa} - L_{pSS}) \quad (4.26)$$

Where:

$mbd_{Igawa}'$  mean bias difference between Igawa model and sky scanner measurement without elements on first almucantar and without element with  $\chi < 15^0$

$n_{X>15}$  Number of patches with scattering angle larger than 15 degrees

In the first step for root mean square differences next equation was used (a sample for Igawa model):

$$rmsd_{Igawa} = \sqrt{\frac{1}{145} \sum_{p=1}^{145} (L_{pIgawa} - L_{pSS})^2} \quad (4.27)$$

Where:

$rmsd_{Igawa}$  root mean square difference between Igawa model and sky scanner measurement,

In the second step for root mean square differences next equation was used (a sample for Igawa model):

$$rmsd_{Igawa}' = \sqrt{\frac{1}{n_{X<15}} \sum_{p=1}^{n_{X<15}} (L_{pIgawa} - L_{pSS})^2} \quad (4.28)$$

Where:

$rmsd_{Igawa}'$  root mean square difference between Igawa model and sky scanner measurement and without elements on first almucantar and without element with  $\chi < 15^0$

In all cases also relative differences were calculated. Relative differences were obtained with normalization of absolute differences with luminance of sky patches measured with sky scanner.

#### 4.4.1 Results of comparison - all cases

Comparisons were done on 13006 cases dating from May 18, 2005 to December 9, 2005. Results are gathered in next tables:

Table 4.4. MBD for the whole sky hemisphere, for the sky hemisphere without sky patches with  $\chi < 15^\circ$  and for the sky hemisphere without 6 degree almucantar and without sky patches with  $\chi < 15^\circ$

Sky luminance Model	Mean bias difference [cd/m <sup>2</sup> ]		
	All patches	Without sky patches with $\chi < 15^\circ$	Without sky patches on 6 <sup>o</sup> almucantar and $\chi < 15^\circ$
Igawa	-1441.18	-422.91	-742.73
ASRC-CIE	-1472.40	-429.89	-713.60
Perez-All weather	-1356.70	-387.80	-778.87

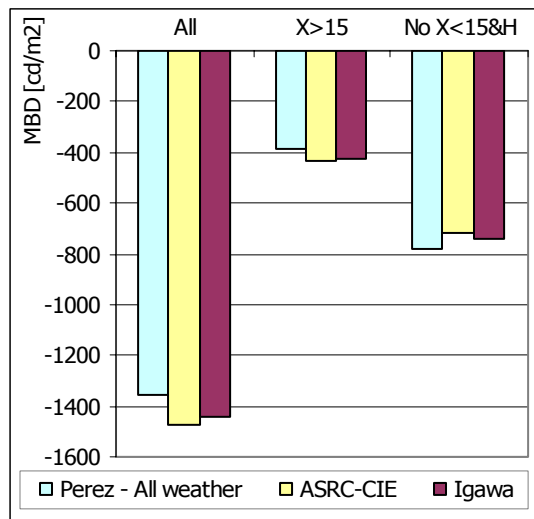


Fig. 4.7. MBD for the whole sky hemisphere, for the sky hemisphere without sky patches with  $\chi < 15^\circ$  and for the sky hemisphere without 6 degree almucantar and without sky patches with  $\chi < 15^\circ$

In our case mean bias difference does not show the real situation and the results (Fig. 4.7) could mislead us if we would trust them without any reflection. The results are misleading because they show that calculations with sky patches on the 6<sup>o</sup> almucantar give better results than calculations without them. Since there are obstacles around IDMP station the sky scanner is not measuring sky patches on the 6<sup>o</sup> almucantar, but it is measuring luminances of façades of surrounding buildings. In most cases, especially on sunny days, luminances measured with the sky scanner are lower than the true sky luminances. This fact can be observed on Fig. 4.3 and Fig. 4.4, where sky scanner luminance for first 30 sky patches (6 degree almucantar) are practically always under modelled luminances. Modelled values can be treated as true values, measurements

performed with sky scanner are underestimating luminance values because the surrounding obstacles. For almost all 30 sky patches on first almucantar the bias difference is positive (Fig. 4.6) while on the other hand for the most of the rest sky elements the difference is negative (sky models underestimate sky luminance). If we calculate mean bias difference with all sky patches the values is lower (because of the above mentioned fact) compared with the one when taking into account sky elements without horizon (6 degree almucantar). Since we are aware of problems regarding surrounding buildings, we can conclude that MBD cannot be trusted and we should move to RMSD.

Table 4.5. RMS differences for the whole sky hemisphere, for the sky hemisphere without sky patches with  $\chi < 15^\circ$  and for the sky hemisphere without 6 degrees almucantar and without sky patches with  $\chi < 15^\circ$

Sky luminance Model	Root mean square difference [cd/m <sup>2</sup> ]		
	All patches	Without sky patches with $\chi < 15^\circ$	Without sky patches on 6 <sup>o</sup> almucantar and $\chi < 15^\circ$
Igawa	9185.39	2335.20	2215.03
ASRC-CIE	9231.04	2240.76	2194.44
Perez-All weather	9016.78	2240.55	2227.75

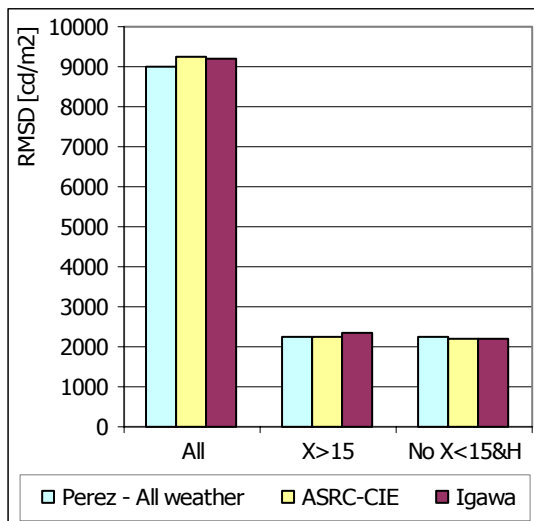


Fig. 4.8. RMS differences for the whole sky hemisphere, for the sky hemisphere without sky patches with  $\chi < 15^\circ$  and for the sky hemisphere without 6 degrees almucantar and without sky patches with  $\chi < 15^\circ$

RMSD is more trustful, since problems with averaging the bias difference are eliminated. From Fig. 4.8 it can be read that the best results are obtained with elimination of first 30 sky patches and patches with scattering angle less than  $15^\circ$ .

Table 4.6. Relative MBD for the whole sky hemisphere, for the sky hemisphere without sky patches with  $\chi < 15^\circ$  and for the sky hemisphere without 6 degree almucantar and without sky patches with  $\chi < 15^\circ$

Sky luminance Model	Relative MB difference [%]		
	All patches	Without sky patches with $\chi < 15^\circ$	Without sky patches on $6^\circ$ almucantar and $\chi < 15^\circ$
Igawa	-20.36	-9.22	-14.11
ASRC-CIE	-20.38	-8.92	-13.57
Perez-All weather	-16.99	-6.48	-14.45

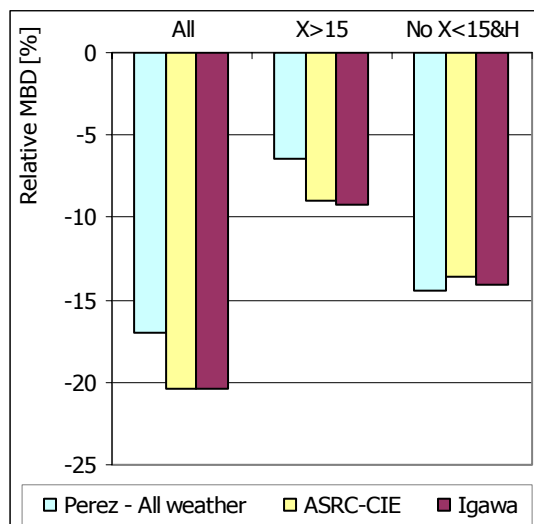


Fig. 4.9. Relative MBD for the whole sky hemisphere, for the sky hemisphere without sky patches with  $\chi < 15^\circ$  and for the sky hemisphere without 6 degree almucantar and without sky patches with  $\chi < 15^\circ$

Table 4.7. Relative RMSD for the whole sky hemisphere, for the sky hemisphere without sky patches with  $\chi < 15^\circ$  and for the sky hemisphere without 6 degree almucantar and without sky patches with  $\chi < 15^\circ$

Sky Model	luminance	Relative RMS difference [%]		
		All patches	Without sky patches with $\chi < 15^\circ$	Without sky patches on $6^\circ$ almucantar and $\chi < 15^\circ$
Igawa		128.02	42.75	40.03
ASRC-CIE		128.78	41.02	40.03
Perez-All weather		127.38	41.02	40.88

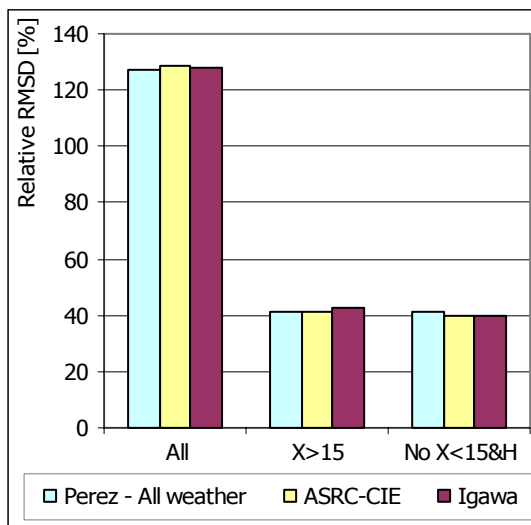


Fig. 4.10. Relative RMSD for the whole sky hemisphere, for the sky hemisphere without sky patches with  $\chi < 15^\circ$  and for the sky hemisphere without 6 degree almucantar and without sky patches with  $\chi < 15^\circ$

Comparison of relative values of MB and RMS difference give practically the same results as comparison of absolute values. If we look at relative MB (Fig. 4.9), we get the best results with elimination of sky patches with scattering angle less than  $15^\circ$ . Since we have the same situation as for absolute values, we know that those results cannot be trusted and we should not ground any further decision on them. On the other hand the relative RMS difference results are more trustful and they suggest eliminating patches on first almucantar and those with scattering angle less than  $15^\circ$ .

If we consider all measurements with all sky patches except the ones with scattering angle below  $15^\circ$ , than only Igawa model deviate from ASRC-CIE and Perez All weather model. From all measurements we can conclude that both ASRC-CIE and Perez All weather model lead to same results and to practically same RMS difference (Table 4.8) between modelled and measured values.

Table 4.8. RMS difference for three sky luminance models

Sky luminance Model	RMS difference cd/m <sup>2</sup>	Relative RMS difference [%]
Igawa	2335.20	42.75
ASRC-CIE	2240.76	41.02
Perez-All weather	2240.55	41.02
Mean luminance: 5462.74 cd/m <sup>2</sup>		

#### 4.4.2 Results of comparison dependent on CIE sky type

When sky scanner data were processed, also a CIE sky type was determined. CIE sky type was defined on three methods, the first one was based on gradation on indicatrix group, the second one was based on Tregenza statistical method and the third was based on Lz/Dv ratio.

In this chapter we are analysing relative RMS difference between sky luminance models for each CIE sky type. Since it is possible to analyse all sky scanner measurements only with the first two methods, we decided to gather sky scanner measurements in groups of CIE sky types only for method based on gradation and indicatrix group and on Tregenza statistical method. After the groups were formed for both methods, RMS difference was calculated for all groups of CIE sky types. Results based on gradation/indicatrix method for hemisphere without 6 degree almucantar and without sky patches with scattering angle below 15° are gathered in Table 4.9 and presented on Fig. 4.11, and in Table 4.10 and on Fig. 4.12, for the whole sky hemisphere without sky patches with scattering angle below 15°. Results based on Tregenza statistical method for hemisphere without 6 degree almucantar and without sky patches with scattering angle below 15° are gathered in Table 4.11 and presented on Fig. 4.13. In Table 4.12 and on Fig. 4.14 are gathered results for statistical method for the whole sky hemisphere without sky patches with scattering angle below 15°.

Table 4.9. Relative RMS differences for different CIE sky types (based on gradation and indicatrix) for the sky hemisphere without 6 degree almucantar and without sky patches with  $\chi < 15^\circ$

Sky luminance Model	Relative RMS difference for hemisphere without 6 deg. almucantar and without sky patches with $\chi < 15^\circ$ [%]														
	CIE Sky type (based on gradation/indicatrix method)														
	CIE01	CIE02	CIE03	CIE04	CIE05	CIE06	CIE07	CIE08	CIE09	CIE10	CIE11	CIE12	CIE13	CIE14	CIE15
Number of cases	1452	392	748	372	439	485	820	663	636	395	782	1024	500	4085	213
Igawa	26.6	38.0	27.0	33.2	36.9	36.2	43.8	47.5	46.7	44.5	40.7	42.9	39.7	43.6	59.0
ASRC-CIE	27.1	37.6	26.8	31.7	35.6	34.3	41.3	45.5	45.3	42.3	40.6	43.3	41.4	44.9	59.9
Perez-All weather	30.1	39.3	28.3	32.7	36.0	35.2	40.6	43.1	44.2	40.8	39.5	43.2	43.4	46.6	61.9

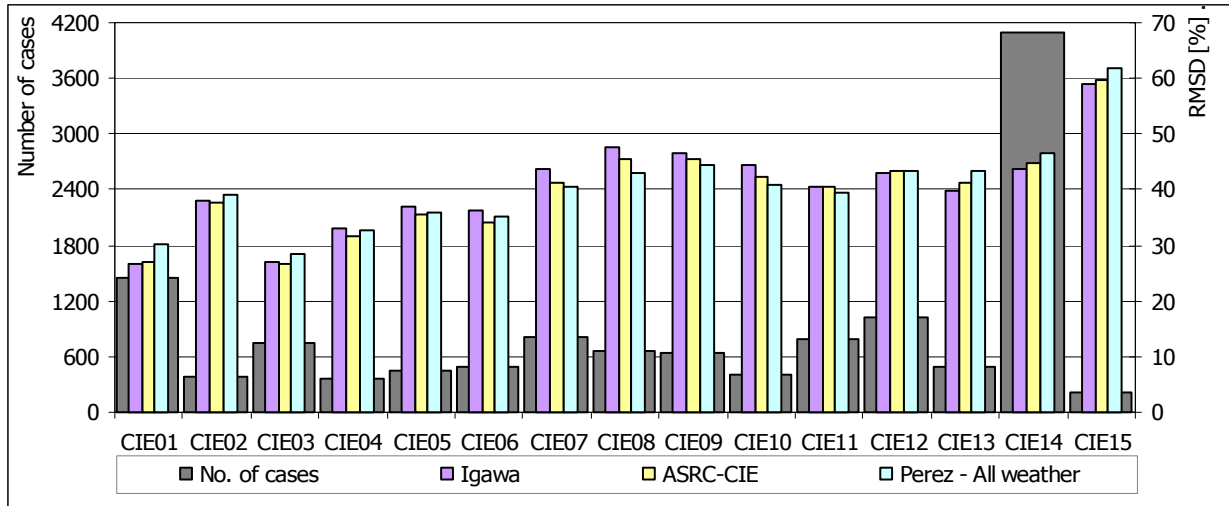


Fig. 4.11. Number of cases and relative RMS differences for different CIE sky types (based on gradation and indicatrix) for the sky hemisphere without 6 degree almucantar and without sky patches with  $\chi < 15^\circ$

Table 4.10. Relative RMS differences for different CIE sky types (based on gradation and indicatrix) for the sky hemisphere without sky patches with  $\chi < 15^\circ$

Sky luminance Model	Relative RMS difference for hemisphere without sky patches with $\chi < 15^\circ$ [%]														
	CIE Sky type (based on gradation/indicatrix method)														
	CIE01	CIE02	CIE03	CIE04	CIE05	CIE06	CIE07	CIE08	CIE09	CIE10	CIE11	CIE12	CIE13	CIE14	CIE15
Number of cases	1452	392	748	372	439	485	820	663	636	395	782	1024	500	4085	213
Igawa	28.9	42.0	29.4	37.3	39.0	40.3	50.7	54.9	48.4	50.9	45.0	44.7	41.1	44.0	57.9
ASRC-CIE	30.0	41.3	29.7	35.9	38.2	37.9	45.3	49.0	46.5	45.6	42.0	43.7	41.6	44.0	57.5
Perez-All weather	36.2	44.8	34.6	38.4	41.2	41.1	46.1	47.1	46.4	45.8	41.0	42.6	42.5	44.1	57.7

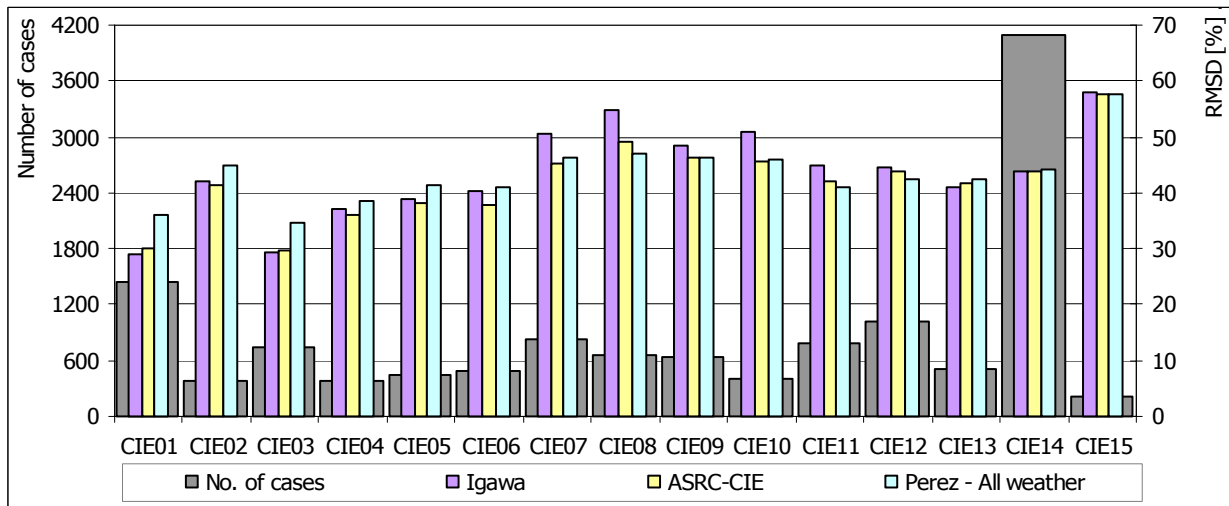


Fig. 4.12. Number of cases and relative RMS differences for different CIE sky types (based on gradation and indicatrix) for the sky hemisphere without sky patches with  $\chi < 15^\circ$

Table 4.11. Relative RMS differences for different CIE sky types (based on Tregenza method) for the sky hemisphere without 6 degree almucantar and without sky patches with  $\chi < 15^\circ$

Sky luminance Model	Relative RMS difference for hemisphere without 6 deg. almucantar and without sky patches with $\chi < 15^\circ$ [%]														
	CIE Sky type (based on Tregenza method)														
	CIE01	CIE02	CIE03	CIE04	CIE05	CIE06	CIE07	CIE08	CIE09	CIE10	CIE11	CIE12	CIE13	CIE14	CIE15
Number of cases	1912	592	559	475	183	221	350	3890	49	45	505	13	3653	24	535
Igawa	24.5	34.7	36.3	36.3	54.8	48.7	48.1	39.8	67.8	57.9	56.0	48.0	44.5	52.8	46.3
ASRC-CIE	25.1	34.4	34.6	34.7	52.2	46.0	46.5	39.0	64.8	55.3	54.4	49.8	46.1	48.7	47.3
Perez-All weather	28.3	35.6	34.1	35.6	49.1	44.5	46.0	39.0	60.0	50.9	50.4	48.5	48.3	47.1	46.9

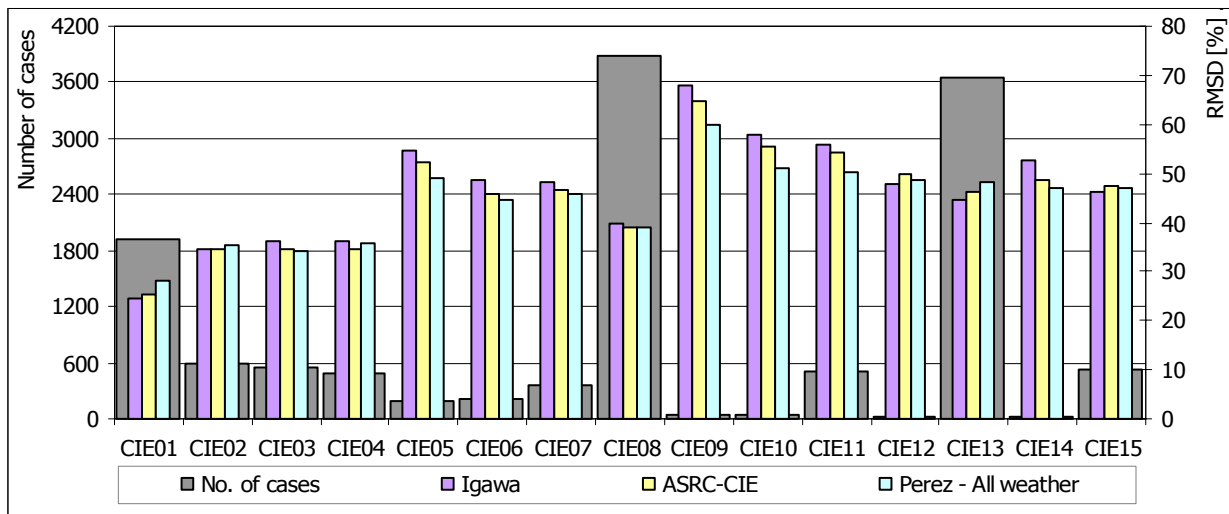


Fig. 4.13. Number of cases and relative RMS differences for different CIE sky types (based on Tregenza method) for the sky hemisphere without 6 degree almucantar and without sky patches with  $\chi < 15^\circ$

Table 4.12. Relative RMS differences for different CIE sky types (based on Tregenza method) for the sky hemisphere without sky patches with  $\chi < 15^\circ$

Sky luminance Model	Relative RMS difference for hemisphere without sky patches with $\chi < 15^\circ$ [%]														
	CIE Sky type (based on Tregenza method)														
	CIE01	CIE02	CIE03	CIE04	CIE05	CIE06	CIE07	CIE08	CIE09	CIE10	CIE11	CIE12	CIE13	CIE14	CIE15
Number of cases	1912	592	559	475	183	221	350	3890	49	45	505	13	3653	24	535
Igawa	26.7	38.5	37.5	38.8	57.6	50.5	50.7	43.6	73.5	62.6	66.7	53.9	44.4	64.1	49.5
ASRC-CIE	28.1	38.9	35.8	37.0	54.9	47.5	48.5	40.7	70.1	60.2	60.7	56.9	44.5	51.5	49.6
Perez-All weather	35.3	42.9	37.3	41.6	51.2	48.9	55.0	39.9	64.1	56.1	56.6	61.9	44.9	54.6	48.0

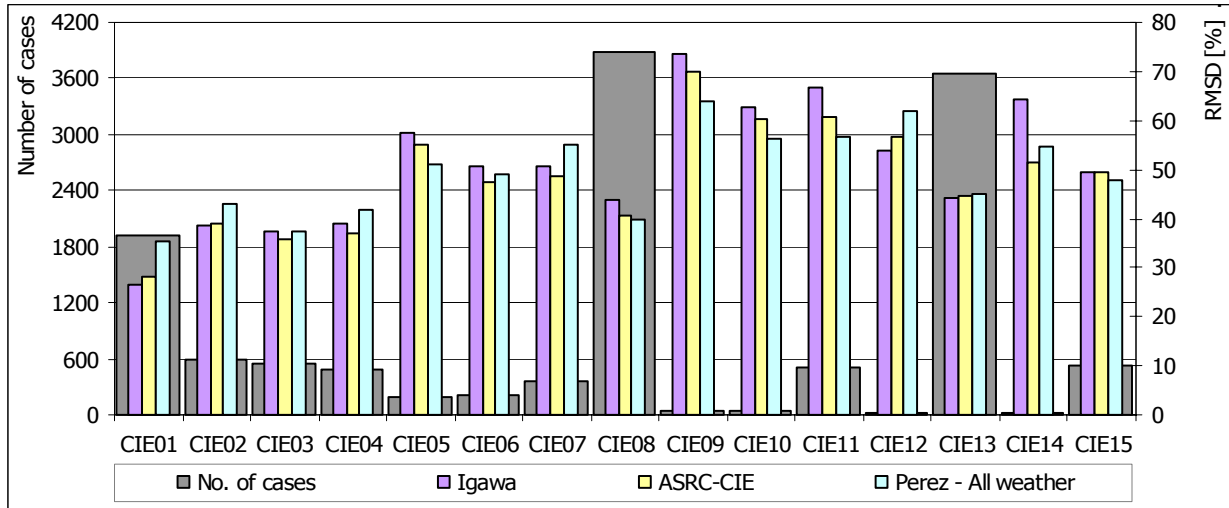


Fig. 4.14. Number of cases and relative RMS differences for different CIE sky types (based on Tregenza method) for the sky hemisphere without sky patches with  $\chi < 15^0$

Table 4.13. Relative RMS differences for different CIE sky types for both methods of CIE sky type determination and for different number of eliminated sky patches.



Number of eliminated sky patches has a meaningful influence to RMS difference. As it is seen from diagrams in Table 4.13 the RMS is lowered if beside sky patches with scattering angle lower than  $15^0$  also sky patches on first almucantar are excluded from calculations.

If CIE sky type is defined with gradation/indicatrix method, then RMS is lowered if first almucantar is eliminated with sky types from 1 to 12. Surprisingly the RMS is higher in cases of clear skies. If the CIE sky type is defined with Tregenza statistical method, than RMS is lowered with elimination of first almucantar practically in all CIE sky types and all three sky luminance models, except for both Perez models (ASRC-CIE and All-Weather) for CIE sky type 13.

#### 4.4.3 Results of comparison

The quality of a model can be expressed as a relative difference between best model and certain model for each sky type. Relative difference is computed with next equation (a sample for Igawa model):

$$rd_{IgawaCIEx} = \frac{rmsd_{IgawaCIEx} - rmsd_{BestCIEx}}{rmsd_{BestCIEx}} \quad (4.29)$$

Where:

$rd_{IgawaCIEx}$  relative difference for Igawa luminance model for CIE sky type X

$rmsd_{IgawaCIEx}$  RMSD for Igawa luminance model for CIE sky type X

$rmsd_{BestCIEx}$  RMSD for best luminance model for CIE sky type X

Quality of luminance models expressed in relative difference for different sky types is presented in Table 4.14 and plotted on Fig. 4.15, for selection based on gradation and indicatrix and in Table 4.15 and plotted on Fig. 4.16 for selection based on Tregenza method.

In Table 4.14 and Table 4.15 the best model for certain CIE sky type has a value 0.0.

Table 4.14. Quality of luminance models expressed in relative difference for different sky types (based on gradation and indicatrix)

Sky luminance Model	Relative difference [%]														
	CIE Sky type														
	CIE01	CIE02	CIE03	CIE04	CIE05	CIE06	CIE07	CIE08	CIE09	CIE10	CIE11	CIE12	CIE13	CIE14	CIE15
Number of cases	1452	392	748	372	439	485	820	663	636	395	782	1024	500	4085	213
Igawa	<b>0.0</b>	1.8	<b>0.0</b>	3.9	2.3	6.2	11.8	16.7	4.2	11.7	9.9	5.0	0.0	<b>0.0</b>	0.6
ASRC-CIE	3.9	<b>0.0</b>	1.0	<b>0.0</b>	<b>0.0</b>	<b>0.0</b>	<b>0.0</b>	4.2	0.1	<b>0.0</b>	2.5	2.7	1.3	<b>0.0</b>	<b>0.0</b>
Perez-All weather	25.5	8.5	17.6	7.1	8.0	8.4	1.8	<b>0.0</b>	<b>0.0</b>	0.4	<b>0.0</b>	<b>0.0</b>	3.4	0.3	0.3

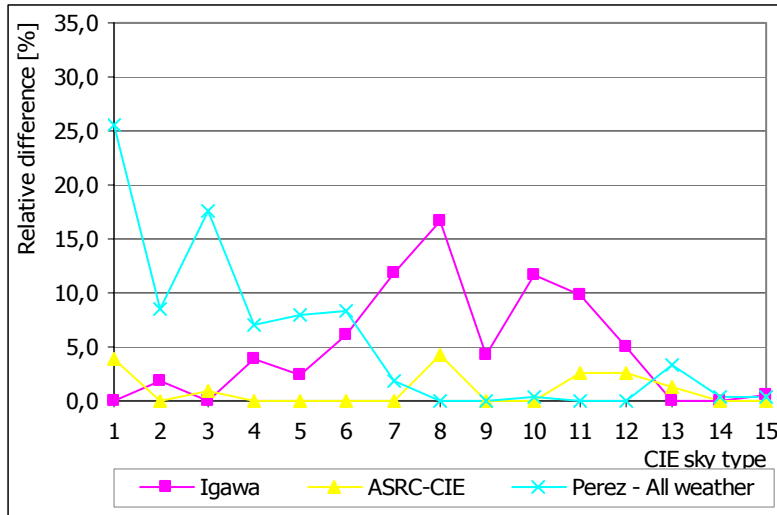


Fig. 4.15. Quality of luminance models expressed in relative difference for different sky types (based on gradation and indicatrix)

Table 4.15. Quality of luminance models expressed in relative difference for different sky types (based on Tregenza method)

Sky luminance Model	Relative difference [%]														
	CIE Sky type														
	CIE01	CIE02	CIE03	CIE04	CIE05	CIE06	CIE07	CIE08	CIE09	CIE10	CIE11	CIE12	CIE13	CIE14	CIE15
Number of cases	1912	592	559	475	183	221	350	3890	49	45	505	13	3653	24	535
Igawa	<b>0.0</b>	<b>0.0</b>	4.7	5.1	12.3	6.3	4.6	9.3	14.6	11.6	17.9	<b>0.0</b>	<b>0.0</b>	24.5	3.1
ASRC-CIE	5.4	1.1	<b>0.0</b>	<b>0.0</b>	7.1	<b>0.0</b>	<b>0.0</b>	1.9	9.4	7.2	7.3	5.4	0.2	<b>0.0</b>	3.2
Perez-All weather	32.4	11.4	4.2	12.6	<b>0.0</b>	3.0	13.4	<b>0.0</b>	<b>0.0</b>	<b>0.0</b>	<b>0.0</b>	14.8	1.2	5.9	<b>0.0</b>

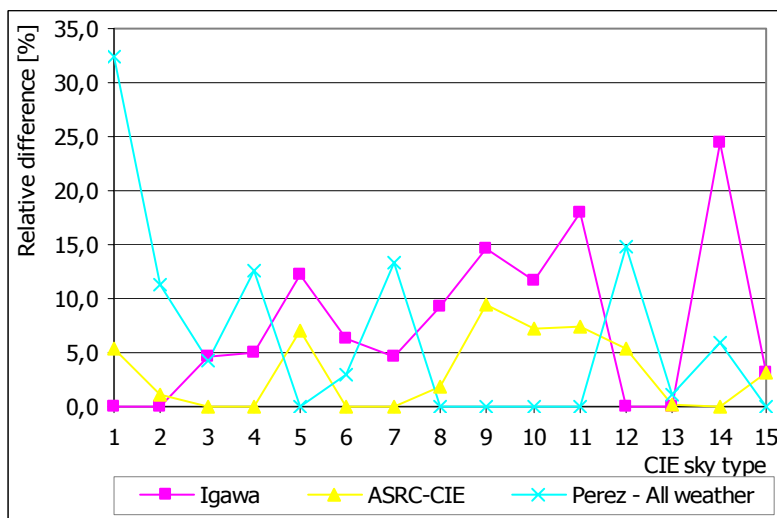


Fig. 4.16. Quality of luminance models expressed in relative difference for different sky types (based on Tregenza method)

*Table 4.16. Average and maximum value of relative difference for sky luminance models*

Sky luminance Model	Relative difference [%]			
	Average value		Maximum value	
	Gradation/indicatrix method	Tregenza statistical method	Gradation/indicatrix method	Tregenza statistical method
Igawa	4,9	7,6	16,7	24,5
ASRC-CIE	1,0	3,2	4,2	9,4
Perez-All weather	5,4	6,6	25,5	32,4

In this model quality evaluation all sky scans (13006) were analysed. In the comparison all sky patches, except the ones with scattering angle lower than  $15^{\circ}$  were used. In Table 4.16 the results are summarized. As it can be seen from the mentioned table, the smallest average relative difference is for ASRC-CIE model. The difference is the smallest for both methods of CIE sky type decision. ASRC-CIE model is the best model for eight CIE sky types (CIE 2, CIE 4, CIE 5, CIE 6, CIE7, CIE 10, CIE 14 and CIE 15) in case of gradation/indicatrix method and for five CIE sky types (CIE 3, CIE 4, CIE 6, CIE 7, CIE 14) in case of Tregenza statistical method. Although in case of Tregenza statistical method Perez-All weather model seem to be better (best model for six CIE sky types), it can not be treated as the best model because of higher relative differences in cases where it is not the best sky model. ASRC-CIE sky luminance model also has smallest maximum value of relative difference. Igawa model gives best results with extreme cloudy skies (CIE 1, CIE 2 and CIE 3) and worse results with intermediate skies (CIE 7, CIE 8, CIE 10 and CIE 11). On the other hand Perez-All weather model provides best results for intermediate and intermediate-sunny skies (CIE 7, CIE 8, CIE 9, CIE 10 and CIE 12) and worse results for extreme cloudy skies (CIE 1, CIE 2 and CIE3). ASRC-CIE model is in most cases in between Igawa and Perez-All weather model, but always close to the best model.

When taking into account also CIE sky types, we can conclude from Table 4.14 and Table 4.15 and from Fig. 4.15 and Fig. 4.16 that the best results are provided with ASRC-CIE sky luminance model. From both diagrams, especially from Fig. 4.15, it's obvious that the ASRC-CIE model has no peaks of high levels of relative difference and gives best results in eight sky types when CIE sky type is selected based on gradation and indicatrix. And also in cases of sky types where is not providing the best results, the relative difference is below 5% and it never provides worse results.

No matter what method was used to define CIE sky type, the ASRC-CIE luminance model provides results with the best average relative difference and the smallest values of maximum relative difference (Table 4.16).

#### **4.4.4 Results of comparison dependent on sky types and sun altitudes**

Similar comparison as we did it in previous chapter was done also in next comparison. In this comparison measured cases were arranged by sun altitude into four bins (Table 4.17). And for each sun altitude bin relative difference for each CIE sky type was calculated.

Table 4.17. Bins of sun altitudes

Bin	Sun altitudes [°]
Bin 1	5 - 20
Bin 2	20 - 35
Bin 3	35 - 50
Bin 4	> 50

For all four bins, CIE sky types were derived from sky scanner measurement with gradation and indicatrix method. In the comparison all sky patches, except the ones with scattering angle lower than 15° were used.

4.4.4.1 Sun altitudes 5 - 20°

Table 4.18. Number of cases and relative RMS differences for different CIE sky types (based on gradation and indicatrix) for sun altitudes between 5 and 20 degrees.

Sky luminance Model	Relative RMS difference for sun altitudes between 5 and 20 degrees [%]														
	CIE Sky type														
	CIE01	CIE02	CIE03	CIE04	CIE05	CIE06	CIE07	CIE08	CIE09	CIE10	CIE11	CIE12	CIE13	CIE14	CIE15
Number of cases	488	96	270	93	175	126	179	153	114	101	175	211	112	1140	49
Igawa	26.4	43.2	29.2	38.7	39.7	39.4	58.7	67.7	56.7	57.0	59.9	51.5	56.9	51.6	80.9
ASRC-CIE	27.0	42.4	28.8	37.2	38.4	38.3	52.3	62.3	54.9	51.1	56.9	52.1	58.8	52.2	80.6
Perez-All weather	36.4	53.5	37.4	40.6	45.2	47.9	58.6	63.6	60.5	58.9	56.5	51.2	58.8	51.9	81.7

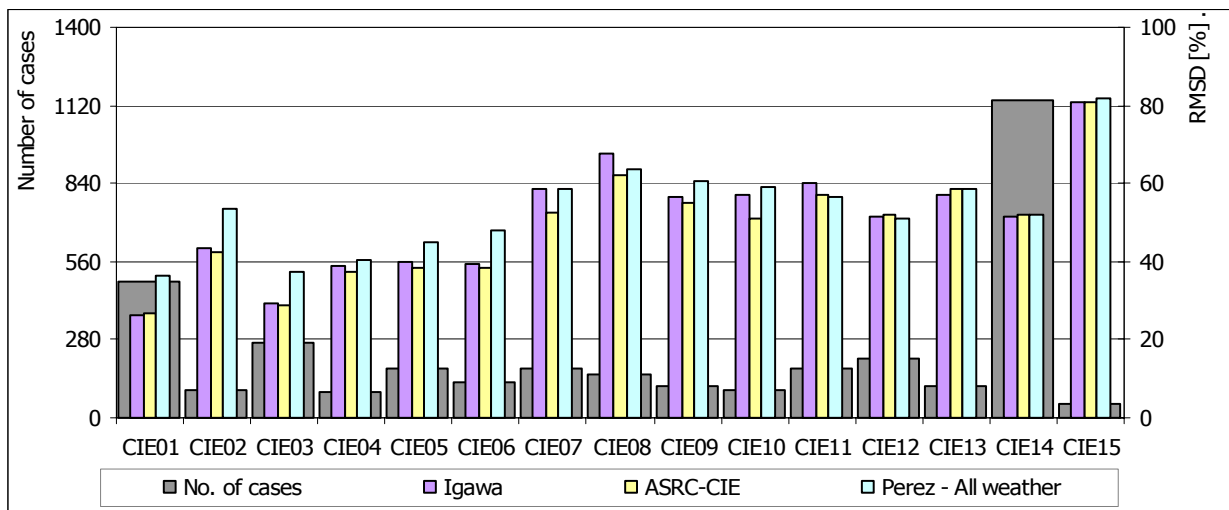


Fig. 4.17. Number of cases and relative RMS differences for different CIE sky types (based on gradation and indicatrix) for sun altitudes between 5 and 20 degrees.

Table 4.19. Quality of luminance models expressed in relative difference for different sky types (based on gradation and indicatrix) for sun altitudes between 5 and 20 degrees.

Sky luminance Model	Relative difference [%]														
	CIE Sky type														
	CIE01	CIE02	CIE03	CIE04	CIE05	CIE06	CIE07	CIE08	CIE09	CIE10	CIE11	CIE12	CIE13	CIE14	CIE15
Number of cases	488	96	270	93	175	126	179	153	114	101	175	211	112	1140	49
Igawa	<b>0.0</b>	2.0	1.3	3.9	3.3	3.0	12.1	8.8	3.3	11.6	6.0	0.6	<b>0.0</b>	<b>0.0</b>	0.5
ASRC-CIE	2.3	<b>0.0</b>	0.6	1.7	3.4	1.2	<b>0.0</b>								
Perez-All weather	38.1	26.2	29.8	9.2	17.7	25.2	12.0	2.1	10.2	15.2	<b>0.0</b>	<b>0.0</b>	3.3	0.7	1.4

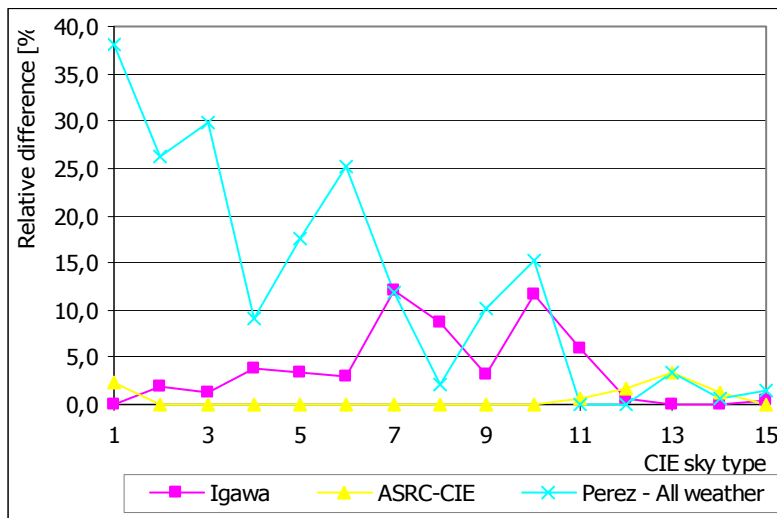


Fig. 4.18. Quality of luminance models expressed in relative difference for different sky types (based on gradation and indicatrix) for sun altitudes between 5 and 20 degrees.

As it can be read from Fig. 4.18 ASRC-CIE is the best model for practically all CIE sky types. Perez-All weather model is good for clear sky and extremely bad for cloudy skies. Relative difference for Perez-All weather model for cloudy sky types is almost in all cases higher than 25 %. Igawa model is acceptable for cloudy and sunny sky types, but not so good for intermediate sky types. Relative difference of Igawa sky luminance model for intermediate sky types is around 10 %. It's interesting that Igawa sky luminance model has quite low relative difference for CIE sky type 9.

4.4.4.2 Sun altitudes 20 - 35°

Table 4.20 Number of cases and relative RMS differences for different CIE sky types (based on gradation and indicatrix) for sun altitudes between 20 and 35 degrees.

Sky luminance Model	Relative RMS difference for sun altitudes between 20 and 35 degrees														
	CIE Sky type														
	CIE01	CIE02	CIE03	CIE04	CIE05	CIE06	CIE07	CIE08	CIE09	CIE10	CIE11	CIE12	CIE13	CIE14	CIE15
Number of cases	459	100	260	108	125	121	235	188	132	100	149	255	134	1320	56
Igawa	27.8	45.0	29.3	38.4	39.4	43.7	56.6	62.4	53.3	63.1	59.7	54.7	47.7	48.5	68.5
ASRC-CIE	29.6	43.9	30.0	37.1	38.8	39.8	48.3	53.0	50.7	53.6	52.6	51.8	47.2	47.7	67.1
Perez-All weather	36.1	47.5	34.0	42.6	40.6	43.0	49.7	48.7	52.2	50.4	49.7	48.6	47.0	47.5	64.7

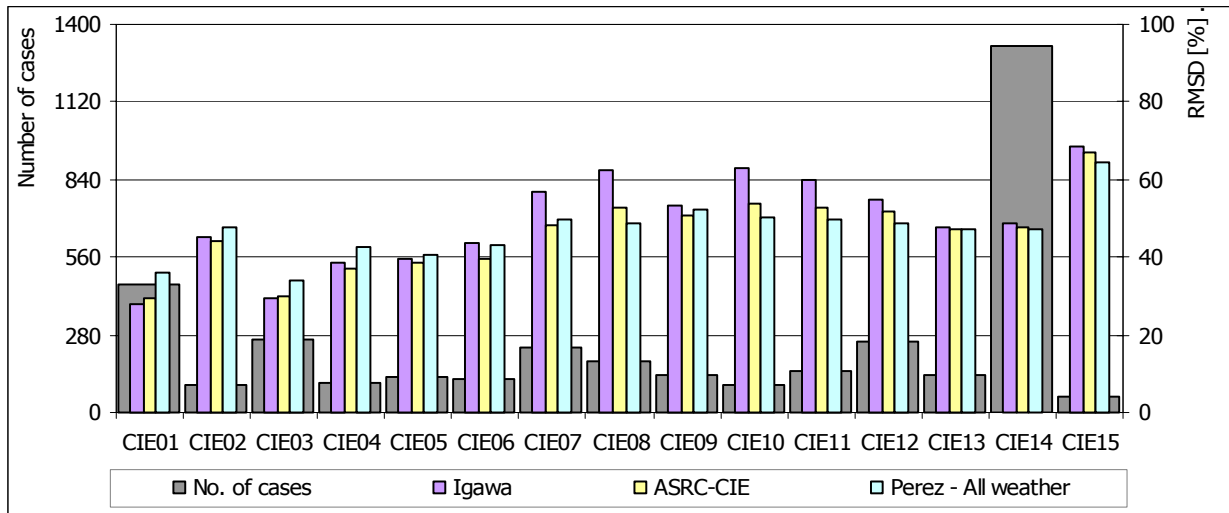


Fig. 4.19. Number of cases and relative RMS differences for different CIE sky types (based on gradation and indicatrix) for sun altitudes between 20 and 35 degrees.

Table 4.21. Quality of luminance models expressed in relative difference for different sky types (based on gradation and indicatrix) for sun altitudes between 20 and 35 degrees.

Sky luminance Model	Relative difference [%]														
	CIE Sky type														
	CIE01	CIE02	CIE03	CIE04	CIE05	CIE06	CIE07	CIE08	CIE09	CIE10	CIE11	CIE12	CIE13	CIE14	CIE15
Number of cases	459	100	260	108	125	121	235	188	132	100	149	255	134	1320	56
Igawa	<b>0.0</b>	2.3	<b>0.0</b>	3.5	1.5	9.7	17.2	28.1	5.1	25.2	20.2	12.5	1.5	2.3	5.9
ASRC-CIE	6.7	<b>0.0</b>	2.2	<b>0.0</b>	<b>0.0</b>	<b>0.0</b>	<b>0.0</b>	8.8	<b>0.0</b>	6.4	5.9	6.6	0.4	0.5	3.7
Perez-All weather	29.9	8.1	15.9	14.8	4.6	8.0	2.9	<b>0.0</b>	3.0	<b>0.0</b>	<b>0.0</b>	<b>0.0</b>	<b>0.0</b>	<b>0.0</b>	<b>0.0</b>

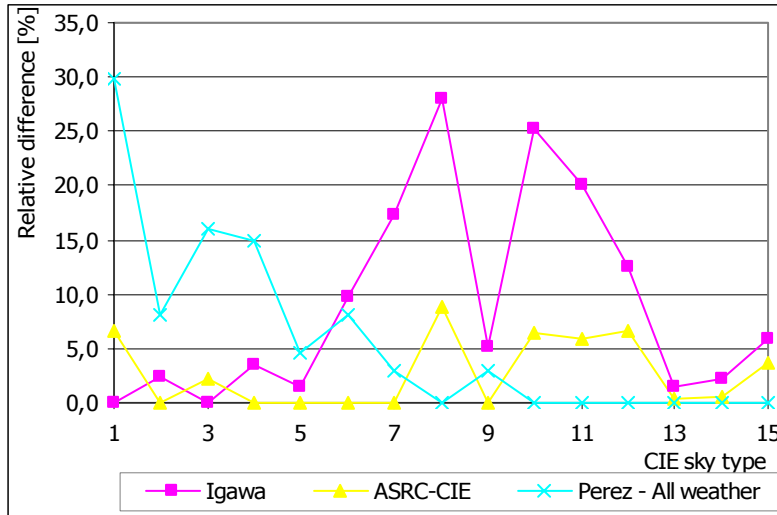


Fig. 4.20. Quality of luminance models expressed in relative difference for different sky types (based on gradation and indicatrix) for sun altitudes between 20 and 35 degrees.

Also for sun altitudes between 20 and 35 degrees the ASRC-CIE is the best model for practically all CIE sky types. Igawa model is good for cloudy and sunny sky types, but not so good for intermediate sky types. Perez-All weather model is the worst for cloudy sky types, but the best model for sunny sky types. Also here we can find an obvious drop in relative difference for Igawa model for intermediate sky types in CIE sky type 9.

#### 4.4.4.3 Sun altitudes 35 - 50°

Table 4.22. Number of cases and relative RMS differences for different CIE sky types (based on gradation and indicatrix) for sun altitudes between 35 and 50 degrees.

Sky luminance Model	Relative RMS difference for sun altitudes between 35 and 50 degrees														
	CIE Sky type														
	CIE01	CIE02	CIE03	CIE04	CIE05	CIE06	CIE07	CIE08	CIE09	CIE10	CIE11	CIE12	CIE13	CIE14	CIE15
Number of cases	265	82	129	104	86	131	186	122	130	79	130	270	113	937	32
Igawa	29.3	40.3	30.0	35.3	39.5	42.5	46.6	55.1	49.9	48.8	45.5	39.2	36.1	37.0	43.0
ASRC-CIE	31.4	40.8	30.9	34.2	38.8	40.3	42.5	48.0	47.5	44.0	42.2	38.4	36.5	37.4	44.3
Perez-All weather	35.8	41.4	32.8	35.2	38.3	41.1	40.0	43.1	45.0	41.4	38.7	38.1	37.5	37.9	46.3

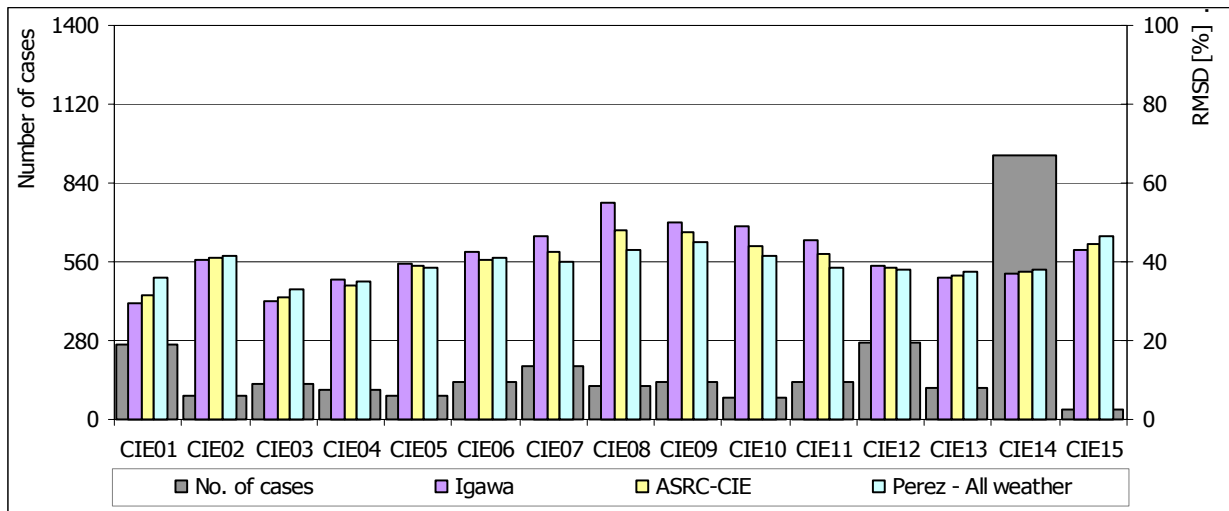


Fig. 4.21. Number of cases and relative RMS differences for different CIE sky types (based on gradation and indicatrix) for sun altitudes between 35 and 50 degrees.

Table 4.23. Quality of luminance models expressed in relative difference for different sky types (based on gradation and indicatrix) for sun altitudes between 35 and 50 degrees.

Sky luminance Model	Relative difference [%]														
	CIE Sky type														
	CIE01	CIE02	CIE03	CIE04	CIE05	CIE06	CIE07	CIE08	CIE09	CIE10	CIE11	CIE12	CIE13	CIE14	CIE15
Number of cases	265	82	129	104	86	131	186	122	130	79	130	270	113	937	32
Igawa	<b>0.0</b>	<b>0.0</b>	<b>0.0</b>	3.2	3.3	5.2	16.6	27.7	10.9	18.0	17.6	2.9	<b>0.0</b>	<b>0.0</b>	<b>0.0</b>
ASRC-CIE	7.0	1.4	3.1	<b>0.0</b>	1.4	0.0	6.1	11.4	5.5	6.2	9.2	0.6	1.1	0.9	3.0
Perez-All weather	21.9	2.7	9.4	2.8	<b>0.0</b>	2.0	<b>0.0</b>	<b>0.0</b>	<b>0.0</b>	<b>0.0</b>	<b>0.0</b>	<b>0.0</b>	4.0	2.3	7.6

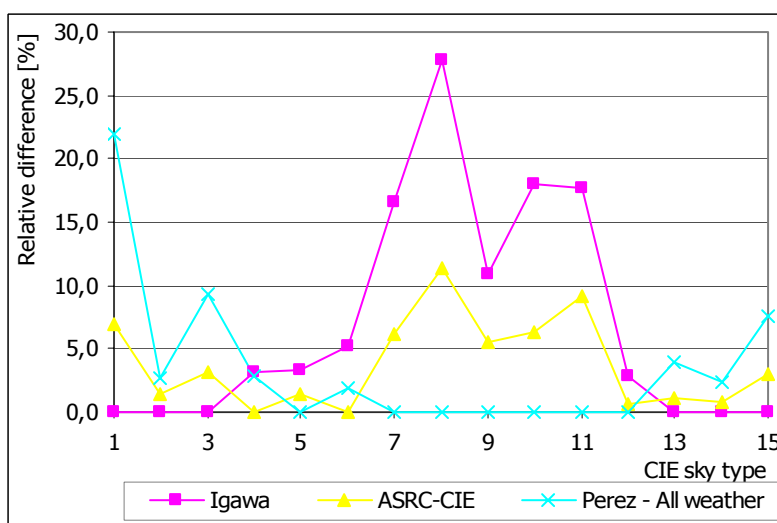


Fig. 4.22. Quality of luminance models expressed in relative difference for different sky types (based on gradation and indicatrix) for sun altitudes between 35 and 50 degrees.

Also for sun altitudes between 35 and 50 degrees the ASRC-CIE is the best model for practically all CIE sky types. Igawa model is best for cloudy and sunny sky types, but not so good for intermediate sky types. Perez-All weather model is the worst for cloudy sky types, but the best model for intermediate sky types. Also here we can find an obvious drop in relative difference for Igawa model for intermediate sky types in CIE sky type 9.

**4.4.4.4 Sun altitudes over 50°**

Table 4.24. Number of cases and relative RMS differences for different CIE sky types (based on gradation and indicatrix) for sun altitudes over 50 degrees.

Sky luminance Model	Relative RMS difference for sun altitudes over 50 degrees														
	CIE Sky type														
	CIE01	CIE02	CIE03	CIE04	CIE05	CIE06	CIE07	CIE08	CIE09	CIE10	CIE11	CIE12	CIE13	CIE14	CIE15
Number of cases	233	114	85	66	53	106	218	197	254	114	323	283	139	666	76
Igawa	36.0	39.7	29.6	36.7	35.4	34.5	41.2	37.7	41.2	36.2	30.0	35.9	26.1	31.5	41.4
ASRC-CIE	35.7	38.3	29.9	34.8	34.8	32.2	38.8	35.5	39.8	34.8	29.0	35.2	26.7	31.7	41.1
Perez-All weather	36.9	37.6	30.6	33.7	34.3	30.7	37.3	35.0	37.8	33.1	29.6	34.9	29.1	32.6	41.8

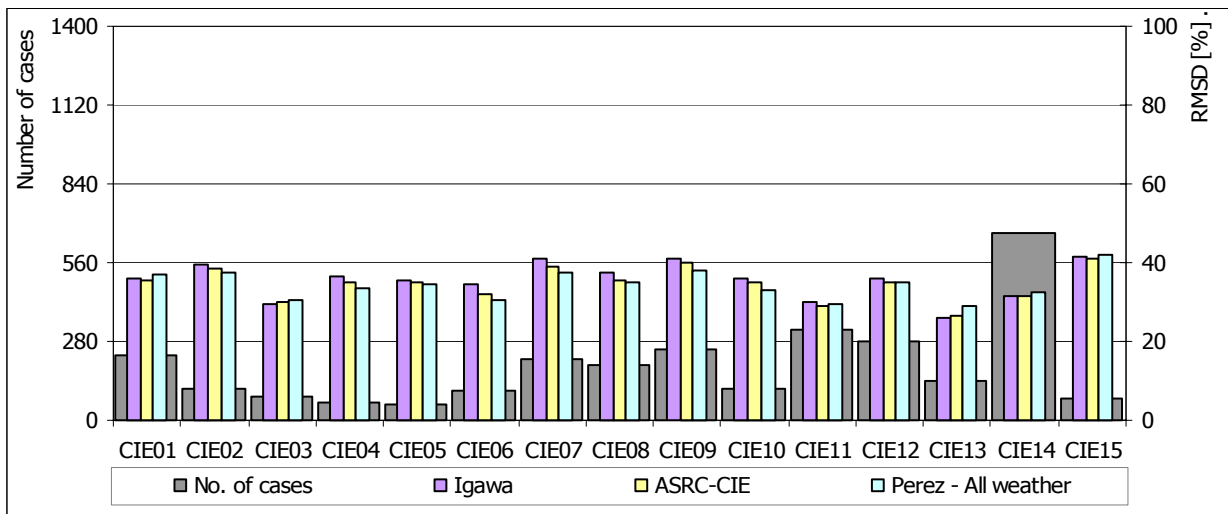


Fig. 4.23. Number of cases and relative RMS differences for different CIE sky types (based on gradation and indicatrix) for sun altitudes over 50 degrees.

Table 4.25. Quality of luminance models expressed in relative difference for different sky types based on gradation and indicatrix) for sun altitudes over 50 degrees.

Sky luminance Model	Relative difference [%]														
	CIE Sky type														
	CIE01	CIE02	CIE03	CIE04	CIE05	CIE06	CIE07	CIE08	CIE09	CIE10	CIE11	CIE12	CIE13	CIE14	CIE15
Number of cases	233	114	85	66	53	106	218	197	254	114	323	283	139	666	76
Igawa	0.6	5.6	<b>0.0</b>	8.7	3.4	12.4	10.6	7.8	9.0	9.3	3.6	2.7	<b>0.0</b>	<b>0.0</b>	0.6
ASRC-CIE	<b>0.0</b>	1.9	0.7	3.1	1.5	4.8	4.0	1.4	5.3	5.1	<b>0.0</b>	0.9	2.1	0.7	<b>0.0</b>
Perez-All weather	3.3	<b>0.0</b>	3.3	<b>0.0</b>	2.0	<b>0.0</b>	11.4	3.6	1.6						

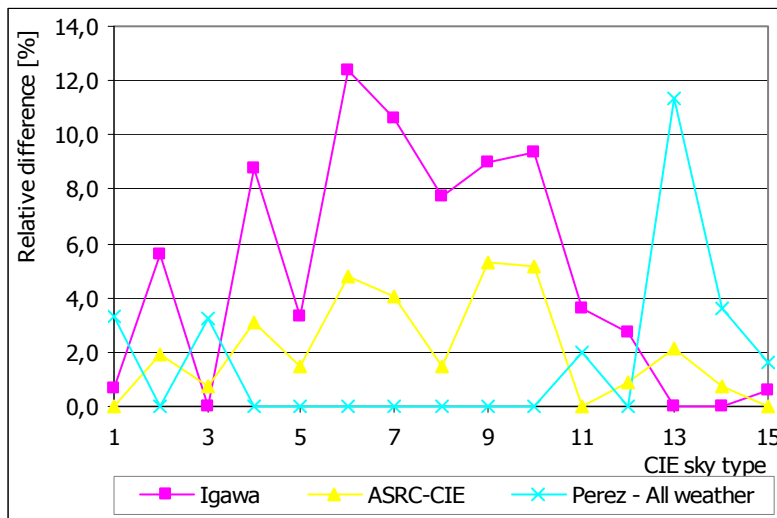


Fig. 4.24. Quality of luminance models expressed in relative difference for different sky types (based on gradation and indicatrix) for sun altitudes over 50 degrees.

For sun altitudes above 50° it is seen from Fig. 4.23 that relative difference is practically the same for all sky types. Relative difference does not differ much from sky type to sky type (from 26% to 41%). The difference is much lower as it is at lower sun altitudes (up to 80% with CIE sky type 15 at sun altitudes between 5 and 20°).

With higher sun altitudes relative difference between models fades away. The difference in worst case (Igawa model for CIE sky type 6) is only 12,4%. Although the differences between models are small, we can conclude that Igawa model is good for cloudy and best for sunny sky types. Perez-All weather model is best for intermediate sky types and ASRC-CIE gives best average results.

Similar to previous case, where all measurements were grouped only by CIE sky type, also in this case we group measurements by CIE sky type and also by sun altitude. From Fig. 4.18, Fig. 4.20, Fig. 4.22 and Fig. 4.24 it is seen that also in this comparison ASRC-CIE sky luminance model provides best results.

Also when we consider average relative difference (Table 4.26) Perez All weather and ASRC-CIE sky luminance share the same number of best results. First one is better for sun altitudes above 50° and the second one is better for sun altitudes below 50°. But a note should be added, that Perez All weather model has high average relative

difference for sun altitudes below 50° and on the other hand ASRC-CIE's average relative difference for sun altitudes above 50° is practically in line with Perez All weather model (Fig. 4.25).

When maximum relative difference (Table 4.27) is considered, at all sun altitudes ASRC-CIE luminance model is the best choice. This models highest maximum relative difference is in bin with sun altitudes between 35° and 50° and has a value of 11.4%. Highest maximum relative differences for Igawa and Perez All weather models are higher and have values of 28.1 and 38.1%.

Table 4.26. Average relative difference for three luminance models dependent on sun altitudes

Sky luminance Model	Average relative difference [%]			
	sun altitude 5° – 20°	sun altitude 20° – 35°	sun altitude 35° – 50°	sun altitude above 50°
Igawa	3.8	9.0	7.0	5.0
ASRC-CIE	0.6	2.8	3.8	2.1
Perez-All weather	12.7	5.8	3.5	1.7

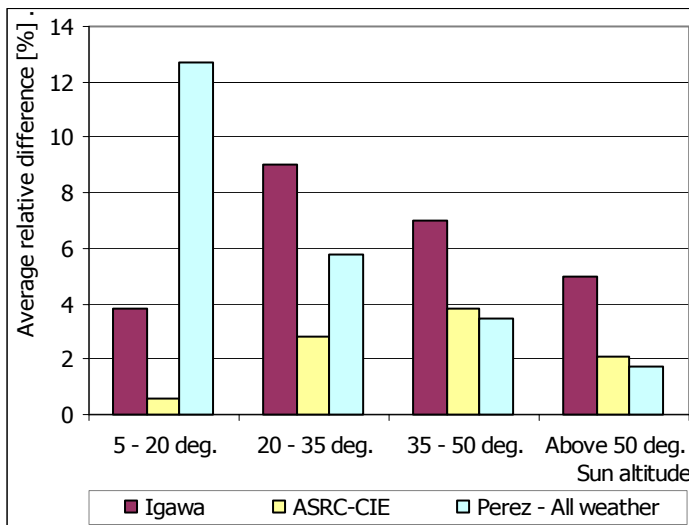


Fig. 4.25. Average relative difference for three luminance models dependent on sun altitudes

Table 4.27. Maximum relative difference for three luminance models dependent on sun altitudes

Sky luminance Model	Maximum relative difference [%]			
	sun altitude 5° – 20°	sun altitude 20° – 35°	sun altitude 35° – 50°	sun altitude above 50°
Igawa	12.1	28.1	27.7	12.4
ASRC-CIE	3.4	8.8	11.4	5.3
Perez-All weather	38.1	29.9	21.9	11.4

#### 4.4.4.5 Problems of Igawa model for intermediate skies

Since Igawa model provides worse results for CIE sky type 8, we decided to search further what is happening with this model in combination with CIE sky type 8.

In Table 4.10 relative RMS differences for different CIE sky types (based on gradation and indicatrix) for the sky hemisphere without sky patches with  $\chi < 15^\circ$  are gathered. If we extract from it only data for CIE sky type 8, we get Table 4.28.

Table 4.28. Relative RMS differences for CIE sky type 8 (based on gradation and indicatrix) for the sky hemisphere without sky patches with  $\chi < 15^\circ$

Sky luminance Model	Relative RMS difference for hemisphere without sky patches with $\chi < 15^\circ$
Number of cases	663
Igawa	54.9
ASRC-CIE	49.0
Perez-All weather	47.1

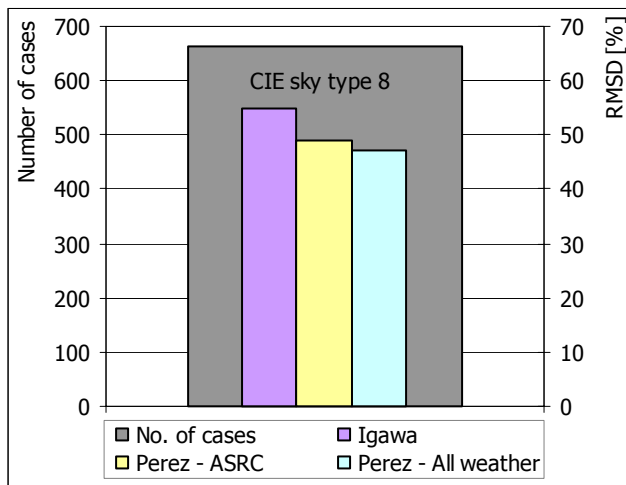


Fig. 4.26. Number of cases and relative RMS differences for CIE sky type 8 (based on gradation and indicatrix) for the sky hemisphere without sky patches with  $\chi < 15^\circ$

From the matrix with gradation and indicatrix groups and CIE sky types (Table 2.8), it can be read that CIE sky type 8 can be achieved with six different combinations of gradation and indicatrix groups. These combinations are (gradation/indicatrix): I/6, II/5, II/6, III/4, III/5, III/6.

All measurements were grouped in bins of combinations of gradation and indicatrix groups and next table was filled.

Table 4.29. Number of cases and relative RMS differences for different combinations of gradation and indicatrix groups for CIE sky type 8

Sky luminance Model	Relative RMS difference [%]					
	Gradation/Indicatrix combination					
	I/6	II/5	II/6	III/4	III/5	III/6
Number of cases	23	55	13	353	189	30
Igawa	52.1	58.2	53.6	54.5	54.3	60.0
ASRC-CIE	49.0	52.4	51.9	48.6	48.0	53.5
Perez-All weather	51.7	51.8	50.9	46.8	44.7	50.9

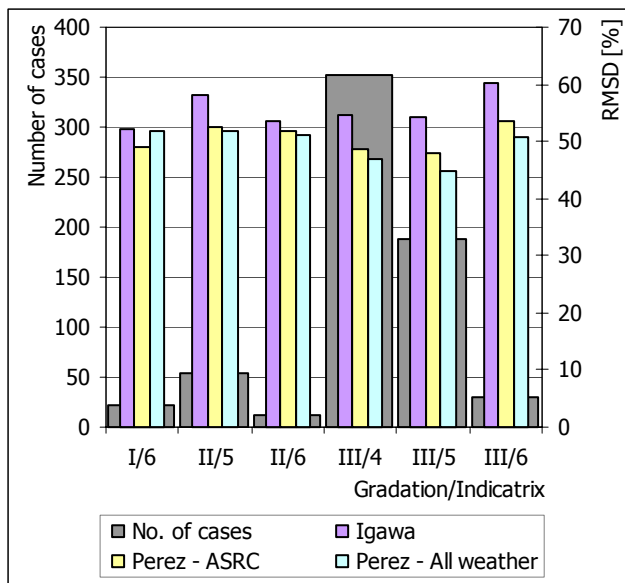


Fig. 4.27. Number of cases and relative RMS differences for different combinations of gradation and indicatrix groups for CIE sky type 8

Most cases of CIE sky type 8 (53.2%) have gradation III and indicatrix 4. From our whole database of measurements we have chosen out four cases of CIE sky type 8 (Table 4.30). The presented four cases were chosen because the RMS difference between Igawa model and measurement was much higher than for other two models.

Table 4.30. Relative RMS differences for three luminance models and four cases of measurement

Sky luminance Model	Relative RMS difference for hemisphere without sky patches with $\chi < 15^\circ$ [%]			
	Date and time			
	June 15, 2005 18:10	July 30, 2005 11:20	October 2, 2005 10:40	November 1, 2005 9:50
Igawa	143.48	117.08	129.37	131.16
ASRC-CIE	83.708	40.823	61.585	75.865
Perez-All weather	56.54	26.388	44.402	47.426

We were intended to plot luminance profiles for all four cases and look for specialities, but in three cases out of previously mentioned four, there was no profile for Igawa luminance model. Luminances of all sky patches on the hemisphere were zero.

In Igawa luminance model, the parameters, that describe luminance distribution of the sky vault, are dependent on sky index. Sky index was especially calculated for the mentioned four cases (Table 4.31).

Table 4.31. Sky index used in Igawa model for four cases of measurement

	Date and time of case measurement			
	June 15, 2005 18:10	July 30, 2005 11:20	October 2, 2005 10:40	November 1, 2005 9:50
Sky index	1.9386	2.1006	2.1417	2.1440

If we take a closer look into equation for parameter  $c'$  of Igawa luminance model (Fig. 4.28), we can see that the equation has a "Not a number" value for all cases where sky index is higher than 2.1.

$$c' = 1.77 \cdot (1.22 \cdot Si)^{3.56} \cdot \exp(0.2 \cdot Si) \cdot (2.1 - Si)^{0.8} \quad (4.30)$$

From the equation it is obvious that in all cases in our database, where sky index is higher than 2.1, values of luminances in Igawa model are zero.

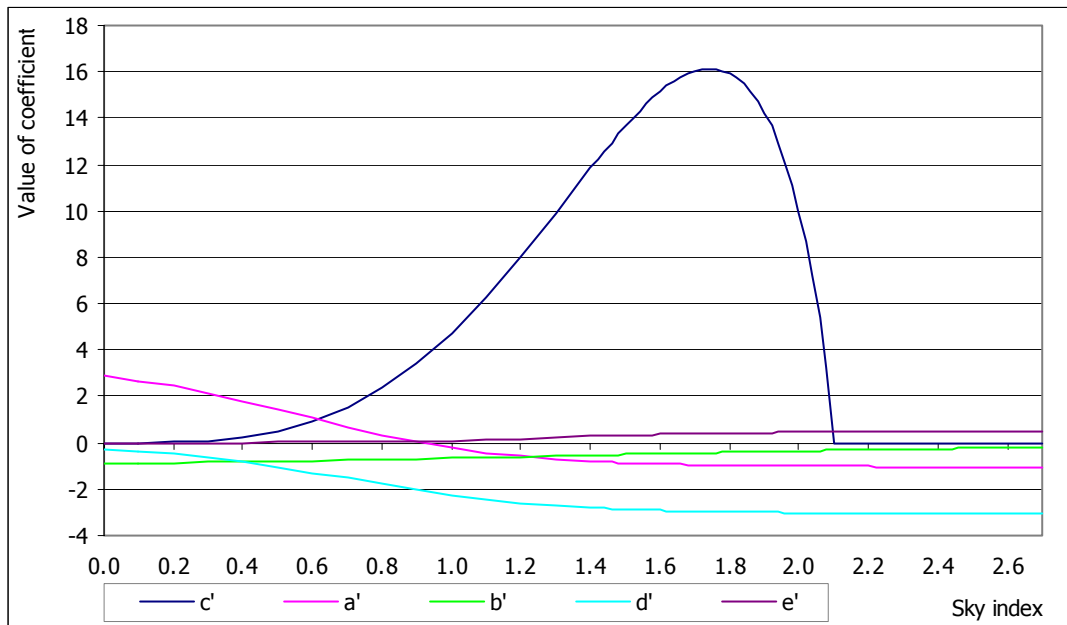


Fig. 4.28. Igawa coefficients against sky index

Sky index was calculated for all 13006 measurements in our data base and grouped in bins of an interval 0.1. Numbers of cases in certain bins are collected in Table 4.32 and presented on Fig. 4.29.

Table 4.32. Sky index bins and number of cases in bins

	Sky index interval													
	0.0 -0.1	0.1 -0.2	0.2 -0.3	0.3 -0.4	0.4 -0.5	0.5 -0.6	0.6 -0.7	0.7 -0.8	0.8 -0.9	0.9 -1.0	1.0 -1.1	1.1 -1.2	1.2 -1.3	1.3 -1.4
No. of cases	445	889	873	711	526	424	398	391	306	276	231	196	178	241
No. of cases [%]	3.42	6.84	6.71	5.47	4.04	3.26	3.06	3.01	2.35	2.12	1.78	1.51	1.37	1.85

	Sky index interval													
	1.4 -1.5	1.5 -1.6	1.6 -1.7	1.7 -1.8	1.8 -1.9	1.9 -2.0	2.0 -2.1	2.1 -2.2	2.2 -2.3	2.3 -2.4	2.4 -2.5	2.5 -2.6	2.6 -2.7	
No. of cases	294	379	635	1239	2428	1720	188	30	4	1	0	2	1	
No. of cases [%]	2.26	2.91	4.88	9.53	18.67	13.22	1.45	0.23	0.03	0.01	0.00	0.02	0.01	

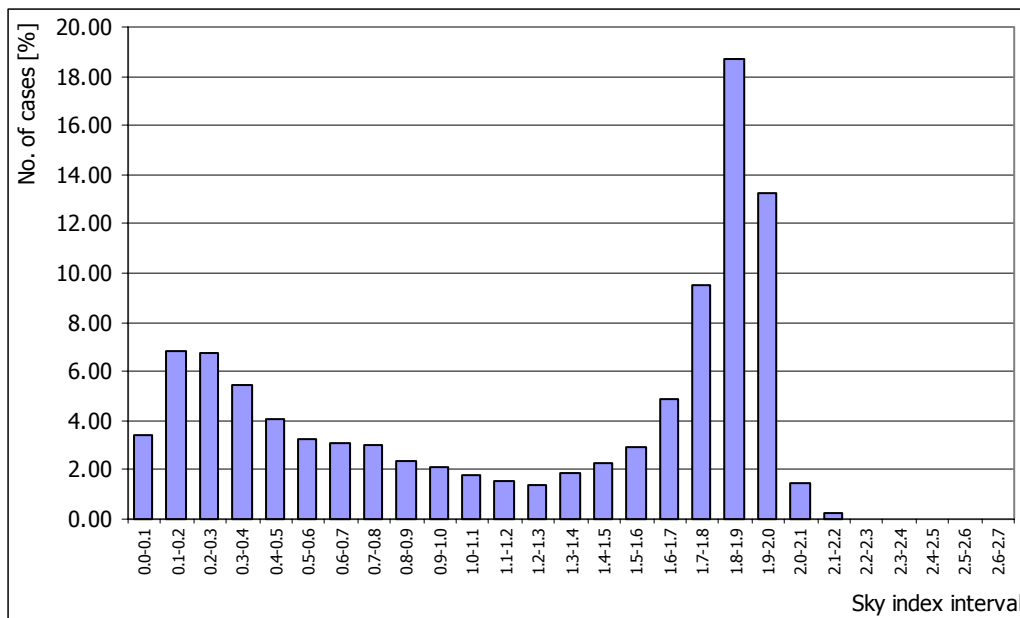


Fig. 4.29. Sky index bins and number of cases in bins

There are not many cases (126 or 1.7%) with sky index higher than 2.0. but for all this cases value of  $c'$  is questionable. In equation 4.31 a new formulation for coefficient  $c'$  is given.

$$c'^* = \frac{6}{1 + 0.5 \cdot \exp(40 \cdot (Si - 2))} + 6 \quad (4.31)$$

If we do not apply a new formulation for  $c'$ , at least we should limit value of sky index for calculations of coefficient  $c'$  to value 2.1.

Original formulation and new formulation of coefficients are plotted on Fig. 4.30

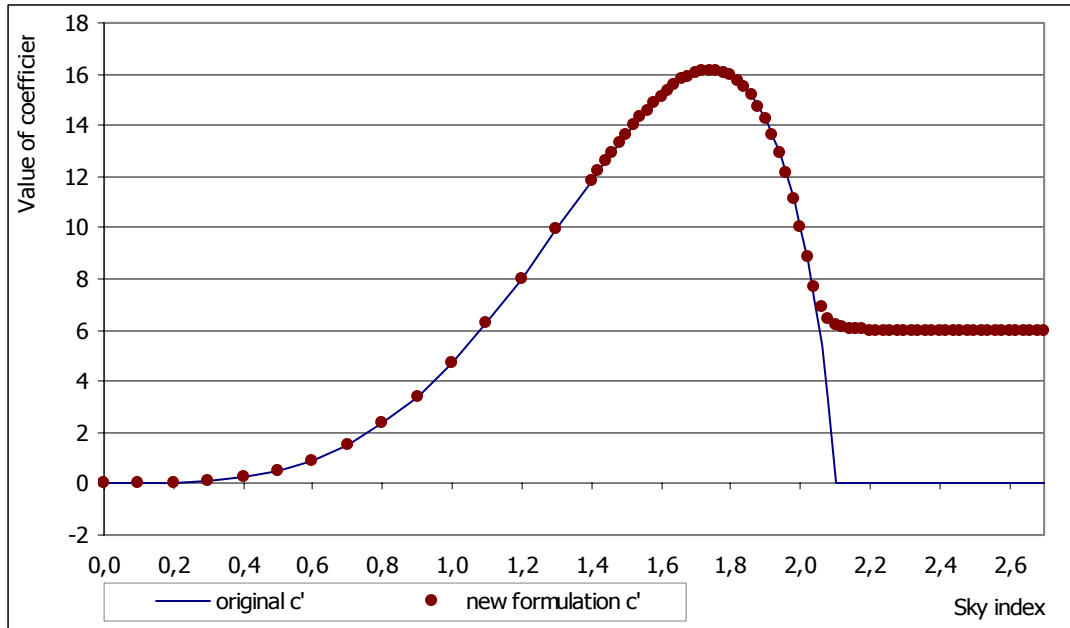


Fig. 4.30. Original and new formulation of coefficients against sky index

If the sky index is limited to value 2.1 in cases where the computed value is higher than 2.1, the luminance distribution can be calculated and luminance profiles can be plotted (Fig. 4.31 -Fig. 4.34).

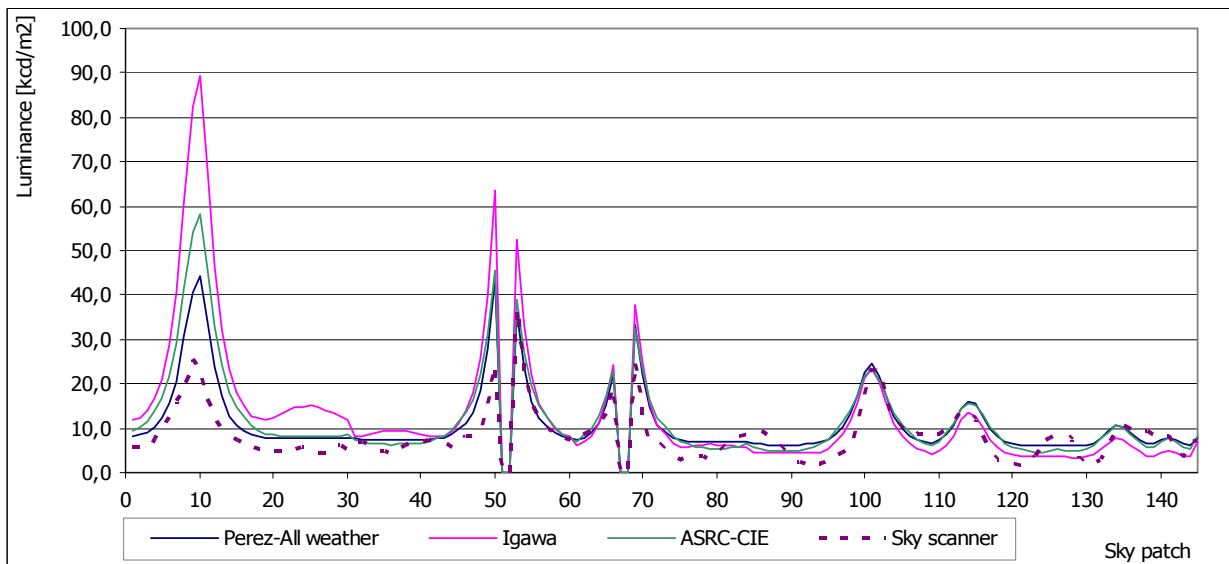


Fig. 4.31. Luminance profile for June 15, 2005 at 18:10 ( $S_i=1.94$ )

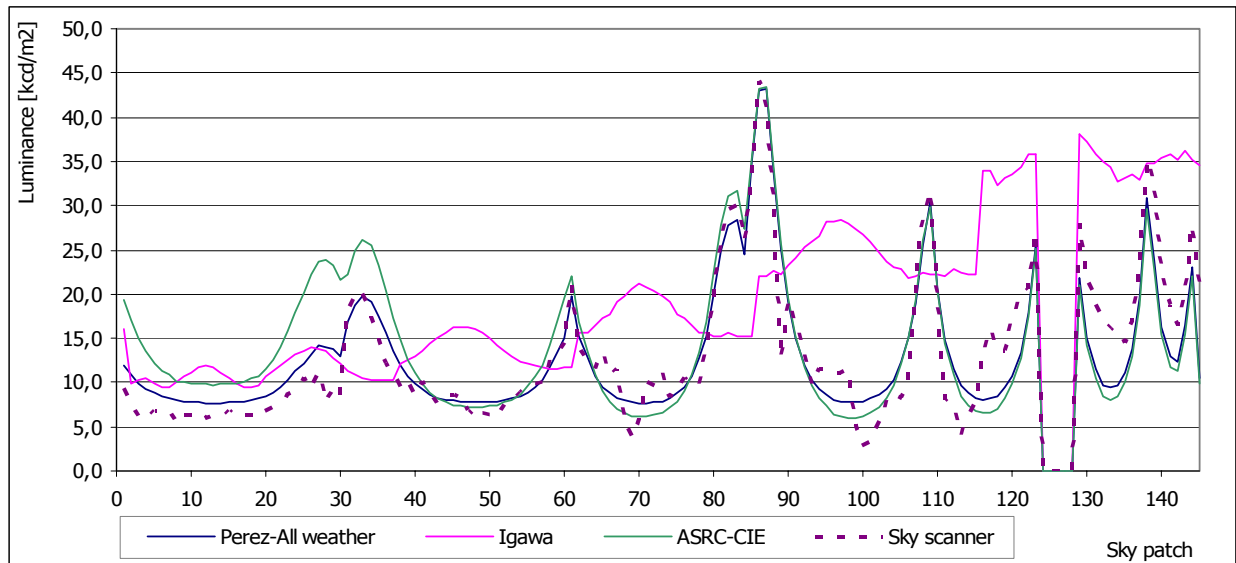


Fig. 4.32. Luminance profile for July 30, 2005 at 11:20 (original  $S_i=2.101$ )

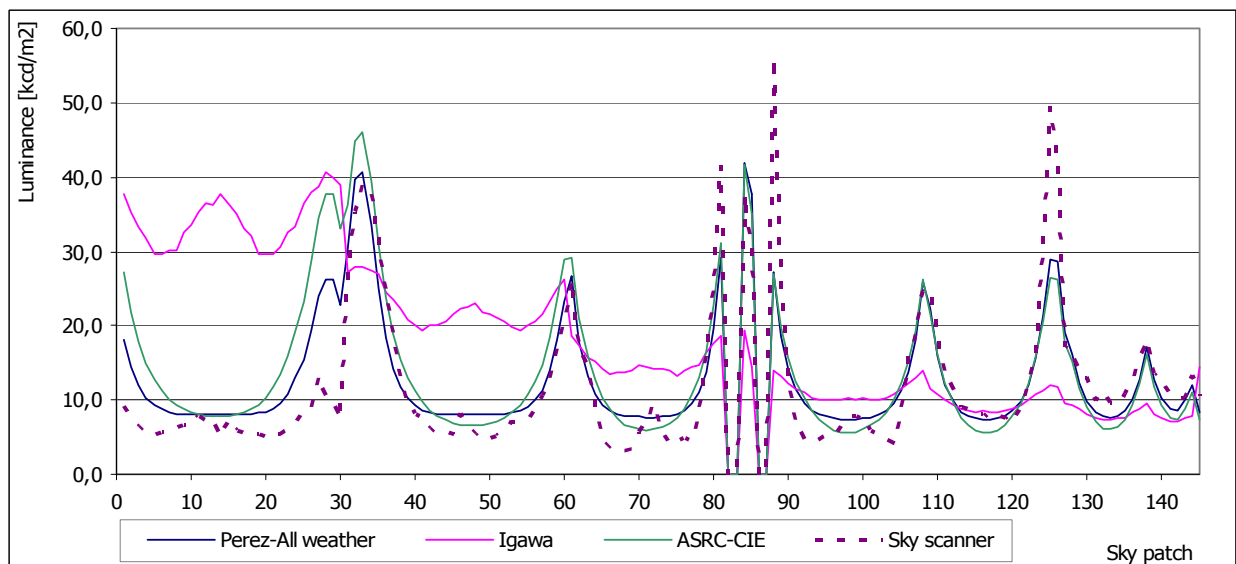


Fig. 4.33. Luminance profile for October 2, 2005 at 10:40 (original  $S_i=2.14$ )

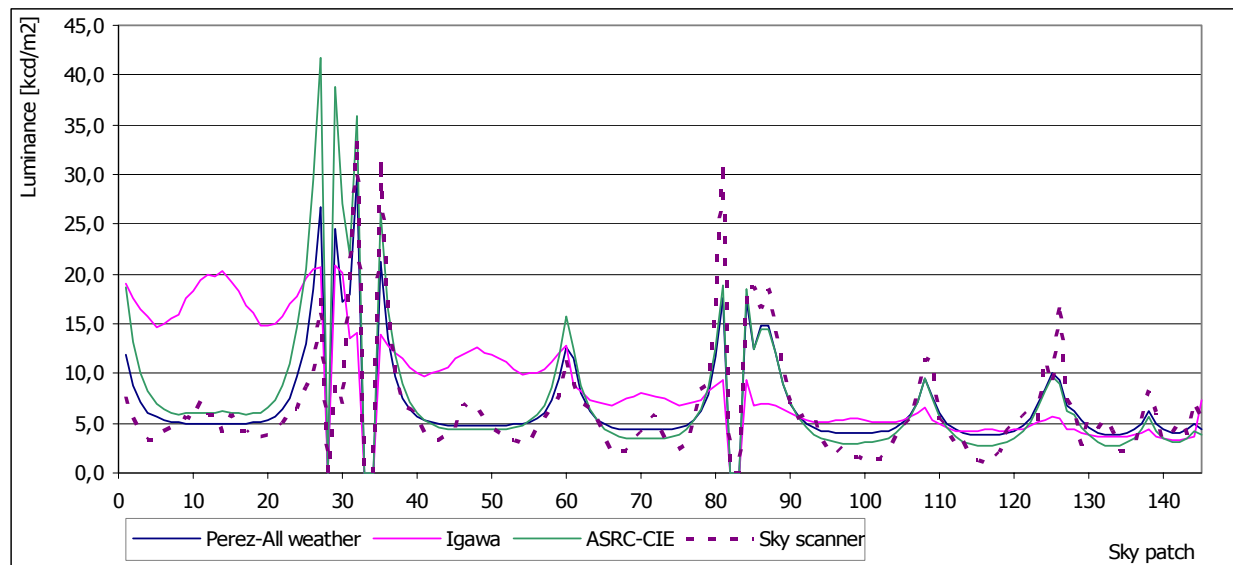


Fig. 4.34. Luminance profile November 1, 2005 at 9:50 (original  $S_i=2.144$ )

All luminance profiles on Fig. 4.31 are in line. Luminances modelled with Igawa model are overestimated, especially around position of sun, but the shape of the profile is same as the shape of the measurements.

On the other hand, the Igawa profile on Fig. 4.32, Fig. 4.33 and Fig. 4.34 is totally different when compared to profiles of Perez All weather, ASRC-CIE or measurements.

Sky index is computed from global and diffuse irradiance and in first case (Fig. 4.30, June 15, 2005 at 18:10) has a value of 1.9386. Sky indices for the other three cases were limited to 2.1 when computing luminances, since their value calculated from global and diffuse irradiances were higher than 2.1.

We can conclude, that Igawa model does not provide comparable luminances for sky index values around 2.1 and higher.

## 4.5 Conclusion on sky luminance models

Sky luminance models have been tested in three different ways:

- All measurements together,
- Measurements sorted by CIE sky type:
  - o with gradation/indicatrix method
  - o with Tregenza statistical method
- Measurements sorted by CIE sky type and sun altitude.

After comparing sky luminance models in all ways, we can conclude that on average ASRC-CIE sky luminance model provides best results for all CIE sky types. Igawa luminance model gives usually good results for cloudy and sunny skies but extremely bad results for intermediate skies. On the other hand Perez-All weather model provides

usually good results for intermediate skies and extremely bad results for cloudy skies. Perez-All weather model cannot model the standard overcast sky and with that is unable to predict sky type 1, which is CIE standard overcast sky.

In any way, ASRC-CIE sky luminance model provides best results for all sky types and we suggest the use of this sky luminance model for calculations of frequencies of occurrence of CIE sky types from satellite images.





In the model, measurements of illuminances were carried out at ten measuring positions with Li-Cor sensors (Fig. 5.2). Sensors were connected to two data loggers (five sensors per logger).

For measurements of luminances on indoor walls, a digital camera with a fish-eye lens was fixed just under the window opening (Fig. 5.2 and Fig. 5.3). With the camera and Photolux we were able to produce luminance maps for practically all indoor walls except the one with window.

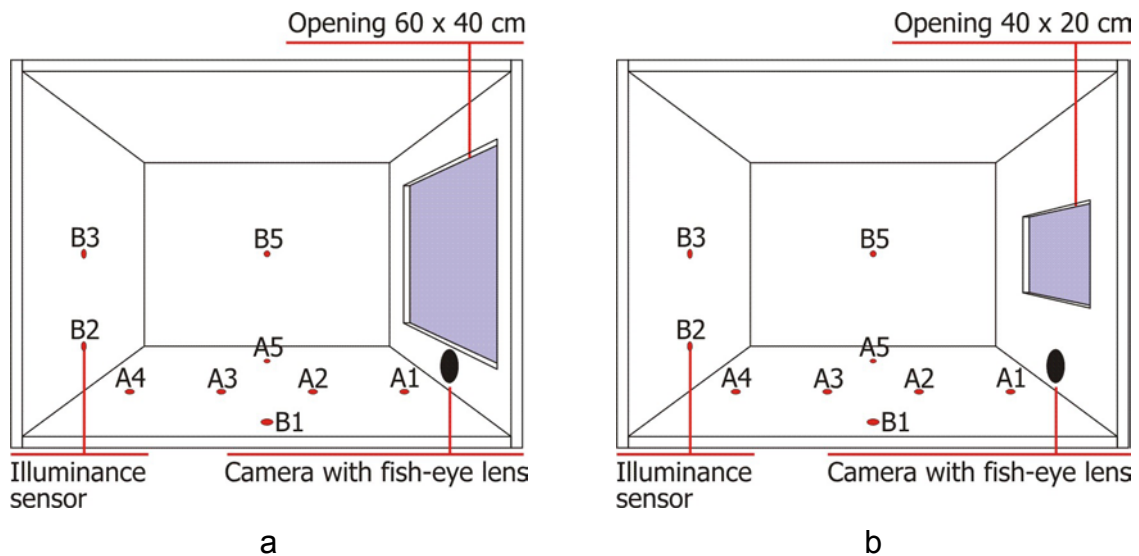


Fig. 5.2. Scale model with illuminance sensors and fish-eye lens



Fig. 5.3. Position of the digital camera with fish-eye lens (black surface is the opening (60 cm x 40 cm) into the scale model)

At the same time also luminance of a view from a window was taken. For this, we used another digital camera also with a fish-eye lens. A Nikon CoolPix 990 digital camera was fixed on the box on the right at the height of the middle of the window (Fig. 5.4).



*Fig. 5.4. Digital camera with fish-eye lens for outdoor luminance measurements*

The wooden box with the Li-Cor sensors, the two data loggers and the two cameras with fish-eye lens was placed on the roof of ENTPE building. Because of the surrounding obstacles we wanted to place the scale model as high as possible. The best choice was to place it on a wooden base, which was fixed in place using spirit level, on the concrete ventilation shaft (Fig. 5.5).



*Fig. 5.5. Scale model was positioned on ventilation shaft*

## 5.2.1 Illuminance and luminance measurements in scale model

### 5.2.1.1 Illuminance

Indoor illuminance was measured at ten places with Li-Cor sensors. Measurements were performed on six different points on floor of the scale model, two on back wall and one on each side wall.

Sensors were connected to data logger and were stored every minute. Every stored measurement is an average value of 1 s measurements.

### 5.2.1.2 Indoor luminances

For indoor luminance purposes a digital camera Nikon CoolPix 5000 with fish-eye was installed under the window opening. For every luminance measurement at least four or five pictures were taken (Fig. 5.6a). Span between the highest and the lowest luminance in model was so high that pictures with different exposure values were needed. All fish-eye images were processed with Photolux (Fig. 5.6b). Luminance measurements were performed when sky scanner started to run (every ten minutes) and when it returned to home position (three minutes after the start). For every sky scan two luminance maps are available for all indoor walls. For comparisons we used the average of both measurements.

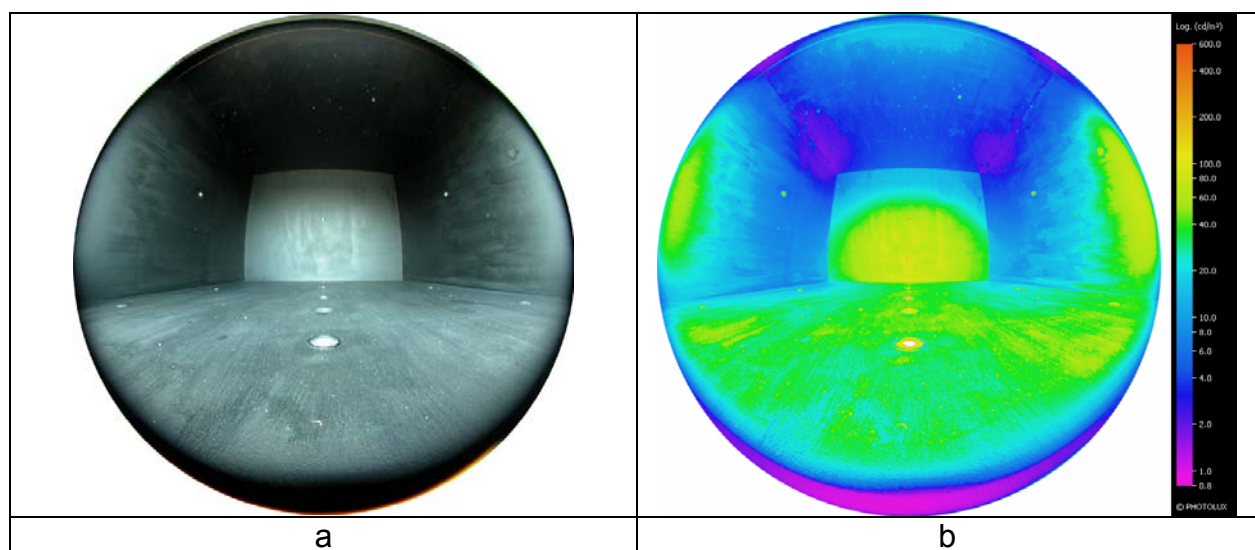


Fig. 5.6. Fish-eye image of indoor (a) and luminance map of indoor walls (b)

### 5.2.1.3 Outdoor luminances

For outdoor luminance purposes a digital camera Nikon CoolPix 990 with fish-eye was installed on the side of the window opening. All fish-eye images (Fig. 5.7a) were processed with Photolux (Fig. 5.7b). Luminance measurements were performed in the same manner as for indoor luminance measurements, one at the time when sky

scanner started to run and one when it returned to home position. For every sky scan two luminance maps are available for the view from the window. For comparisons we used the average of both measurements.

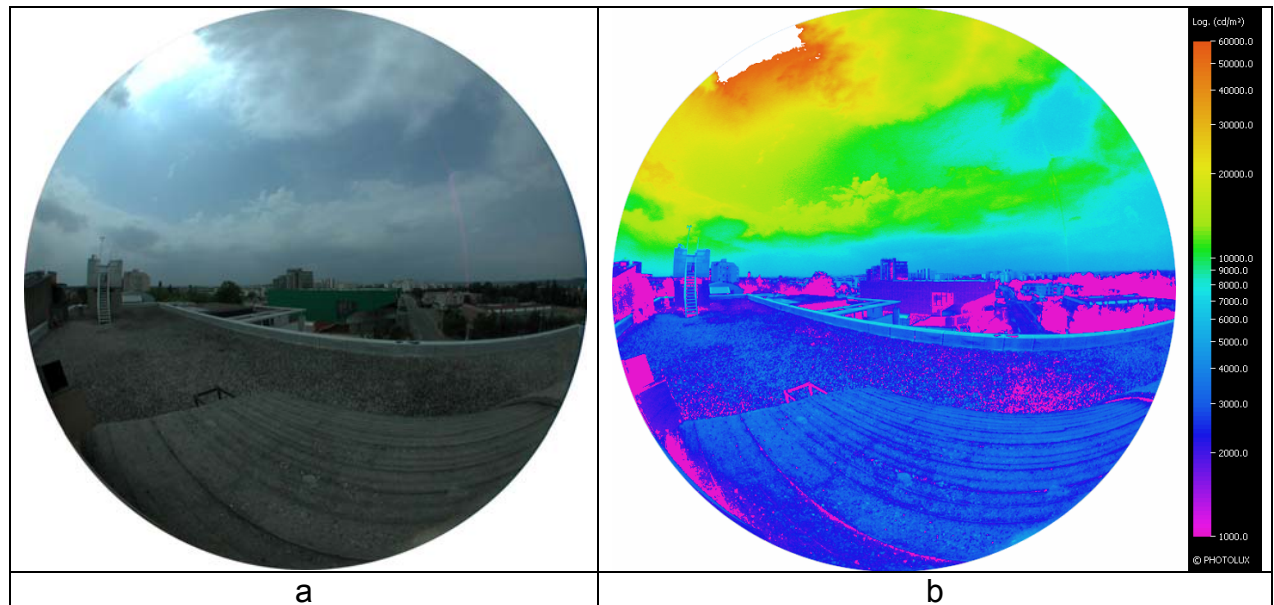


Fig. 5.7. Fish-eye image of a view from the window (a) and luminance map of the same view (b)

### 5.2.2 View from a scale model

View from a scale model is dependant on position of observation. A view from each point is differently obstructed with wall surrounding the window opening. For all ten points in which we measured illuminances, we calculated vertical and horizontal angles of view through the window opening. Calculated angles are listed in Table 5.1. Angles listed in the table are defined with Fig. 5.8 and Fig. 5.9.

Table 5.1. Angles of view through the window for a window opening 60x40 cm

Point of measurement	Coordinates in a room			Angles of view for a window opening 60x40 cm				Angles of view for a window opening 40x20 cm			
	X (m)	Y (m)	Z (m)	$\alpha_{V1}$ (°)	$\alpha_{V2}$ (°)	$\gamma_{V1}$ (°)	$\gamma_{V2}$ (°)	$\alpha_{V1}$ (°)	$\alpha_{V2}$ (°)	$\gamma_{V1}$ (°)	$\gamma_{V2}$ (°)
A1	0	-0.1	0	-68.53	68.53	45.00	76.72	-59.46	59.46	63.43	73.56
A2	0	-0.3	0	-43.33	43.33	18.43	57.54	-32.17	32.17	33.69	51.52
A3	0	-0.5	0	-30.08	30.08	11.31	43.99	-21.11	21.11	21.80	37.68
A4	0	-0.7	0	-22.68	22.68	8.13	34.85	-15.57	15.57	15.95	29.12
A5	-0.3	-0.4	0	-55.14	0.00	14.04	50.10	-50.10	-14.04	26.57	43.74
B1	0.3	-0.4	0	0.00	55.14	14.04	50.10	14.04	50.10	26.57	43.74
B2	0	-0.8	0.1	-20.14	20.14	0.00	26.06	-13.74	13.74	7.13	20.14
B3	0	-0.8	0.3	-20.14	20.14	-13.74	13.74	-13.74	13.74	-6.97	6.97
B4	0.4	-0.4	0.3	14.04	59.16	-25.57	25.57	26.57	55.14	-13.45	13.45
B5	-0.4	-0.4	0.3	-59.16	-14.04	-25.57	25.57	-55.14	-26.57	-13.45	13.45

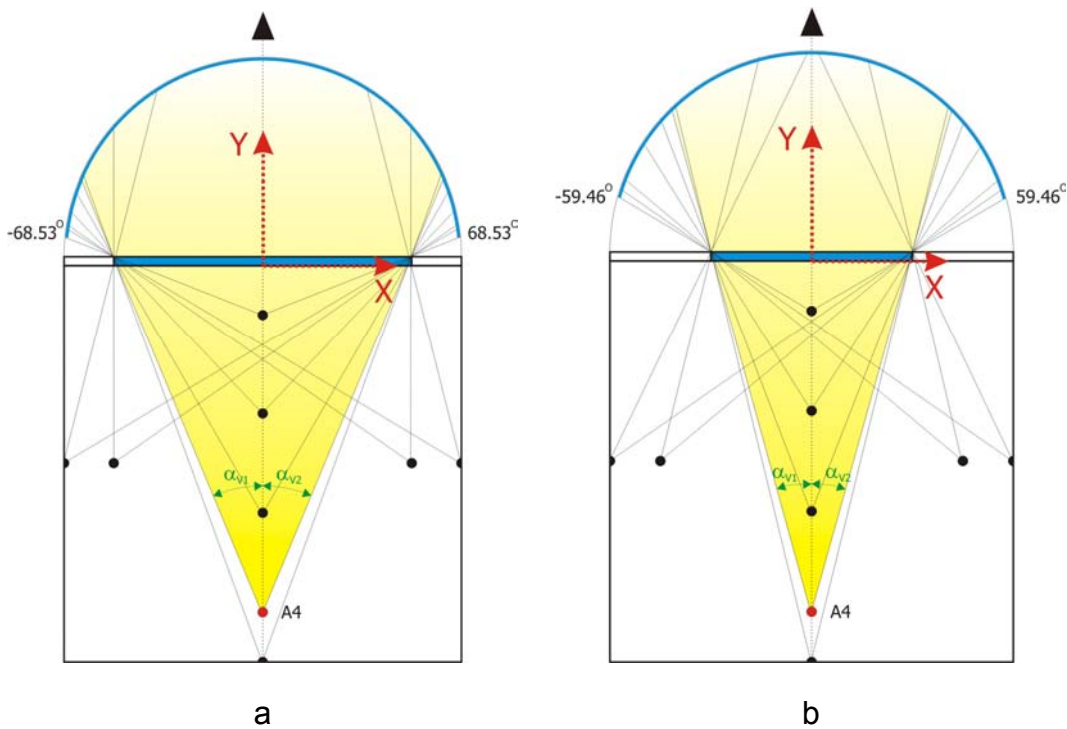


Fig. 5.8. Horizontal angles defining view from a window with sample angles for point A4 (a-opening 60x40 cm, b-opening 40x20 cm)

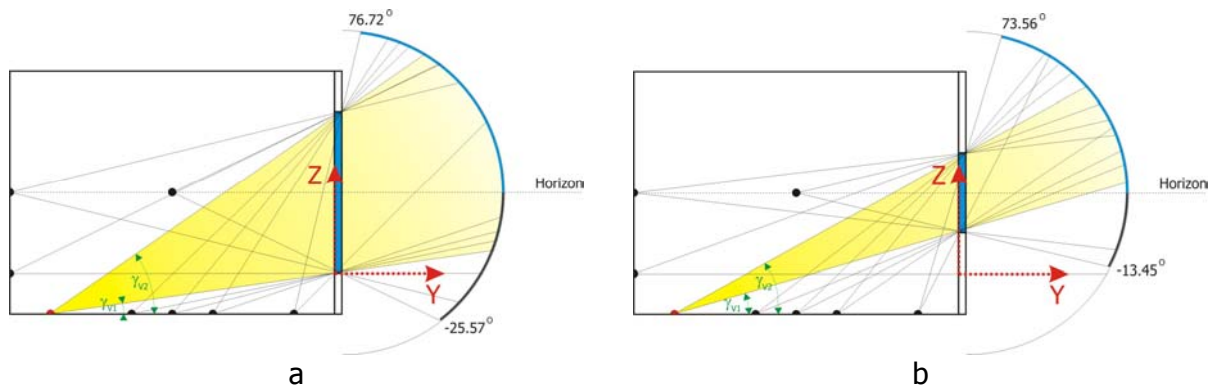


Fig. 5.9. Vertical angles defining view from a window with sample angles for point A4 (a-opening 60x40 cm, b-opening 40x20 cm)

Points of measurements can be divided into three groups. In the first group are the points where we measured the horizontal illuminance. This group consists of points A1, A2, A3, A4, A5 and B1. In the second group are two points (B2 and B3) on the wall opposite the wall with the window opening. And in the last group there are the remaining two points (B4 and B5), which are placed on side walls. At these last four points, we measured the vertical illuminance.

For all measuring points we also created images of view from a point through the window opening. Images are presented in Fig. 5.10.

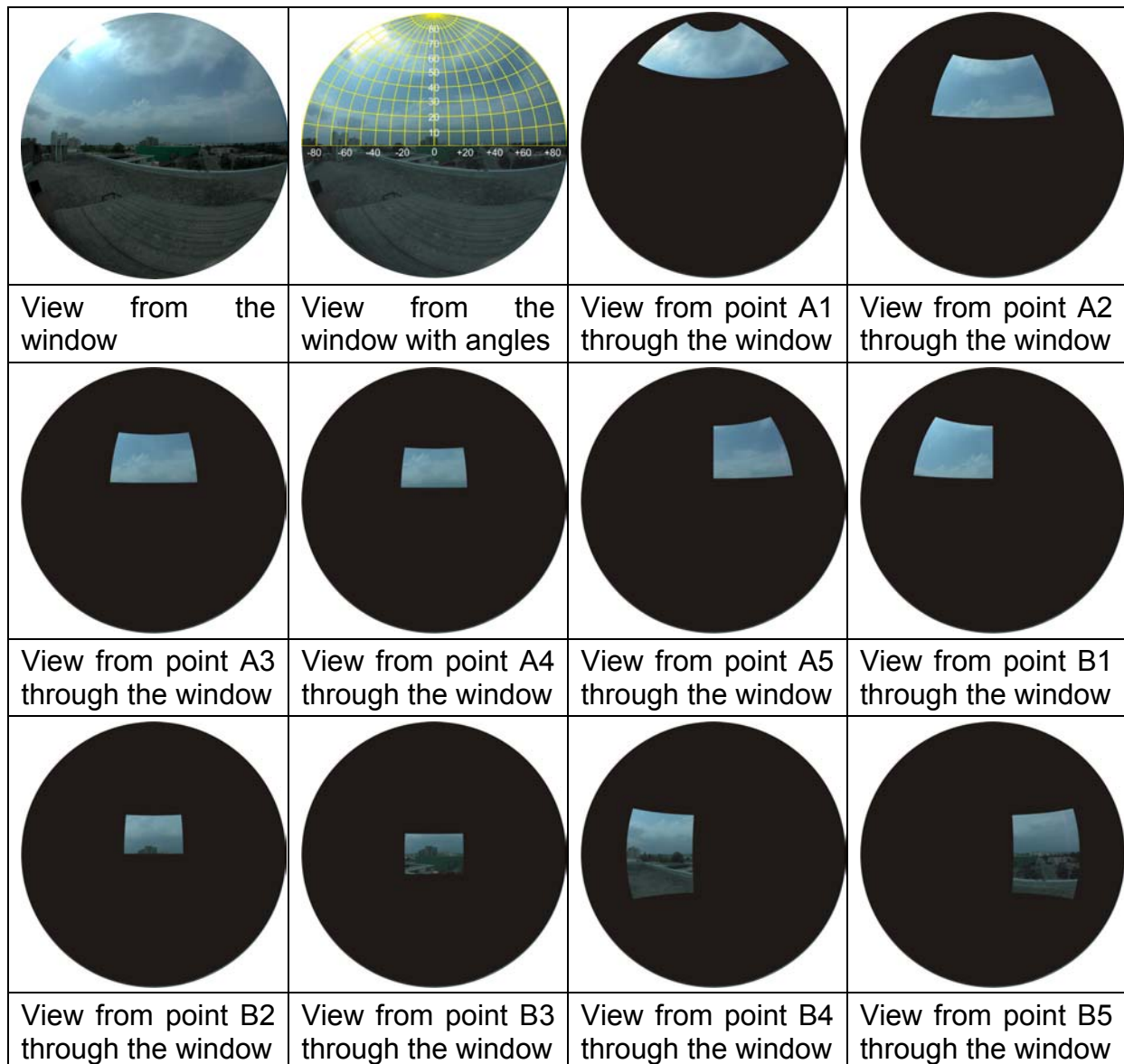


Fig. 5.10. Images of view from the window opening for all points of measurement for a window opening 60x40 cm

### 5.3 Calculation of directional daylight factors

In our work, we calculated directional daylight factors (DDF) for different celestial hemisphere partitioning. The hemisphere can be divided into different number of discrete sky elements. To investigate the influence of the number of sky elements on the error in illuminance calculations, we calculated DDF's and latter illuminance values for the hemisphere divided into 212, 145, 97, 26 and 13 sky elements (Fig. 5.11). All the grids except the 13 elements grid, are of the Genelux type. Genelux grid is characterized by a constant interval in zenith angle and in quasi constant solid angles. The numbers of sky elements are defined with the density of the grid. In the first case, the interval in zenith angle is 10 degrees, in second 12 degrees then 15 and 30 degrees respectively. Grid with 13 elements is not of the Genelux type. In this case the hemisphere is divided into three different altitude zones: a horizontal band, a zenith

zone and intermediate band. The horizontal band is divided into 8 zones and the intermediate band into 4 zones. Each zone has the same zenith angle.

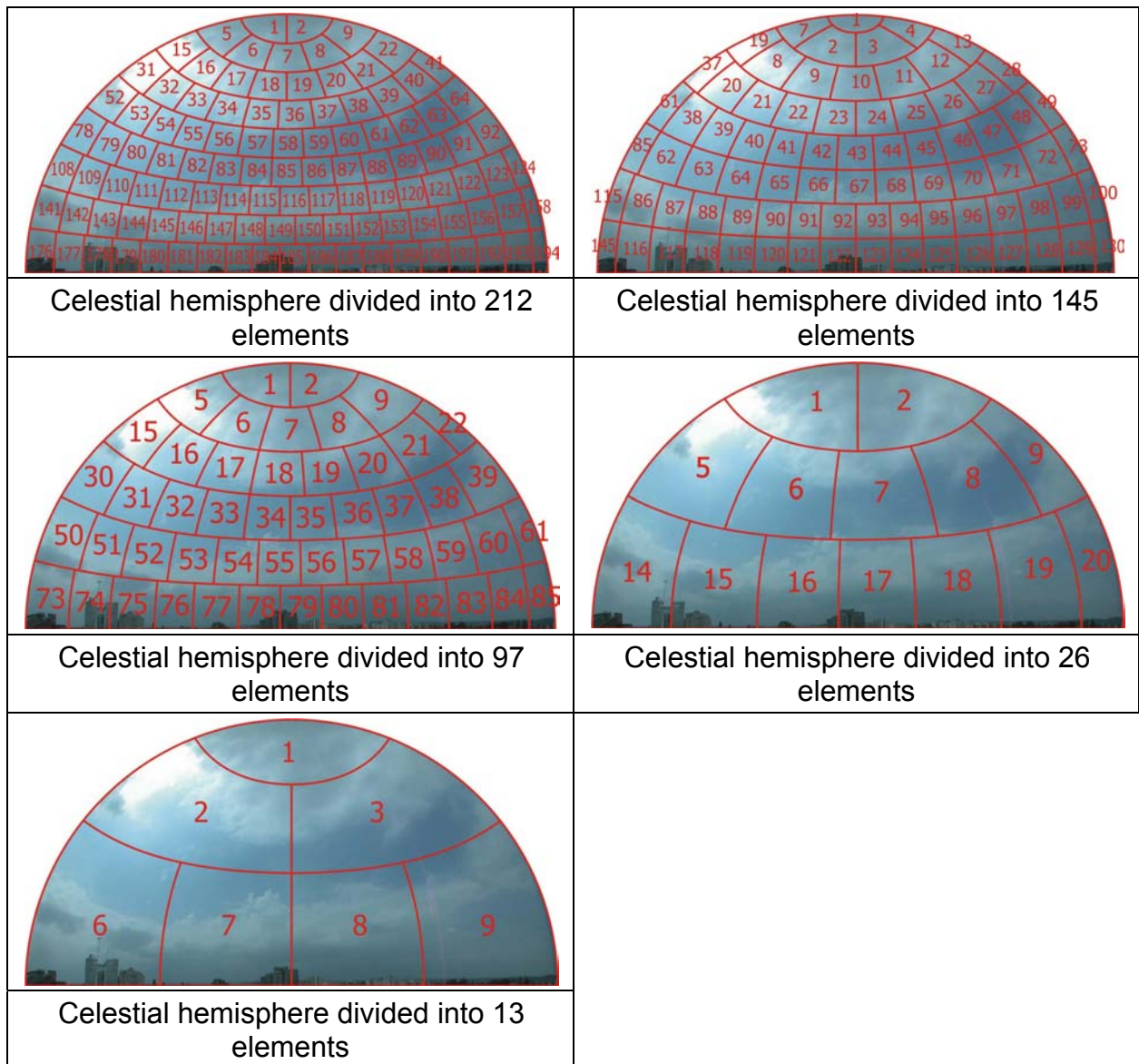


Fig. 5.11. Different sky partitions with different grid density (view to the east)

The quantity of daylight that penetrates into indoor premises can be represented in different ways. The most common way is to represent it with daylight factor.

Daylight factor is ratio of the illuminance at a point on a given plane due to the light received directly or indirectly from a sky of assumed or known luminance distribution, to the illuminance on a horizontal plane due to an unobstructed hemisphere of this sky. The contribution of direct sunlight to both illuminances is excluded. Glazing, dirt effects, etc. are included. When calculating the lighting of interiors, the contribution of direct sunlight must be considered separately. Unless stated otherwise the sky luminance distribution is assumed to be that of the CIE standard overcast sky.

In our work we would like to evaluate the contribution of individual sky elements to the illuminance at a point on a given plane. Since daylight factor describes the contribution of the whole sky, we should implement more sophisticated daylight representation – directional daylight factor.

Directional daylight factor (DDF) is the daylight factor at a point P due to the light received from only a patch of the sky. In other words: DDF is the ratio between the illuminance at a given point due to a sky element over the illuminance produced outdoor by the same sky element (eq. 5.1).

$$DDF_{Ap} = \frac{E_{AIntp}}{E_{AExtp}} \quad (5.1)$$

Where:

- $DDF_{Ap}$  directional daylight factor related to a sky element p at a given point A
- $E_{AIntp}$  indoor illuminance at a given point A, produced by sky element p
- $E_{AExtp}$  outdoor (unobstructed) illuminance at a given point A, produced by sky element p

As seen, the DDF related to a sky element at a given point, can be expressed with indoor and outdoor illuminances. Indoor and outdoor illuminances are defined with equations 5.2 and 5.3.

The equation 5.2 describes only the direct component of daylight. Indirect component in this equation is neglected because the walls of the scale model were painted in black and there are no multiple reflections inside the scale model. Besides neglecting the indirect component, we should not forget the glazing. In the scale model we do not have any glazing and the luminance of a sky element that is seen from inside, is the same as its true luminance. In real buildings the luminance of a sky element should be corrected with the influence of the transmission factor and the incidence angle between the sky element and glass surface.

$$E_{AIntp} = L_p \cdot \cos(Z_p') \cdot \Delta S' \quad (5.2)$$

$$E_{AExtp} = L_p \cdot \cos(Z_p) \cdot \Delta S \quad (5.3)$$

Where:

- $L_p$  mean luminance of a sky element
- $Z_p'$  incidence angle between surface in point and sky element
- $\Delta S_p'$  solid angle of a sky element seen from indoor
- $Z_p$  zenith angle of a sky element
- $\Delta S_p$  solid angle of a sky element

If we combine equations 5.1, 5.2 and 5.3, DDF related to a sky element at a given point can be expressed:

$$DDF_{Ap} = \frac{E_{AIntp}}{E_{AExtp}} = \frac{L_p \cdot \cos(Z_p') \cdot \Delta S'}{L_p \cdot \cos(Z_p) \cdot \Delta S} = \frac{\cos(Z_p') \cdot \Delta S'}{\cos(Z_p) \cdot \Delta S} \quad (5.4)$$

In our scale model all six points, that were taken latter into account for evaluation, are on horizontal plane – floor. The floor plane is parallel to ground and because of that the incidence angle between surface in a point and sky element is the same as the zenith angle of a sky element:

$$Z_p = Z_p' \quad (5.5)$$

For the six points on the floor the DDF notation can be simplified to:

$$DDF_{Ap} = \frac{\Delta S'}{\Delta S} \quad (5.6)$$

A reader can see from equation 5.6 that DDF for six points in the scale model is just a ratio between a solid angle of a sky element seen from indoor and solid angle of a sky element. If a whole sky element is seen from the point in the scale model, that DDF equals 1, if a sky element is not seen from a point, the DDF equals 0. If only a part of a sky element is seen from the point, the value of the DDF is between 0 and 1.

The sky is divided into zones of altitude and azimuth, and the directional daylight factor can be computed for each zone. The total illuminance at a point is the sum of the products of the mean luminance of each sky element, the solid angle of the each sky element, the cosine of the mean zenith angle of each sky element and the corresponding directional daylight factor (eq. 5.7):

$$E_A = \sum_{p=1}^n DDF_{Ap} \cdot \Delta S_p \cdot \cos(Z_p) \cdot L_p \quad (5.7)$$

Where:

- $E_A$  total illuminance at a given point (in this example for point A)
- $DDF_{Ap}$  directional daylight factor related to a sky element p for a point A in the model
- $\Delta S_p$  solid angle of a sky element
- $Z_p$  zenith angle of a sky element
- $L_p$  mean luminance of a sky element

Zenith angle of a sky element and solid angle of a sky element are unique for each sky element. Regarding this fact a product of DDF, solid angle and zenith angle can be replaced with so called directional daylight quotient (DDQ):

$$DDQ_{Ap} = DDF_{Ap} \cdot \Delta S_p \cdot \cos(Z_p) \quad (5.8)$$

DDQ is unique for each sky element.

Illuminance values in different points in our scale model will be calculated directly from luminance values of sky elements.

For these calculations it's possible to rewrite equation 5.2. In equation 5.9 a product of DDF, solid angle and zenith angle is replaced with directional daylight quotient (DDQ): With new notation the total illuminance at a given point can be computed with:

$$E_A = \sum_{p=1}^n DDQ_{Ap} \cdot L_p \quad (5.9)$$

Where:

- $E_A$  total illuminance at a given point (in this example for point A)
- $DDQ_{Ap}$  directional daylight quotient related to a sky element p for a point A in the model
- $L_p$  mean luminance of a sky element

DDF is without units and is expressed in per cents, on the other hand the DDQ has a unit  $lx \cdot m^2 / Cd$ . Directional daylight quotients describe contribution of each sky element to the illuminance at a given point in the model.

When directional daylight quotients were calculated we were taking into account the window opening and position of a point in a model.

Since most of the sky elements are obstructed with walls of the model (window only on one wall) there are only few sky elements that penetrate light into the model. The numbers of sky elements that are visible from measuring points in the model depend on the sky partitioning and position of a point in the model. Some elements that are seen from the points in the model are seen totally and on the other hand some elements are seen only partly. In the calculation of a solid angle  $\Delta S_{Ap}$  we have taken this into account.

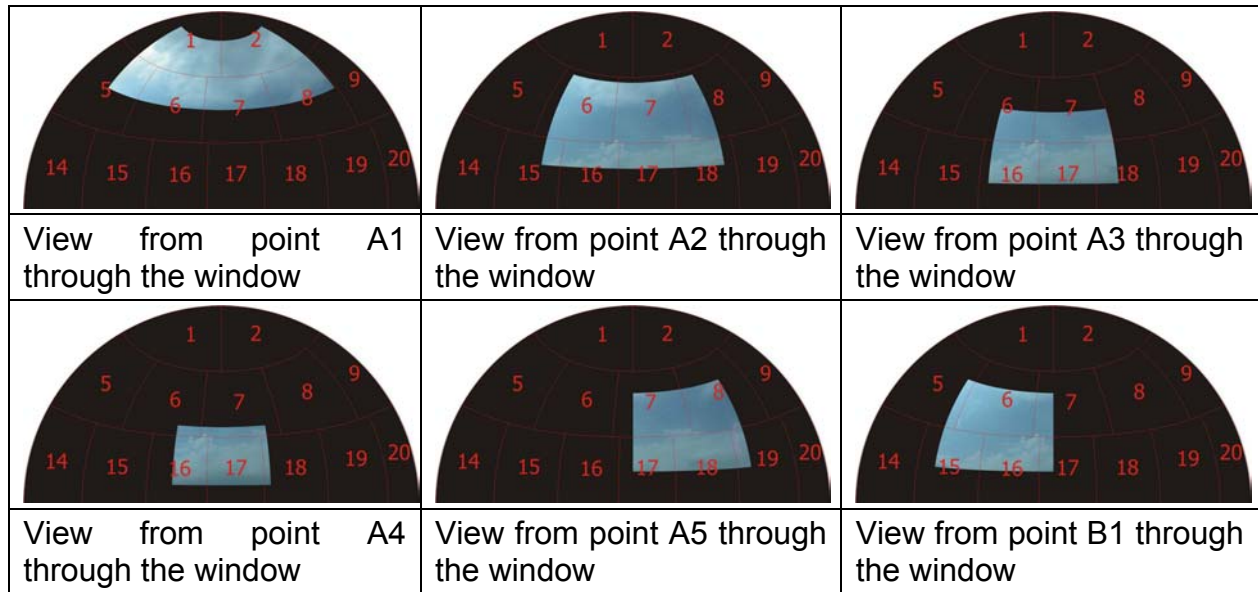


Fig. 5.12. Fish eye images of view from points of measurement on floor with a mask of sky model with 26 sky elements (view to the east) for a window opening 60x40 cm

For each sky element a percentage of the element that is seen from a measuring point (Fig. 5.12) in the model was calculated. Then those percentages were multiplied with solid angles of the sky elements, the results are “visible solid angles” of sky elements from a measuring point in the model. For all sky partitioning, tables similar to Table 5.2 were designed.

For the evaluation purposes of the solid angle calculation we also calculated the sum of solid angles of all sky elements viewed from measuring points on floor of the model. As we supposed the sum should be practically the same for all sky partitioning. The results are listed in Table 5.3 and presented in diagrams Fig. 5.13a and Fig. 5.13b. As it can be read from the diagrams the solid angles do not differ much regarding the sky partitioning. The highest difference was seen at sky partitioning into 26 elements, smaller window opening and measuring point A1. The most probable reason for the difference lies in small zenith angle and the fact that window opening is covering parts of only two sky elements.

Table 5.2. Percentages and solid angles of a sky element visible from measuring points in the model for a window opening 60x40 cm (sky partitioned into 26 elements)

Sky element	Solid angle	Percentage of sky element visible from point in a model						Solid angle of sky element visible from point in a model					
		A1	A2	A3	A4	A5	B1	A1	A2	A3	A4	A5	B1
	$S_r$	%						$S_r$					
1	0.210447	42.44	0	0	0	0	0	0.0893	0	0	0	0	0
2	0.210447	42.44	0	0	0	0	0	0.0893	0	0	0	0	0
3	0.210447	0	0	0	0	0	0	0	0	0	0	0	0
4	0.210447	0	0	0	0	0	0	0	0	0	0	0	0
5	0.255534	23.16	0	0	0	8.61	0	0.0592	0	0	0	0.0220	0
6	0.255534	50	76.49	23.41	5.12	67.00	0	0.1278	0.1955	0.0598	0.0131	0.1712	0
7	0.255534	50	91.80	46.63	13.21	16.75	50.25	0.1278	0.2346	0.1192	0.0338	0.0428	0.1284
8	0.255534	48.16	30.59	0.09	0	0	42.11	0.1231	0.0782	0.0002	0	0	0.1076
9	0.255534	0	0	0	0	0	0	0	0	0	0	0	0
10	0.255534	0	0	0	0	0	0	0	0	0	0	0	0
11	0.255534	0	0	0	0	0	0	0	0	0	0	0	0
12	0.255534	0	0	0	0	0	0	0	0	0	0	0	0
13	0.255534	0	0	0	0	0	0	0	0	0	0	0	0
14	0.241661	0	0	0	0	0	0	0	0	0	0	0	0
15	0.241661	0	12.13	0	0	39.42	0	0	0.0293	0	0	0.0953	0
16	0.241661	0	38.57	52.09	41.48	53.20	0	0	0.0932	0.1259	0.1002	0.1286	0
17	0.241661	0	38.57	62.30	72.90	13.30	39.90	0	0.0932	0.1506	0.1762	0.0321	0.0964
18	0.241661	0	31.42	20.95	5.03	0	53.20	0	0.0759	0.0506	0.0122	0	0.1286
19	0.241661	0	0	0	0	0	12.83	0	0	0	0	0	0.0310
20	0.241661	0	0	0	0	0	0	0	0	0	0	0	0
21	0.241661	0	0	0	0	0	0	0	0	0	0	0	0
22	0.241661	0	0	0	0	0	0	0	0	0	0	0	0
23	0.241661	0	0	0	0	0	0	0	0	0	0	0	0
24	0.241661	0	0	0	0	0	0	0	0	0	0	0	0
25	0.241661	0	0	0	0	0	0	0	0	0	0	0	0
26	0.241661	0	0	0	0	0	0	0	0	0	0	0	0

Table 5.3. Table of solid angles of view from measuring points for different sky partitioning

Sky partitioning	Solid angles of view with window opening 60x40 cm						Solid angles of view with window opening 40x20 cm					
	A1	A2	A3	A4	A5	B1	A1	A2	A3	A4	A5	B1
13	0.636	0.789	0.520	0.343	0.495	0.495	0.129	0.237	0.190	0.116	0.154	0.154
26	0.616	0.800	0.506	0.335	0.492	0.492	0.094	0.244	0.170	0.119	0.141	0.141
97	0.628	0.796	0.523	0.338	0.499	0.499	0.140	0.253	0.175	0.115	0.154	0.154
145	0.631	0.796	0.520	0.340	0.503	0.503	0.138	0.254	0.176	0.114	0.153	0.153
212	0.635	0.795	0.521	0.339	0.506	0.506	0.134	0.257	0.176	0.115	0.153	0.153
20763	0,637	0,798	0,523	0,340	0,505	0,505	0,134	0,256	0,177	0,115	0,154	0,154
CIE145	0,629	0,796	0,520	0,340	0,503	0,503	0,138	0,254	0,176	0,114	0,153	0,153

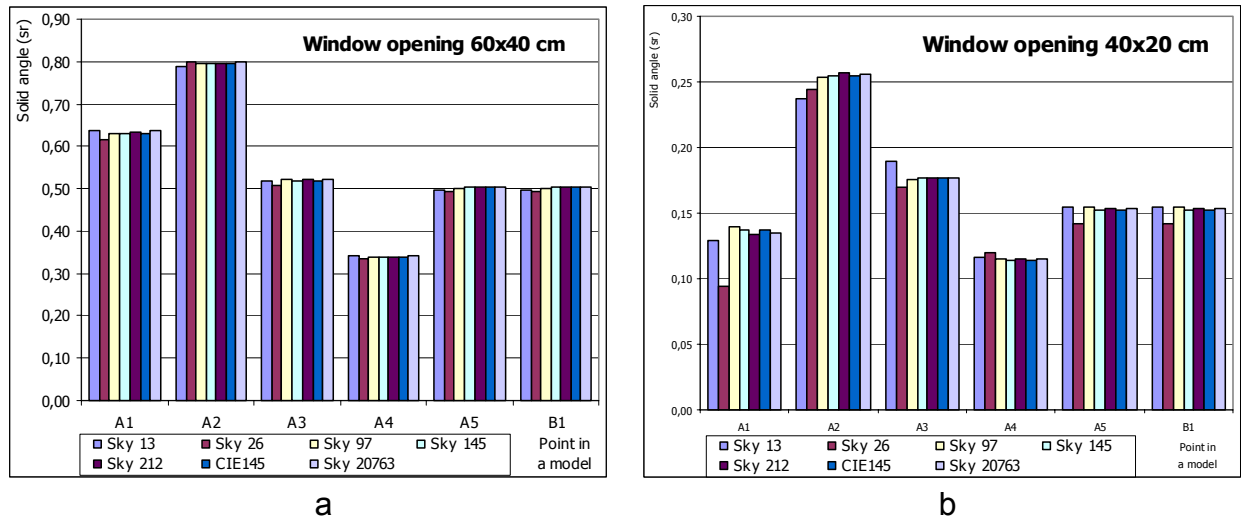


Fig. 5.13. Solid angle of view from measuring points for different sky partitioning (a-window opening 60x40cm, b- window opening 40x20cm)

With the calculated solid angles it was possible to calculate DDQ's with use of equation 5.8 for all sky partitioning, all measuring points, all sky elements and both window opening. As a sample we show a table for DDQ's for sky partitioning into 26 elements with window opening 60x40 cm.

Table 5.4. Directional daylight quotients for sky partitioning into 26 elements with window opening 60x40 cm.

Sky element	Directional daylight quotient for points in a model					
	A1	A2	A3	A4	A5	B1
	lx m <sup>2</sup> /cd					
1	0.08627	0	0	0	0	0
2	0.08627	0	0	0	0	0
3	0	0	0	0	0	0
4	0	0	0	0	0	0
5	0.04185	0	0	0	0.01556	0
6	0.09034	0.13821	0.04230	0.00926	0.12106	0
7	0.09034	0.16587	0.08426	0.02387	0.03027	0.09080
8	0.08702	0.05528	0.00017	0	0	0.07609
9	0	0	0	0	0	0
10	0	0	0	0	0	0
11	0	0	0	0	0	0
12	0	0	0	0	0	0
13	0	0	0	0	0	0
14	0	0	0	0	0	0
15	0	0.00759	0	0	0.02466	0
16	0	0.02412	0.03258	0.02594	0.03327	0
17	0	0.02412	0.03897	0.04560	0.00832	0.02496
18	0	0.01965	0.01310	0.00315	0	0.03327
19	0	0	0	0	0	0.00803
20	0	0	0	0	0	0
21	0	0	0	0	0	0
22	0	0	0	0	0	0
23	0	0	0	0	0	0
24	0	0	0	0	0	0
25	0	0	0	0	0	0
26	0	0	0	0	0	0

## 5.4 Calculation of illuminance values in scale model

Illuminance values were calculated for all points in the scale model for all cases of scale model measurements. Values are presented in a database of scale model measurements.

Illuminance calculations were done with equation 5.9.

Since illuminance values depend on luminance of sky elements it was necessary to first calculate luminance values of sky elements for all sky partitioning.

### 5.4.1 Calculation of luminance values of sky elements

Luminance values of sky elements were defined with digital image of the view from the window. All images were edited in Photolux software and luminances saved in Genelux format. Using the Genelux format we kept 20673 patches of the view. Each patch is defined with left and right bordering azimuth, upper and lower bordering zenith angle, solid angle of the patch and its luminance. Unfortunately azimuths and zenith angles

would have the right meaning if the picture would be taken horizontally, but the pictures were taken vertically. To get the azimuths and zenith angles with the right meaning we had to transform vertical values into horizontal values (Fig. 5.14).

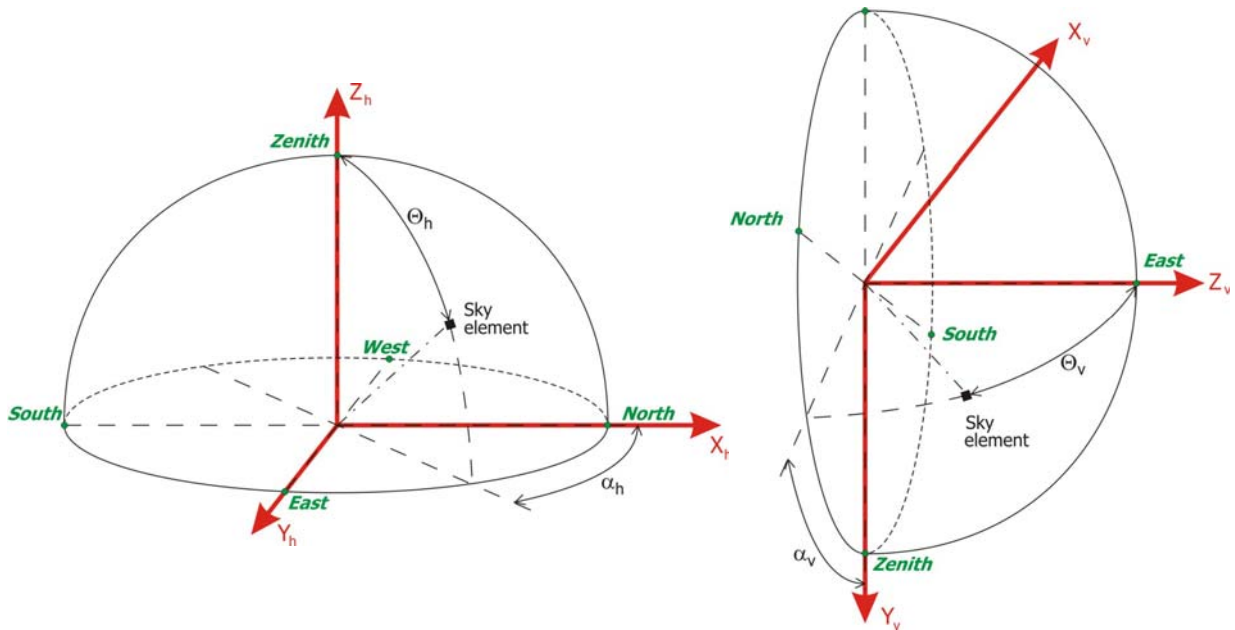


Fig. 5.14. Angles defining sky element at horizontal and vertical camera position

Cartesian coordinates of a sky element are defined with next equation:

$$\begin{aligned} X_h &= \cos \alpha \cdot \sin \Theta \\ Y_h &= \sin \alpha \cdot \sin \Theta \\ Z_h &= \cos \Theta \end{aligned} \quad (5.10)$$

From the Fig. 5.14 next relation between angles can be read:

$$\begin{aligned} X_v &= -Y_h \\ Z_v &= X_h \\ Y_v &= -Z_h \end{aligned} \quad (5.11)$$

With a combination of equations 5.10 and 5.11 it is possible to express vertical azimuth and zenith angles with horizontal ones:

$$\begin{aligned} \alpha_v &= \arctan(\sin \alpha_h \cdot \tan \Theta_h) \\ \Theta_v &= \arccos(\cos \alpha_h \cdot \sin \Theta_h) \end{aligned} \quad (5.12)$$

When the equation 5.12 was applied to all 20673 sky elements, bordering angles of 20673 sky elements and bordering angles of different sky partitioning were in the same system of coordinates and luminance values could be calculated for all sky partitioning.

Luminance values were then multiplied with directional daylight quotients (equation 5.9).

### 5.4.2 Calculation of illuminance values in scale model with daylight factors

For comparison reasons we calculated the illuminance values in the scale model also with daylight factors. Daylight factors were calculated in two different ways. The first way was using the lighting software DIALux and the second one was with DDF for 20673 sky elements.

Illuminance values in measuring points are calculated with next equation:

$$E_A = DF_A \cdot E_{diff} \quad (5.13)$$

where:

$E_A$	total illuminance at a given point
$DF_A$	daylight factor for a given point
$E_{diff}$	diffuse illuminance on an unobstructed horizontal plane

#### 5.4.2.1 Daylight factors with DIALux

In the DIALux lighting software we defined our scale model with both window openings (Fig. 5.15). The walls of the scale model were in black colour with approximate reflectance 6%. Measuring points in the scale model were defined in DIALux as *daylight calculation points*. To get the whole image of daylight factors on floor, also a *Daylight Quotient Surface* was added to the floor.

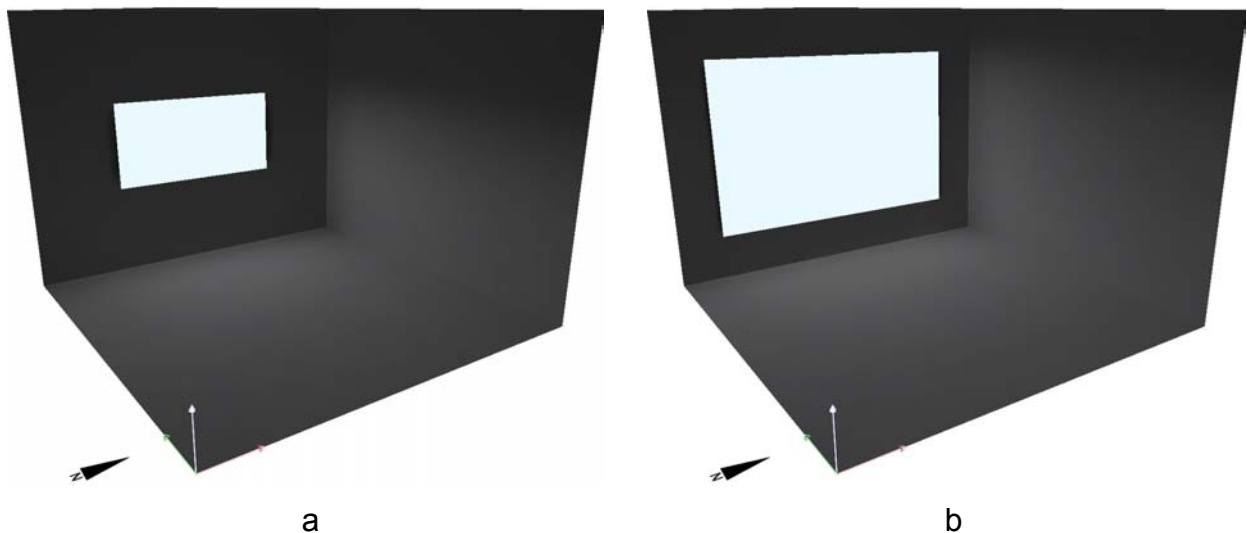


Fig. 5.15. 3D view of a scale model with both window openings in DIALux (a - window opening 40x20 cm, b - window opening 60x40 cm )

Daylight calculations in DIALux are performed in accordance with DIN 5034, this means that the sky is overcast. Calculation results (daylight factors) for measuring points are listed in Table 5.5, results for calculation surfaces are shown on Fig. 5.16.

Table 5.5. Daylight factors calculated with DIALux

Point in scale model	DIALux daylight factors [%]	
	Window opening 60x 40 cm	Window opening 40x 20 cm
A1	18	5.85
A2	11	4.43
A3	4.92	1.87
A4	2.51	0.83
A5	5.07	1.78
B1	5.15	1.73

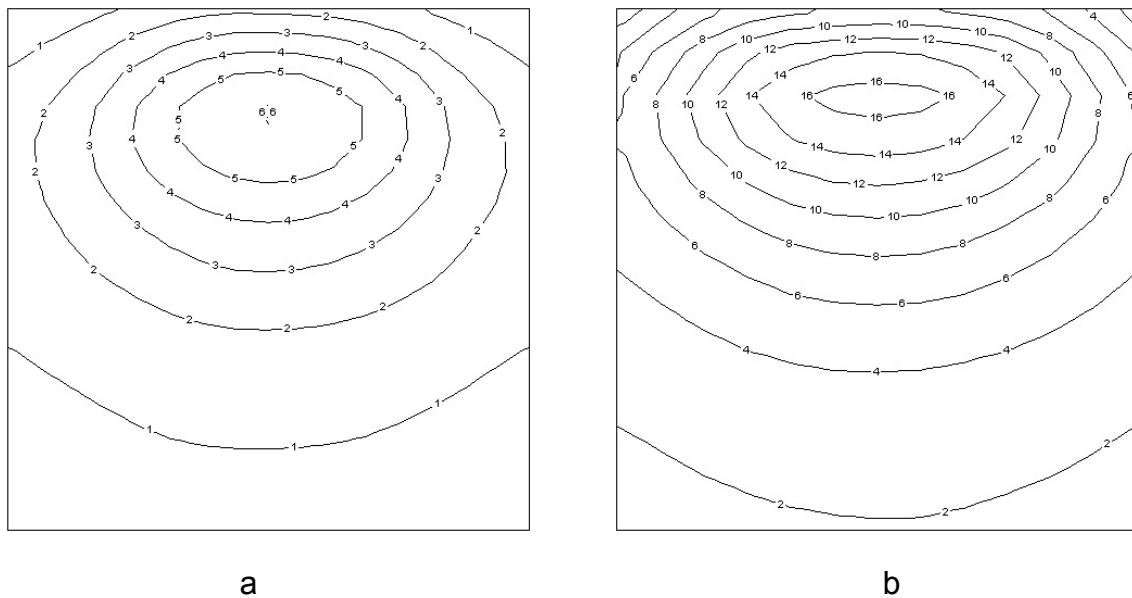


Fig. 5.16. Results of daylight calculations for calculation surfaces (a - window opening 40x20 cm, b - window opening 60x40 cm)

#### 5.4.2.2 Daylight factors with illuminance

Uniform hemisphere was divided into 20673 elements with constant interval in zenith angle ( $1^{\circ}$ ) and quasi constant solid angles. The partitioning was the same as it was used when calculating directional daylight factors. With the same method as it was used in section 5.2, percentage of each sky element that is visible from point in a model was calculated. Percentage was multiplied with solid angle of a sky element and the result (modified solid angle) was used in equation 5.9.

After the summation of contributions of all 20763 sky elements to the illuminance at a given point, the result was divided by theoretical illuminance on horizontal plane under uniform sky.

So called illuminance daylight factors are listed in Table 5.6.

Table 5.6. Illuminance daylight factors

Point in scale model	Illuminance daylight factors [%]	
	Window opening 60x 40 cm	Window opening 40x 20 cm
A1	17.03	3.96
A2	14.73	5.45
A3	7.42	2.76
A4	3.86	1.40
A5	8.11	2.78
B1	8.11	2.78

### 5.4.3 Calculation of illuminance values in scale model from luminance values from sky scanner

During scale model measurements, the sky scanner was also performing measurements of luminance values of the sky. The EKO sky scanner we used is measuring luminance of 145 sky elements. For this reason we had to calculate DDF also for CIE partitioning of the sky. With the same method as used in sections 5.2 and 5.3 the illuminance values were calculated for all measuring points in the scale model.

## 5.5 Mean bias error between measured and calculated illuminance values in scale model

In the scale model illuminance values were measured with Licor sensors. Calculated values (from sky scanner luminances, fish-eye luminances averaged over different number of sky zones and from daylight factors) were compared with measured ones and mean bias error was calculated with next equation (shown for fish-eye luminances averaged over 13 sky zones):

$$MBE_{sky13} = \frac{\frac{E_{sky13-A1} - E_{Licor-A1}}{E_{Licor-A1}} + \frac{E_{sky13-A2} - E_{Licor-A2}}{E_{Licor-A2}} + \dots + \frac{E_{sky13-A5} - E_{Licor-A5}}{E_{Licor-A5}} + \frac{E_{sky13-B1} - E_{Licor-B1}}{E_{Licor-B1}}}{6} \quad (5.14)$$

Where:

- $MBE_{sky13}$  mean bias error for sky modelled with 13 zones
- $E_{sky13-A1}$  calculated illuminance from 13 sky zone luminances in point A1
- $E_{Licor-A1}$  measured illuminance with Licor sensor in point A1

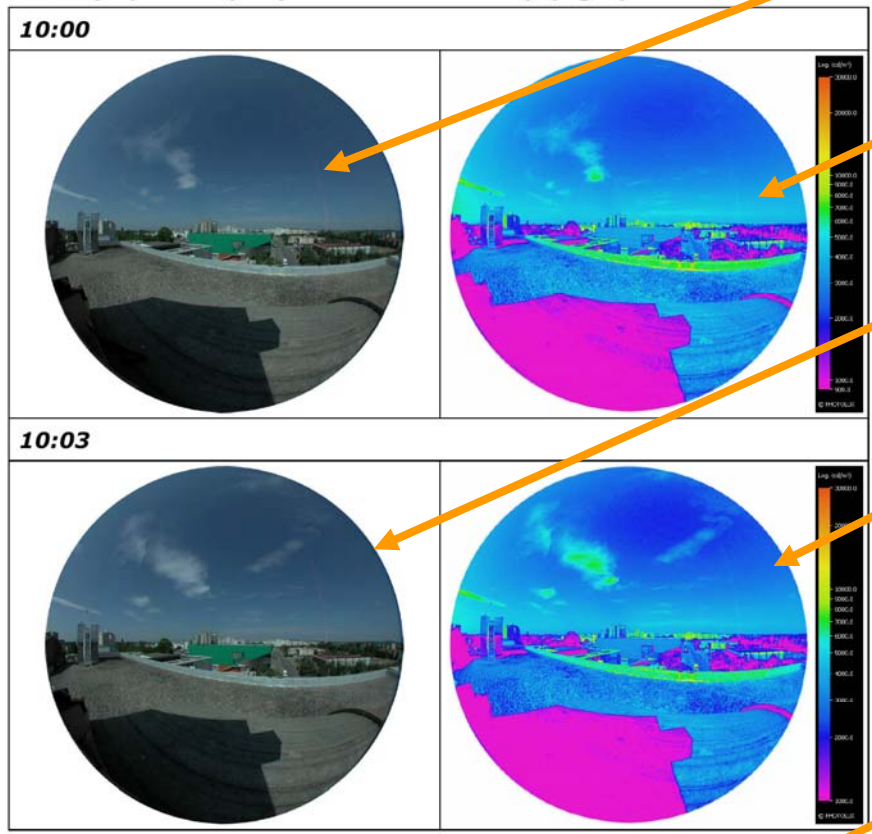
## 5.6 Database of scale model measurements

In the database we include all relevant data of whole sky measurements and all data measured and calculated for inside of the scale model. The database consists of three pages for each measurement. On the first page, one can find data about outdoor situation (fish-eye pictures, sky luminance maps and illuminance data), on the second page there are data about indoor situation (luminance maps of walls and measured and calculated illuminance values in all 6 points) and on the last page, there is an analysis of the calculated data.

The measurements were carried out on July 25<sup>th</sup>, 26<sup>th</sup>, 27<sup>th</sup> and 28<sup>th</sup>, 2005. All together we performed 153 measurements. All measurements are collected in the database, although some of the data are missing at certain measurements.

**July 28, 2005, 10:00 - 10:03 (GMT+1)**

**View seen from the scale model opening (40x20) facing WEST**  
**Fish-eye picture (left) and luminance map (right)**



Fish-eye picture of a view seen from the window opening. Picture is taken at the start of sky scanner measurement.

Luminance map of the fish-eye view from the window opening at the start of sky scanner measurement.

Fish-eye picture of a view seen from the window opening. Picture is taken at the end of sky scanner measurement.

Luminance map of the fish-eye view from the window opening at the start of sky scanner measurement.

Outdoor illuminance values on the scale model wall with the window opening vertical. Values are calculated from luminance map. In the left column illuminance is calculated with all elements of luminance map (also ground) and in the right column we take into account only elements above horizon.

**Whole sky measurements**

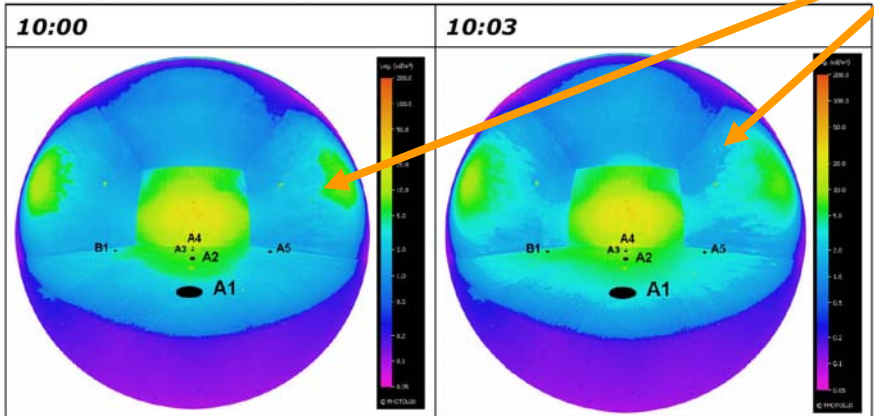
Time GMT+1	IDMP station			Sky scanner		Luminance map	
	Global horizontal illuminance lux	Diffuse horizontal illuminance lux	WEST global vertical illuminance lux	Diffuse horizontal illuminance lux	WEST diffuse vertical illuminance lux	Vertical illuminance on opening (Sky+Ground) lux	Vertical illuminance on opening (Sky only) lux
10:00	72800	17163	7060	18513	7121	9934	5420
10:01	73500	17194	7140			-	-
10:02	74000	17331	7240			-	-
10:03	74800	17388	7410			10055	5572

Global horizontal, diffuse horizontal and vertical illuminance measured by IDMP station

Illuminance values calculated from sky scanner luminances

**July 28, 2005, 10:00 - 10:03 (GMT+1)**

**Fish-eye luminance maps of scale model surfaces**



Fish-eye luminance map of scale model surfaces. Fish-eye images are taken at the start and at the end of sky scanner measurement.

**Illuminances inside the scale model**

(from Licor sensor measurements; from integration of sky scanner luminances, from integration of fish-eye picture luminances averaged over sky zones larger and larger and from daylight factors)

Illuminance values inside the scale model

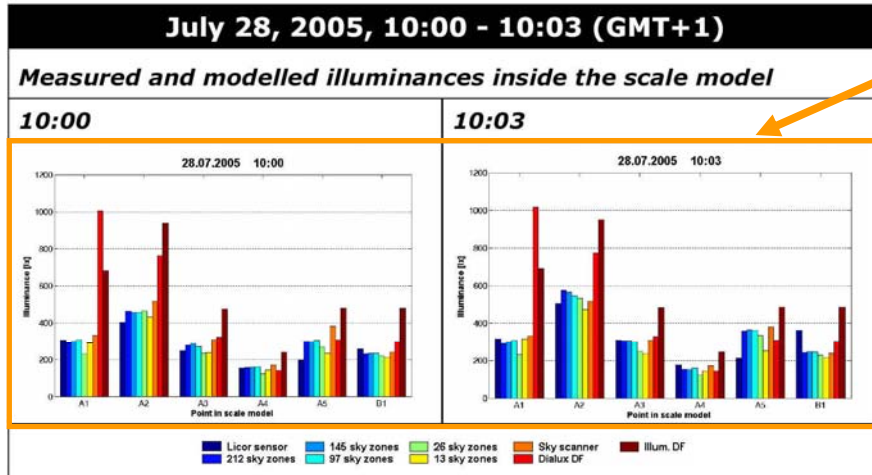
Point	Time GMT+1	Licor	Scanner luminances	Fish-eye luminances averaged over # sky zones					Daylight factor	
				212	145	97	26	13	Dialux	Illum.
A1	10:00	304	330	291	299	305	228	292	1004	680
	10:03	314		292	300	305	231	315	1017	689
A2	10:00	401	517	461	457	457	464	430	760	936
	10:03	505		573	565	545	532	471	770	948
A3	10:00	248	310	279	285	271	233	236	321	474
	10:03	310		305	303	300	247	236	325	481
A4	10:00	153	171	156	159	162	124	144	142	239
	10:03	176		155	150	160	121	144	144	243
A5	10:00	197	382	298	297	303	269	233	306	478
	10:03	211		357	364	362	333	251	310	484
B1	10:00	260	238	232	234	234	219	212	297	478
	10:03	362		241	245	244	228	214	301	484

Illuminances inside the scale model measured with Licor sensors

Illuminances inside the scale model calculated with  $DDF_{CIE145}$  from sky scanner luminances

Illuminances inside the scale model calculated with DDF's from fish-eye luminance maps

Illuminances inside the scale model calculated with daylight factors and IDMP diffuse horizontal illuminance

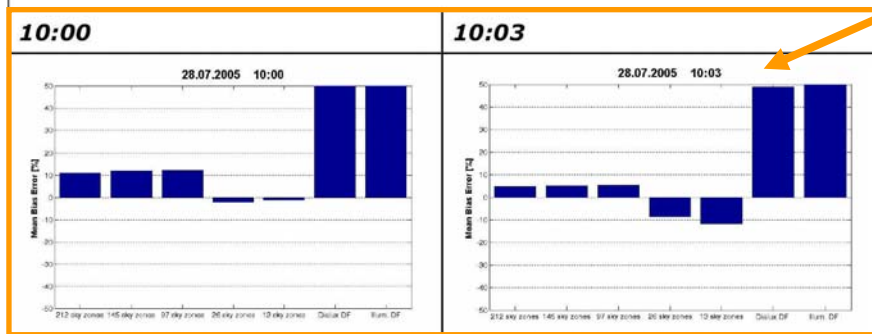


Graphical presentation of measured and modelled illuminances inside the scale model. Left diagram presented the conditions at the start of the sky scanner measurement and the right diagram presents the conditions at the end of the sky scanner measurement.

**Mean bias error of luminance based models and models based on daylight factors**

Time GMT+1	Mean bias error [%]						
	Number of sky zones					Daylight factors	
	212	145	97	26	13	Dialux	Luminance
10:00	10,88	11,97	12,20	-2,28	-1,23	68,53	105,13
10:03	4,72	5,13	5,28	-8,69	-11,71	48,91	77,23

Table with mean bias errors of luminance based models and models based on daylight factors



Graphical presentation of mean bias errors of luminance based models and models based on daylight factors. Left diagram presents the MBE for the conditions at the start of the sky scanner measurement and the right one presents the MBE for the conditions at the end of the sky scanner measurement.

**Comments**

## 5.7 Results of the scale model measurements

Our expectations were simple. We expected that the error would be inversely proportioned to the number of elements used at sky partitioning. So we expected that the error would be the smallest with the sky partitioning into 212 sky zones.

From all measurements where calculation of the MBE was possible, we calculated average MBE. Average MBE are collected in next table and presented in Fig. 5.17.

Table 5.7. Table of mean bias error

	Fish-eye luminances averaged over # sky zones					Daylight factors	
	212	145	97	26	13	Dialux	Illumin.
MBE for T0 [%]	11,29	11,29	11,54	0,19	2,15	45,36	88,84
MBE for T3 [%]	9,45	9,46	9,66	-1,28	0,85	44,43	87,34

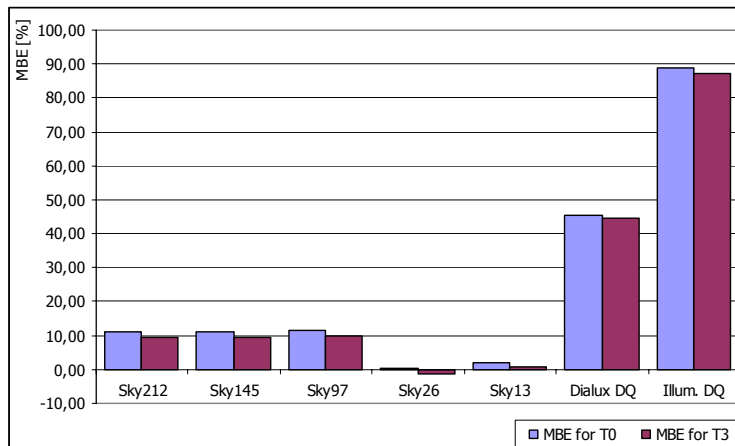


Fig. 5.17. Mean bias error

To present results in a more evident way, diagrams of cumulative MBE frequency distribution were also plotted (Fig. 5.18 - Fig. 5.24). In this graphs mean bias errors are sorted by the height of the error.

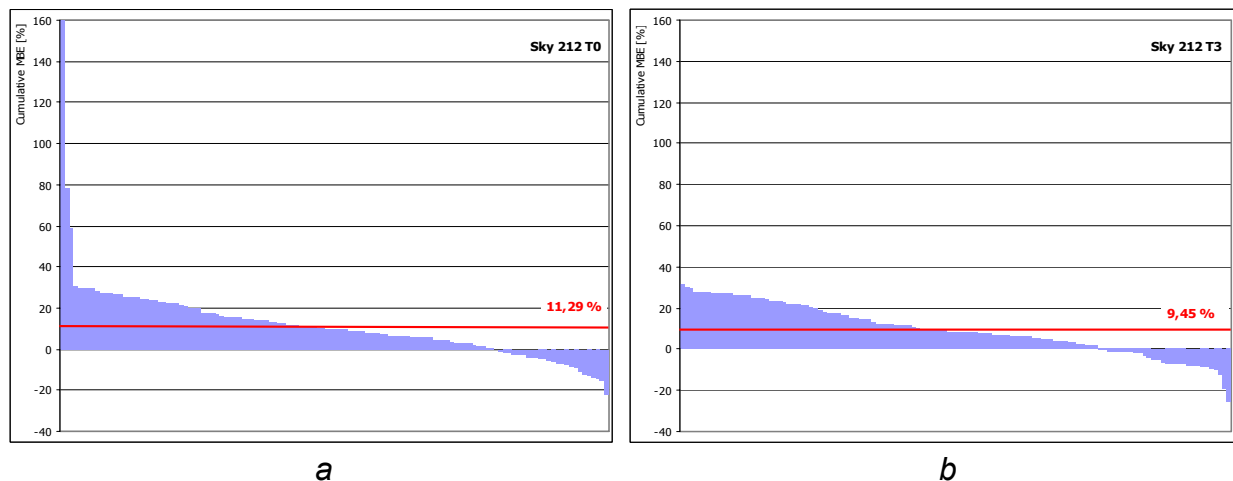


Fig. 5.18. Cumulative MBE frequency distribution for sky modeled with 212 zones (a - time T 0 min, b - time T 3 min)

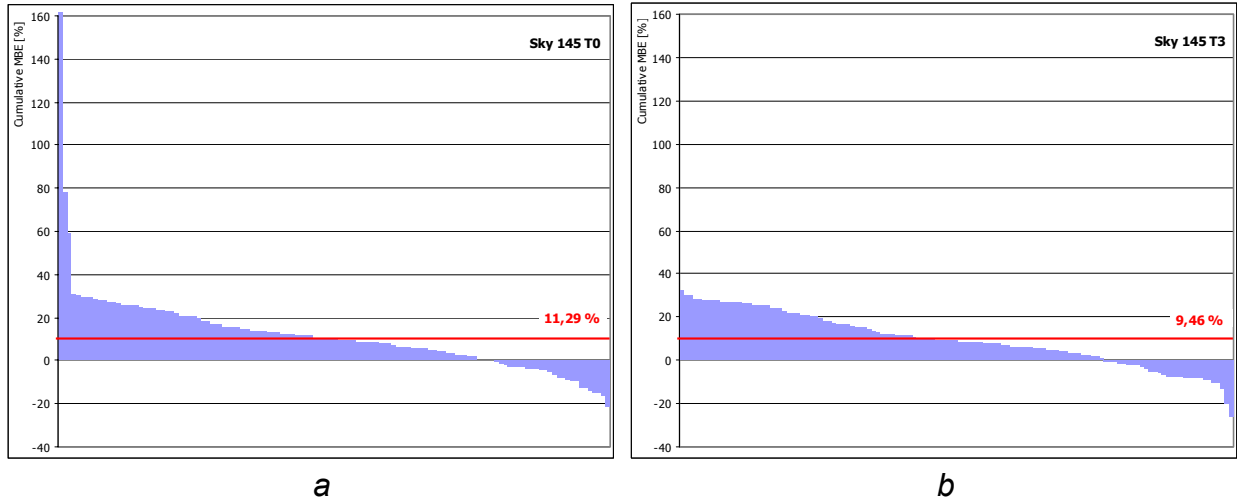


Fig. 5.19. Cumulative MBE frequency distribution for sky modeled with 145 zones (a - time T 0 min, b – time T 3 min)

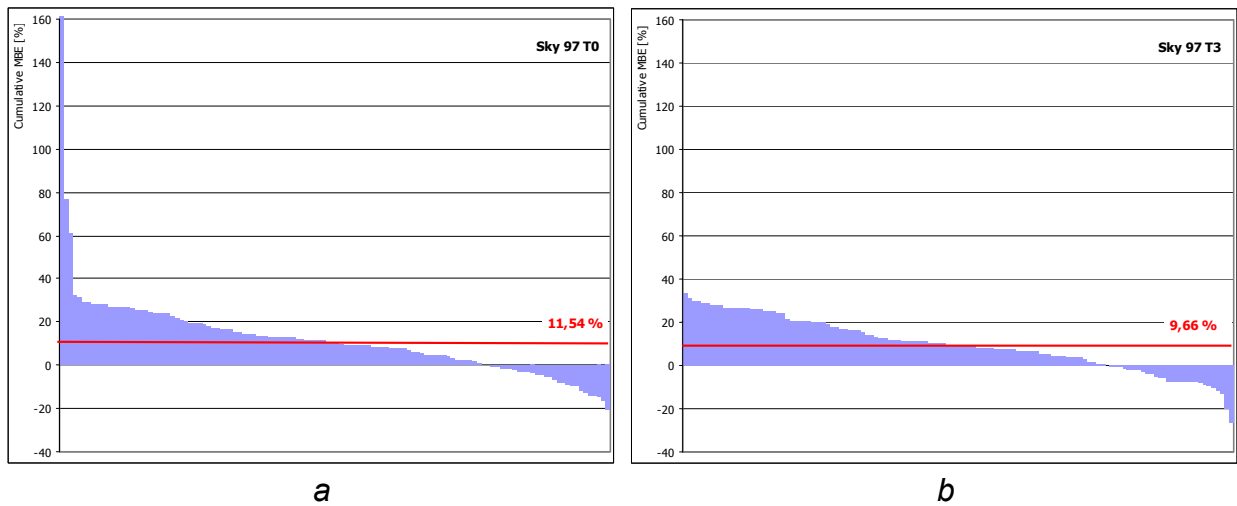


Fig. 5.20. Cumulative MBE frequency distribution for sky modeled with 97 zones (a - time T 0 min, b – time T 3 min)

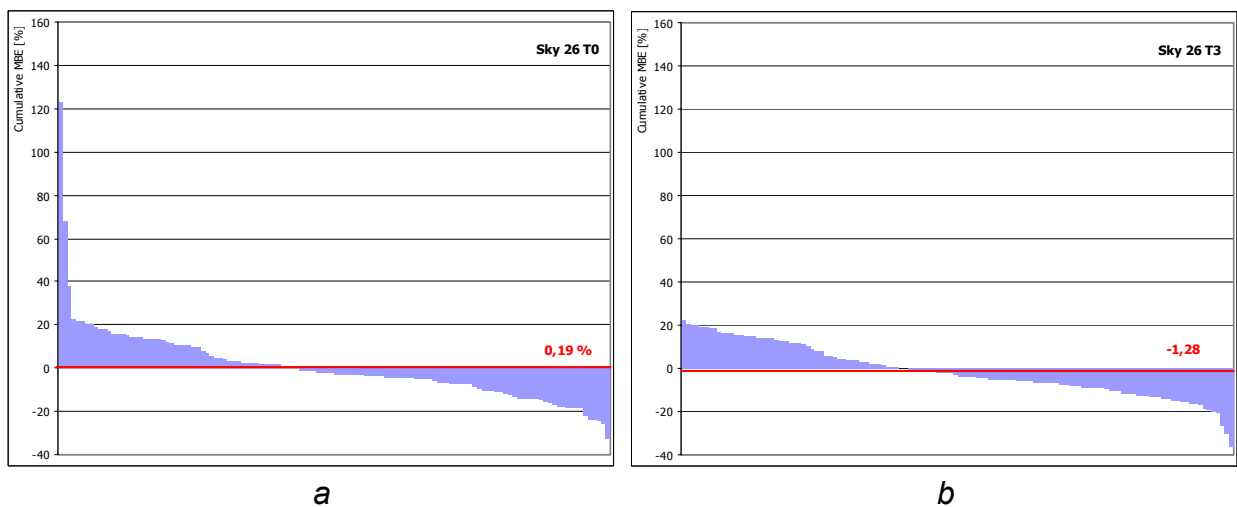


Fig. 5.21. Cumulative MBE frequency distribution for sky modeled with 26 zones (a - time T 0 min, b – time T 3 min)

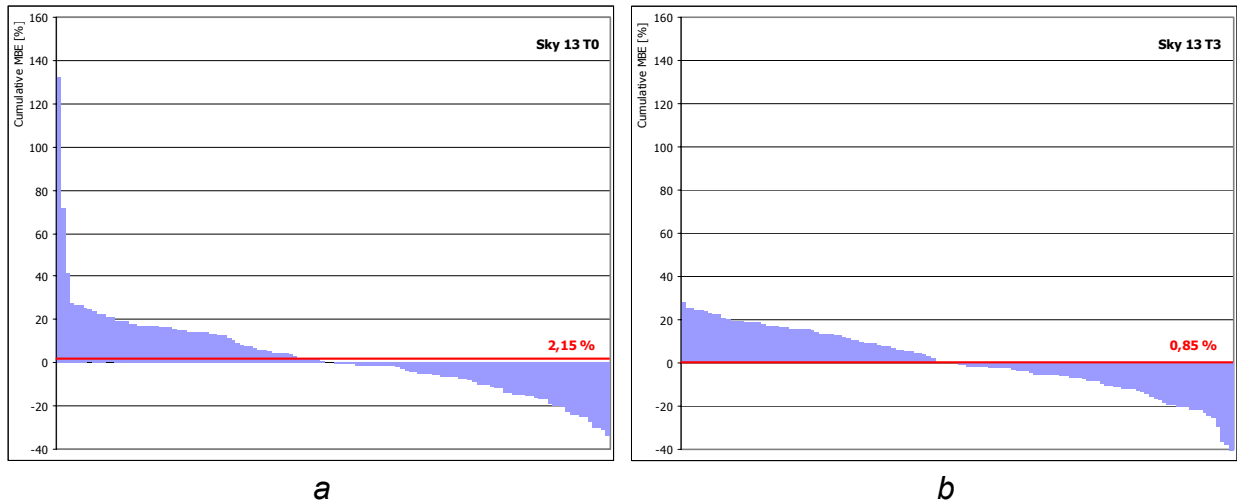


Fig. 5.22. Cumulative MBE frequency distribution for sky modeled with 13 zones (a - time T 0 min, b - time T 3 min)

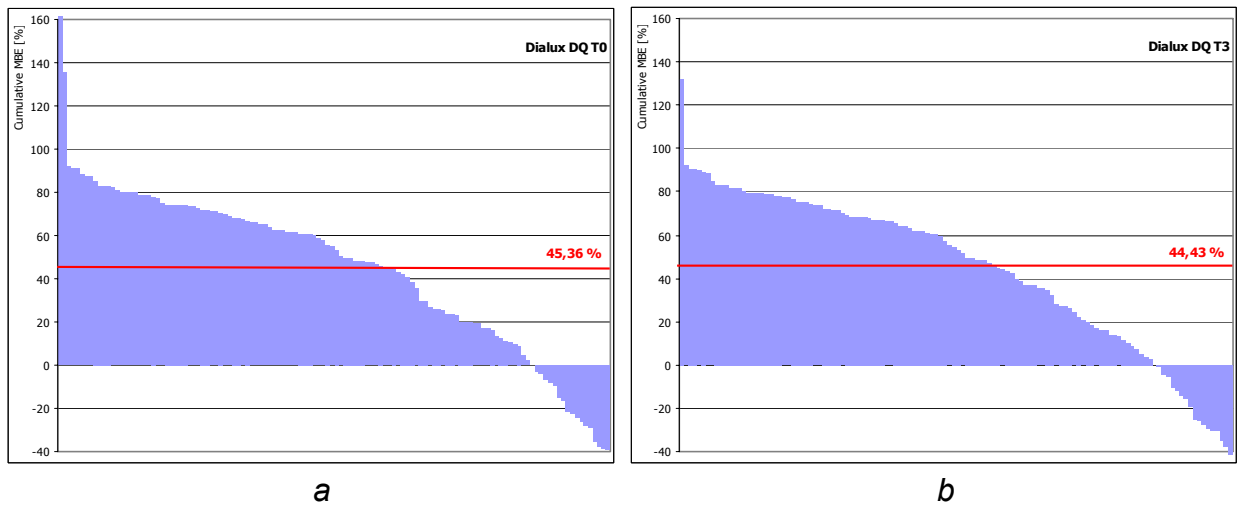


Fig. 5.23. Cumulative MBE frequency distribution for sky modeled with Dialux daylight factors (a - time T 0 min, b - time T 3 min)

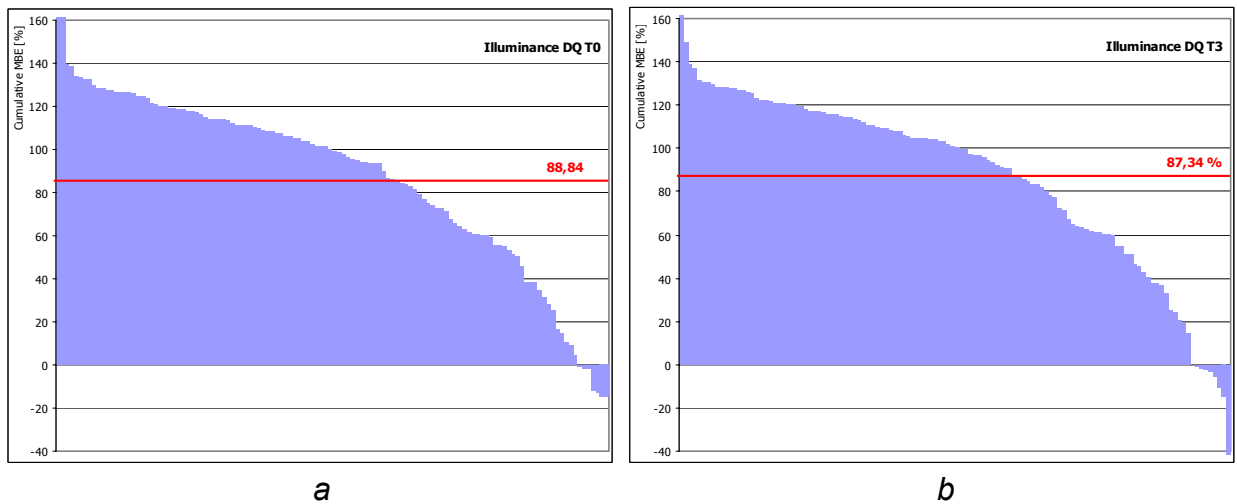


Fig. 5.24. Cumulative MBE for sky modeled with illuminance daylight factors (a - time T 0 min, b - time T 3 min)

One can see that the graphs of cumulative frequency distribution of mean bias error for both daylight factors are quite full and also the mean bias error (Table 5.7) is not in favour of the daylight factors. Daylight factor in all cases overestimate illuminances in the model. The reason is that daylight factors are calculated with overcast sky in case of Dialux factors and with uniform sky in case of illuminance factors.

Average value of the MBE can be misleading, since the average MBE can be close to zero, but the individual values could be far from zero. To eliminate this possible misleading, also RMSE was calculated and results are presented in Table 5.8 and on Fig. 5.25. Relative RMSE was calculated with next equation (shown for fish-eye luminances averaged over 13 sky zones):

$$RMSE_{sky13} = \sqrt{\frac{\left(\frac{E_{sky13-A1} - E_{Licor-A1}}{E_{Licor-A1}}\right)^2 + \left(\frac{E_{sky13-A2} - E_{Licor-A2}}{E_{Licor-A2}}\right)^2 + \dots + \left(\frac{E_{sky13-A5} - E_{Licor-A5}}{E_{Licor-A5}}\right)^2 + \left(\frac{E_{sky13-B1} - E_{Licor-B1}}{E_{Licor-B1}}\right)^2}{6}} \quad (5.15)$$

Where:

- $RMSE_{sky13}$  root mean square error for sky modelled with 13 sky zones
- $E_{sky13-A1}$  Calculated illuminance from 13 sky zone luminances in point A1
- $E_{Licor-A1}$  Measured illuminance with Licor sensor in point A1

Table 5.8. Table of RMS error

	Fish-eye luminances averaged over # sky zones					Daylight factor	
	212	145	97	26	13	Dialux	Illumin.
RMSE for T0 [%]	25,21	25,37	25,42	24,28	23,69	75,31	97,98
RMSE for T3 [%]	22,56	22,69	22,65	22,42	21,84	74,23	95,91

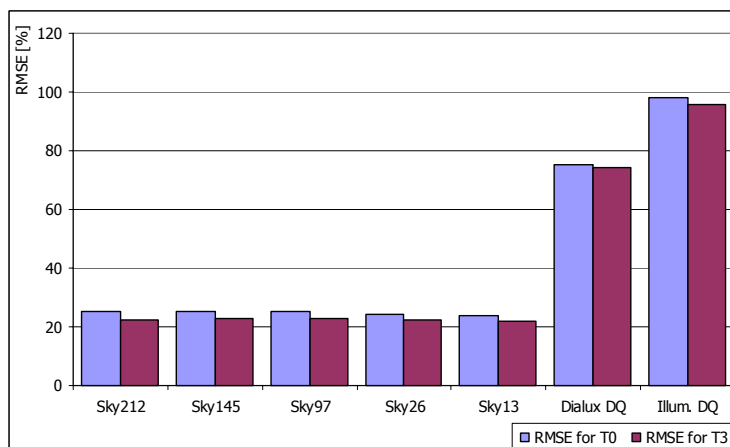


Fig. 5.25. Root mean square error

As can be seen from Table 5.7 and Table 5.8, the results are not in line with our expectations. As mentioned in the beginning of this paragraph the error should be

inversely proportional to the number of sky zones used in the model. Mean bias error has practically the same value for sky models with 212, 145 and 97 zones and is around 11,5 % for measurements performed at the start of the sky scanner measurements and around 9,5 for measurements performed at the end of the sky scanner measurements (three minutes after the first measurements). Surprisingly the values of MBE with sky models with 26 and 13 zones are lower and they are less than 2,5% for both measurements (T0 and T3). Illuminances modelled with Dialux and illuminance daylight factors are over estimated in more than 85% cases for Dialux and in 95% for illuminance daylight factors (Fig. 5.23 and Fig. 5.24). The results for daylight factors did not surprised us, since the daylight factors are supposed to be used with uniform and overcast skies, what was not a case with our measurements.

If we base our conclusion on root mean square error the figure is similar but not the same. Practically all scale model illuminances based on sky partitioning give the same RMS error, which is around 25 % for T0 measurements and 23 % for measurements performed at the end of the sky scanner measurements. Also with RMS error we get much higher values for both methods with daylight factors. RMS error is around 75 % for Dialux daylight factors and around 95% for illuminance quotient.

## **5.8 Conclusions for scale model measurements**

As already mentioned we get most of the light in indoor premises from the sky and not from the sun. If there is direct component of the sun penetrating into premises it is usually screened with blinds or other similar devices.

In our research we wanted to investigate the influence of the number of sky elements in the sky model on the accuracy of indoor illuminance calculations. All the measurements that were performed with scale model were without direct sun and for that the difference in luminance of the darkest and brightest part of the sky was not great. If also direct sun would be taken into account, then the difference could be larger.

As it can be carried out from the scale model measurements, in cases of homogeneous sky or sky without extreme differences in luminance, the number of sky elements is not playing an important role.

Surprisingly the mean bias error is not inversely proportional with the number of the elements used in the sky model and from results (Table 5.7 and Table 5.8) we can conclude that the most convenient number of sky zones used for sky models is 13. Results are pretty the same for 26 and 13 sky zones, but a smaller number of zones, means a shorter computing time.

In this place we should also think about the simplifications we made. One of the most important simplifications is that in our scale model we did not use any glazing. Since the transmission factor of the glazing depend on the direction of the light penetrating into the rooms, it is difficult to say for certain that 13 elements are enough.

## 6 Conclusion

The main topics of the thesis are daylight measurements and calculations connected with daylight availability. The most important contribution of the thesis is selection of the sky luminance model that can be used to derive frequencies of appearance of CIE sky types from satellite images (global and diffuse horizontal irradiances) and to calculate time values of indoor daylight illuminances.

Selection of the best performing sky luminance model is based on sky luminance distribution measurements performed in Lyon between April 2005 and December 2005.

Sky luminance distribution measurements were carried out with an EKO sky scanner, borrowed from Kyushu University (Japan). This scanner measures sky luminance distribution with accuracy over 145 sky zones in approximately 3 minutes. The sky scanner was calibrated under artificial sky and under real sky conditions before performing measurements.

Together with the installation of the sky scanner we carried out also some modifications to vertical illuminance sensors on ENTPE IDMP station.

Measurement data were analysed in different ways. The most important analysis was deriving the CIE sky type. CIE sky type was defined firstly on basis of indicatrix and gradation groups, which are defined with CIE standard CIE S 011/2003. Secondly the CIE sky type was defined with ratio between zenith luminance and diffuse horizontal illuminance. The last method we used was a statistical method. With all three methods, for every sky scan, one of the 15 CIE sky types was determined. At the end of chapter two, we present frequencies of CIE sky types derived with different methods are shown. All the data were analysed and the complete database is available online at <http://lrf.fe.uni-lj.si/ekoscan.htm>.

There are only a few working sky scanners in the world. The main reason is that this equipment is expensive and it needs regular attendance and servicing. We tried to find a new, more effective method, for a reasonable price by using a digital camera with a fish-eye lens. We compared more than 160 pairs of digital images and sky scans. The results show that a digital camera with a fish-eye lens can be used as a sky scanner with some limitation. For instance there are problems with rain, temperature variations, and it's easy to burn a CCD if we do not use a single-lens reflex (SLR) camera.

When selecting the sky luminance model that can be used to derive frequencies of occurrence of CIE sky types from satellite images, we have reviewed the following sky luminance models: Perez all weather model, ASRC-CIE model and Igawa model. For the times, when we had sky scanner measurements (13.006 cases), sky luminance distributions were produced with all three models. The modelled luminances are calculated with model's equations and irradiance data measured by IDMP station. Based on all comparisons, we can conclude that Igawa model is best for extremely cloudy sky types, Perez All weather model gives best results with intermediate sky types and ASRC-CIE model is in most cases in between upper two models, but on average the best model.

In last part of the thesis, we draw conclusions on needed density of the grid of sky luminance model. To come to those conclusions we performed measurements on scale model. Measurements were carried out on scale model with black indoor walls to eliminate multiple indoor reflections. In the scale model, illuminances were measured and the same illuminances were modelled with different methods. One method was by means of directional daylight factor (DDF). DDFs were calculated for different densities of sky luminance model grid (212, 145, 97, 26 and 13 zones). The other method was with traditional daylight factor. Results show that the number of sky zones has almost no influence to MBE and after that we can conclude that 13 zones are enough to model sky luminance if we are considering only sky vault without direct sun.

Conclusions about the use of digital camera as a sky scanner and needed accuracy of the sky luminance model and with that needed number of sky zones that should be used in a model are based on analysis of a large amount of measured data. The measured data and the complete analysis are gathered in two databases. The first one is a database of outdoor measurements (comparison of sky scanner measurements and images taken with digital camera) and the second one is a database of scale model measurements (measurements of illuminances in the scale model accompanied with pictures of the sky vault and luminance maps in the scale model). Both databases are available to public on CD upon request.

During our research, we have realized that there is still much work that could be done in this field. When we were talking with the daylight designer, we got the impression that one of the first things that could be done is a table with frequencies of occurrences of CIE sky types for at least capital cities of EU countries. In next iteration we could broaden this table with all bigger cities in EU and in countries which are covered with Meteosat geostationary satellite (<http://www.satellight.com>).

Performing measurements on scale models is easy and cheap if we compare it with measurements in real buildings. But in our future work we should change model with real building. Those measurements should be long-term and during the measurements we should consider also different sorts of glazing and different sorts of blinds. When working with real buildings or bigger scale models (size of a window should be compared to real window situation) also the luminance intensity distribution could be measured with an automated goniophotometer on the inner side of a window. In our work we conclude that a digital camera could be used as a sky scanner with some limitations, we could also perform long-term measurements of sky luminance distribution with digital camera. A camera should be put in a tempered box, covered with a spherical glass cover, such as used for collectors with light-pipes. A problem with burning CCD could be eliminated with use of single-lens reflex (SLR) camera.

## **Contributions of the thesis to the science**

Main contribution of the thesis to the science is a selection of a sky luminance model that allows the determination of frequency of emergence of CIE sky types at a specific location on the basis of global and diffuse horizontal irradiances. The model is defined and it can be used on data available from satellite images.

Another contribution to the science is definition of partitioning of the sky vault. In the thesis we suggest the number of zones that should be used when calculating daylight availability without direct sun.

Beside the selection of the sky luminance model and suggested number of sky zones the contribution to the science are also next large databases:

- database of all sky scanner measurement that were performed at ENTPE in year 2005. In the database a reader can find measured sky luminance values together with the analysis of the sky luminance distribution (CIE sky type, indicatrix and gradation group...)
- database of outdoor measurements (comparison of sky scanner measurements and images taken with digital camera)
- database of scale model measurements (measurements of illuminances in the scale model accompanied with pictures of the sky vault and luminance maps in the scale model).



## **Statement of the authorship**

Undersigned Matej B. Kobav, born on March 21st 1974 in Ljubljana, declare that I have written the PhD thesis "Development and validation of methods used to compute time values of indoor daylight illuminances" on my own under the supervision of dr. Grega Bizjak and dr. Dominique Dumortier. Help of other collaborator is indicated in acknowledgements.

Matej B. Kobav



## References

- [1] Dumortier D., Mesure, analyse et modélisation du gisement lumineux. Application à l'évaluation des performances de l'éclairage naturel des bâtiments. (1995) *PhD Thesis*, Université de Savoie, France, 350 pages.
- [2] Darula S., Kittler R., Kmeto P., New CIE General Sky Defining Luminance Distributions, SUSTAINABLE BUILDING & SOLAR ENERGY 2001, Brno, 2001
- [3] Nakamura H., Oki M., Hayashi Y., Luminance distribution of intermediate sky, *J. Light and Vis. Env.*, 9, 1, pp. 6-13.
- [4] Igawa N., Nakamura H., Matsuzawa T., Koga Y., Goto K., Kojo S., Sky luminance distribution between two CIE standard skies 1,2, *Pros. Lux Pacifica*, pp. 359-373.
- [5] Igawa N., Nakamura H., Matsuura K., Sky luminance distribution model for simulation of daylight environment, BS99 (Building Simulations 1999), 1999, Kyoto.
- [6] CIE, Spatial Distribution of Daylight - Luminance Distributions of Various Reference Skies, Pub. CIE No.110 1994 ISBN 3 900 734 52 6, 1994.
- [7] CIE, Daylight International recommendations for calculation of natural daylight, Pub. CIE no. 16 (E-3.2) 1970.
- [8] ISO 15469/CIE S003, Spatial Distribution of Daylight – CIE Standard overcast and clear sky, 1996.
- [9] <http://genelux.entpe.fr/sommaire.html>
- [10] <http://www.satellight.com/guide/advday.htm>.
- [11] Kaehler K., Flächenhelligkeit des Himmels und Beleuchtungsstärke in Raumen. *Meteorol. Zeitschr.*, 25, 2, pp 52-57, 1908.
- [12] Kimball H., Hand I. F. Sky brightness and daylight illumination measurements. *Monthly Weather Rev.* 49, 9, pp. 481-488, 1921
- [13] Moon P., The scientific basis of illuminating engineering, Dover publications, New York, 1961.
- [14] Perez R., Seals R., Michalsky J., All Weather Model for sky luminance distribution – preliminary configuration and validation, *Solar Energy*, Volume 50, Issue 3, PP 234-245, 1993.
- [15] Kittler R., Darula S., Perez R., A set of standard skies, characterizing daylight conditions for computer and energy conscious design, American-Slovak grant project, US-SK 92 052, 1998.
- [16] CIE DS 011.1/E:2003 Spatial distribution of daylight – CIE standard general sky, Standard, CIE Central Bureau, Vienna, 2003.
- [17] KOBAV Matej Bernard, Razvoj nadomestnega svetlobnega vira za izračun osvetljenosti prostora z dnevno svetlobo, magistrsko delo, Fakulteta za elektrotehniko Univerza v Ljubljani, Ljubljana, 2003.

- [18] Michalsky J., Perez R., Seals R., Evaluation of Algorithms for Sky Luminance Distribution Prospects for Performance Improvements, ISES World Congress, Denver Colorado, 1991.
- [19] Esteban C., Torres A., Fasulo A., Tocho J, Adjusted Model of Linke's Turbidity Factor, EuroSun 98, Portorož, Slovenia, 1998.
- [20] Roy G. G., Ruck N., Reid G., Winkelmann C. F., Julian W., The Development of Modelling Strategies for Whole Sky Spectrum under Real Conditions for International Use, University of Sydney, 1995.
- [21] Daylight Simulation: Methods, Algorithms and Resources, A report of IEA SHC 21/ECBCS ANNEX 29, December 1999, Berkeley, California.
- [22] Kittler R., Perez R., Darula S., A New Generation of Sky Standards, Proceedings Conference Lux Europa 1997, pp 359-373, Amsterdam, 1997.
- [23] Perez R., Ineichen P., Seals R., Michalsky J., Stewart R., Modeling daylight availability and irradiance components from direct and global irradiance, Solar Energy, Vol. 44, Issue 5, PP 271-289, 1990.
- [24] Perez R., Ineichen P., Moore K., Kmiecik M., Chain C., George R., Vignola, F., A new operational model for satellite-derived irradiances: description and validation Solar Energy, Vol. 73, Issue 5, PP 307-317, 2002.
- [25] Chain C, Dumortier D., Fontoynt M., A Comprehensive Model of Luminance, Correlated Colour Temperature and Spectral Distribution of Skylight: Comparison with Experimental Data, Solar Energy, Volume 65, Issue 5, PP 285-295, 1999.
- [26] Ineichen P., Molineaux B., Perez R., Sky luminance data validation: Comparison of seven models with four data banks, Solar Energy, Volume 52, Issue 4, PP 337-346, 1994
- [27] Rutten AJF, Sky luminance measurements for design and control of indoor daylight illumination, Lighting Research and Technology, Volume 22, PP 189–192, 1990
- [28] Littlefair PJ, A comparison of sky luminance models with measured data from Garston, United Kingdom. Solar Energy, Volume 53, PP 315–322, 1994
- [29] Dumortier, D., Van Roy F., Daylighting information throughout Europe from the SATEL-LIGHT and SODA Internet servers. CIE 25th Conference San Diego, 2003, 1, D3-4.
- [30] Karayel M, Navvab M, Ne'eman E, Selkowitz S, Zenith luminance and sky luminance distributions for daylighting calculations, Energy and Buildings, Volume 6, PP 283–291, 1984.
- [31] Moon P, Spencer DE, Illumination from a non-uniform sky, Illuminating Engineering, Volume 37, PP 707–726, 1942
- [32] Kittler R., Ruck N., Definition of typical and average exterior daylight conditions in different climatic zones, Energy and Buildings, Volume 6, Issue 3, PP 253-259, 1984.
- [33] Tregenza P.R., Subdivision of the sky hemisphere for luminance measurements, Lighting Research and Technology, Volume 19, Issue1, PP. 13–14, 1987.

- [34] Kittler R., Darula S., Perez R., Advantages of new sky standards: more realistic modelling of daylight conditions in energy and environmental studies. *International Journal of Energy, Environment and Economics*, Volume 8, Issue 1, PP 65–71, 1999.
- [35] Bartzokas A., Sky luminance distribution in Central Europe and the Mediterranean area during the winter period, *Journal of Atmospheric and Solar-Terrestrial Physics*, Volume 65, Issue 1, PP 113-119, 2003.
- [36] Darula S., Kittler R., Parametric definition of the daylight climate, *Renewable Energy*, Volume 26, Issue 2, PP 177-187, 2002.
- [37] Tregenza, P.R., Analysing sky luminance scans to obtain frequency distribution of CIE Standard General Sky. *Lighting Research and Technology*, 2004. 36(4): pp 271-281
- [38] Kittler, R. Darula, S., New trends in daylighting theory based on the new ISO/CIE sky standard. 1. Zenith luminance on overcast skies. *Building research journal*, Vol. 52, No. 3, 2004
- [39] Igawa, N. Koga, Y. Matsuzawa, T. Nakamura, H. Models of sky radiance distribution and sky luminance distribution. *Solar Energy* Vol. 77, No. 4, 2004: pp. 137-157.
- [40] Perez, R. Michalsky, J. Seals, R., Modelling sky luminance angular distribution for real sky conditions. Experimental evaluation of existing algorithms, *J. Illumin. Eng. Soc.* 21(2), pp 84-92. 1992.
- [41] Moon, P. Spencer, D. E., Illumination from a nonuniform sky, *Illum. Eng. (N.Y)*, 37, pp. 707-726, 1942.
- [42] Kittler, R. Darula, S., New trends in daylighting theory based on the new ISO/CIE sky standard. 2. Typology of cloudy skies and their zenith luminance. *Building research journal*, Vol. 52, No. 4, 2004
- [43] Kittler, R. Darula, S., New trends in daylighting theory based on the new ISO/CIE sky standard. 2. Zenith luminance formula verified by measurement data under cloudless skies. *Building research journal*, Vol. 53, No. 1, 2005
- [44] Tregenza, P.R., Perez, R., Seals, R., Michalsky, J., Guide to recommended practice of daylight measurement, CIE TC 3.07, 1993
- [45] Kittler, R., Relative scattering indicatrix: derivation from regular radiance/luminance distribution sky scans, *Lighting Res. Technol.* Vol. 25, No. 3, pp 125-127, 1993
- [46] Kittler, R., Hayman, S., Ruck, N., Julian, W., Daylight measurement data: Methods of evaluation and representation, *Lighting Res. Technol.* Vol. 24, No. 4, pp 173-187, 1992
- [47] Schramm, W., Über die Verteilung des Lichtes in der Atmosphäre. *Schriften d. Naturw. Veriens f. Schl.-Holst.*, Vol. 12, No. 1, 1901, pp 81-129
- [48] Pokrowski, G. I., Über die Helligkeitsverteilung am Himmel. *Phys. Zeitsch*, Vol. 30, No. 20, 1929, pp 697-700
- [49] Boldyrev, N. G., O raspredeleniyi jarkosti po nebu (About the distribution of luminance on sky), *Svetotekhnka*, Vol. 6., 1935, pp 16-18
- [50] Krat, V.A., Indikatrisa rasseyaniya sveta v zemnoj atmosfere. (Indictrix of light diffusion in earth atmosphere), *Astronom. J.*, Vol. 20, 1943, pp 5-6.

## *References*

---

- [51] Kittler, R., Standardisation of the outdoor conditions for the calculation of the Daylight factor with clear skies, Sunlight in buildings, Bouwcentrum Rotterdam, 1967, pp 273-286.
- [52] CIE, Standardization of luminance distribution on clear skies, Pub. CIE No. 22, 1973.